NOTE TO USERS

This reproduction is the best copy available.

UMI®

DISSERTATION

SYNTHESIS AND CHARACTERIZATION OF TETRAALKYLATED AND FUNCTIONALIZED POLYALKYLATED FERROCENES AND THEIR APPLICATIONS FOR THE SELECTIVE REDOX-RECYCLABLE EXTRACTION AND DETECTION OF AQUEOUS ANIONS

Submitted by

Brady J. Clapsaddle

Department of Chemistry

In partial fulfillment of the requirements

for the Degree of Doctor of Philosophy

Colorado State University

Fort Collins, Colorado

Spring, 2002

COLORADO STATE UNIVERSITY

January 23, 2002

WE HEREBY RECOMMEND THAT THE DISSERTATION PREPARED UNDER OUR SUPERVISION BY BRADY J. CLAPSADDLE ENTITLED, *SYNTHESIS AND CHARACTERIZATION OF TETRAALKYLATED AND FUNCTIONALIZED POLYALKYLATED FERROCENES AND THEIR APPLICATIONS FOR THE SELECTIVE REDOX-RECYCLABLE EXTRACTION AND DETECTION OF AQUEOUS ANIONS*, BE ACCEPTED AS FULFILLING IN PART THE REQUIREMENTS FOR THE DEGREE OF DOCTOR OF PHILOSOPHY.

Committee on Graduate Work

Advisor

Department Head

ABSTRACT OF DISSERTATION

SYNTHESIS AND CHARACTERIZATION OF TETRAALKYLATED AND FUNCTIONALIZED POLYALKYLATED FERROCENES AND THEIR APPLICATIONS FOR THE SELECTIVE REDOX-RECYCLABLE EXTRACTION AND DETECTION OF AQUEOUS ANIONS

Several new tetraalkylated ferrocenes and functionalized polyalkylated ferrocenes have recently been synthesized and used for the selective ion exchange and detection of aqueous anions. The synthesis of new, functionalized polyalkylated ferrocenes is key to the development of novel, robust ion exchange compounds that can be used in materials synthesis or surface modification. The resulting materials have applications in both the remediation and detection of pollutant anions in aqueous media. The goal of this work is the synthesis and characterization of several novel polyalkylated ferrocenes and the study of their applications toward the remediation and detection of aqueous media containing pollutant anions. Several new functionalized polyalkylated ferrocenes have been synthesized and used for materials synthesis or surface modification toward this end. In addition, a novel method of electrochemical anion detection is discussed using some of the electroactive polyalkylated ferrocenyl materials synthesized. Due to the importance of selectivity for both remediation and detection, the ion-exchange selectivity of these novel polyalkylated ferrocenes for both applications was determined as further characterization of the new ion-exchange materials.

Brady John Clapsaddle
Department of Chemistry
Colorado State University
Fort Collins, CO 80523
Spring, 2002

ACKNOWLEDGEMENTS

I would like to thank all of those people who helped with this research for their valuable time and advice. I would specifically like to thank Mr. Don Dick for all mass spectral characterization, Dr. Oren Anderson for help with X-ray crystallography, Dr. Nancy Levinger and Ms. Liz Corbiel for training on and use of the particle size analyzer, and Dr. David W. Grainger and Dr. Farazad Parsepour for use of a spin-coater. Very special thanks need to be given to Dr. C. Michael Elliott for both teaching me and helping me with electrochemistry. Your expert advice and somewhat "unorthodox" teaching methods, which I am sure are going to cause a renaissance of sorts in the teaching field, were invaluable. Finally, many thanks need to be given to Susie M. Miller for her unfathomable crystallographic skills, patience, and encouragement.

I would also like to thank all my classmates, who by default have also become my friends. The support and encouragement I have received from you I can only hope has been returned by me at every opportunity to do so. Special thanks go to Dr. Jon Lorenz, for organic synthesis advice, and Dr. Shawn Sapp, for electrochemical advice.

Special thanks goes to the entire Strauss Research Group, both past and present, especially Dr. Kristina Gansle, Dr. C. Kevin Chambliss, Dr. Alex Gash, Gretchen Hebert, Preston Craig, and Elisha Kosak. Dr. Matthew Odom and I were an inseparable team for this research and he contributed his time, valuable data, and friendship.

Dr. Steve Strauss, the job of training scientists to be successful at this level is the most important thing you do and no research result will ever be equal to your accomplishments in this area. I will never be able to thank you enough.

It is with much appreciation and love that I end with thanks to my sister Wendy and parents Jerry and Susan Clapsaddle. You have been there for EVERY moment of my life with encouragement, understanding, and most importantly love. It is extremely important that you are acknowledged in my biggest accomplishment. Thank you.

To my wife Trisha, who's support, patience, and love exceeds anything I could have imagined. I don't care what your hair looks like, I love you anyway.

Table of Contents

Chapter 1. An Overview: Redox-Recyclable Extraction and Recovery (R^2ER) and its Application to Remediation and Detection of Aqueous Ions

Introduction 1

Ionic Pollutants 2

Current Extraction and Recovery Techniques 4

A New Approach Towards Extraction and Recovery of Pollutant Ions 7

The Low-Level Detection of Pollutant Anions Using the R^2ER Extractants 12

Selectivity of R^2ER Extractants 16

Scope of the Dissertation 24

References 33

Chapter 2. Synthesis, Characterization, and Crystal Structures of Polyalkylated Ferrocenes and Ferrocenium Salts

Introduction 38

Experimental Section 40

Results and Discussion 46

Preparation of 1,1',3,3'-tetra(2-methyl-2-alkyl)ferrocenes 46

Structures of New Tetraalkylated Ferrocenes 49

Structures of New Tetraalkylated Ferrocenium Salts 55

Layered Ferrocene Structures 67

Electronic Properties 75

Conclusions 78

References 81

Chapter 3. Synthesis and Characterization of Novel Functionalized Polyalkylated Ferrocenes and Ferrocenium Salts

Introduction 84

Experimental Section 86

Results and Discussion 99

Preparation and Functionalization of Trialkylated Ferrocenes 100

Functionalization of Trialkylated Ferrocenes 100

Functionalization of Tetraalkylated Ferrocenes 120

Hydrosilation Reactions of Vinylferrocene and Olefinic Polyalkylated Ferrocenes 133

Functionalization of Longer Alkyl Chain Polyalkylated Ferrocenes 144

Conclusions 154

References 156

Chapter 4. Selectivity Studies and Sensor Applications of Tetraalkylated Ferrocene Ion-Exchange Materials Confined to Electrically Conducting Substrates

Introduction 160

Experimental Section 163

Results and Discussion 170

Electrochemical Properties of HEP Physisorbed onto Indium-Tin Oxide (ITO) Surfaces 170

HEP/ITO Electrode Materials Prepared by Spin-Coating 174

11-Thioundecanoyl Tetraalkylated Ferrocene Monolayers on Gold 182

Electrochemical Determination of Effective Formation Constants (K_{eff}) of Tetraalkylated Ferrocenium Salts 192

Comparison of Effective Formation Constants (K_{eff}) and Ion-Exchange Selectivity of Tetraalkylated Ferrocenium Cations 198
Amperometric Sensing of Aqueous Anions 207
Conclusions 212
References 213
Chapter 5. Comparison of $HEP^+NO_3^-$ and $DEC^+NO_3^-$ for the Liquid-Liquid Anion Exchange of Aqueous ReO_4^-
Introduction 217
Experimental Section 219
Results and Discussion 222
Preliminary Extraction Studies 223
Aggregation of HEP^+ and DEC^+ Cations in Chlorobenzene 226
Particle Size Analysis of Extraction Media 232
Conclusions 239
References 241
Chapter 6. Scope of the Dissertation and Future Work
Introduction 243
Important Results and Conclusions 243
Increased Ion-Exchange Selectivity and Aqueous Anion Detection 243
Functionalization, Surface Modification, and Electrochemical Sensing 244
Future Work 246
Liquid-Liquid Extractions 246
Synthesis of new Tetraalkylated Ferrocenes 247
Functionalization of Tetraalkylated Ferrocenes 248
Electrochemical Sensors 248

References 250

Appendix A. Structures, Tables, and Experimental Data for All Novel X-ray Crystallographic Structures 251

Appendix B. Final Concentrations of $HClO_4$ Used in Electrochemical Determinations of K_{eff} 279

Appendix C. Derivation of Equation 4.2 281

Appendix D. Complete Tables of Observed Distribution Ratios for the Liquid-Liquid Extraction of ReO_4^- by $HEP^+NO_3^-$ and $DEC^+NO_3^-$ in Chlorobenzene 284

List of Tables

Table		Page
1.1	Structures, names, and abbreviations for the ligands, polyalkylated ferrocenes and functionalized polyalkylated ferrocenes presented in this dissertation	27
2.1	Summary of crystallographic data	44
2.2	Selected bond distances for HEP	51
2.3	Selected bond distances for DEC	53
2.4	Structural parameters for tetraalkylated ferrocenes and ferrocenium cations	54
2.5	Selected bond distances and angles for $BUT^{+}ReO_4^{-}$·acetone	57
2.6	Selected bond distances and angles for $HEP^{+}NO_3^{-}$	59
2.7	Selected bond distances and angles for $DEC^{+}NO_3^{-}$	60
2.8	Selected bond distances and angles for $BUT2^{+}ReO_4^{-}$	62
2.9	Electronic properties of polyalkylated ferrocenes and ferrocenium cations	76
3.1	Comparison of reaction data for functionalized tri-BUT and BUT	121
3.2	Summary of hydrosilation reactions with vinylferrocene	136
3.3	Mass spectral data for 11-bromoundecanoyl polyalkylated ferrocenes	147
3.4	Summary of mass spectral data for compounds prepared in Scheme 3.10	151
4.1	The HEP/ITO cathodic peak potential shifts obtained from reductive differential pulse voltammograms for various anions	178
4.2	Theoretical and experimental monolayer surface coverages calculated for 11-thiolundecanoyl tetraalkylated ferrocenes	188

4.3	Electrochemically determined effective formation constants (K_{eff}) for surface-confined $Fc'^{+}ClO_4^-$ ion pairs	197
4.4	K_d* values for the extraction of ReO_4^- with tetraalkylated ferrocenium nitrate ion-exchange materials	200
4.5	Potential shifts observed for partial tetraalkylated ferrocenyl monolayers in 1 M H_2SO_4 containing 5 mM $HClO_4$	208
5.1	Results from preliminary liquid-liquid extractions of ReO_4^- using $HEP^+NO_3^-$ and $DEC^+NO_3^-$ in dichloromethane	224
5.2	Least squares analysis and aggregation numbers of partial ReO_4^- loading data for $HEP^+NO_3^-$ and $DEC^+NO_3^-$ in chlorobenzene	230
5.3	Particle size analysis of partial ReO_4^- loading in chlorobenzene	238
A.1	Crystal data and structure refinement for HEP	252
A.2	Atomic coordinates and equivalent isotropic displacement parameters for HEP	255
A.3	Bond lengths and angles for HEP	256
A.4	Anisotropic displacement parameters for HEP	258
A.5	Hydrogen coordinates and isotropic displacement parameters for HEP	259
A.6	Crystal data and structure refinement for DEC	261
A.7	Atomic coordinates and equivalent isotropic displacement parameters for DEC	264
A.8	Bond lengths and angles for DEC	265
A.9	Anisotropic displacement parameters for DEC	267
A.10	Hydrogen coordinates and isotropic displacement parameters for DEC	268
A.11	Crystal data and structure refinement for $DEC^+NO_3^-$	270

A.12 Atomic coordinates and equivalent isotropic displacement parameters for $DEC^+NO_3^-$ 273

A.13 Bond lengths and angles for $DEC^+NO_3^-$ 274

A.14 Anisotropic displacement parameters for $DEC^+NO_3^-$ 276

A.15 Hydrogen coordinates and isotropic displacement parameters for $DEC^+NO_3^-$ 277

B.1 Volumes of 1 M $HClO_4$ added to 10 mL of 1 M H_2SO_4 electrolyte and resulting concentrations of $HClO_4$ used for electrochemical determination of K_{eff}. 280

D.1 Observed distribution ratios for the extraction of ReO_4^- by $HEP^+NO_3^-$ 285

D.2 Observed distribution ratios for the extraction of ReO_4^- by $DEC^+NO_3^-$ 286

List of Figures

Figure		Page
1.1	General representation of the complete Redox-Recyclable Extraction and Recovery process (R^2ER)	8
1.2	R^2ER cycle for the extraction and recovery of the surfactant anion PFOS ($C_8F_{17}SO_3^-$) using the $HEP^+NO_3^-$/XAD-7 material	13
1.3	Time dependent ATR-FTIR spectra of a thin film of water insoluble $DEC^+NO_3^-$ on a silicon ATR-FTIR sensing crystal immersed in a 5 μM(*aq*) solution of $LiClO_4$	15
1.4	Model representing the liquid-liquid ion exchange of ReO_4^- for NO_3^-	17
1.5	Plot of the relationship between anion-exchange rate versus the anion-exchange selectivity for four commercial anion-exchange resins	22
2.1	Structures of the neutral HEP molecule from the HEP structure and one of the unique HEP^+ cations from the $HEP^+NO_3^-$ structure	50
2.2	Structures of neutral DEC from the DEC structure and the DEC^+ cation from the $DEC^+NO_3^-$ structure	52
2.3	Structure of the BUT^+ cation from the $BUT^+ReO_4^-$·acetone structure	56
2.4	Structure of the $BUT2^+$ cation from the $BUT2^+ReO_4^-$ structure	61
2.5	Distribution of Fe–C distances for the tetraalkylated ferrocenes and ferrocenium salts	64
2.6	The geometric orientation of the iron atom relative to the perpendicular to the Cp' plane that passes through the centroid of the plane	65

2.7	Graphs showing the correlation between Fe–Ct–C angle and Fe–C bond distance for BUT^+, HEP^+, and DEC^+	66
2.8	Solid state packing diagram of DEC showing the layered structure and 3-demensional channels formed by the alkyl chain interdigitation within a single layer	68
2.9	Packing diagrams showing hexagonal packing of the iron(II) atoms between three layers of DEC and the "face on" view of the hexagon formed between the iron(II) atoms in the *ab* plane	70
2.10	Solid state packing diagram of $DEC^+NO_3^-$	71
2.11	Diagrams of the packing arrangement of iron(III) atoms in $DEC^+NO_3^-$ and the "face on" view of the pseudo-rectangle formed between the iron(III) atoms in the *ab* plane	73
2.12	Diagram depicting the different orientations of the *t*-decyl methyl groups in the interlayer spacing for DEC and $DEC^+NO_3^-$	74
2.13	Linear relationship between the reduction potential and wavelength of maximum absorption ($\lambda_{max}(+)$) for the polyalkylated ferrocenium nitrate salts	79
3.1	LSIMS mass spectrum of the reaction mixture of 1,1',3,3'-mono–, di–, tri– , and tetra(3-ethyl-3-pentyl)ferrocene	102
3.2	^{1}H-NMR spectrum of tri-HEP2	103
3.3	^{1}H-NMR spectrum of tri-BUT-Ac	106
3.4	LSIMS mass spectra of crude and purified tri-HEP2-Ac and tri-BUT-Ac	107
3.5	LSIMS mass spectra of tri-HEP2-Ac and tri-BUT-OH	109
3.6	^{1}H-NMR spectrum of tri-BUT-OH	110
3.7	LSIMS mass spectrum of tri-BUT-Vn	112

3.8	^{1}H-NMR spectrum of tri-BUT-Vn	113
3.9	LSIMS mass spectrum of tri-BUT-Pr	115
3.10	^{1}H-NMR spectrum of tri-BUT-Pr	116
3.11	FTIR spectra of tri-BUT, PVBC, and PVB-triBUT	119
3.12	LSIMS mass spectrum of BUT-Pr	124
3.13	^{1}H-NMR spectrum of BUT-Pr	125
3.14	LSIMS mass spectrum of BUT-PtOH	129
3.15	^{1}H-NMR of BUT-PtOH	130
3.16	LSIMS mass spectrum of BUT-diPt	131
3.17	^{1}H-NMR of BUT-diPt	132
3.18	^{1}H-NMR spectrum and the LSIMS mass spectrum of Fc-DMES	138
3.19	^{1}H-NMR spectrum and the LSIMS mass spectrum of Fc-TES	139
3.20	Cyclic voltammogram of Fc-TES covalently attached to an ITO coated glass electrode	141
3.21	LSIMS mass spectrum of the product mixture obtained from the hydrosilation of BUT-diPt with triethoxysilane	143
3.22	LSIMS mass spectra of the hydrosilation reaction of BUT-diPt with trimethoxysilane at time intervals of 2 hours, 16 hours, and 24 hours	145
3.23	^{1}H-NMR spectrum of DEC-Br	148
4.1	Cyclic voltammograms of $HEP^+NO_3^-$ physisorbed onto an ITO electrode	172
4.2	Reductive differential pulse voltammograms for three different ITO electrodes spin coated with HEP	175
4.3	Differential pulse voltammograms of HEP/ITO in a KCl(*aq*) electrolyte with NO_3^-, ReO_4^-, and $CB_{11}H_{12}^-$ anion	177

4.4	Magnified pictures of ITO electrodes spin coated with HEP before and after 100 electrochemical cycles	181
4.5	A magnified picture of a two-week-old HEP/ITO electrode before electrochemical cycling	183
4.6	Cyclic voltammograms of HEP-SH SAMs on a gold electrode	185
4.7	Cyclic voltammograms of gold disk electrodes modified with BUT-SH, PENT-SH, HEX-SH, HEP-SH, and DEC-SH	191
4.8	Plots of E_{pk} vs. log[ClO_4^-] for partial monolayers of the 11-thiolundecanoyl tetraalkylated ferrocenes on gold disk electrodes	196
4.9	Plot of $K_d^*(ReO_4^-)$ for the extraction of ReO_4^- from 1.0 M $NaNO_3$ vs. the increasing size of the tetraalkylated ferrocenium cations	202
4.10	Plot of $K_{eff}(ClO_4^-)$ vs. the increasing size of the tetraalkylated ferrocenium cations	203
4.11	Plot of $K_{eff}(ClO_4^-)$ vs. $K_d^*(ReO_4^-)$ for tetraalkylated ferrocenium cations	206
4.12	Plots of current vs. time for the chronamperometric sensing of ClO_4^- and $CB_{11}H_{12}^-$ using a partial monolayer of HEP-SH	211
5.1	Plots of $D(ReO_4^-)/[Fc'^+NO_3^-]_{tot}$ vs. $[ReO_4^-]_{org}/[Fc'^+NO_3^-]_{tot}$ for 1 mM, 10 mM, and 0.1 M $HEP^+NO_3^-$ and $DEC^+NO_3^-$ in chlorobenzene at 25 °C	229
5.2	Particle size distribution of 10 mM dichloromethane solutions of $DEC^+NO_3^-$ and $HEP^+NO_3^-$ measured by dynamic light scattering	233
5.3	Particle size distribution of 1 mM and 10 mM chlorobenzene solutions of $DEC^+NO_3^-$ and $HEP^+NO_3^-$	235
A.1	Diagram showing the asymmetric unit of the HEP structure	253

A.2 Diagram showing the HEP structure 254

A.3 Diagram showing the asymmetric unit of the DEC structure 262

A.4 Diagram showing the DEC structure 263

A.5 Diagram showing the asymmetric unit of the $DEC^{+}NO_3^{-}$ structure 271

A.6 Diagram showing the $DEC^{+}NO_3^{-}$ structure 272

Chapter 1

An Overview: Redox-Recyclable Extraction and Recovery (R^2ER) and its Application to Remediation and Detection of Aqueous Ions

Introduction

The separation and recovery of inorganic ions (i.e., nuclear fission products, precious metals), organic ions (i.e., antibiotics), and ionic pollutants (i.e., ClO_4^-, CN^-, $C_nF_{2n+1}SO_3^-$) from aqueous media is an important area of research that addresses both environmental and industrial concerns. Traditionally, anion separation has been carried out using commercially available anion-exchange resins such as Dowex, Reillex-HPQ, Amberlite, Purolite, and Sybron Ionac, which contain quaternary ammonium or pyridinium sites with exchangeable anions. More recently, efforts have been made to make extractants with varying sized exchange sites that combine both high selectivity and fast ion-exchange kinetics.[1-3] The majority of research has been focused on improving the selectivity, capacity, and kinetics of the ion-exchange materials for the specific ions of interest. When ion-exchange chromatography has been used for the remediation of toxic and/or radioactive aqueous waste streams, however, minimization of the volume of secondary waste (i.e., the strip solution) destined for permanent disposal has been a significant challenge. Waste minimization becomes even more problematic as the concentration of the target ion in primary hazardous waste streams becomes dilute. Generally, as the concentration of the target ion in the primary waste stream decreases, the volume of the secondary waste stream generated increases.[4] Furthermore, tougher environmental regulations and high initial cost of new, more effective, and more selective extractants have made the recyclability of the extractant an increasingly important issue.[5]

Ionic Pollutants. The need to clean contaminated areas and properly dispose of nuclear waste has been a problem that many communities continue to face across the country.[6,7] The bulk of the nuclear waste accumulated during the cold war era was in the form of aqueous acidic process waste, containing fission products, uranium, transuranic elements, and some heavy metals. The waste was made alkaline and stored in large underground tanks.[8,9] Recently, reports of leaking tanks and potentially explosive gas generation in some tanks have raised environmental as well as safety concerns at such storage sites as the Hanford Reservation site in Hanford, Washington.[6,10-13] Radioactive technetium (^{99}Tc) along with several other radioactive byproducts, including $^{137}Cs^{+}$ and $^{90}Sr^{2+}$, are produced in ~ 6% yield or higher from the thermal neutron fission of ^{235}U.[14] The cations $^{137}Cs^{+}$ and $^{90}Sr^{2+}$ are high-activity γ- and/or β-emitters with half-lives of ca. 30 years and still account for 97% of the penetrating radiation and 98% of the thermal energy in high-level waste 30 years after fuel irradiation.[15] The radioactive ^{99}Tc is a weak β^{-} emitter and does not contribute significantly to the heat and radiation load. Its relatively long half-life of 213,000 years, however, makes it a radioactive pollutant of concern. Furthermore, once ^{99}Tc is in the form of the pertechnetate ion ($^{99}TcO_4^{-}$), it becomes a water soluble species that is mobile in the environment.[16-18] Greater than 1,800 kg of ^{99}Tc are believed to be present in the Hanford tank waste, and new estimates of $[^{99}TcO_4^{-}]/[^{99}Tc]$ range from 40% to 80%.[19,20]

The current site for long-term storage of nuclear waste is the Yucca Mountain repository in Nevada. The site has a maximum capacity of 70,000 metric tons. The Hanford nuclear site alone contains an estimated 770,000 metric tons of process waste and contaminated soil.[6] Without an efficient cost effective means to minimize hazardous waste, current repositories would only hold a fraction of the total nuclear waste in this country. Ion exchange processes are planned to remove $^{137}Cs^{+}$ and $^{90}Sr^{2+}$ from liquid fractions of contaminated waste. This will essentially separate the waste into high-level waste (HLW) and low-level waste (LLW). In the past, zeolites, as well as other ion-

exchange materials, have been used to separate both cesium and strontium from solutions containing high levels of sodium, but they tend to have low distribution coefficients, and it has proven difficult to recover the radioactive ions from the ion-exchange matrix.[21]

Contamination of groundwater with ionic pollutants is also of recent concern. Anionic pollutants such as cyanide (CN^-) and perchlorate (ClO_4^-) are known to be common pollutants of groundwater in certain areas.[22-27] Perchlorate is present in groundwater in the Western states, most notably Utah, California, and Nevada. The most common source of perchlorate in the environment appears to be from NH_4ClO_4, a common additive in rocket fuel.[27] Perchlorate is believed to have been introduced into the environment at rocket fuel manufacturing or testing sites. Cyanide is commonly found in water near mines due to its use for extracting silver or gold from mine tailings. Due to leaching from these mine tailing ponds, cyanide has been implicated in a substantial wildlife mortality rate in the western United States during the 1980's.[22,28] The current US Environmental Protection Agency (USEPA) drinking-water standards and drinking-water reference doses for cyanide and perchlorate are 200 μg/L and 4–18 μg/L, respectively.[27,29,30]

In addition to remediation problems, there is an ongoing need to detect and quantify anionic pollutants such as CN^- and ClO_4^-. Currently, the most common method used to detect aqueous ClO_4^- is ion chromatography (IC), but the method relies on retention times as a means of detection and is prone to error if the matrix is unknown.[31] Ion chromatography techniques can also be used to detect CN^- but due to the weak acidity of hydrogen cyanide ($pK_a = 9.22$), the detection limit is much higher than that for ClO_4^-.[32] Other methods of cyanide analysis include potentiometry,[33] spectrofluorometry,[34] and spectrophotometry.[35] Detection of CN^- and ClO_4^- by the above methods is typically problematic due to the lack of a selective means of identifying the two anions.

Another anion that has recently been shown to be persistent in the environment

is the surfactant anion perfluorooctylsulfonate, $C_8F_{17}SO_3^-$ (PFOS).[7,36-40] The surfactant anion PFOS was formerly used in Scotchgard®-brand fabric treatments and aqueous film-forming foams (AFFF's), which are commonly used to fight liquid fuel fires, manufactured by the 3M company.[7,36,37,39,40] As an additive in AFFF, PFOS is used on Navy aircraft carriers to fight fires and subsequently is washed into the ship's bilge water tanks. Treatment of this bilge water at publicly owned treatment works upon returning to port, however, causes excessive foaming and shutdowns of the treatment plants. Due to the robust nature of the C–F bonds, the surfactant cannot be destroyed by conventional methods, so it needs to be removed from the water before treatment. PFOS has also been found in groundwater at abandoned military bases and fire-fighting training centers.[41] Furthermore, AFFF is also commonly used in urban areas for fighting fires. The production of PFOS has recently been halted due to large levels of the anionic surfactant found in tissue samples of workers at 3M production plants.[39,40]

Current Extraction and Recovery Techniques. To date, both liquid-liquid and chromatographic techniques have been employed to extract $^{99}TcO_4^-$ from ground water and process nuclear waste. New anion-exchange resins have been developed for the efficient removal of $^{99}TcO_4^-$ from aqueous solutions.[42-46] Schroeder and co-workers at the Los Alamos National Laboratory have demonstrated that Reillex™–HPQ (a strong base anion-exchange resin containing both methylpyridinium and pyridinium sites) can selectively remove $^{99}TcO_4^-$ from acidic, neutral, and alkaline waste simulants containing a complicated matrix of interfering ions.[44,45] The traditional method of recovery involves passing large volumes of an aqueous solution containing a high concentration of a displacing ion (8 M HNO_3) through the column. An alternative stripping solution used by Schroeder and co-workers contained 1.0 M NaOH, 1.0 M ethylenediamine, and 5 mM Sn^{2+}. When this solution was passed through the column, Tc was reduced to a lower valent species that was subsequently complexed by ethylenediamine and eluted from the column. Although the extractant can be reused, this was a fairly lengthy process, taking

up to 11 hours to regenerate the extractant material.

Another approach for removing $^{99}TcO_4^-$ from aqueous solutions has been developed by Rogers *et. al* at the University of Alabama and his collaborators at Argonne National Laboratory.[47-49] Their system involves high-molecular-weight polyethylene glycol (PEG) covalently bonded to a polystyrene support. The resin material behaves as an aqueous biphasic system when the mobile phase contains a high concentration of water structuring ions (e.g., SO_4^{2-}, CO_3^{2-}, OH^-). Weakly hydrated ions, present in the mobile phase, preferentially partition into the PEG phase. Selective partitioning of $^{99}TcO_4^-$ from Hanford waste simulants has been demonstrated using ABEC™-5000.[49] Stripping was accomplished by simply washing the resin with water. When the mobile phase was changed from high ionic strength to low ionic strength, an aqueous biphasic environment was no longer supported, and the weakly hydrated ions partitioned out of the PEG phase. A major limitation of this innovative approach was that a high-salt mobile phase was required for extraction. Though this extraction system might work well for high ionic strength matrices such as Hanford tank waste, this type of process would not be applicable to removal of $^{99}TcO_4^-$ or other ionic contaminants from low-ionic-strength matrices such as groundwater.

Liquid-liquid solvent extraction systems have been successfully used for the removal of >99% of the $^{99}TcO_4^-$ from simulated nuclear waste in a single contact. For example, Strauss and co-workers used organic solutions containing the commercially available anion-exchange reagent Aliquot™–336 nitrate ($[NMe(C_8H_{17})_3][NO_3]$) to establish benchmarks for the extraction of $^{99}TcO_4^-$ from a number of aqueous waste simulants.[50] Greater than 99% of the $^{99}TcO_4^-$ was extracted form the aqueous phase when organic solutions of the quaternary ammonium salt were contacted with various acidic, neutral, and alkaline waste simulants containing high concentrations of NO_3^-. Although the extractant performed quite well, the recovery of $^{99}TcO_4^-$ in a small volume still posed significant problems. As mentioned above, recovery has traditionally involved

using a strip solution containing a high concentration of a displacing ion (i.e., NO_3^-). Many investigators have used 8 M HNO_3 to strip (i.e., back-extract) $^{99}TcO_4^-$ from the organic phase.[51-53] Typically, several aliquots of stripping solution were required to fully displace $^{99}TcO_4^-$ and regenerate the extractant material. This regeneration/stripping method is undesirable for two reasons. The recovered $^{99}TcO_4^-$ is contained in a *large volume* of stripping solution. In addition, the secondary waste remains quite hazardous because of the corrosive and oxidizing nature of 8 M HNO_3. Both the large volume of secondary waste and the corrosive nature of the secondary waste have prevented the implementation of a convenient and efficient extraction cycle based on these traditional anion-exchange strategies.

As a solution to these recovery issues, Moyer *et. al* at Oak Ridge National Laboratory have developed a solvent extraction process in which the extracted $^{99}TcO_4^-$ can be recovered by simply washing the organic phase with water.[54] The extraction mechanism involves the extraction of an alkali metal ion (i.e., Na^+ or K^+) by the crown ether-type extractant bis-4,4'(5')[(*tert*-butyl)cyclohexano]-18-crown-6 (CE). Since an anion was necessary to maintain charge neutrality, $^{99}TcO_4^-$ was also extracted to maintain charge neutrality, as can be seen in the equation below:

$$Na^+(aq) + TcO_4^-(aq) + CE(org) \rightleftharpoons (CE)NaTcO_4(org)$$

When the organic phase containing the crown ether complex was contacted with water, the equilibrium was reversed, which promoted dissociation of the complex to free alkali metal salt in the aqueous phase and free crown ether in the organic phase. A complete extraction-recovery cycle was demonstrated based on this principle, and a patent covering the process has been issued.[55] An inverse relationship between the degree of extraction and the stripping efficiency was identified; therefore, multiple contacts of the aqueous and organic phases were required for complete extraction and recovery to be achieved.

A method for the removal of cationic pollutants in a minimal volume of secondary waste using a recyclable extractant has also been demonstrated. The method, called electrically switched ion exchange (ESIX), has been tested at Pacific Northwest National Laboratory by Lilga *et. al.*[56-59] The ESIX system operates by *electrochemically* reducing and oxidizing nickel hexacyanoferrate or hexacyanouranate films for activation and deactivation, respectively, prior to extraction and recovery. Extraction and recovery with *minimal secondary waste volumes* has been demonstrated for K^+ and Cs^+ cations in aqueous media containing high concentrations of Na^+ cations. The extractant films can then be regenerated electrochemically without the further use of chemicals. A similar system using Cobalt hexacyanoferrate modified electrodes has also been demonstrated for the extraction of Cs^+ cations form high ionic strength aqueous solutions.[60] Currently, ESIX systems for anion extraction, specifically $^{99}TcO_4^-$, using poly(vinylferrocene) films are also being exploring.[61] These processes are limited by the size of the electrodes containing the extractant films, but have been demonstrated to be viable ion-exchange systems on a small scale. The use of redox processes clearly represents a novel way of addressing ion-exchange processes and other issues associated with aqueous waste remediation.

A New Approach Towards Extraction and Recovery of Pollutant Ions. To address the need for new extractants, organometallic complexes have been developed that are address the need for new extractants, organometallic complexes have been developed that are (i) highly selective, (ii) have high capacities, (iii) undergo rapid ion-exchange, and (iv) are recyclable. These extractants are incorporated into a Redox-Recyclable Extraction and Recovery (R^2ER) scheme in which the target ion is selectively removed from the bulk waste and recovered in a minimal volume. A general R^2ER scheme is depicted in Figure 1.1.[62,63] The R^2ER process begins with the redox-active organometallic compound, confined to a water- immiscible organic phase or immobilized onto an inert solid support. In its neutral state, this compound is denoted EXTR. When

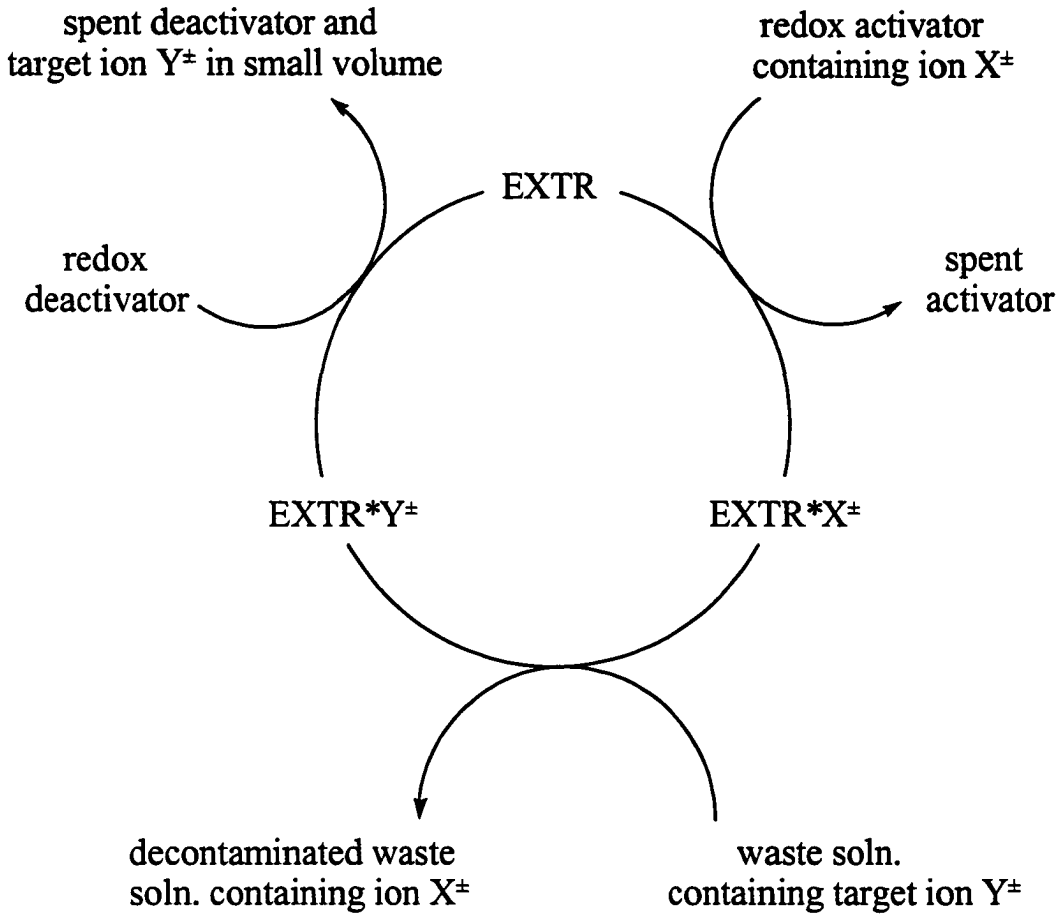

Figure 1.1. A general representation of the complete Redox-Recyclable Extraction and Recovery process (R^2ER). The species, EXTR, is a neutral, redox-active, transition-metal complex. The species, EXTR*, is the oxidized, cationic transition metal species (for extraction of anions) or the reduced, anionic transition-metal species (for the extraction of cations). The species, EXTR, EXTR*$X^{\pm}$, and EXTR*$Y^{\pm}$, are confined to a water-immiscible organic phase or a stationary phase for solvent extraction or ion-exchange chromatography, respectively.

the extractant becomes activated by oxidation to its cationic form (for the extraction of anions) or reduction to its anionic form (for the extraction of cations) in the presence of an abundant exchangeable ion, $X^{\pm}$, the species, EXTR, is converted to the organometallic salt, $EXTR^*X^{\pm}$, which exchanges its ion, $X^{\pm}$, for the target ion, $Y^{\pm}$, in the subsequent extraction step. In this case, EXTR* represents the cationic or anionic extractant. After extraction, a final redox deactivation step regenerates the neutral form of the extractant and releases the target ion into a minimal volume of secondary waste.

The R^2ER strategy offers a novel stripping/regeneration method based on an extractant redox-process rather than a displacement principle. Typically, ion-exchange materials are stripped of their target ions with large volumes of highly concentrated acid solutions during regeneration. The ease with which the new redox-active extractant can be switched "on" and "off" allows for a strategy in which pollutant ions are selectively removed from complex matrixes, efficiently recovered, and the extractant reused multiple times without loss of selectivity or capacity. Since the extractant is simply switched "off," the target ion may be quantitatively concentrated into a small volume without the use of a high concentration of a displacing ion (e.g., 8 M HNO_3) or complexing reagent.

Certain criteria are required for the successful application of an organometallic extractant to the R^2ER process. First, the organometallic complex must undergo facile one-electron oxidation and reduction electrochemically or with mild chemical oxidizing or reducing agents. Secondly, the complex must remain stable with respect to ligand substitution, hydrolysis, and irreversible over-oxidation or over-reduction. Third, loss of the extractant to the aqueous phase must also be prevented, thus the extractant must be extremely hydrophobic/lipophilic. Furthermore, when immobilization of the extractant onto a solid support is desired, the structure of the extractant must also provide for favorable interfacial forces or covalent bonding to the surface. Finally, the extractant must exhibit high selectivity for a target ion, which can be achieved by adding specific functionality or increasing the size of the organometallic complex, as will be discussed

below.

Recently, redox-active transition metal-containing extractants for the separation and recovery of $^{137}Cs^{+}$ and $^{90}Sr^{2+}$ have been developed by Strauss, Chamberlin, and co-workers at Los Alamos National Laboratory.[15] The anionic complexes, Na[Fe(η^5-C_5H_5)(η^5-(3)-1,2-$C_2B_9H_9$(n-$C_{12}H_{25}$)$_2$)] (I) and Na[Fe(η^5-C_5H_5)(η^5-(3)-1,2-$C_2B_9H_9$(n-$C_{12}H_{25}$)$_2$-9,12-Br_2)] (II) were synthesized and were found to be highly selective towards $^{137}Cs^{+}$ and $^{90}Sr^{2+}$. The active forms of the redox-active extractants I and II are shown below. Most importantly, the radioactive cations were recovered in a minimal volume of

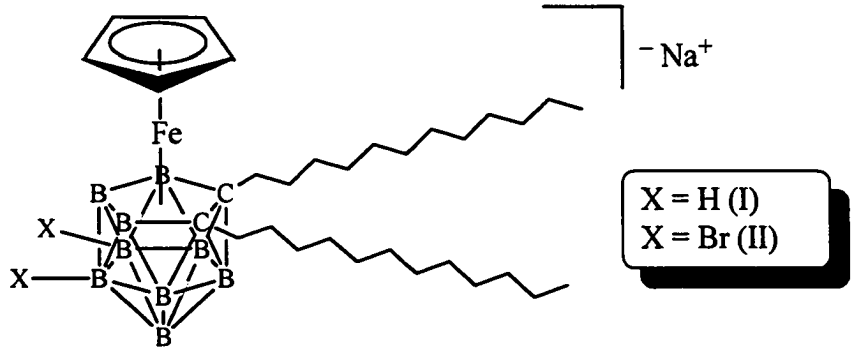

secondary waste, and the extractants were recyclable.

The R^2ER strategy has also been applied towards the difficult separation of anions from aqueous waste streams.[62-65] To address some of the concerns presented by difficult separations, Strauss and co-workers have applied the new R^2ER strategy towards the extraction and recovery of $^{99}TcO_4^{-}$. In one study $^{99}TcO_4^{-}$ was extracted from an aqueous waste simulant containing 1 M NaOH, 1.5 M $NaNO_3$, and 10^{-5} M $^{99}TcO_4^{-}$ using the hydrophobic organometallic complex 1,1',3,3'-tetra(2-methyl-2-hexyl)ferrocenium nitrate ($HEP^{+}NO_3^{-}$) dissolved in a variety of organic solvents.[62] The active form of the redox-active, tetraalkylated ferrocenium extractant is shown below. This organometallic complex in its active, oxidized form, ion paired with an exchangeable anion (NO_3^{-}), was able to selectively extract anions with lower hydration energies than nitrate from aqueous media. In its reduced form (HEP), no extraction was

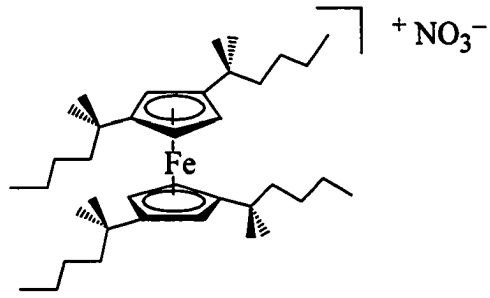

observed. Interestingly, a color change accompanies the activation (green) and deactivation (orange) of the extractant HEP, which gives a useful visual indication of the activation and deactivation processes. In its active form, the extractant was found to be highly selective towards the removal of $^{99}TcO_4^-$ from the waste simulant, and upon deactivation of the extractant material with powdered iron, the secondary waste produced contained a mixture of solids containing >99% of the radioactivity originally in the primary waste and a total volume less than 1% of the primary waste volume. This new type of redox-recyclable extraction and recovery process (R^2ER) was found to accomplish three important things simultaneously: (i) high selectivity with large capacity for the target ion (TcO_4^-), (ii) efficient reuse of the extractant, and (iii) recovery of the target ion in a minimal volume. The primary advantage of this type of extraction/recovery process is not the selectivity of HEP^+ for pertechnetate but the *minimization* of the volume of the secondary waste containing the target ion.

More recently, redox-recyclable materials have been developed by adsorbing highly selective redox-recyclable extractant salts, HEP^+X^-, onto high surface area silica gels.[63] These materials were then evaluated for their selectivity towards $^{99}TcO_4^-$ and ReO_4^-, and their effectiveness over multiple R^2ER cycles. (ReO_4^- has been shown to be a non-radioactive surrogate for $^{99}TcO_4^-$, and as such, can be used for the evaluation of extractants in laboratories not equipped to handle radioactive waste or radioactive simulants.[64]) The results of these investigations indicated that: (i) salts of HEP^+ can be adsorbed onto silica gels using organic solvents and will not appreciably desorb into the

aqueous phase when the dried materials are treated with 1 M HNO_3, (ii) NO_3^- co-adsorbed with HEP^+ will selectively exchange with both $^{99}TcO_4^-$ and ReO_4^- in aqueous solutions, and (iii) adsorbed HEP^+ can be rapidly activated and deactivated using water-soluble redox reagents.[62-65] These materials have the added advantage that no organic solvents are used once the organometallic complex has been loaded onto the support, unlike the case with the solvent extraction systems.

Similar to the silica supported $HEP^+NO_3^-$ ion-exchange material, $HEP^+NO_3^-$ has also been supported on high surface area polymer substrates and used in ion-exchange chromatographic extraction experiments.[65] The polymer support that seemed to give the best extraction results was XAD-7, a commercially available poly(acrylic ester). This material, $HEP^+NO_3^-$/XAD-7, was also prepared by physisorption of $HEP^+NO_3^-$ onto the solid support's surface. As with the silica materials, the $HEP^+NO_3^-$ was not observed to desorb from the surface upon prolonged exposure to aqueous media.[65] In addition to the extraction of ReO_4^- and $^{99}TcO_4^-$, the newly prepared material was also used for the extraction of the PFOS anion from aqueous solutions.[65,66] Extraction of PFOS was performed from solutions containing pure PFOS as well as solutions of AFFF. Ion-exchange chromatography experiments utilizing a proprietary recovery technique resulted in 88 to 100% extraction and recovery of the PFOS anions from these solutions. Furthermore, due to the low solubility of PFOS in water, the PFOS anion was recovered as the solid, potassium salt. The ion chromatographic extraction and recovery of PFOS using $HEP^+NO_3^-$/XAD-7 is shown in Figure 1.2. The recovery of PFOS in a pure, crystalline form represents the largest obtainable reduction in secondary waste volume possible since the recovered pollutant is not in a stripping solution.

The Low-Level Detection of Pollutant Anions Using the R^2ER Extractants. As stated above, in addition to extraction and remediation applications, there is an ongoing need to detect and quantify anionic pollutants in aqueous media. In addition to the remediation of aqueous media, the R^2ER process has also been used in the attenuated

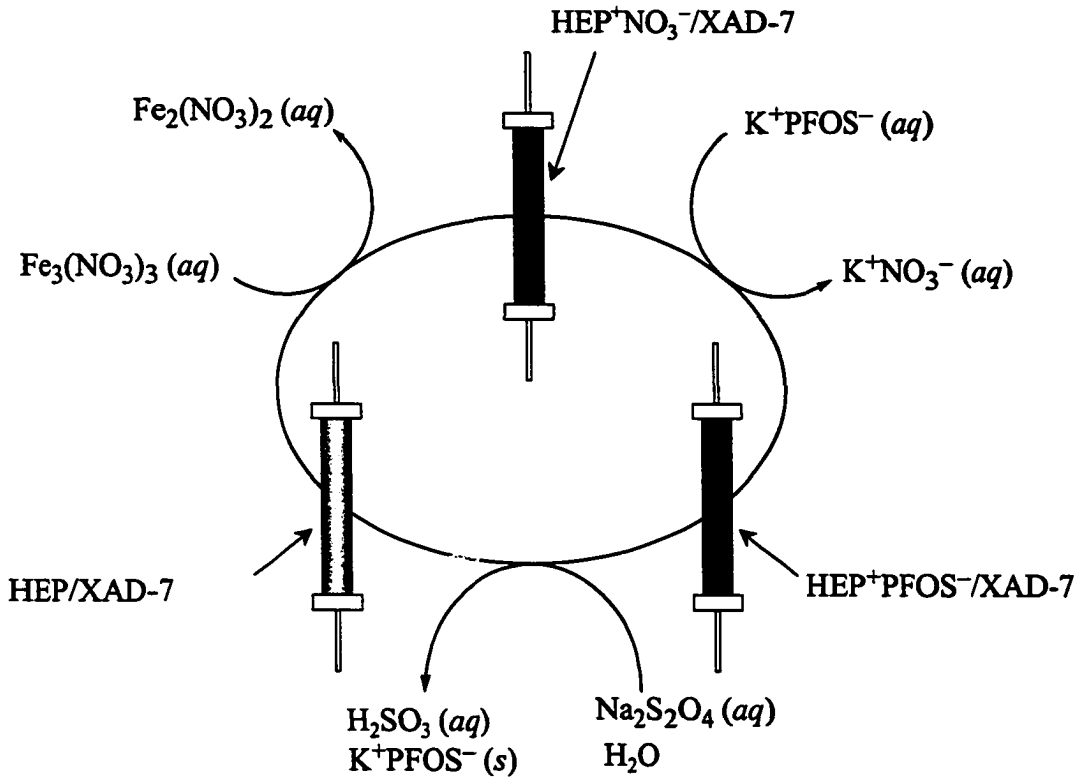

Figure 1.2. The R^2ER cycle for the extraction and recovery of the surfactant anion PFOS ($C_8F_{17}SO_3^-$) using the $HEP^+NO_3^-$/XAD-7 material in a chromatographic ion-exchange process. The PFOS contaminated aqueous media is pumped through the columns from bottom to top at a rate of 3.5 mL min-1. Typical column dimensions are 3.5 cm (inner diameter) × 28 cm in length. Aqueous dithionite anion ($Na_2S_2O_4$) was used as the deactivation/recovery reagent (reduction) and aqueous ferric nitrate (Fe_3NO_3) was used as the reactivation reagent (oxidation). The color changes accompanying the deactivation (orange) and activation (green) cycles are also shown. This figure is reprinted with permission from reference 65.

total reflectance (ATR) Fourier transform infrared detection and identification of several IR active anionic pollutant molecules.[67] This technique is useful due to the low-level detection and subsequent *identification* of the analyte from its unique IR spectrum. Such a technique greatly diminishes (if not eliminates) the occurrence of false positive or negative detection due to the corresponding identification.

Detection of anions in aqueous media was accomplished by depositing a thin film of the organometallic extractant, 1,1',3,3'-tetra(2-methyl-2-nonyl)ferrocenium nitrate ($DEC^+NO_3^-$) onto the surface of the ATR-FTIR sensing element. (DEC is a tetraalkylated ferrocene similar to HEP, but its carbon chains contain ten carbon atoms instead of seven. The higher lipophilicity of this extractant causes better adhesion to the silicon ATR-FTIR sensing crystal.) The thin film then undergoes ion exchange with anions in the aqueous media, resulting in the concentration of the target anion in the thin film close to the ATR-FTIR sensing crystal. Due to the increasing amounts of target anion in the thin film, an IR signal from that anion is seen to increase as ion exchange occurs. As a result, anions can be detected in water at concentrations previously unobtainable due to the large IR-absorption bands observed for water.

A variety of anions have been detected by this method. Parts per billion (ppb) levels of both ClO_4^- and PFOS have been detected by this method using a $DEC^+NO_3^-$ thin film.[65,67] The detection limit (defined as three times signal to noise) for ClO_4^- using this method is currently 3 ppb (30 nM) in 30 minutes and the detection limit for PFOS is 25 ppb (50 nM) in 30 minutes. The time dependant ion-exchange process for the detection of 5 μM ClO_4^- is shown in Figure 1.3. The T_2-symmetry $\nu(ClO_4^-)$ of the tetrahedral anion can be seen to grow in at 1096 cm^{-1} over time as the anion becomes more concentrated in the thin film according to the following ion-exchange equilibrium:

$$DEC^+NO_3^-(probe) + ClO_4^-(aq) \rightleftharpoons DEC^+ClO_4^-(probe) + NO_3^-(aq)$$

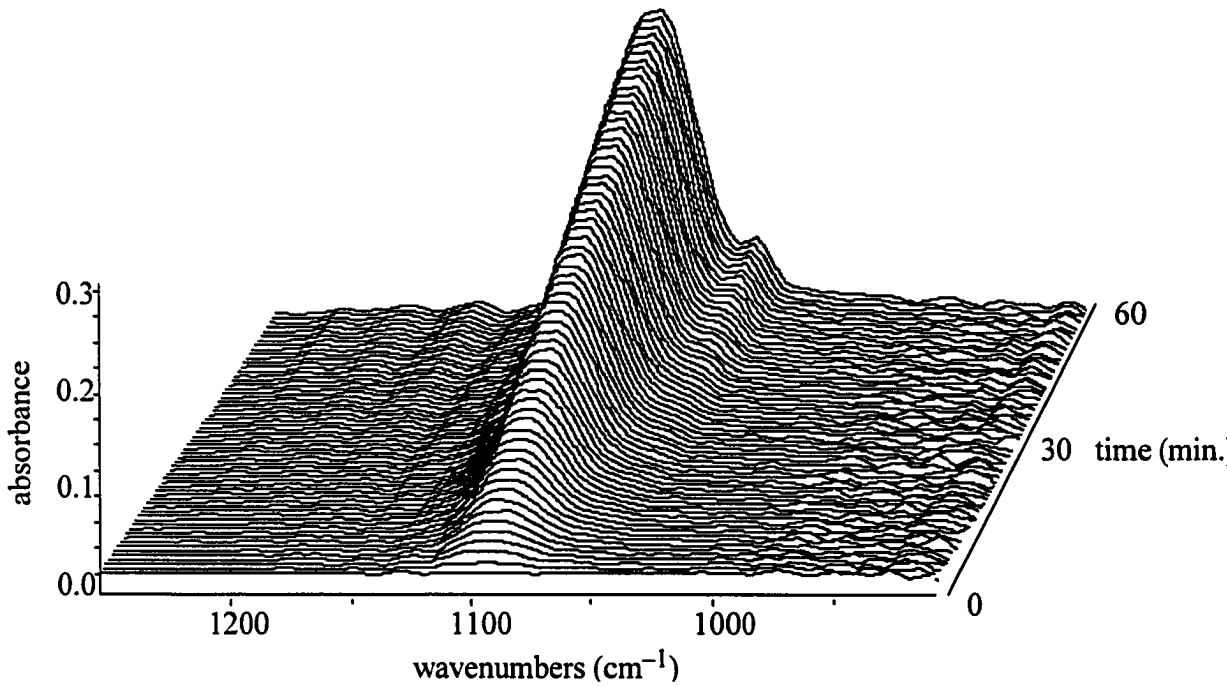

Figure 1.3. The time dependent ATR-FTIR spectra of a thin film of water insoluble $DEC^+NO_3^-$ on a silicon ATR-FTIR sensing crystal immersed in a 5 μM(*aq*) solution of $LiClO_4$ (DEC^+ = 1,1',3,3'-tetra(2-methyl-2-nonyl)ferrocenium cation). The band that grows in at 1096 cm^{-1} over time is assigned to a Cl–O band from the water insoluble compound $DEC^+ClO_4^-$, which is formed throughout the film by an ion-exchange reaction. This detection experiment was performed by Gretchen Hebert.

The detection of CN^- by this method has also been performed; detection, however, could not be accomplished using an R^2ER extractant. Instead, the compound 1,3-bis(diphenylphosphino)propanedichloronickel(II) ($NiCl_2$(dppp)) was used as the organometallic thin film and a CN^- anion displaced a Cl^- anion in the Ni(II) coordination sphere. The detection limit achieved for CN^- using this technique was 2.6 ppb (100 nM) in 45 minutes.

In addition to detection, this technique has also been shown to be quantitative.[68] Due to diffusional effects in the thin film, however, the concentration of the target anion in solution is not directly proportional to the absorbance. Instead, a calibration curve of the change in absorbance over time (dA/dt) versus concentration has been used. These calibration curves are constructed by measuring the change in absorption over time at a variety of concentrations of target anion. By measuring the slope of the line of a plot of absorbance vs. time, the quantity dA/dt can be obtained. Once constructed, the calibration curve of dA/dt vs. concentration has been shown to be accurate at low level concentrations for a variety of anions, including ClO_4^-, PFOS, and CN^-.

Selectivity of R^2ER Extractants. Though recyclability and minimization of secondary waste have been emphasized to this point, an important property of any extractant material is its selectivity towards the target ion in complex matrices. Although one of the primary advantages of redox-recyclable materials is the ability to easily reuse the material, the selectivity of the material is related to the volume of secondary waste upon deactivation of the material. The more selective the extractant material, the greater the fractional composition of the target ion in the secondary waste. In a recent paper by Moyer and Bonnesen, the physical factors that describe the basis for anion separations (selectivity) were outlined.[69] The two predominant factors controlling selectivity in anion separation are the solvation environment and the concept of size bias. A simple model generalizing the exchange of anions in a liquid-liquid anion-exchange process is shown in Figure 1.4. The extractant (R^+) is ion paired with NO_3^- and is dissolved in the

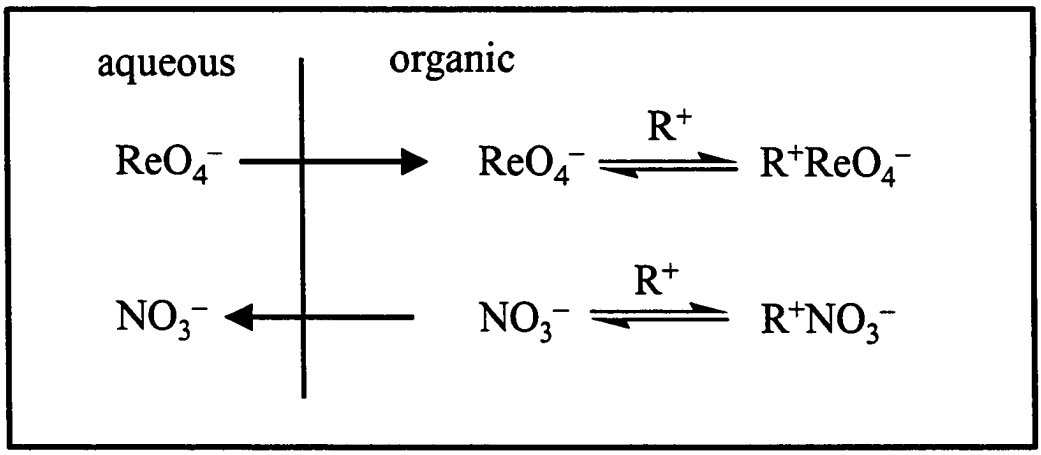

Figure 1.4. Model representing the liquid-liquid ion exchange of ReO_4^- for NO_3^-. R^+ represents a lipophilic cation soluble in organic solvents.

organic solvent. Upon contact with an aqueous solution containing an extractible anion such as ReO_4^-, NO_3^- partitions into the aqueous phase while simultaneously, ReO_4^- partitions into the organic phase. This exchange maintains electroneutrality of the system, but electroneutrality does not initiate this exchange. The net driving force for this transfer is the difference in the standard Gibbs energy of transfer ($\Delta\Delta G°_{tr}$) for the two ions. This process refers to the removal of an ion from water into the gas phase as the bare ion and resolvating it in a dry solvent. As shown in Equation 1.1, the $\Delta\Delta G°_{tr}$, therefore, reflects the differences in solvation energy ($\Delta\Delta G°_{solv}$) and hydration energy ($\Delta\Delta G°_{hyd}$) and the differences in the two ion pairing energies ($\Delta\Delta G°_{ion\text{-}pair}$) for the ion pairs formed with the extractant cation.

(1.1) $$\Delta\Delta G°_{tr} \approx \Delta\Delta G°_{hyd} + \Delta\Delta G°_{solv} + \Delta\Delta G°_{ion\text{-}pair}$$

Again considering the liquid-liquid extraction model depicted in Figure 1.4 where the target ion is $ReO_4^-(aq)$ and $R^+(org)$ will be used as the extractant cation, NO_3^- is ion paired with R^+ and dissolved in an organic solvent. Upon contact with an aqueous solution containing ReO_4^-, NO_3^- replaces ReO_4^- in the aqueous solution as indicated below:

$$ReO_4^-(aq) + R^+NO_3^-(org) \rightleftharpoons NO_3^-(aq) + R^+ReO_4^-(org)$$

The over all $\Delta G°$ for this process is:

$$R^+NO_3^-(org) \rightleftharpoons R^+(org) + NO_3^-(org) \qquad \Delta G°_{ion\text{-}pair}$$

$$NO_3^-(org) \rightleftharpoons NO_3^-(aq) \qquad \Delta G°_{hyd}$$

$$ReO_4^-(aq) \rightleftharpoons ReO_4^-(org) \qquad \Delta G^\circ_{solv}$$

$$R^+(org) + ReO_4^-(org) \rightleftharpoons R^+ReO_4^-(org) \qquad \Delta G^\circ_{ion\text{-}pair}$$

The solvation of ReO_4^- requires the unfavorable transfer from the aqueous solution into the organic solvent. The ion pairing energy of $R^+NO_3^-$ must also be overcome before ReO_4^- can be ion-paired with R^+. These processes both work against the ion-exchange of ReO_4^-. Conversely the transfer of NO_3^- from the organic phase into the aqueous phase is favorable, however, the ion pairing energy of $R^+NO_3^-$, especially in an organic solvent, must also be overcome before this transfer may occur. The hydration energies for ReO_4^- and NO_3^- are –240 and –314 kcal mol^{-1} respectively.[69] The difference in hydration energies ($\Delta\Delta G^\circ_{hyd}$), therefore, is –74 kcal mol^{-1}, which indicates an overall favorable exchange. In order to take full thermodynamic advantage of this favorable difference in hydration energies, however, minimization of $\Delta\Delta G^\circ_{solv}$ and $\Delta\Delta G^\circ_{ion\text{-}pair}$ has to occur. Closer inspection of Equation 1.1 shows that if these two terms are reduced to zero, $\Delta\Delta G^\circ_{hyd}$ will drive the ion exchange. Physically, minimizing $\Delta\Delta G^\circ_{solv}$ can be accomplished by using a solvent with a low dielectric constant. In general, differences in solvation energies become less pronounced in solvents with dielectric constants below 10. Minimizing $\Delta\Delta G^\circ_{ion\text{-}pair}$ can be accomplished by using an organic solvent with a high dielectric constant or using a large extractant. Tight ion-pairs occur in solvents with low-permitivity, therefore, solvents with high dielectric constants will produce ions with lower ion-pair energy. Since using a high dielectric solvent is undesirable, however, and the ion pairing energy is also inversely dependent on the radius of the ions, using a large cationic extractant will also lower the ion pairing energies. Once the effects of $\Delta\Delta G^\circ_{solv}$ and $\Delta\Delta G^\circ_{ion\text{-}pair}$ have been physically reduced to zero, the extraction is only driven by the difference in hydration energies of the two anions, and the ion exchange takes place as described.

The above factors are summarized in a modified Born model, which describes the quantity $\Delta\Delta G^{\circ}_{tr}$.[69] This modified Born model is shown in Equation 1.2

(1.2)

$$\Delta\Delta G^{\circ}_{tr}(\text{kJ/mol}) = B\left\{\frac{1}{\varepsilon_S}\left[\left(\frac{1}{r_X}-\frac{1}{r_Y}\right)+2\left(\frac{1}{r_Y+r_R}-\frac{1}{r_X+r_R}\right)\right]+\frac{1}{\varepsilon_W}\left(\frac{1}{r_Y}-\frac{1}{r_X}\right)\right\}$$

where B is a temperature independent constant equal to –69.47 kJ nm mol^{-1}, r_Y and r_X are the size of the respective anions, r_R is the radius of the cationic extractant, ε_W is the dielectric of water, and ε_S is the dielectric of the solvent. Equation 1.2 shows an inverse relationship between $\Delta\Delta G^{\circ}_{tr}$ and the radii of the ions, as may be expected due to the dependence of ΔG°_{hyd} on anion size. Equation 1.2 also demonstrates that a low dielectric solvent both helps and hinders the ion-exchange process. To physically obtain the most negative $\Delta\Delta G^{\circ}_{tr}$, a compromise between a low dielectric solvent and a large cation (R^+) is made. It can be seen that if an infinite quantity is substituted into Equation 1.2 for r_R, the term containing the size of the cation is reduced to zero and $\Delta\Delta G^{\circ}_{tr}$ is dependent upon only the anion radii and solvent dielectric. In this case, a lower dielectric solvent can now be used without compromising the selectivity. For these reasons, the alkyl chains present in the tetraalkylated ferrocenium extractants of the R^2ER system are important because they impart size to the extractant molecule in addition to lipophilicity.

According to Equations 1.1 and 1.2, a thermodynamic point of diminishing returns will be met in this model since an infinite sized cation will only give a driving force equal to the difference in hydration energies of the anions. At this point, further increases in the size of the cationic extractant will not provide any more driving force (selectivity) for the ion exchange to take place. Work performed by Chambliss *et al* demonstrated a point of diminishing returns when increasing the size of R^+.[70] This work compared the selectivity of $HEP^+NO_3^-$ to that of $(heptyl)_4N^+NO_3^-$ by measuring the

liquid-liquid extraction of $^{99}TcO_4^-$ from a range of $NaNO_3$ containing solutions. The extraction data was examined by slope analysis and fit with the equilibrium modeling program SXLSQI, a program that uses a modification of the Hildebrand-Scott treatment and the Pitzer treatment to estimate the neutral contribution to the organic-phase solute activity coefficients and aqueous-ion activity coefficients, respectively.[71] The refined equilibrium constants as a result of these experiments suggested that the selectivities are nearly the same for both extractants ($logK_{exch}$ (chlorobenzene, 25 °C) was 3.86 ± 0.01 for $HEP^+NO_3^-$ and 3.70 ± 0.01 for $(heptyl)_4N^+NO_3^-$). Electrostatic principles predicted that these large cations ($r(HEP^+)$ = 0.600nm and $r(heptyl_4N^+)$ = 0.548 nm) had reached the point of "diminishing returns", such that a further increase in cation size would yield only a small increase in selectivity. It was also found that the selectivity under these conditions was primarily governed by the difference in the Gibbs energies of solvation, ΔG°_{solv}, and hydration, ΔG°_{hyd}, for the two anions (NO_3^- and $^{99}TcO_4^-$).[66,70]

These concepts were further demonstrated in the extraction of $^{99}TcO_4^-$ by tetraalkylammonium ion-exchange resins.[66] Studies using commercially available anion-exchange resins showed an increase in selectivity as the size of the exchange site increased which supports the assumption that the size of the exchange site (up to a certain point) has a large effect on selectivity. It is important to note that the time needed to reach equilibrium becomes greater as the size of the exchange site in the resin becomes larger. Further work performed by Chambliss *et al* measured the selectivity of four commercially available anion-exchange resins for TcO_4^-.[66,70] The size of cation ion-exchange sites in the resins increased in size from P–NMe_3^+, to P–NEt_3^+, to P–NPr_3^+, to P–NBu_3^+, where P denotes a covalent attachment to a polymer backbone. Figure 1.5 is a plot of the percentage of the $K_d^*(TcO_4^-)_{48h}$ value observed for a 20 min contact for commercial anion-exchange resins with increasing size of exchange sites. (K_d^* is a figure of merit used to evaluate the selectivity of an ion-exchange resin and is described in detail in Chapter 4. In general, the larger the K_d^*, the more selective the extractant

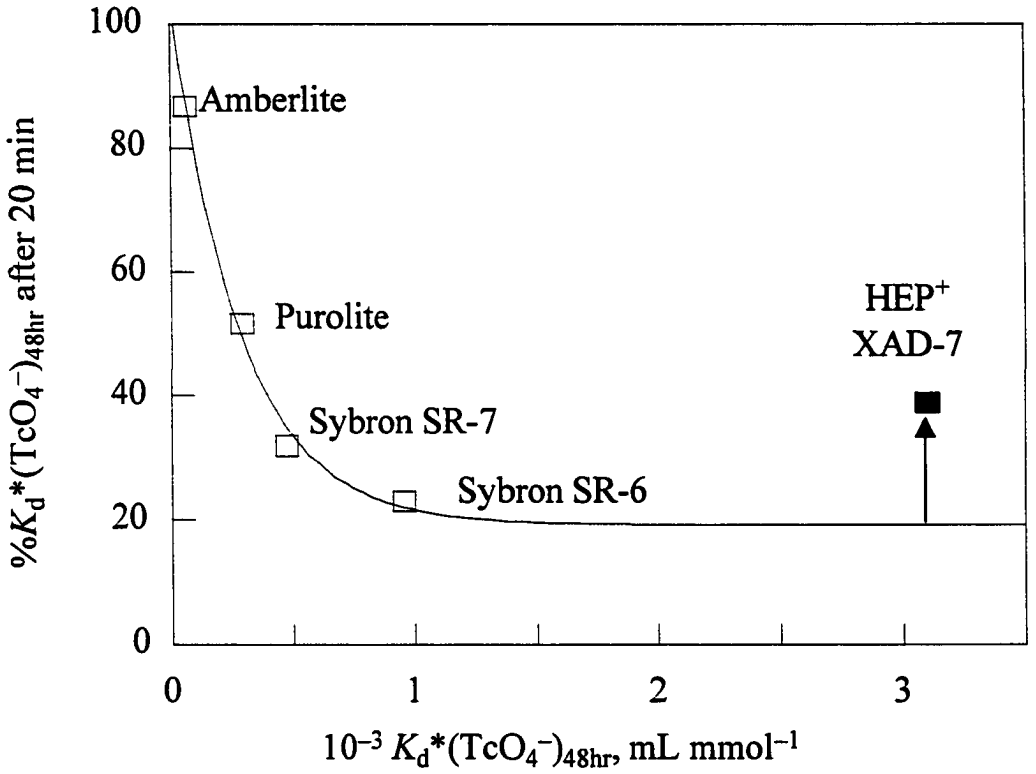

Figure 1.5. A plot of the relationship between anion-exchange rate (i.e., fractional attainment of K_d*($^{99}TcO_4^-$)$_{48h}$ for a 20-min contact) versus the anion-exchange selectivity (i.e., K_d*($^{99}TcO_4^-$)$_{48h}$) for the extraction of 1.0 x 10^{-5} M $^{99}TcO_4^-$ from aqueous 1 M $NaNO_3$ for four commercial anion-exchange resins (Amberlite = Amberlite® IRA-900 (P–NMe_3^+), Purolite = Purolite® A-520E (P–NEt_3^+), Sybron SR-7 = Sybron®-Ionac SR-7 (P–NPr_3^+), Sybron SR-6 = Sybron® Ionac SR-6 (P–NBu_3^+)) and the redox-recyclable anion-exchange material 0.25 mmol g^{-1} $HEP^+NO_3^-$/XAD-7. The line is a simple exponential fit to the first four data points. This figure is reprinted with permission from reference 66.

resin.) The observed trend was that the equilibrium $K_d^*(TcO_4^-)$ increased as the size of the cationic ion-exchange site increased. The increase in selectivity was consistent with a systematic decrease in the contribution of Gibbs free energy of ion-pairing terms to the overall free energy for extraction with increasing cation size, as described by equations 1.1 and 1.2. Another trend observed in Figure 1.5 was that the more selective the resin, the slower the rate of anion-exchange. The optimal case for ion-exchange resins would be to have high selectivity (high $K_d^*(A^-)$) with fast kinetics (large % $K_d^*(A^-)_{48hr}$ after 20 min). A comparison of the commercial anion-exchange resins with $HEP^+NO_3^-$/XAD-7 under similar extraction conditions shows this material does not follow the trend displayed by the tetraalkylammonium resins. The $HEP^+NO_3^-$/XAD-7 material was approximately three times more selective than Sybron®-Ionac SR-6 after 48 hr, but reached 39% of its $K_d^*(TcO_4^-)_{48hr}$ after 20 min. In comparison Sybron®-Ionac SR-6 reached only 23% of its $K_d^*(TcO_4^-)_{48hr}$ after 20 min. A tentative conclusion is that the new redox-recyclable material $HEP^+NO_3^-$/XAD-7 exhibits both faster ion-exchange kinetics and greater selectivity due to the
interfacial nature of the anion-exchange sites.

Finally, it is important to note that the selectivity described by this modified Born model is not recognition. The ion-exchange processes described here represent a "bias" for the anion with the least negative hydration energy in aqueous media. Using the liquid-liquid ion-exchange example presented in Figure 1.4, if an anion with a hydration energy less negative than that of ReO_4^- was also in the aqueous phase, this anion would be preferentially extracted over ReO_4^-. Recognition generally refers to specifically distinguishing between two anions based on shape, size, electrostatic interactions, and/or other properties.[72,73] Extractants can be synthesized to incorporate recognition, but selectivity in extractions using these systems is dependent upon different physical factors than those presented here.

Scope of the Dissertation.

Several new tetraalkylated ferrocenes have recently been synthesized and used for the selective ion exchange and detection of aqueous anions. The synthesis of new, functionalized polyalkylated ferrocenes is key to the development of novel, robust ion exchange compounds that can be used in materials synthesis or surface modification. The resulting materials have applications in both the remediation and detection of pollutant anions in aqueous media. The scope of this dissertation, therefore, is the advancement of the R^2ER process in three major areas: 1) synthesis and evaluation of new tetraalkylated ferrocenes for anion-exchange processes, 2) further functionalization of tetraalkylated ferrocenes for use as surface modifying reagents or materials precursors, and 3) electrochemical characterization of the functionalized tetraalkylated ferrocenes in terms of ion-exchange selectivity and their potential uses as aqueous anion sensors. The work described in this dissertation expands upon the development of ferrocenyl, organometallic anion-exchange materials and their use in the R^2ER process. Further synthesis of novel tetraalkylated ferrocenes and functionalized tetraalkylated ferrocenes is explored. Table 1.1 shows the structures, names, and abbreviations used for all novel compounds discussed in this dissertation as well as compounds and ligands previously prepared. Their applications toward remediation and detection of anionic pollutants are further explored. The selectivity observed for these extractants will be explored and discussed in terms of the modified Born model presented above.

Chapter 2 describes in detail the synthesis of tetraalkylated ferrocenes and ferrocenium salts. The novel tetraalkylated ferrocene, 1,1',3,3'-tetra(2-methyl-2-nonyl)ferrocenium nitrate (DEC) is presented for the first time. Crystal structures and electronic properties of all the tetraalkylated ferrocenes prepared in our laboratory will be compared and discussed. This work has been submitted for publication in Inorganic Chemistry.

Chapter 3 describes in detail the synthetic functionalization of the sterically

hindered, dialkylated Cp rings of the tetraalkylated ferrocenes prepared in our laboratories. Synthetic methodology for over-coming the sterically challenged environment around these Cp rings is discussed. Functionalities, which allow for the attachment of the tetraalkylated ferrocenyl moiety to surfaces are emphasized. Though robust ion-exchange materials have been made without covalent modification of surfaces, applications such as ion-exchange from organic media, studies of extractants that are water soluble, or the modification of electrically conducting surfaces make the need for covalent attachment of these tetraalkylated ferrocenes to surfaces desirable. Furthermore, physisorption of $HEP^{+}NO_3^{-}$ on metal-oxide surfaces has shown that the $HEP^{+}NO_3^{-}$ aggregates on the metal oxide surface, thus decreasing the materials capacity. Since metal oxide solid supports are generally cheaper than polymer solid supports, the covalent attachment of tetraalkylated ferrocenes to these surfaces is desirable for both higher capacity and cheaper ion-exchange materials. Towards these ends, several novel compounds are presented and their characterization discussed. Surface modification using these functionalized tetraalkylated ferrocenes is also demonstrated. Various methodology and compounds presented in this chapter are currently undergoing patent approval.

The focus of Chapter 4 is the study of tetraalkylated ferrocenes confined to electrically conducting surfaces. The use of 11-thiolundecanoyl functionalized tetraalklylated ferrocenes, prepared by methods discussed in Chapter 3, for formation of self assembled monolayers (SAMs) on gold electrodes is also explored. The resulting monolayers were used to explore the electrochemical properties of the tetraalkylated ferrocenes when confined to electrically conducting substrates. These properties are important for both electrochemically modulated ion-exchange chromatography and electrochemical sensing applications. A novel method of electrochemically determining extractant selectivity is also presented. Electrochemical sensing applications using these materials is currently undergoing patent approval.

Finally, Chapter 5 describes the liquid-liquid extraction properties of the novel extractant 1,1',3,3'-tetra(2-methyl-2-nonyl)ferrocenium nitrate ($DEC^{+}NO_3^{-}$). The extractant is compared to $HEP^{+}NO_3^{-}$. Differences in selectivity observed for the two extractants is discussed in terms of the aggregation properties of the two molecules in chlorobenzene.

Table 1.1. The structures, names, and abbreviations for the ligands, polyalkylated ferrocenes and functionalized polyalkylated ferrocenes presented in this dissertation. All compounds listed with the exception of BUT2,[74] tri-BUT, BUT, PENT,[75] HEX, HEP, and DEC are novel and have not been previously reported.

Structure	Name	Abbrev.
	cyclopentadiene anion	Cp
	mono– or polyalkylated cyclopentadiene anion (n = 1 or 2)	Cp'
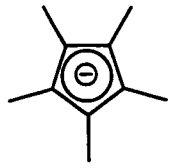	decamethylcylcopentadiene anion	Cp*
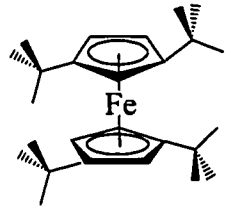	1,1',3,3'-tetra(2-methyl-2-propyl)ferrocene	BUT
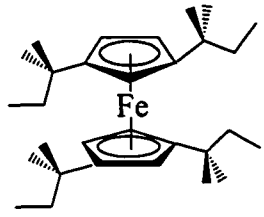	1,1',3,3'-tetra(2-methyl-2-butyl)ferrocene	PENT
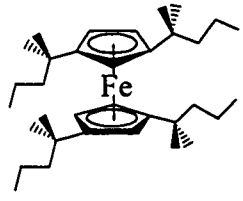	1,1',3,3'-tetra(2-methyl-2-pentyl)ferrocene	HEX
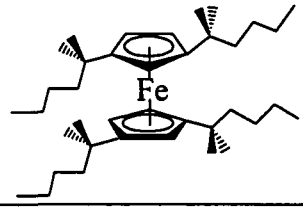	1,1',3,3'-tetra(2-methyl-2-hexyl)ferrocene	HEP

Table 1.1 (continued).

Structure	Name	Abbrev.
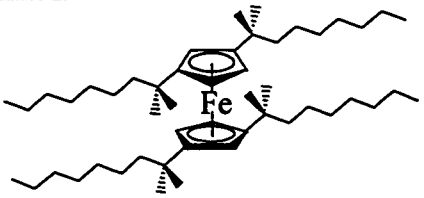	1,1',3,3'-tetra(2-methyl-2-nonyl)ferrocene	DEC
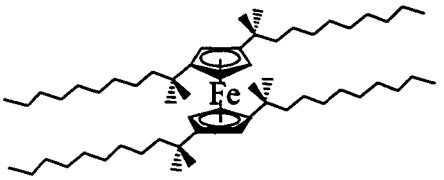	1,1',3,3'-tetra(2-methyl-2-undecyl)ferrocene	DoDEC
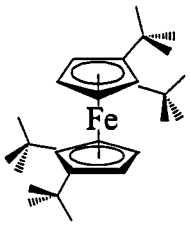	1,1',2,2'-tetra(2-methyl-2-propyl)ferrocene	BUT2
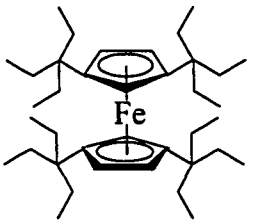	1,1',3,3'-tetra(3-ethyl-3-pentyl)ferrocene	HEP2
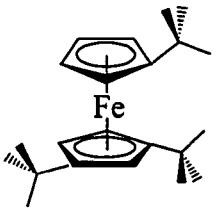	1,1',3-tri(2-methyl-2-propyl)ferrocene	tri-BUT
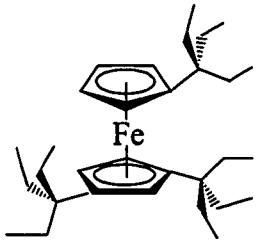	1,1',3-tri(3-ethyl-3-pentyl)ferrocene	tri-HEP2
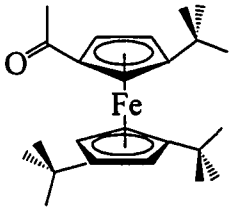	1,1',3-tri(2-methyl-2-propyl)- 3'-acylferrocene	tri-BUT-Ac

Table 1.1 (continued).

Structure	Name	Abbrev.
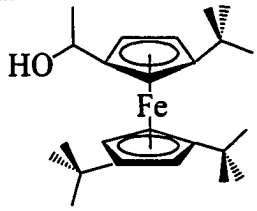	1,1',3-tri(2-methyl-2-propyl)- 3'-(2-hydroxyethyl)ferrocene	tri-BUT-OH
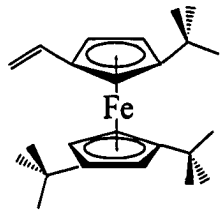	1,1',3-tri(2-methyl-2-propyl)- 3'-vinylferrocene	tri-BUT-Vn
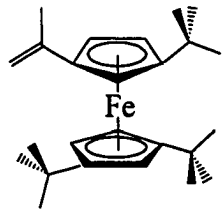	1,1',3-tri(2-methyl-2-propyl)- 3'-(2-propenyl)ferrocene	tri-BUT-Pr
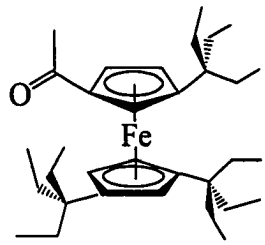	1,1',3-tri(3-ethyl-3-pentyl)-3'-acylferrocene	tri-HEP2-Ac
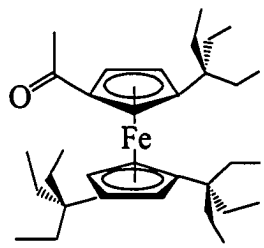	1,1',3-tri(3-ethyl-3-pentyl)-3'-(2-hydroxyethyl)ferrocene	tri-HEP2-OH
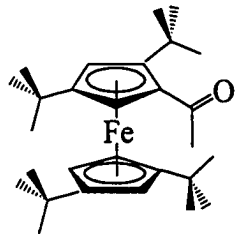	1,1',3,3'-tetra(2-methyl-2-propyl)-4-acylferrocene	BUT-Ac
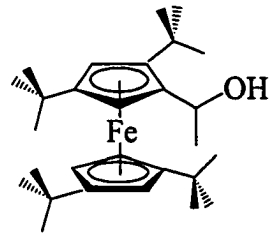	1,1',3,3'-tetra(2-methyl-2-propyl)-4-(2-hydroxyethyl)ferrocene	BUT-OH

Table 1.1 (continued).

Structure	Name	Abbrev.
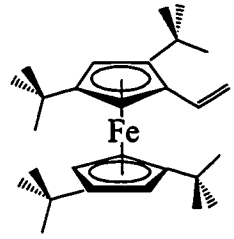	1,1',3,3'-tetra(2-methyl-2-propyl)-4-vinylferrocene	BUT-Vn
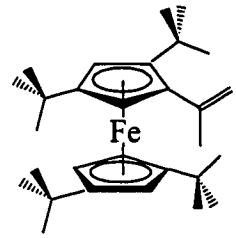	1,1',3,3'-tetra(2-methyl-2-propyl)-4-(2-propenyl)ferrocene	BUT-Pr
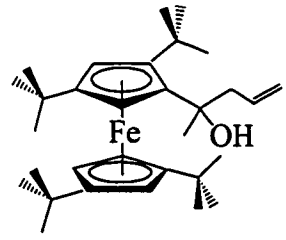	1,1',3,3'-tetra(2-methyl-2-propyl)-4-(4-hydroxy-4-(pentenyl))ferrocene	BUT-PtOH
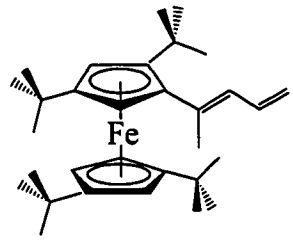	1,1',3,3'-tetra(2-methyl-2-propyl)-4-(4-(1,3-dipentenyl))ferrocene	BUT-diPt
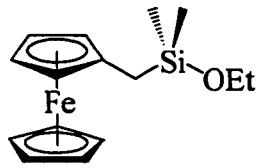	ferrocenylethyl-dimethylmethoxysilane	Fc-DMES
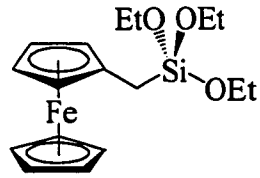	ferrocenylethyl-triethoxysilane	Fc-TES
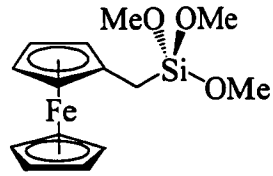	ferrocenylethyl-trimethoxysilane	Fc-TMS

Table 1.1 (continued).

Structure	Name	Abbrev.
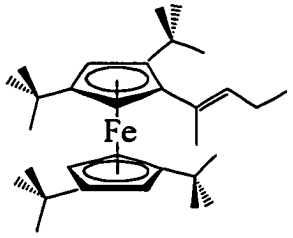	1,1',3,3'-tetra(2-methyl-2-propyl)-4-(2-(2-pentenyl))ferrocene	BUT-2Pt
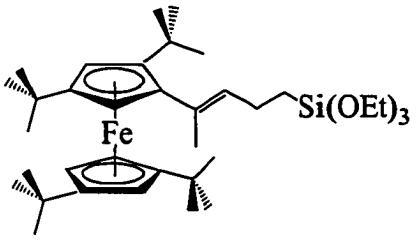	1,1',3,3'-tetra(2-methyl-2-propyl)-4-(2-(5-triethoxysilyl-2-pentenyl))ferrocene	BUT-PtTES
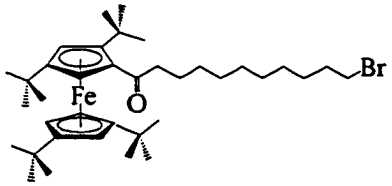	1,1',3,3'-tetra(2-methyl-2-propyl)-4-(11-bromoundecanoyl)ferrocene	BUT-Br
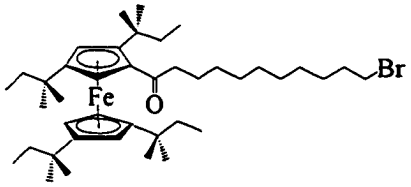	1,1',3,3'-tetra(2-methyl-2-butyl)-4-(11-bromoundecanoyl)ferrocene	PENT-Br
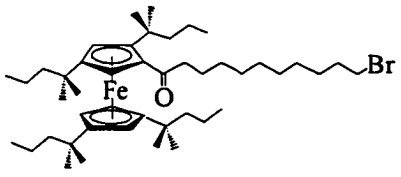	1,1',3,3'-tetra(2-methyl-2-pentyl)-4-(11-bromoundecanoyl)ferrocene	HEX-Br
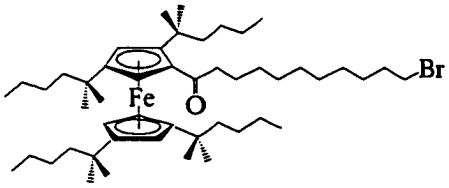	1,1',3,3'-tetra(2-methyl-2-hexyl)-4-(11-bromoundecanoyl)ferrocene	HEP-Br
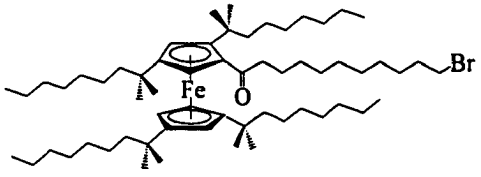	1,1',3,3'-tetra(2-methyl-2-nonyl)-4-(11-bromoundecanoyl)ferrocene	DEC-Br
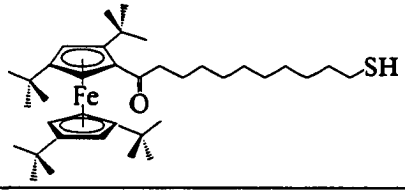	1,1',3,3'-tetra(2-methyl-2-propyl)-4-(11-thiolundecanoyl)ferrocene	BUT-SH

Table 1.1 (continued).

Structure	Name	Abbrev.
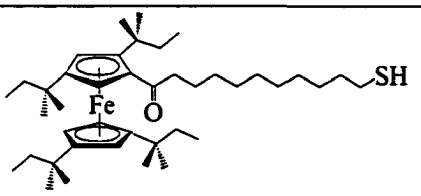	1,1',3,3'-tetra(2-methyl-2-butyl)-4-(11-thiolundecanoyl)ferrocene	PENT-SH
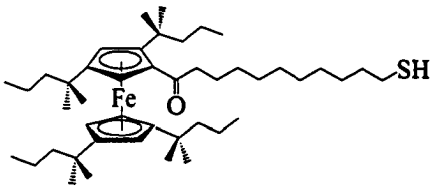	1,1',3,3'-tetra(2-methyl-2-pentyl)-4-(11-thiolundecanoyl)ferrocene	HEX-SH
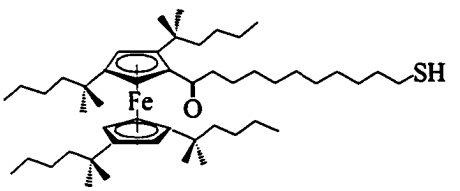	1,1',3,3'-tetra(2-methyl-2-hexyl)-4-(11-thiolundecanoyl)ferrocene	HEP-SH
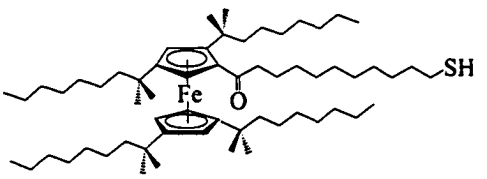	1,1',3,3'-tetra(2-methyl-2-nonyl)-4-(11-thiolundecanoyl)ferrocene	DEC-SH
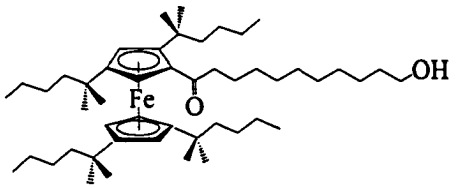	1,1',3,3'-tetra(2-methyl-2-hexyl)-4-(11-hydroxyundecanoyl)ferrocene	HEP-OH
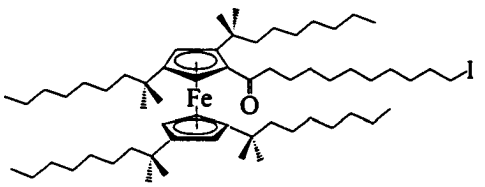	1,1',3,3'-tetra(2-methyl-2-nonyl)-4-(11-iodoundecanoyl)ferrocene	DEC-I
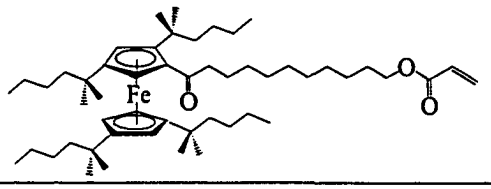	1,1',3,3'-tetra(2-methyl-2-hexyl)-4-(11-acrolylundecanoyl)ferrocene	HEP-acr

References

1. Marsh, S. F.; Jarvinen, G. D.; Bartsh, R. A.; Nam, J.; Barr, M. E. *J. Radioanal. Nucl. Chem.* **1998**, *235*, 37.
2. Gu, B.; M., B. G.; Bonnesen, P. V.; Liang, L.; Moyer, B. A.; Ober, R.; Alexandratos, S. D. *Eviron. Sci Technol.* **2000**, *34*, 1075.
3. Bonnesen, P. V.; M., B. G.; Alexandratos, S. D.; Bavoux, L. B.; Patel, V.; Ober, R.; Moyer, B. A. *Eviron. Sci Technol.* **2000**, *34*, 3761.
4. Tedder, D. W. *Sep. Purif. Methods* **1992**, *21*, 23.
5. Kirschner, E. M. *Chem. Eng. News* **1994**, ***June 20***, 13.
6. Illman, D. L. *Chem. Eng. News* **1993**, ***June 21***, 9.
7. Renner, R. *Eviron. Sci. Technol.* **1997**, *31*, 134A.
8. Babad, H.; Fulton, J. C.; DeFigh-Price, B. C. *A Strategy for Resolving High-Priority Hanford Site Radioactive Waste Storage Tank Safety Issues*; report WHC-SA-1661-FP; Westinghouse Hanford Co., 1993.
9. Barker, S. A.; Thornhill, C. K.; Holton, L. K. *Pretreatment Technology Plan*; report WHC-EP-0629; Westinghouse Hanford Co., 1993.
10. Babad, H.; Johnson, G. D.; Reynolds, D. A.; Pederson, L. R.; Strachan, D. M.; Meisel, D.; Jonah, C.; Ashby, E. C. *Evaluation of the Generation and Release of Flammable in Tank 241-SY-101*; report WHC-EP-0517; Westinghouse Hanford Co., 1991.
11. Babad, H.; Turner, M. D.; Gerber, M. A. *Resolving Safety Issues for Radioactive Waste Tanks with Organic Content*; report WHC-SA-1671-FP; Westinghouse Hanford Co., 1993.
12. Babad, H.; Camaioni, D. M.; Lilga, M. A.; Samuels, W. D.; Strachan, D. M. *Tank Waste Chemistry - A New Understanding of Waste Aging*; report WHC-SA-1661-FP; Westinghouse Hanford Co., 1993.

13. Simpson, B. C.; Babad, H.; Cash, R. J. *Recent Results from Characterization of Ferrocyanide Wastes at the Hanford Site*; report WHC-AS-1701-FPM; Westinghouse Hanford Co., 1993.

14. Katcoff, S. *Nucleonics* **1958**, *16*, 78.

15. Clark, J. F.; Chamberlin, R. M.; Abney, K. D.; Strauss, S. H. *Environ. Sci. Technol.* **1999**, *33*, 2489.

16. Schroeder, N. C.; Morgan, D.; Rokop, D. J.; Fabryka-Martin, J. *Radiochim. Acta* **1993**, *60*, 203.

17. Garten, J., C. T. *Environment International* **1987**, *13*, 311.

18. Wildung, R. E.; McFadden, K. M.; Garland, T. R. *J. Environ. Qual.* **1979**, *8*, 156.

19. Schroeder, N. C., Los Alamos National Laboratory, Los Alamos, NM. Personal communication, 1996.

20. Blanchard, J., D. L.; Brown, G. N.; Conradson, S. D.; Fadeff, S. K.; Golcar, G. R.; Hess, N. J.; Klinger, G. S.; Kurath, D. E. *Technetium Removal and Characterization: A Progress Report*; unpublished report prepared for Westinghouse Hanford Co. by PNL, May 30, 1996.

21. Clearfield, A. In *Inorganic Ion Exchange Materials for Nuclear Waste Effluent Treatment: Industrial Environmental Chemistry*; Sawyer, D. T., Martell, A. E., Eds.; Plenum Press: New York, 1992.

22. Boening, D. W.; Chew, C. M. *Water, Air, Soil Pollut.* **1999**, *109*, 67.

23. Otu, E. O.; Byerley, J. J.; Robinson, C. W. *Int. J. Environ. Anal. Chem.* **1996**, *63*, 81.

24. Christen, K. *Environ. Sci. Technol.* **2000**, *34*, 374A.

25. Okamoto, H. S.; Rishi, D. K.; Steeber, W. R.; Baumann, F. J.; Perera, S. K. *Jour. AWWA* **1999**, *91*, 73.

26. Susarla, S.; Collette, T. W.; Garrison, A. W.; Wolfe, N. L.; McCutcheon, S. C. *Environ. Sci. Technol.* **1999**, *333*, 469.

27. Urbansky, E. T. *Bioremediation J.* **1998**, *2*, 81.

28. Federal Register, 1991 *Testing Consent Order for Sodium Cyanide.*

29. U.S. EPA, 2000 www.epa.gov/safewater/mcl.html.

30. Pontius, F. W. *Jour. AWWA* **2000**, *92*, 40.

31. Gullick, R. W.; Lechevallier, M. W.; Barhorst, T. S. *Jour. AWWA* **2001**, 66.

32. Caliamanis, A.; McCormick, M. J.; Carpenter, P. D. *J. Chromatog. A* **2000**, *75*, 884.

33. Frenzel, W.; Liu, C. Y.; Oleksy-Frenzel, J. *Anal. Chim. Acta* **1990**, *77*, 233.

34. Linares, P.; Luque de Castro, M. D.; Valcarcel, M. *Anal. Chim. Acta* **1984**, *161*, 257.

35. Chinaka, S.; Takayama, N.; Michigami, Y.; Ueda, K. *J. Chromatog. B* **1998**, *713*, 353.

36. Moody, C. A.; Field, J. A. *Environ. Sci. Technol.* **1999**, *33*, 2800.

37. Moody, C. A.; Hebert, G. N.; Strauss, S. H.; Field, J. A. *Eviron. Sci. Technol.* **2001**, accepted for publication.

38. Olsen, G. W.; Burris, J. M.; Mandel, J. H.; Zobel, L. R. *J. Occup. Environ. Med.* **1999**, *41*, 799.

39. Tullo, A. *Chem. Eng. News* **2000**, *May 29*, 12.

40. Tullo, A. *Chem. Eng. News* **2000**, *May 22*, 9.

41. Moody, C. A.; Field, J. A. *Environ. Sci. Technol.* **2000**, *34*, 3864.

42. Kawasaki, M.; Omori, T.; Hasegawa, K. *Radiochimica Acta* **1993**, *63*, 53.

43. Ashley, K. R.; Ball, J. R.; Pinkerton, A. B.; Abney, K. D.; Schroeder, N. C. *Solv. Extr. Ion Exch.* **1994**, *12*, 239.

44. Ashley, K. R.; Whitener, G. D.; Schroeder, N. C.; Ball, J. R.; Radzinski, S. *submitted for publication.*

45. Liang, L.; Gu, B.; Yin, X. *Sep. Technol.* **1996**, *6*, 111.

46. Bonnesen, P. V.; Alexandratos, S. D.; Brown, G. M. Recent Developments and Future Opportunities in Separations Technology, Topical Conference Preprints. *American Institute of Chemical Engineers Annual Meeting*; American Institute of Chemical Engineers: New York, 1995; 294-299.

47. Rogers, R. D.; Bond, A. H.; Griffin, S. T.; Horwitz, E. P. *Solv. Extr. Ion Exch.* **1996**, *14*, 919.

48. Rogers, R. D.; Zhaung, J.; Griffin, S. T. *Sep. Sci. Technol.* **1997**, *32*, 699.

49. Rogers, R. D.; Griffin, S. T.; Horwitz, E. P.; Diamind, H. *Solv. Extr. Ion Exch.* **1997**, *15*, 547.

50. Rohal, K. M.; Van Seggen, D. M.; Clark, J. F.; McClure, M. K.; Chambliss, C. K.; Strauss, S. H.; Schroeder, N. C. *Solvent Extr. Ion Exch.* **1996**, *14*, 401.

51. Tse, P. K.; Horwitz, E. P. *Solv. Extr. Ion Exch.* **1990**, *8*, 353.

52. Dyrkacz, G. R.; Vandegrift, G. F.; W., T. M.; Horwitz, E. P. *J. Phys. Chem.* **1979**, *83*, 670.

53. Macásek, F.; Rajec, P.; Mikulaj, V.; Kopunec, R.; Cech, R. *Coll. Cxech. Chem.Commun.* **1978**, *43*, 200.

54. Bonnesen, P. V.; Moyer, B. A.; Presley, D. J.; Armstrong, V. S.; Haverlock, T. J.; Counce, R. M.; Sachleben, R. A. *Alkaline-Side Extraction of Technetium from Tank Waste Using Crown Ethers and Other Extractants*; report ORNL/TM-13241; Oak Ridge National Laboratory, 1996.

55. Moyer, B. A.; Sachleben, R. A.; Bonnesen, P. V. Process for Extracting Technetium from Alkaline Solutions. U. S. Patent 5,443,731, August 22, 1995.

56. Lilga, M. A.; Orth, R. J.; Sukamto, J. P. H.; Rassat, S. D.; Genders, J. D.; Gopal, R. *Sep. Purif. Technol.* **2001**, *24*, 451.

57. Sukamto, J. P. H.; Rassat, S. D.; Josephson, G. J.; Lawrence, W. E.; Mendoza, D. P.; Viswanathan, V. V.; Hallen, R. T.; Orth, R. J.; Lilga, M. A.; Malmberg, B. J.; Gu, Y. X.; Edwards, L. L. *Tappi J.* **2000**, *83*, 53.

58. Rassat, S. D.; Sukamto, J. P. H.; Orth, R. J.; Lilga, M. A.; Hallen, R. T. *Sep. Purif. Technol.* **1999**, *15*, 207.

59. Lilga, M. A.; Orth, R. J.; Sukamto, J. P. H.; Haight, S. M.; Schwartz, D. T. *Sep. Purif. Technol.* **1997**, *11*, 147.

60. Green-Pedersen, H.; Korshin, G. V. *Environ. Sci. Technol.* **1999**, *33*, 2633.

61. Hubler, T. L.; Anderson, G. M.; Sukamto, J. P. H.; Lilga, M. A.; Rassat, S. D. Polyvinylferrocene Polymers as Electroactive Ion-Exchange Materials for Separation of Pertechnetate Ion from High Nitrate Ion-containing Wates: Issues and Synthetic Strategies. *Book of Abstracts,. 218th ACS National Meeting*; Aug. 22-26, 1999;

62. Clark, J. F.; Clark, D. L.; Whitener, G. D.; Schroeder, N. C.; Strauss, S. H. *Environ. Sci. Technol.* **1996**, *30*, 3124.

63. Chambliss, C. K.; Odom, M. A.; Morales, C. M. L.; Martin, C. R.; Strauss, S. H. *Anal. Chem.* **1998**, *70*, 757.

64. Gansle, K. M. Investigation and Development of Liquid-Liquid Extraction Systems for the Removal of Pertechnetate from Aqueous Nuclear Waste-Stream Simulants. Ph.D. Dissertation, Colorado State University, Fort Collins, CO, 1998.

65. Odom, M. A. Development of Strategies for the Detection, Extraction, and Recovery of Aqueous Anions Using Highly Selective Redox-Recyclable Materials. Ph.D. Dissertation, Colorado State University, Fort Collins, CO, 2001.

66. Chambliss, C. K.; Odom, M. A.; Martin, C. A.; Moyer, B. A.; Strauss, S. H. *Inorg. Chem. Commun.* **1998**, *1*, 435.

67. Strauss, S. H.; Odom, M. A.; Hebert, G. N.; Clapsaddle, B. J., 2001 *ATR-FTIR Detection and Quantification of Anionic Pollutants in Water.*

68. Hebert, G. N.; Strauss, S. H. *unpublished results.*

69. Moyer, B. A.; Bonnesen, P. V. In *Supramolecular Chemistry of Anions*; Bianchi, A., Bowman-James, K., Garcia-Espana, E., Eds.; VCH: New York, 1997.

70. Chambliss, C. K.; Martin, C. A.; Strauss, S. H.; Moyer, B. A. *Solvent Extr. Ion Exch.* **1999**, *17*, 553.

71. Baes, C. F. J.; Moyer, B. A.; Case, G. N.; Case, F. I. *Sep. Sci. Technol.* **1990**, *25*, 1675.

72. Beer, P. D.; Gale, P. A. *Angew. Chem. Int. Ed. Eng.* **2001**, *40*, 486.

73. Beer, P. D.; Gale, P. A.; Chen, G. Z. *J. Chem. Soc., Dalton Trans.* **1999**, 1897.

74. Hughes, R. P.; Kowalski, A. S.; Lomprey, J. R.; Rheingold, A. L. *Organometallics* **1994**, *13*, 2691.

75. Leigh, T. J. *J. Chem. Soc.* **1964**, 3294..

Chapter 2

Synthesis, Characterization, and Crystal Structures of Polyalkylated Ferrocenes and Ferrocenium Salts

Introduction

The functionalization of ferrocene, $Fe(Cp)_2$, with various types of organic moieties has been widely performed for uses in catalysis, organic synthesis, and materials science.[1] Functional groups have also been used to tune redox properties of ferrocenes by virtue of their electron donating or withdrawing properties.[2] Alkylation of ferrocenes is often desirable because the addition of inductively donating alkyl groups to the Cp rings lowers the reduction potential of ferrocene, as in the case of decamethylferrocene ($Fe(Cp^*)_2$; $E_{1/2}$ = –0.548V vs. $Fe(Cp)_2^+/Fe(Cp)_2$).[3,4] Alkylation of ferrocene is also desirable as a means to increase its solubility in organic solvents.

Recently, several new polyalkylated ferrocenes have been prepared in our laboratories for use as redox-recyclable ion exchange materials.[5,6] These highly lipophilic ferrocenes remain insoluble in water even when oxidized, which allows for the biphasic ion exchange between an aqueous anion and the polyalkylated ferrocenium salt in a non-aqueous phase. Biphasic ion-exchange processes utilizing polyalkylated ferrocenium salts have been demonstrated by liquid-liquid and by solid-liquid ion-exchange techniques.[5,7,8] Furthermore, the relatively low $HEP^{+/0}$ and $DEC^{+/0}$ reduction potentials of these polyalkylated ferrocenes allow for easy recycling of these ion-exchange materials by redox switching between the cationic and neutral state of the molecule using mild chemical oxidizing and reducing agents. The high lipophilicity of the tetraalkylated ferrocenes allows for preparation of surface coatings by physisorption onto a variety of solid supports (polymers, metal oxides, etc.), eliminating the need for

covalent attachment and making the preparation of novel ion exchange materials quite simple.[6-8] The robust ion-exchange properties of physisorbed thin films of these polyalkylated ferrocenium salts have also recently been applied to ATR FTIR aqueous sensing.[6] These thin films have increased the ATR FTIR detection limits of aqueous anions by > 10,000 times in some cases.[6]

Preparation of polyalkylated ferrocenes, however, is typically difficult and plagued by the production of product mixtures containing mono to tetraalkylated ferrocenes.[9,10] These product mixtures are intractable oils that are difficult to separate and purify, and as a result alkylation reactions typically have low yields.[11,12] As a way to avoid these problems, a 2-step procedure involving acylation followed by a subsequent reductive deoxygenation of the carbonyl is often employed.[9,10,13] Such procedures, however, only result in mono- and dialkylated ferrocenes and still require a separation of mono and di-substituted ferrocenes from unreacted ferrocene. Other procedures use complicated multi-step organic synthesis schemes to first synthesize a functionalized cyclopentadienyl ring before formation of the desired sandwich complex.[14] The disadvantage of these preparation methods is the need for several reaction steps for the production of polyalkylated ferrocenes.

In synthesizing the polyalkylated ferrocenes used in these studies, several novel tetraalkylated ferrocenes and ferrocenium salts have been prepared and characterized. It has been shown that tetraalkylated ferrocenes can be easily prepared and crystallized using *t*-butyl chloride as the alkylating agent.[15] When used in excess, the reaction of *t*-butyl chloride with ferrocene and aluminum trichloride or zinc chloride resulted exclusively in the 1,1',3,3'-tetra-*t*-butylferrocene that was crystallized from ethanol. By extending this procedure to longer chain *t*-alkyl chlorides, a series of novel, lipophilic, tetraalkylated ferrocenes have been synthesized and isolated as crystalline solids. Their preparation, electronic properties, and structures will be discussed.

Experimental Section

The abbreviations used for all synthesized compounds discussed in this chapter are summarized in Table 1.1 in Chapter 1 of this dissertation. All inert atmosphere synthetic procedures were performed under dried nitrogen using standard procedures.[16] Dichloromethane (Fisher Scientific) was distilled over P_2O_5 and stored under nitrogen. Zinc chloride (Mallinkrodt) was dried by mechanically stirring with $SOCl_2$ for 48 hours and subsequent removal of $SOCl_2$ under vacuum. Dryness of the $ZnCl_2$ was determined by monitoring water peaks in the IR spectrum. Dry zinc chloride was stored in a glovebox under an N_2 atmosphere. Ferrocene (Lancaster Synthesis) was sublimed once and stored in a glovebox under an N_2 atmosphere. Tetra-*n*-butyl ammonium perchlorate (TBAP; Alfa) was recrystallized from acetone/ether (1:3, v:v) and dried under vacuum. 1,1',3,3'-tetra(2-methyl-2-propyl) ferrocene (BUT)[15], 1,1',3,3'-tetra(2-methyl-2-butyl) ferrocene (PENT),[15] and 1,1',2,2'-tetra(2-methyl-2-ethyl) ferrocene (BUT2)[14] were synthesized according to literature methods. A sample of BUT2 was generously donated by Dr. Russell P. Hughes. Water was distilled and deionized (Barnstead NANOpure) and had a resistivity of 18 MΩ cm. The following reagents were obtained commercially and used without further purification: diethyl ether (Fisher Scientific); hexanes (Fisher Scientific); acetonitrile (Fisher Scientific); sodium hydroxide (Fisher Scientific); *t*-butyl-chloride (Fisher Scientific); thionyl chloride (ACROS); 37% hydrochloric acid (Mallinckrodt); silver oxide (Mallinckrodt); 2-methyl-2-pentanol (Aldrich); 2-methyl-2-hexanol (Lancaster); 2-methyl-2-nonanol (Aldrich); 3-ethyl-3-pentanol (Aldrich); absolute ethanol (Pharmco); zinc metal (granular, 20 mesh; Fisher Scientific); silver nitrate (Aldrich); perrhenic acid (Aldrich), silica gel (60 – 200 mesh; J. T. Baker). All deuterated solvents were obtained from Cambridge Isotope Labs.

Synthesis of 2-chloro-2-methylhexane. 2-methyl-2-hexanol (100 g, 861 mmol) was stirred with an equal volume of concentrated HCl (~100 mL) in a round-bottom flask for 4 to 5 hours. The yellow organic layer was then separated and passed over a small

column of dry silica gel. The product, 2-chloro-2-methylhexane, was obtained as a viscous clear liquid in > 90% yield and was stored in the dark. ^{1}H-NMR (acetone-d_6, 300 MHz, 25 °C) δ 1.75 (m, 2H), 1.58 (s, 6H), 1.45 (m, 2H), 1.37 (s, 2H), 0.93 (t, 3H). Liquid secondary ion mass spectrometry (LSIMS) m/z=135.1 (135.7 calc.)

Synthesis of 2-chloro-2-methylpentane. The synthesis of 2-chloro-2-methylpentane was the same as that for 2-chloro-2-methylhexane described above. ^{1}H-NMR (acetone-d_6, 300 MHz, 25 °C) δ 1.8 – 1.6 (m, 2H), 1.54 (s, 6H), 1.53 – 1.40 (m, 2H), 0.92 (t, 3H). LSIMS m/z=107.6 (107.1 calc.)

Synthesis of 2-chloro-2-methylnonane. The synthesis of 2-chloro-2-methylnonane was the same as that for 2-chloro-2-methylhexane described above. ^{1}H-NMR (benzene-d_6, 300 MHz, 25 °C) δ 1.5 (t, 2H), 1.35 (s, 6H), 1.28 – 1.00 (m, 12H), 0.81 (t, 3H). LSIMS m/z=177.1 (177.7 calc.)

Synthesis of 1,1',3,3'-tetra(2-methyl-2-hexyl)ferrocene (HEP). In a glovebox, ferrocene (14.0 g; 75.3 mmol) was weighed into a Schlenk flask. Also in a glovebox, dry zinc chloride (30.9 g; 227 mmol) was weighed into a three neck round-bottom flask equipped with a stir bar. Both flasks were then removed from the glovebox under N_2 purge and connected to a Schlenk line. Under nitrogen purge, 2-chloro-2-methylhexane (75 g; 557 mmol) was added to the zinc chloride, and the round-bottom flask was then equipped with a condenser and an addition funnel. In the separate Schlenk flask, the ferrocene was dissolved in CH_2Cl_2 (200 mL) and then cannulated into the addition funnel attached to the round-bottom flask. The ferrocene solution was then added drop wise over 1 hour to the zinc chloride/2-chloro-2-methylhexane slurry while heating and stirring. The reaction mixture was allowed to reflux for 24 hours, at which time the reaction mixture was opened to air and washed with an equal volume of 10 vol% concentrated HCl in water. After separation, the organic layer was stirred under mild heat with granular zinc metal until the solution turned bright orange. After filtering, the organic layer was washed with an equal volume of 1 M NaOH followed by 2 washings

with an equal volume of water. After separating the organic phase and removing the solvent, the resulting orange oil was recrystallized from absolute ethanol. The resulting orange crystals were obtained in an 85 to 90% yield after recrystallization. ^{1}H-NMR (acetone-d_6, 300 MHz, 25 °C) δ 3.96 (m, 4H), 3.87 (m, 2H), 1.26 (s, 24H), 1.2-1.0 (m, 24H), 0.78 (t, 12H). LSIMS m/z=578.5 (578.8 calc.)

Synthesis of 1,1',3,3'-tetra(2-methyl-2-pentyl)ferrocene (HEX). HEX was prepared in the same manner as HEP using 2-chloro-2-methylpentane as the alkylating agent. The product was obtained as orange crystals in an 88% yield. ^{1}H-NMR (acetone-d_6, 300 MHz, 25 °C) δ 3.96 (m, 4H), 3.87 (m, 2H), 1.25 (s, 24H), 0.8-1.2 (m, 8H), 0.74 (t, 12H). LSIMS m/z=522.4 (522.7 calc.)

Synthesis of 1,1',3,3'-tetra(2-methyl-2-nonyl)ferrocene (DEC). DEC was prepared in the same manner as HEP using 2-chloro-2-methylnonane as the alkylating agent. A refluxing time of 48 hours was necessary for complete tetra-alkylation. Needle-like, orange crystals were obtained in a 75% to 85% yield. ^{1}H-NMR (benzene-d_6, 300 MHz, 25 °C) δ 4.01 (d, 4H), 3.97 (t, 2H), 1.2-1.6 (m, 64H), 0.93 (t, 12H). Liquid secondary ion mass spectrometry (LSIMS) m/z=746.8 (747.1 calc.)

Synthesis of Tetraalkylated Ferrocenium Nitrate Salts. A solution of silver(I) nitrate (0.252 g; 1.48 mmol) was prepared in absolute ethanol (20 mL) by gently heating the solution while stirring. The resulting solution was added drop wise to a dichloromethane solution of the tetraalkylated ferrocene (1.78 mmol) and stirred for 6 hours in the dark. The solution was then filtered to remove precipitated silver metal and the solvent removed under vacuum. The resulting dark green solid was washed three times with hexanes to remove any unoxidized starting material and then filtered. The tetraalkylated ferrocenium nitrate salt was then recrystallized from a mixture of dichloromethane and cold ether. The product was obtained as dark green crystals in an 80% yield.

Preparation of silver(I) perrhenate. A suspension of silver(I) oxide (6.47 g;

27.9 mmol) was prepared in a minimal amount of water (~500-750 mL) and was gently heated to 70 °C. Perrhenic acid ($HReO_4$; 17.0 g; 67.7 mmol) was added to the suspension, at which point the remaining silver(I) oxide dissolved. After filtering, the solution was then cooled to –20 °C overnight. The resulting gray/silver crystals were obtained in a 75-80% yield and stored in the dark.

Synthesis of Tetraalkylated Ferrocenium Perrhenate Salts. A solution of silver(I) perrhenate (0.530 g; 1.48 mmol) was prepared in acetonitrile (20 mL) by gently heating the solution while stirring. The resulting solution was added drop wise to a dichloromethane solution of the tetraalkylated ferrocene (1.78 mol) and stirred for 6 hours in the dark. The solution was then filtered and solvent removed under vacuum. The resulting dark green solid was washed three times with hexanes to remove any unoxidized starting material and then filtered. The tetraalkylated ferrocenium perrhenate salt was then recrystallized from a mixture of dichloromethane and cold ether. The product was obtained as dark green crystals in 80% yield.

Determination of Reduction Potentials. Reduction potentials for all tetraalkylated ferrocenes were determined anaerobically by cyclic voltammetry using a model 263A potentiostat/galvanostat (EG&G Princeton Applied Research). All reduction potentials ($E_{1/2}$ taken as the average of the cathodic and anodic peak potentials) were measured in dichloromethane solutions of 0.1 M TBAP supporting electrolyte, 0.1 M ferrocene, and 0.1 M tetraalkylated ferrocene using a scan rate of 50 mV/s, platinum or glassy carbon disc working electrode, platinum gauze counter electrode, and a silver wire quasi-reference electrode. All $E_{1/2}$ values are referenced to the ferrocene$^{+/0}$ redox couple.

Electronic Spectra. All electronic spectra were measured using a Lambda 40 UV-vis spectrometer (Perkin Elmer). Spectra were taken of 1 mM acetonitrile solutions of tetraalkylated ferrocene and ferrocenium salts in 1 cm pathlength quartz cuvettes (Wilmad).

Single Crystal X-ray Crystallography. Table 2.1 contains a summary of the

Table 2.1. Summary of crystallographic data.

	$HEP^+NO_3^-$	HEP	$BUT^+ReO_4^-$·acetone	$BUT2^+ReO_4^-$	DEC	$DEC^+NO_3^-$
space group	$P\bar{1}$	Fdd2	$P2_12_12_1$	$P2_1/c$	$C2/c$	$P2/n$
unit cell dimensions:						
a, Å	10.7055(7)	18.833(12)	9.784(1)	16.3501(1)	18.7606(8)	9.3909(15)
b, Å	14.3445(9)	43.00(2)	15.303 (1)	16.7310(2)	8.7418(4)	8.6829(14)
c, Å	25.815(2)	8.849(5)	20.588(3)	20.9034(4)	28.808(1)	29.713(5)
α, deg	76.265(2)	90	90	90	90	90
β, deg	83.174(2)	90	90	106.785 (1)	101.736(1)	93.772(3)
γ, deg	77.547(2)	90	90	90	90	90
Z	2	8	4	8	4	2
abs coeff, cm^{-1}	4.36	4.43	44.27	49.75	3.56	3.51
data/param ratio	13.7	23.8	14.6	22.6	23.0	13.9
R_1[a]	0.0750	0.0726	0.0385	0.0462	0.0675	0.0580
w$R2$[b]	0.1309	0.1602	0.0901	0.0786	0.1385	0.1158
GOF	0.878	0.756	0.990	0.946	0.865	1.084

a. $R_1 = \Sigma||F_o| - |F_c||/\Sigma|F_o|$. b. $wR2 = [\Sigma w(|F_o| - |F_c|)^2/\Sigma w|F_o|^2]^{1/2}$.

crystallographic and computational parameters associated with the six compounds that were characterized by X-ray diffraction in this study. Complete tables of atomic coordinates, bond distances and angles, and anisotropic displacement parameters for the structures of HEP, DEC, and $DEC^{+}NO_3^{-}$, which are structures obtained for this dissertation by the author, can be seen in Appendix A. Complete tables of atomic coordinates, bond distances and angles, and anisotropic displacement parameters for the structures of $BUT^{+}ReO_4^{-}$·acetone (structure obtained by Dr. Alexander E. Gash), $HEP^{+}NO_3^{-}$ (structure obtained by Mr. Dustin L. Clark), and $BUT2^{+}ReO_4^{-}$ (structure obtained by Dr. Kristina M. Gansle) can be found in references 17 and 18. All structures were solved at Colorado State University by Susie M Miller, except the structure of $BUT^{+}ReO_4^{-}$·acetone, which was solved by Dr. Alexander E. Gash. Other structures discussed in this Chapter and not obtained in our laboratories are referenced as appropriate in the text.

X-ray diffraction data were recorded on a Siemens P4 4-circle diffractometer (for $BUT^{+}ReO_4^{-}$·acetone) or on a Bruker SMART CCD diffractometer (for all other structures reported herein) employing MoKα radiation (graphite monochromator). Standard Siemens/Bruker data collection and data reduction software was employed in all cases as appropriate, and Bruker SHELXTL[19] software was used for structure solution, refinement, and graphics. Absorption and other corrections were applied by using SADABS,[20] except in the case of the $BUT^{+}ReO_4^{-}$·acetone structure, in which case an empirical absorption correction based on ψ scans for selected reflections was utilized. All structures were initially solved by direct methods and refined (on F^2, using all data) by a full matrix, weighted least-squares process. All non-hydrogen atoms were refined using anisotropic displacement parameters. Hydrogen atoms were generally placed in idealized positions and refined by using a riding model. Further details of the data collection and structure determination for the structures of HEP, DEC, and $DEC^{+}NO_3^{-}$ are listed in Appendix A.

Results and Discussion

Preparation of 1,1',3,3'-tetra(2-methyl-2-alkyl)ferrocenes. The Friedel-Crafts polyalkylation of ferrocene with an excess of 2-chloro-2-methylalkane leads to a 1,1',3,3'-tetraalkylferrocene in high yield and with excellent compositional and isomeric purity. The preparation and general structure of the 1,1',3,3'-tetra(2-methyl-2-alkyl)ferrocenes is shown in Scheme 2.1. For simplification, the 1,1',3,3'-tetra(2-methyl-2-alkyl)ferrocenes are named according to the total number of carbon atoms contained in each tertiary alkyl chain, as shown in Scheme 2.1. (Geometric isomers of these ferrocenes are referred to by addition of the number "2" to the name.) The tertiary chloroalkanes were first prepared by stirring the corresponding 2-methyl-2-alkanol with an equal volume of concentrated hydrochloric acid. Interestingly, no olefinic elimination product is seen with this preparation method. Apparently the tertiary alcohols afford very stable carbocation intermediates resulting exclusively in the tertiary chloroalkane products. All tertiary alkanols used in this study were chlorinated in this manner with yields > 90%.

Friedel-Crafts alkylation of ferrocene with zinc chloride and the desired tertiary alkylchloride containing 4-10 carbon atoms was then performed. It was found that the use of zinc chloride as the Lewis acid catalyst, instead of the more reactive aluminum chloride, resulted in a product with fewer side products and gave a reaction product that was less likely to emulsify upon work-up of the reaction. The cleaner work-up and production of fewer impurities generally gave a more crystalline final product with higher yields (≥ 85%) than previously reported (68%).[15] For these reasons, even though the reaction time is longer and heat is required, we chose to use zinc chloride as the catalyst for the Friedel-Crafts reactions. Reactions were performed under an N_2 atmosphere in a single-pot by adding a dry dichloromethane solution of ferrocene drop wise to a mixture of anhydrous zinc chloride and the tertiary chloroalkane while stirring vigorously. The mixture was then refluxed for 24 to 48 hours depending on the chain length of the alkyl chloride. Following work-up with 1 M HCl, 1 M NaOH, and water, the product was

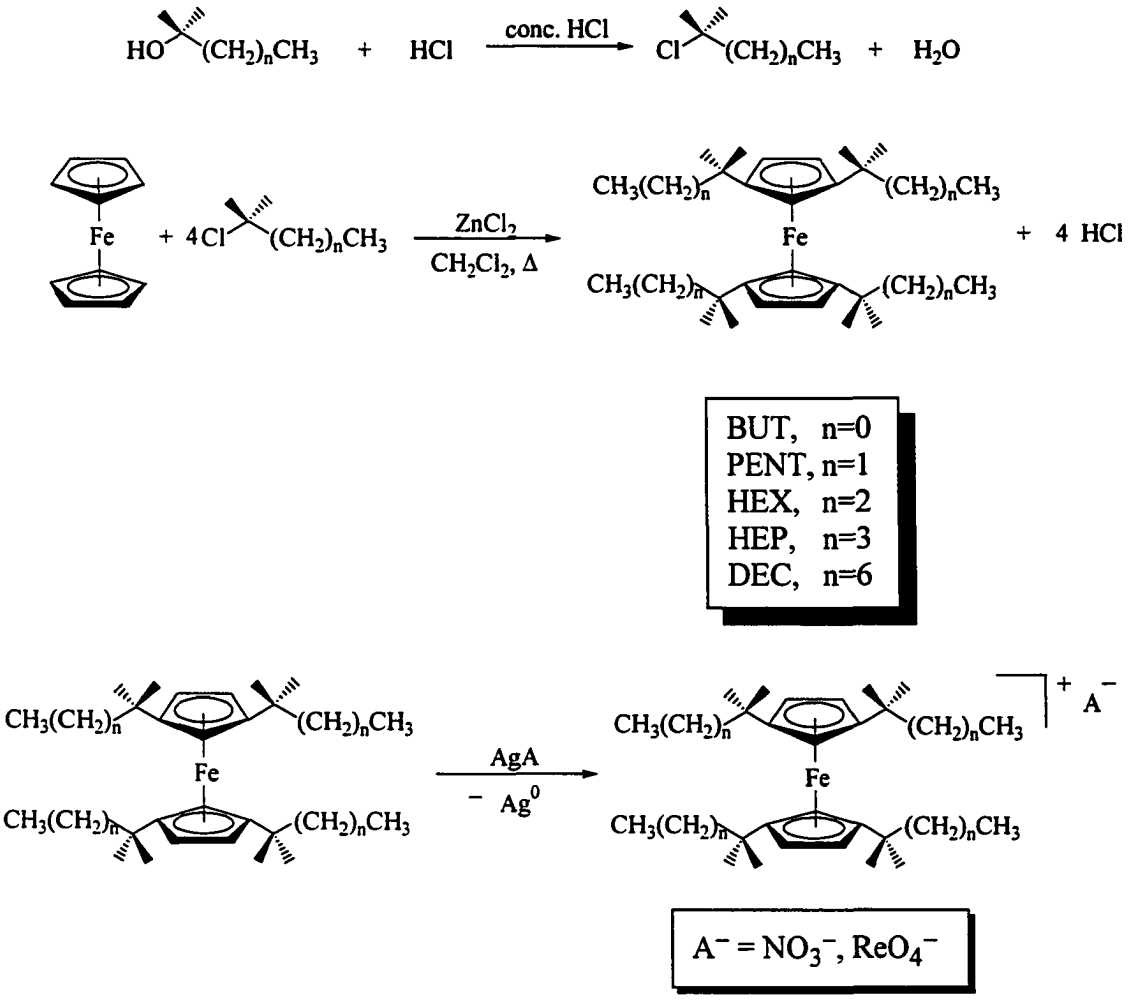

Scheme 2.1. Preparation of 1,1',3,3'-tetra(2-methyl-2-alkyl)ferrocenes and ferrocenium salts. The structural isomer, BUT2, was also oxidized to its corresponding ReO_4^- and NO_3^- salts as shown in the bottom reaction.

reduced over granular zinc metal and recrystallized from ethanol. The resulting orange, needle-like crystals were pure tetraalkylated ferrocenes that are exclusively alkylated in the 1 and 3 positions of both Cp rings. Yields are typically between 80% and 90% and the resulting crystals are soluble in a variety of organic solvents, including hexanes, toluene, diethyl ether, and dichloromethane.

Oxidation of the tetraalkylated ferrocenes, also shown in Scheme 2.1, was accomplished by the reaction of a dichloromethane solution of the tetraalkylated ferrocene with an ethanolic solution of a silver(I) salt of the desired anion. After filtering off silver metal and removal of the solvent, the resulting dark green oil was washed with hexanes to remove any unoxidized tetraalkylated ferrocene. The tetraalkylated ferrocenium salt was then recrystallized from a mixture of dichloromethane and cold ether. Yields for tetraalkylated ferrocenium salts prepared in this manner are greater than 80% after recrystallization. The tetraalkylated ferrocenium salts also have good solubility in many organic solvents, including toluene, dichloromethane, benzene, and acetonitrile.

Crystals suitable for X-ray diffraction of various tetraalkylated ferrocenes and ferrocenium salts were obtained and their structures and electronic properties are described below. Novel NO_3^- and ReO_4^- salts of all the tetraalkylated ferrocenes discussed in this work with the 1,1',3,3'-alkylation pattern were isolated as pure, crystalline compounds. Crystals of HEP and DEC suitable for single-crystal X-ray diffraction were grown from absolute ethanol and a mixture of dichloromethane and acetonitrile, respectively. Crystals of $HEP^+NO_3^-$ suitable for single-crystal X-ray diffraction were grown from toluene. Crystals of $DEC^+NO_3^-$ suitable for single-crystal X-ray diffraction were grown from chlorobenzene. Crystals of $BUT^+ReO_4^-$suitable for single-crystal X-ray diffraction were grown from acetone. In the case of $BUT^+ReO_4^-$, the crystals contained one molecule of acetone per formula unit. None of the other compounds investigated crystallized with the inclusion of solvent molecules. In addition, the 1,1',2,2'-tetra-*t*-butylferrocene (BUT2), prepared previously by Hughes *et. al.*,[14] was

isolated as a nitrate and perrhenate salt by the methods described above. Crystals of $BUT2^{+}ReO_4^{-}$ suitable for single-crystal X-ray diffraction were grown from acetone.[17] Details of the structure determinations, data collections, and refinements for all compounds crystallized in our labs are provided in Table 2.1 and Appendix A.

Structures of New Tetraalkylated Ferrocenes. New structures of neutral tetraalkylated ferrocenes were obtained in this study for HEP and DEC. The structure of a full molecule of HEP is shown in Figure 2.1 and selected bond distances and angles are listed in Table 2.2. The crystal of HEP obtained was a racemic twin and crystallized in the orthorhombic space group *Fdd2*. The asymmetric unit contains one independent half-molecule of HEP that contains half of the iron(II) atom on a two-fold axis, two partial Cp rings consisting of two and three carbon atoms, and two alkyl chains, one each attached to each partial Cp ring. Diagrams of the asymmetric unit of HEP can be seen in Appendix A. Eight symmetry related molecules are contained in the unit cell ($Z = 8$) and the structure of the full molecule is subsequently generated by symmetry operations as described in Appendix A.

The structure of DEC also contains one independent half-molecule in the asymmetric unit. The half-molecule of DEC, however, crystallized in the centrosymmetric space group *C2/c*. The half molecule of DEC differs from that of HEP in that it contains half of the iron(II) atom on a two-fold axis, and one full Cp ring with two covalently attached alkyl chains. Diagrams of the asymmetric unit can be seen in appendix A. Four symmetry related molecules are contained in the unit cell ($Z = 4$) and the structure of the full molecule is subsequently generated by symmetry operations as described in Appendix A. The structure of a full molecule of DEC is shown in Figure 2.2 and selected bond distances and angles are listed in Table 2.3. Table 2.4 shows other structural parameters of interest for both HEP and DEC and the other tetraalkylated ferrocenes and ferrocenium salts discussed in this work.

Before this work, the only 1,1',3,3'-tetra-*t*-alkylferrocene species that had

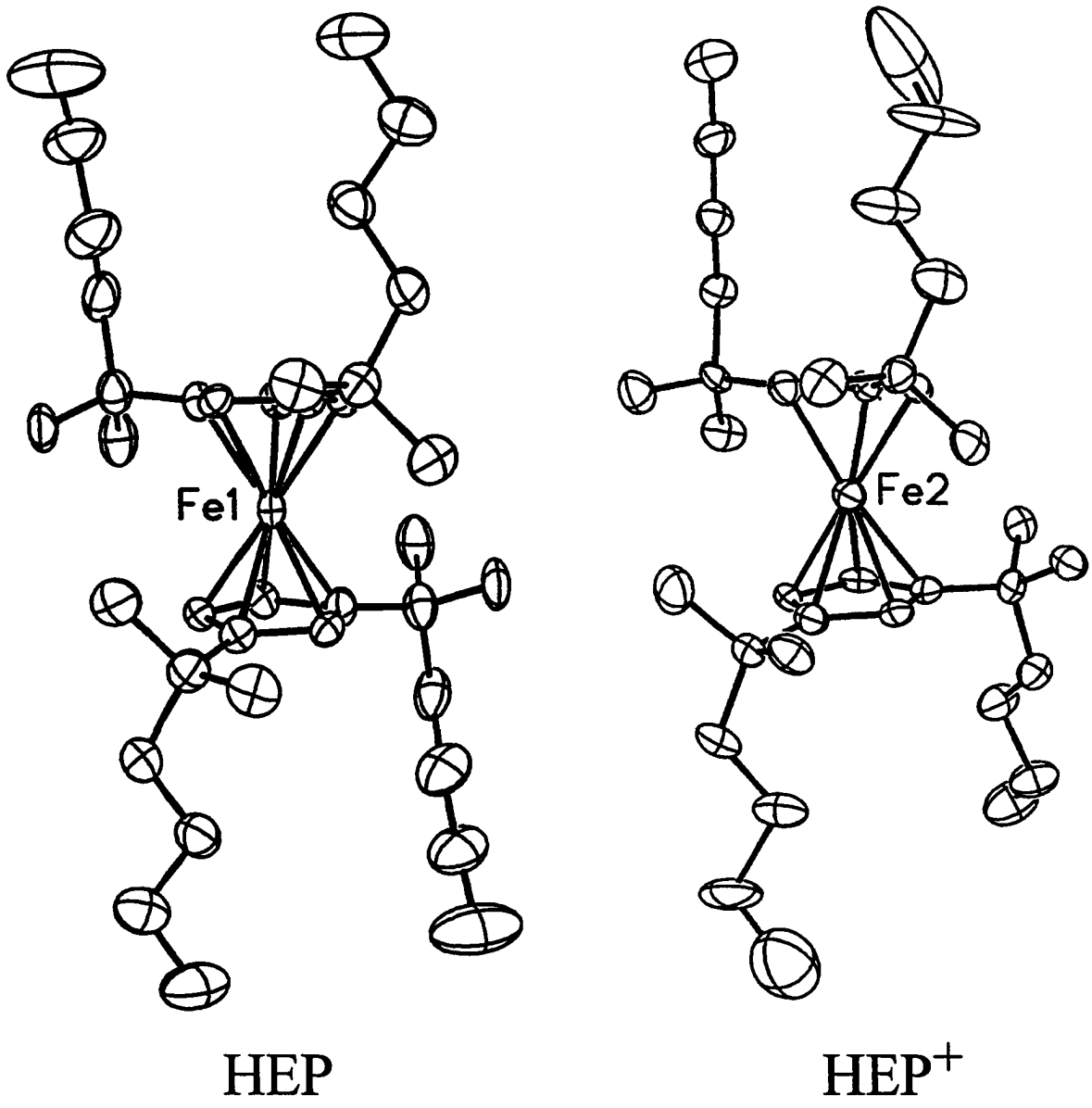

Figure 2.1. Structures of the neutral HEP molecule (50% probability ellipsoids, left) and one of the unique HEP^+ cations from the $HEP^+NO_3^-$structure (50% probability ellipsoids, right). Hydrogen atoms have been omitted for clarity. The structure of $HEP^+NO_3^-$ was obtained by Mr. Dustin L. Clark.[18]

Table 2.2. Selected bond distances (Å) for HEP.[a]

Fe1–C1	2.052(5)	Fe1–C2	2.019(6)
Fe1–C3	2.044(5)	Fe1–C4	2.105(6)
Fe1–C5	2.070(5)		

[a] One estimated standard deviation is shown in parentheses.

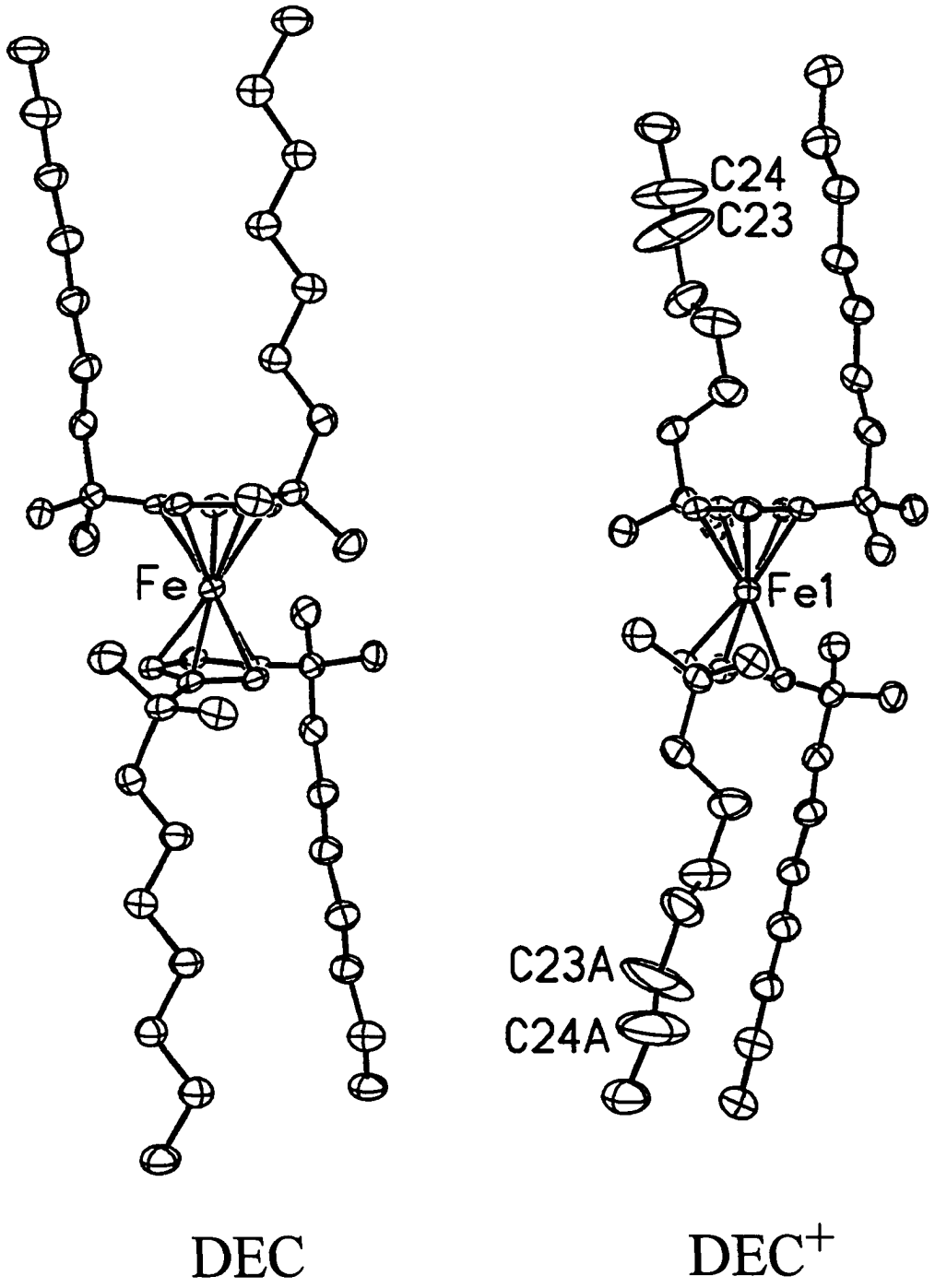

Figure 2.2. Structures of the neutral DEC molecule (50% probability ellipsoids, left) and the DEC^+ cation (50% probability ellipsoids, right) from the $DEC^+NO_3^-$ structure. Hydrogen atoms have been omitted for clarity.

Table 2.3. Selected bond distances (Å) for DEC.[a]

Fe–C1	2.100(3)	Fe–C2	2.058(3)
Fe–C3	2.054(3)	Fe–C4	2.037(3)
Fe–C5	2.059(3)		

[a] One estimated standard deviation is shown in parentheses.

Table 2.4. Structural parameters for tetraalkylated ferrocenes and ferrocenium cations.[a]

parameter	DEC	DEC^+	HEP	HEP^+	BUT[b]	BUT^+	BUT2[c]	$BUT2^+$
ave. R(Fe–C) (Å)	2.062(3)	2.111(3)	2.058(6)	2.107(7),2.108(7) 2.109(7),2.112(7)	2.063(2),2.063(2)	2.113(8),2.112(8)	2.061(4)	2.113(5),2.110(5), 2.107(5), 2.110(5)
ave. R(Fe–Ct) (Å)	1.670	1.731	1.667	1.726, 1.727 1.733, 1.730	1.670, 1.668	1.730, 1.730	1.664	1.722, 1.725
Ct–Fe–Ct' (deg.)	174.1	175.6	174.4	173.7, 174.7	174.5, 174.6	174.7	180	179.4, 179.2
interplane angle (deg.)	8.7	9.1	9.5	9.9, 11.1	8.3, 8.9	11.6	0	1.2, 1.0
Fe–Ct–C (deg.)	88.6–91.6	87.5–92.3	88.3–92.0	87.0–92.5	88.5–91.6	86.5–93.2	—	88.0–91.7

[a] All data is from this work unless otherwise noted. One estimated standard deviation is shown in parentheses. [b] Reference 22. [c] Reference 14.

been structurally characterized was the neutral compound BUT. The structure of this compound was first reported by Kalushi *et al.* in 1972[21] and was re-determined by Boese *et al.* in 1993.[22] There are two unique but very similar molecules in the asymmetric unit; each of the two iron atoms sits on a crystallographic two-fold axis, as was observed for both HEP and DEC. The most interesting feature of this structure is that the dialkylated cyclopentadienyl (Cp') rings within each ferrocene molecule are not co-planar; the two interplane angles are 8.3° and 8.9°. Similar interplane angles have been previously reported for substituted ferrocenes.[23] Similarly, the interplane angles for the two discrete molecules in the HEP unit cell are 9.2 and 9.3° and the interplane angle for DEC is 8.7°. The interplane angles for the neutral 1,1',3,3'-tetra-*t*-alkylferrocenes described in this study range from 8.3 – 9.5° in comparison to a range of 9.1 – 11.6° for the 17 electron 1,1',3,3'-tetra-*t*-alkylferrocenium cations. This may be due in part to the longer Fe–C bonds observed for the cations. The longer Fe–C bonds allow for a greater interplane angle and thus, greater relief from the steric strain present due to the interaction of *t*-alkyl groups on the two Cp' rings in a single molecule. The average Fe–C of 2.062(3) Å and 2.058(6) Å for DEC and HEP respectively, are shorter than those of their corresponding cations. The average Fe–C bond length is 2.111(3) Å for $DEC^+NO_3^-$ and 2.109(7) Å for $HEP^+NO_3^-$. The same trend is observed for BUT[21,22] and $BUT^+ReO_4^-$ with average Fe–C distances of 2.063(8) Å and 2.113(8) Å respectively.

Structures of New Tetraalkylated Ferrocenium Salts. The structure of the BUT^+ cation from the $BUT^+ReO_4^-$·acetone structure is shown in Figure 2.3. The asymmetric unit consists of a discrete BUT^+ cation and a ReO_4^- anion separated by more than 6 Å and a noninteracting molecule of acetone (the closest approach of the acetone oxygen atom to any non-hydrogen atom of the ferrocenium cation is 3.82 Å to C13, one of the methyl carbon atoms). Selected bond distances and angles are listed in Table 2.5. The bond distances and angles for the virtually tetrahedral ReO_4^- anion and the molecule of acetone are normal.

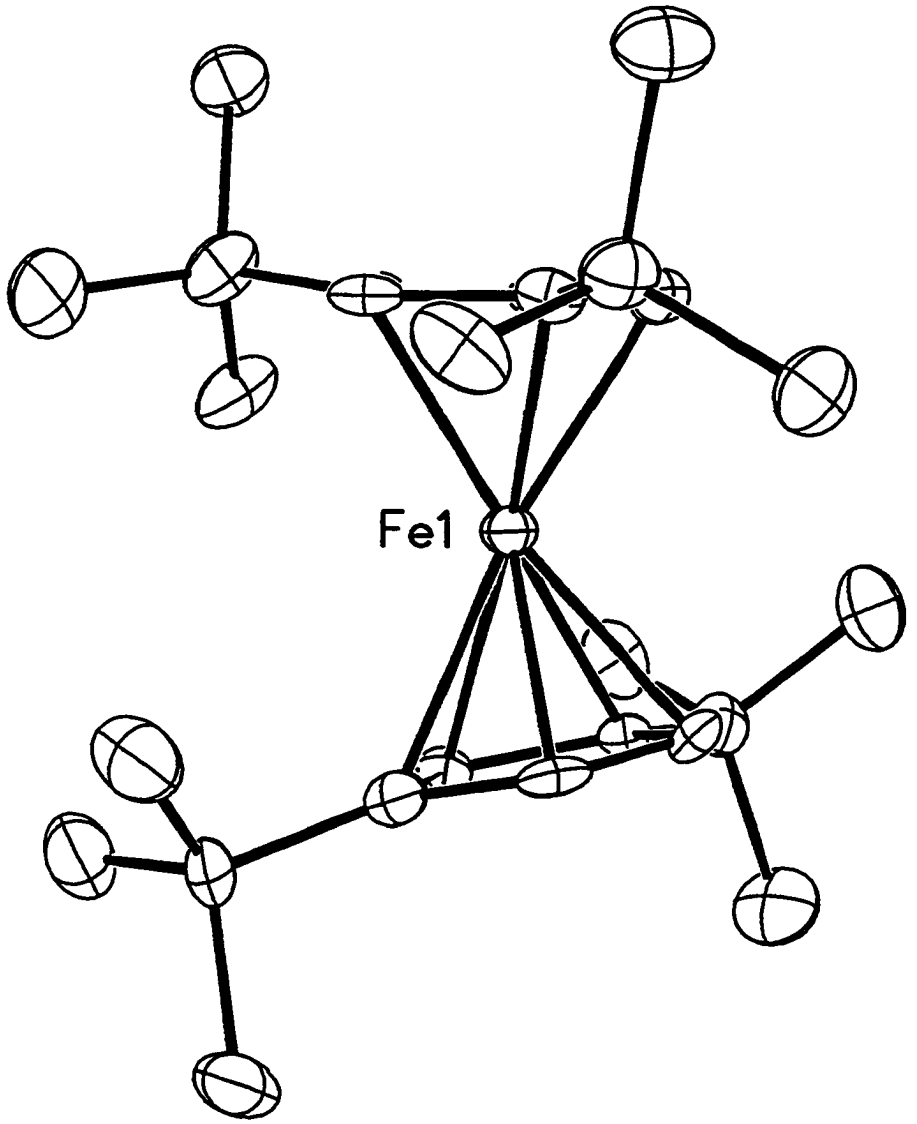

Figure 2.3. Structure of the BUT^+ cation from the $BUT^+ReO_4^-$·acetone structure (50% probability ellipsoids). Hydrogen atoms have been omitted for clarity. The structure of $BUT^+ReO_4^-$·acetone was obtained by Dr. Alexander E. Gash.[18]

Table 2.5. Selected bond distances (Å) and angles (deg) for $BUT^{+}ReO_4^{-}$·acetone.[a]

Fe–C1	2.149(8)	Fe–C2	2.077(7)
Fe–C3	2.049(6)	Fe–C4	2.121(7)
Fe–C5	2.166(6)	Fe–C6	2.177(7)
Fe–C7	2.152(7)	Fe–C8	2.161(7)
Fe–C9	2.075(7)	Fe–C10	2.057(7)
Re–O1	1.698(8)	Re–O2	1.718(7)
Re–O3	1.734(7)	Re–O4	1.702(8)
C27–C29	1.49(2)	C28–C29	1.44(2)
C29–O5	1.20(1)	O–Re–O	107.0(5)–111.8(7)
C27–C29–O5	121.0(1)	C28–C29–O5	119.5(1)
C27–C29–C28	119.3(1)		

[a] One estimated standard deviation is shown in parentheses.

Unlike the structure of neutral HEP, which only contained half of a molecule in the asymmetric unit, the structure of $HEP^+NO_3^-$ consists of two discrete HEP^+ cations and two discrete NO_3^- anions in the asymmetric unit. The structure of one of the HEP^+ cations is shown in Figure 2.1. Selected bond distances and angles are listed in Table 2.6. The bond distances and angles for the virtually planar NO_3^- anions are normal.

Similar to the structure of its neutral counterpart DEC, the structure of $DEC^+NO_3^-$ contains only half of a DEC^+ cation and half of a NO_3^- anion in the asymmetric unit. As with DEC, $DEC^+NO_3^-$ is centrosymmetric and the partial iron(III) atom again sits on a two-fold axis. Selected bond distances and angles for the $DEC^+NO_3^-$ asymmetric unit are listed in Table 2.7. A full molecule of $DEC^+NO_3^-$ can be generated by symmetry operations as described in Appendix A and the full molecular structure of the DEC^+ cation is shown in Figure 2.2. The asymmetric unit can be seen in Appendix A. Bond distances and angles for the planar NO_3^- anion are normal.

The unique interplane angle in $BUT^+ReO_4^-$·acetone is 11.6° and in $DEC^+NO_3^-$ is 9.1°. The two interplane angles of the two discrete cations in the $HEP^+NO_3^-$ structure are 9.9° and 11.1°. Clearly, an interplane angle of > 8° is a common feature of 1,1',3,3'-tetra-*t*-alkylferrocene species, with the interplane angles for the tetraalkylated ferrocenium salts being larger than those of their neutral counterparts as discussed above.

The structure of the $BUT2^+$ cation from the $BUT2^+ReO_4^-$ structure is shown in Figure 2.4.[17] Selected bond distances and angles for $BUT2^+$ are listed in Table 2.8. Like $HEP^+NO_3^-$, the structure of $BUT2^+ReO_4^-$ contains two full $BUT2^+$ cations and two full ReO_4^- anions in the asymmetric unit. For comparison, the structure of the neutral compound, BUT2, contains one independent half-molecule in the asymmetric unit, which resides on an inversion center.[14] The bond distances and angles for the virtually tetrahedral ReO_4^- anions are normal.

In comparison to the three structures of the ferrocenium cations with 1,1',3,3'-alkylation pattern, the two Cp' rings within each ferrocenium moiety of $BUT2^+ReO_4^-$,

Table 2.6. Selected bond distances (Å) and angles (deg) for $HEP^{+}NO_3^{-}$.[a]

Fe1–C11	2.130(7)	Fe1–C12	2.139(7)
Fe1–C13	2.134(7)	Fe1–C14	2.058(7)
Fe1–C15	2.076(7)	Fe1–C16	2.118(7)
Fe1–C17	2.130(7)	Fe1–C18	2.156(7)
Fe1–C19	2.080(7)	Fe1–C20	2.056(7)
Fe2–C1	2.137(7)	Fe2–C2	2.139(7)
Fe2–C3	2.127(7)	Fe2–C4	2.065(7)
Fe2–C5	2.077(7)	Fe2–C6	2.157(7)
Fe2–C7	2.096(7)	Fe2–C8	2.069(7)
Fe2–C9	2.113(7)	Fe2–C10	2.127(7)
N1–O1	1.258(8)	N1–O2	1.255(8)
N1–O3	1.242(8)	N2–O4	1.227(8)
N2–O5	1.239(8)	N2–O6	1.260(8)
O–N–O	119.4(8)–120.5(7)		

[a] One estimated standard deviation is shown in parentheses.

Table 2.7. Selected bond distances (Å) and angles (deg) for $DEC^{+}NO_3^{-}$.[a]

Fe–C1	2.161(3)	Fe–C2	2.123(3)
Fe–C3	2.119(3)	Fe–C4	2.063(3)
Fe–C5	2.090(3)	N1–O1	1.250(5)
N1–O1, N1–O2	1.238(3)	O1–N–O2	119.5(3)
O1–N–O2'	119.5(3)	O2–N–O2'	121.0(3)

[a] One estimated standard deviation is shown in parentheses.

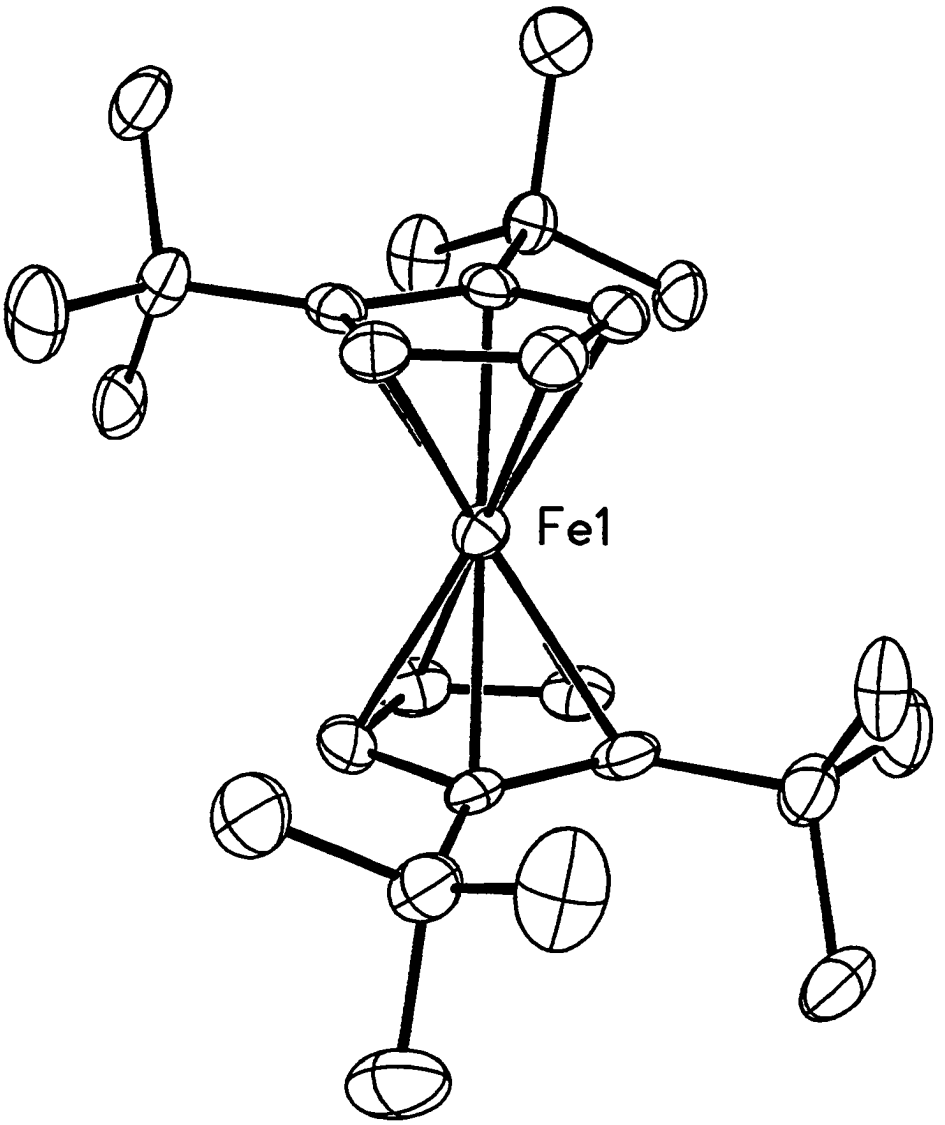

Figure 2.4. Structure of one of the unique $BUT2^{+}$ cations from the $BUT2^{+}ReO_4^{-}$ structure (50% probability ellipsoids). The interplane angle of the two Cp' rings is only 1.2°. The interplane angle observed for the neutral BUT2 molecule is 0° (ref. 14). The structure of $BUT2^{+}ReO_4^{-}$ was obtained by Dr. Kristina M. Gansle.[17]

Table 2.8. Selected bond distances (Å) and angles (deg) for $BUT2^{+}ReO_4^{-}$.[a]

Fe1–C1	2.144(5)	Fe1–C2	2.154(5)
Fe1–C3	2.102(5)	Fe1–C4	2.086(5)
Fe1–C5	2.077(5)	Fe1–C6	2.126(5)
Fe1–C7	2.146(5)	Fe1–C8	2.113(5)
Fe1–C9	2.082(5)	Fe1–C10	2.084(5)
Fe2–C27	2.155(5)	Fe2–C28	2.128(5)
Fe2–C29	2.071(5)	Fe2–C30	2.073(5)
Fe2–C31	2.107(5)	Fe2–C32	2.153(5)
Fe2–C33	2.142(5)	Fe2–C34	2.084(5)
Fe2–C35	2.079(5)	Fe2–C36	2.093(5)
Re1–O1	1.702(5)	Re1–O2	1.703(6)
Re1–O3	1.700(4)	Re1–O4	1.718(5)
Re2–O5	1.718(5)	Re2–O6	1.721(4)
Re2–O7	1.732(5)	Re2–O8	1.721(4)
O–Re1–O	107.8(3)–112.1(3)	O–Re2–O	108.4(3)–110.3(3)

[a] One estimated standard deviation is shown in parentheses.

which has a 1,1',2,2'-alkylation pattern, are co-planar to within ~1°. The 1,1',2,2'-alkylation pattern allows the *t*-butyl substituents on one ring to avoid a close approach with the *t*-butyl substituents on the other ring, as can be seen in Figure 2.4, thus enabling the Cp' rings to remain parallel to one another. In comparison with the structure of neutral BUT2,[14] there are small interplane angles of 1.2° and 1.0° between the Cp' rings for the two unique $BUT2^+$ cations in the asymmetric unit. The structure of neutral BUT2 has a Cp' interplane angle of 0°.

Relevant distances and angles for the structures of these tetraalkylated ferrocenium salts are listed in Table 2.4. In addition to the longer Fe–C bond lengths described above, the Fe–Ct distances (Ct = the centroid of the five carbon atoms that comprise an individual Cp' ring) in the 17-electron complexes DEC^+, HEP^+, and BUT^+ are also longer than in the 18-electron complexes DEC, HEP, and BUT. Furthermore, the ranges of Fe–C distances in DEC^+, HEP^+ and BUT^+ are wider than those in neutral DEC, HEP and BUT, as shown in Figure 2.5. These observations are also true when the structures of $BUT2^+$ vs. BUT2 are compared. The longer average Fe–C distances for the ferrocenium cations relative to the corresponding ferrocene is due to fact that the HOMO of ferrocene is an Fe–C bonding MO.[24] This does not, however, explain the wider range of Fe–C distances for a ferrocenium cation relative to its homologous ferrocene. There appears to be a greater degree of "ring slippage" in the ferrocenium cations; that is, the iron atom is not along the vector that passes through the centroid (Ct) of the Cp' ring and is perpendicular to the least-squares plane of the ring, as shown in Figure 2.6. For reasons that are not clear at this time, the displacement of the iron atom from this vector is greater for $Fe(Cp')_2^+$ than for $Fe(Cp')_2$. The ranges of Fe–Ct–C angles for each structure are listed in Table 2.4. As might be expected from the drawing in Figure 2.6, there is a correlation between the Fe–Ct–C angle and the Fe–C distance for a given carbon atom, as shown for DEC^+, HEP^+ and BUT^+ in Figure 2.7. The smaller the Fe–C distance for a given carbon atom, the smaller the Fe–Ct–C angle. Interestingly, the

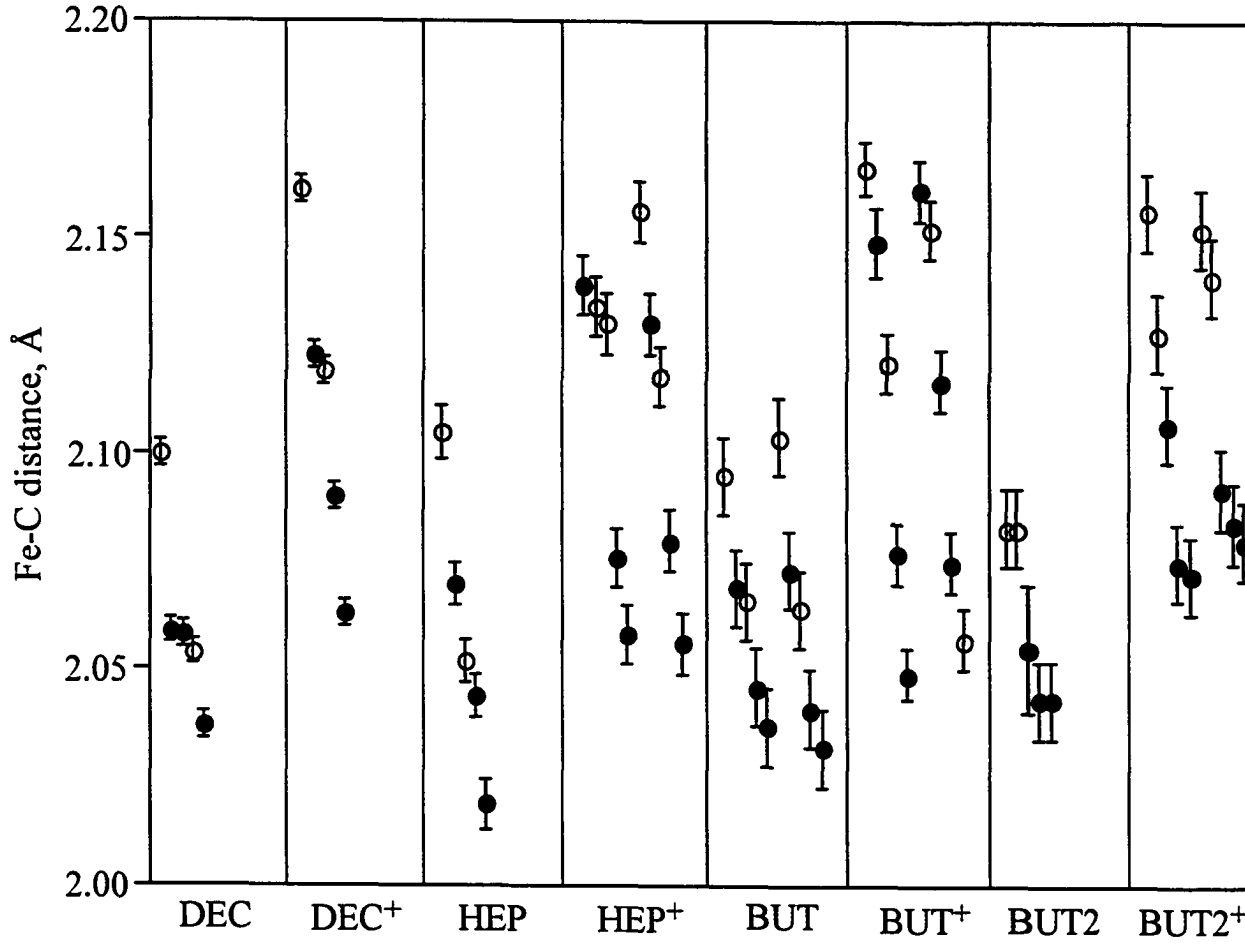

Figure 2.5. Distribution of the Fe–C distances for the tetraalkylated ferrocenes and ferrocenium salts. Open circles indicate the alkylated Cp' carbon atoms. The errors bars shown represent ± 3σ.

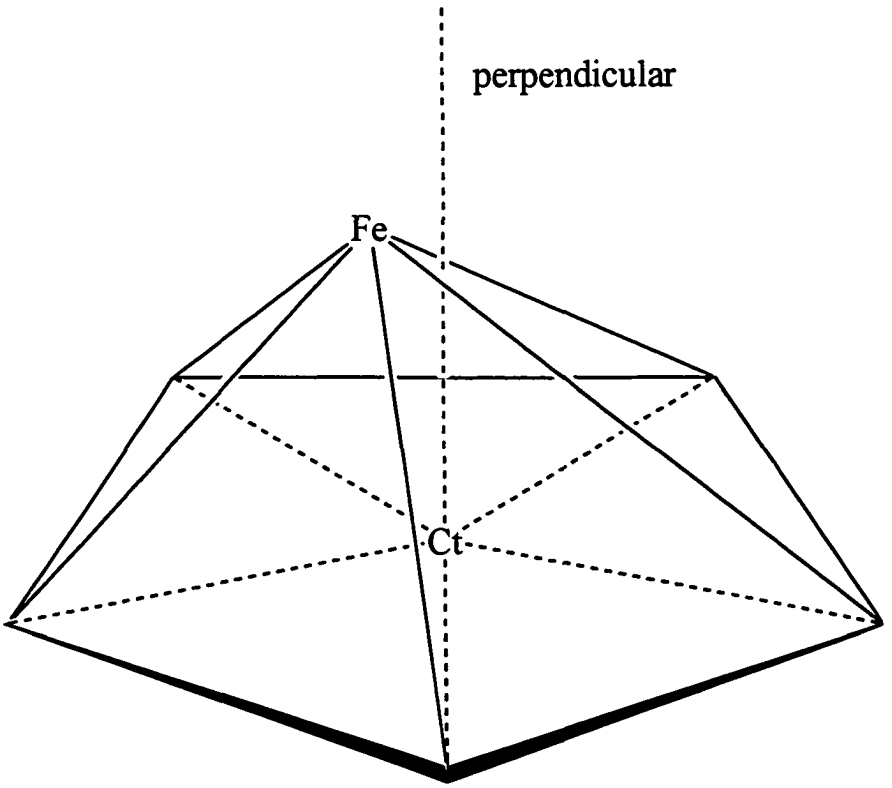

Figure 2.6. The geometric orientation of the iron atom relative to the perpendicular to the Cp' plane that passes through the centroid (Ct) of the plane.

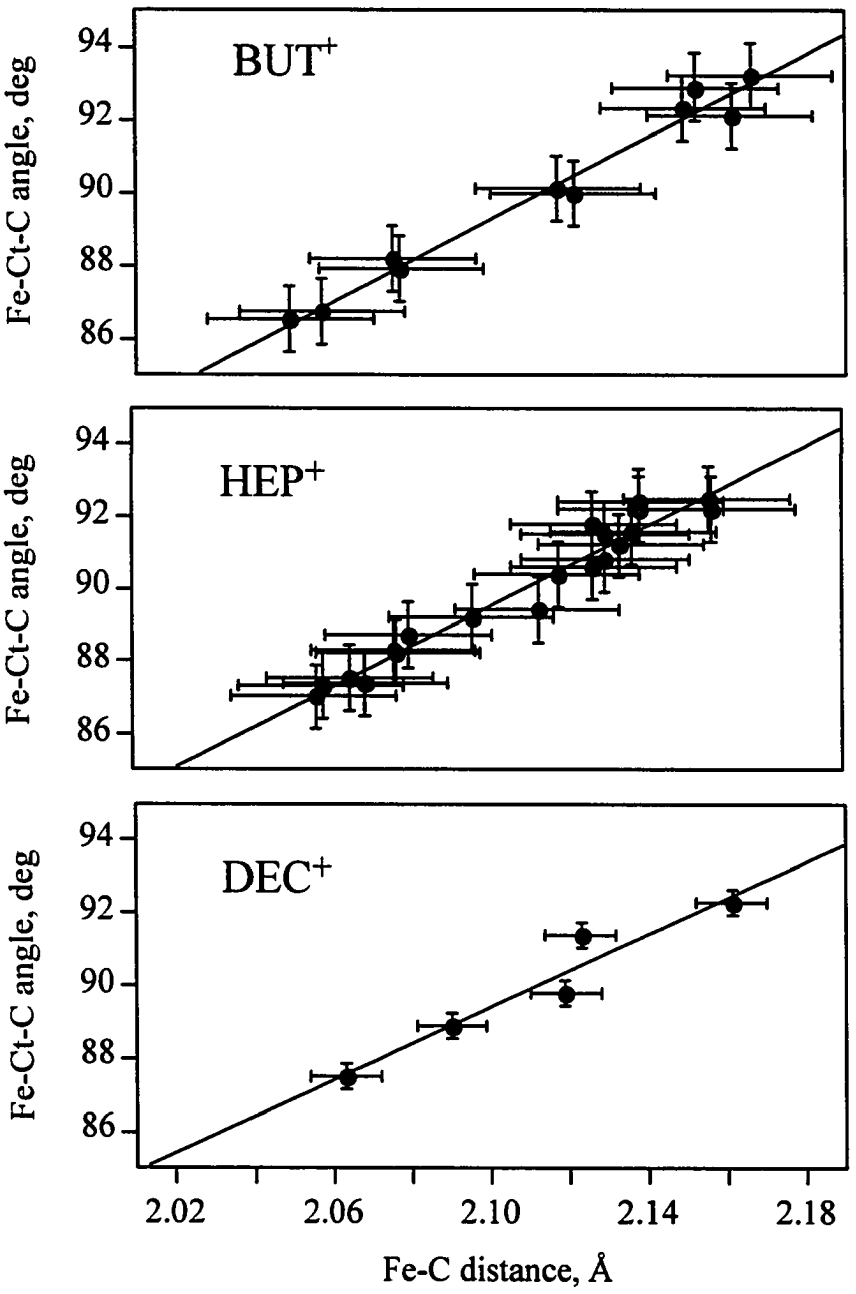

Figure 2.7. Graphs showing the correlation between Fe–Ct–C angle and Fe–C bond distance for BUT^+, HEP^+, and DEC^+. The errors bars shown represent ± 3σ.

carbon atoms in the Cp' rings that are bonded to the alkyl chains may influence the Fe–C distance and Fe–Ct–C angle. As can be seen in Figure 2.5, the presence of an alkyl chain bonded to a Cp ring carbon tends to favor a longer Fe–C bond distance for the tetraalkylated ferrocenium salts. In contrast, the neutral tetraalkylated ferrocenes have a wider distribution of Fe–C distances for Cp' carbon atoms with alkyl chains.

Layered Ferrocene Structures. Unlike the other neutral and cationic tetraalkylated ferrocene and ferrocenium structures obtained in this study, DEC and $DEC^{+}NO_3^{-}$ have layered packing structures. In contrast, the crystal packing structure of HEP, for example, consists of rows of ferrocene centers, but the alkyl chains of individual rows are staggered between those of HEP molecules from other rows. The DEC and $DEC^{+}NO_3^{-}$ crystal packing structures consist of discrete layers of DEC molecules or cations in which the alkyl chains of a single DEC molecule are interdigitated only with the alkyl chains of DEC molecules in the same layer.

The extended structure of DEC is shown in Figure 2.8. In the extended structure of neutral DEC, by defining the plane containing the iron atoms as the center of a layer, the center-to-center distance between layers is 9.38 Å. The closest approach of atoms between two layers is 2.44 Å between two hydrogen atoms of two methyl groups. In a single layer, the closest approach of iron(II) centers is 8.74 Å in the *b* direction. Iron(II) centers of different layers form a plane parallel to the *ab* plane and the closest approach between iron(II) centers of different layers is 10.35 Å in the *a* direction. Iron(II) atoms of every fifth layer are directly in line with one another in a direction that runs perpendicular to the individual layers. Between two adjacent layers, the iron (II) centers of closest proximity in the *ab* plane are offset from each other by 4.37 Å in the *b* direction due to the interaction of methyl groups between the alkyl chains of the two layers. The offset distance of 4.37 Å is exactly half the distance between iron(II) centers in a single layer, and thus creates layers in which each DEC molecule lies halfway between two other DEC molecules above and below in adjacent layers (i.e., each layer is staggered from the layers

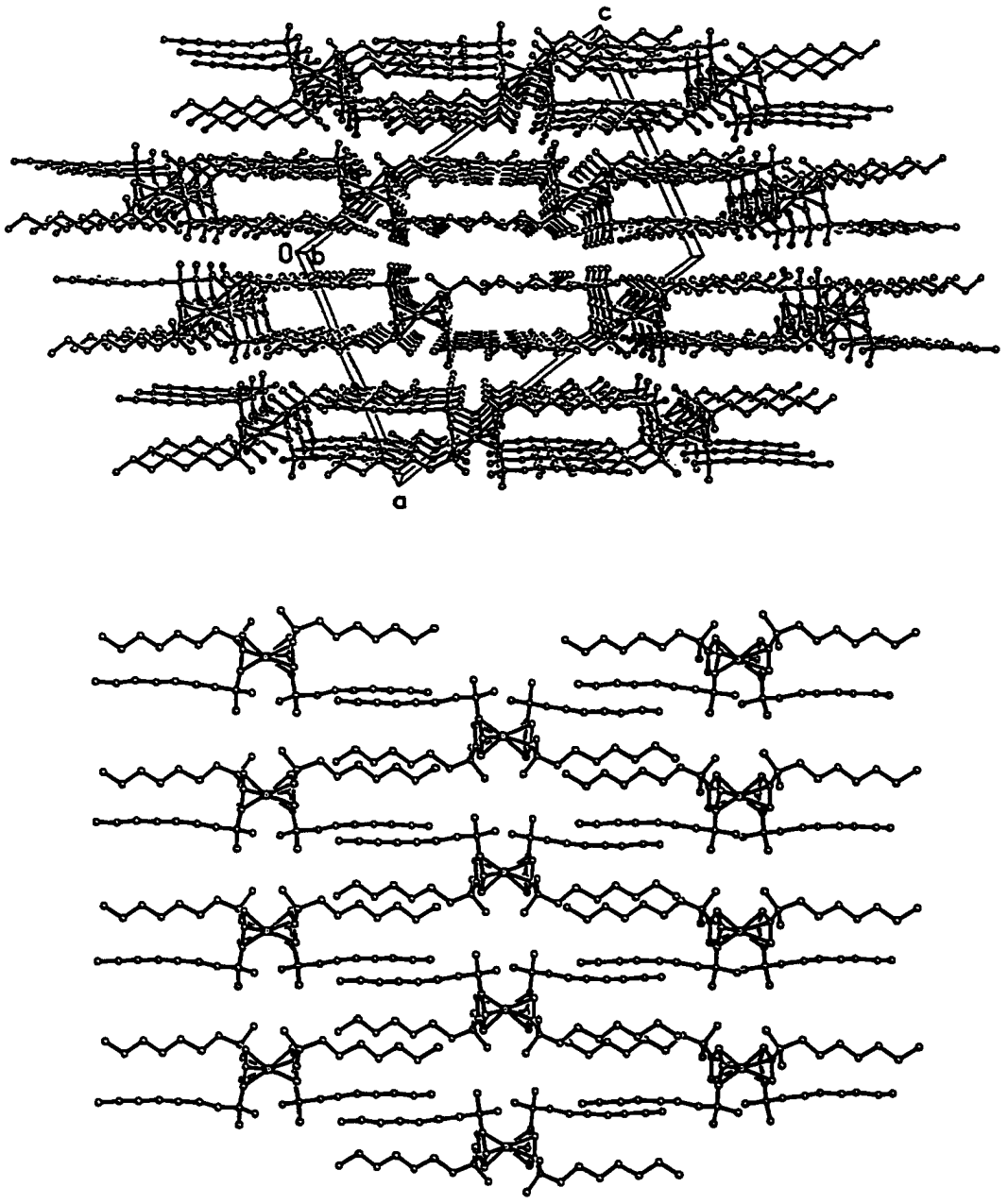

Figure 2.8. The solid state packing diagram of DEC showing the layered structure and 3-demensional channels (top) formed by the alkyl chain interdigitation within a single layer (bottom; viewed from above a single layer). The atoms shown are of arbitrary size and the hydrogen atoms have been omitted for clarity.

above and below it by 4.37 Å). As a result, the iron(II) centers of three adjacent layers form a perfect hexagon in the *ab* plane. This "pseudo hexagonal packing" of the iron(II) centers is shown in Figure 2.9. No deviation from the plane formed by these 7 iron(II) atoms is observed.

A single layer of DEC molecules consists of rows of DEC molecules that are packed end-on-end with adjacent rows of DEC molecules. As is the case between layers, the rows in a single layer are staggered from each other by 4.37 Å in the *b* direction. This results in the alkyl chains of a single DEC molecule being interdigitated with those of four surrounding DEC molecules from the same layer (Figure 2.8, bottom). The result is channels formed by the alkyl chains of the DEC molecules of the end-on-end rows in a single layer. The channels formed run the length of a single layer in the *b* direction (Figure 2.8, top) and are approximately 8.86 x 0.21 Å.

In addition to the formation of channels, the interdigitation of alkyl chains in a single layer displays a highly ordered packing of the alkyl chains. The alkyl chains of end-on-end DEC molecules pack in an alternating pattern in which the planes containing the carbon atoms of each adjacent alkyl chain are exactly perpendicular to each other. This highly ordered packing is best viewed in Figure 2.8 down the *b* axis (top) and from the top of a single layer (bottom).

The extended structure of $DEC^{+}NO_3^{-}$ is shown in Figure 2.10. As with DEC, the packing structure of $DEC^{+}NO_3^{-}$ consists of stacked layers of DEC^{+} cations, but as may be expected, when DEC is oxidized to the 17-electron cationic nitrate salt, the nitrate anions are present in the interlayer spaces. The presence of the nitrate anions between the layers, however, does not have the expected effect of making the interlayer spacing larger. Again defining the plane containing the iron(III) atoms as the center of a layer, the distance between layers is 9.13 Å, 0.25 Å shorter than that observed for neutral DEC. In addition, the closest approach between iron(III) centers of different layers is also shorter at 9.39 Å as compared to 10.35 Å for neutral DEC. This shortening of interlayer

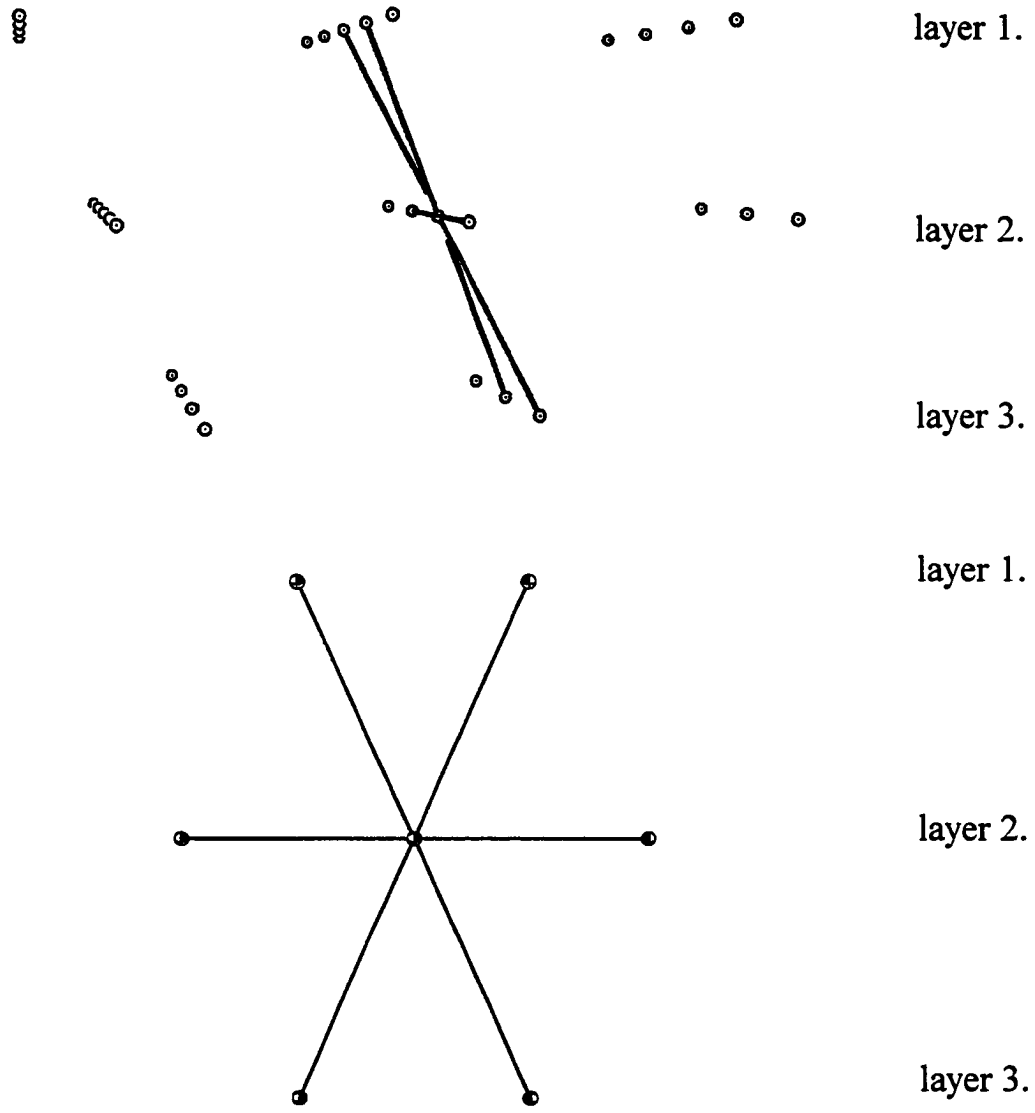

Figure 2.9. Packing diagrams showing hexagonal packing of the iron(II) atoms between three layers of DEC (top) and the "face on" view of the hexagon formed between the iron(II) atoms in the *ab* plane(bottom). The top view is the same as that seen in Figure 2.8 (top) with the hydrogen and carbon atoms omitted for clarity. Solid and dashed lines show atoms in the same plane and do not represent bonding.

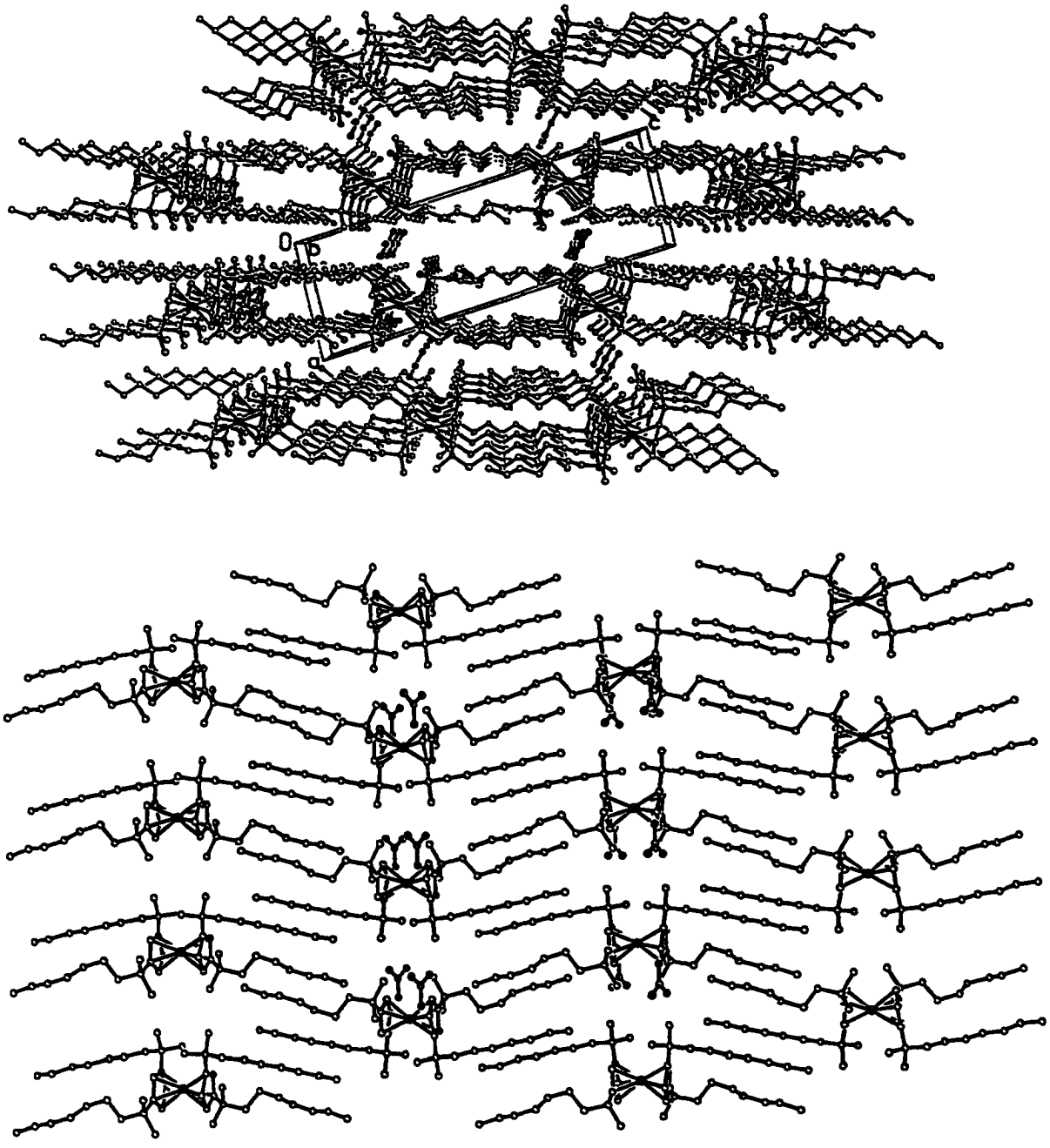

Figure 2.10. The solid state packing diagram of $DEC^{+}NO_3^{-}$. The layered structure contains nitrate anions in the interlayer spacing (top). The interdigitation of the alkyl chains within a single layer (bottom) is maintained upon oxidation of DEC to DEC^{+} despite the disorder present in some of the alkyl chains. The atoms shown are of arbitrary size and the hydrogen atoms have been omitted for clarity.

distances is due to a slightly different packing arrangement of the DEC^+ cations in each layer as compared to neutral DEC. Whereas the iron(II) centers in DEC formed a hexagon in the *ab* plane, the iron(III) centers of DEC^+ form a rectangle in the *ab* plane, as shown in Figure 2.11. No deviation from the plane formed by these 4 iron(III) atoms is observed. As a result, the DEC^+ cations of adjacent layers are stacked directly above each other instead of staggered as seen in the neutral complex. Furthermore, the nitrate anion sits in a position, which causes a different ordering of the *t*-decyl methyl groups between adjacent layers for DEC^+. The *t*-decyl methyl groups of the alkyl chains are rotated out of the interlayer spacing to avoid interaction with those in an adjacent layer. Figure 2.12 shows a diagram demonstrating the different packing arrangement of the *t*-decyl methyl groups for neutral DEC and DEC^+ cations. The *t*-decyl methyl groups in DEC are oriented towards each other and out in to the interlayer spacing due to the staggering of DEC molecules in the *b* direction between layers. The result is an alternation of methyl groups from adjacent layers in the interlayer spacing (Figure 2.8, top).

In addition to the smaller interlayer spacing, another possible result of this rotation of the *t*-decyl groups may be the disorder observed for some of the methylene carbon atoms of one alkyl chain in the DEC^+ cation. One of the alkyl chains in the half molecule of the asymmetric unit of $DEC^+NO_3^-$ contains two disordered methylene carbon atoms. The resulting full molecule generated by symmetry thus has disorder in two of its four alkyl chains. This disorder is evidenced by the large thermal ellipsoids seen for C(23), C(23A), C(24), and C(24A) in Figure 2.2.

The rotation of the *t*-decyl groups and disorder in the methylene carbon atoms may also be responsible for less organization in the interdigitation of the alkyl chains in a single layer of DEC^+ cations. The high degree of order discussed above for the packing of alkyl chains in the neutral DEC is not observed in $DEC^+NO_3^-$ as seen down the *b*-axis (Figure 2.10, top). The alkyl chains containing the disordered methylene groups are

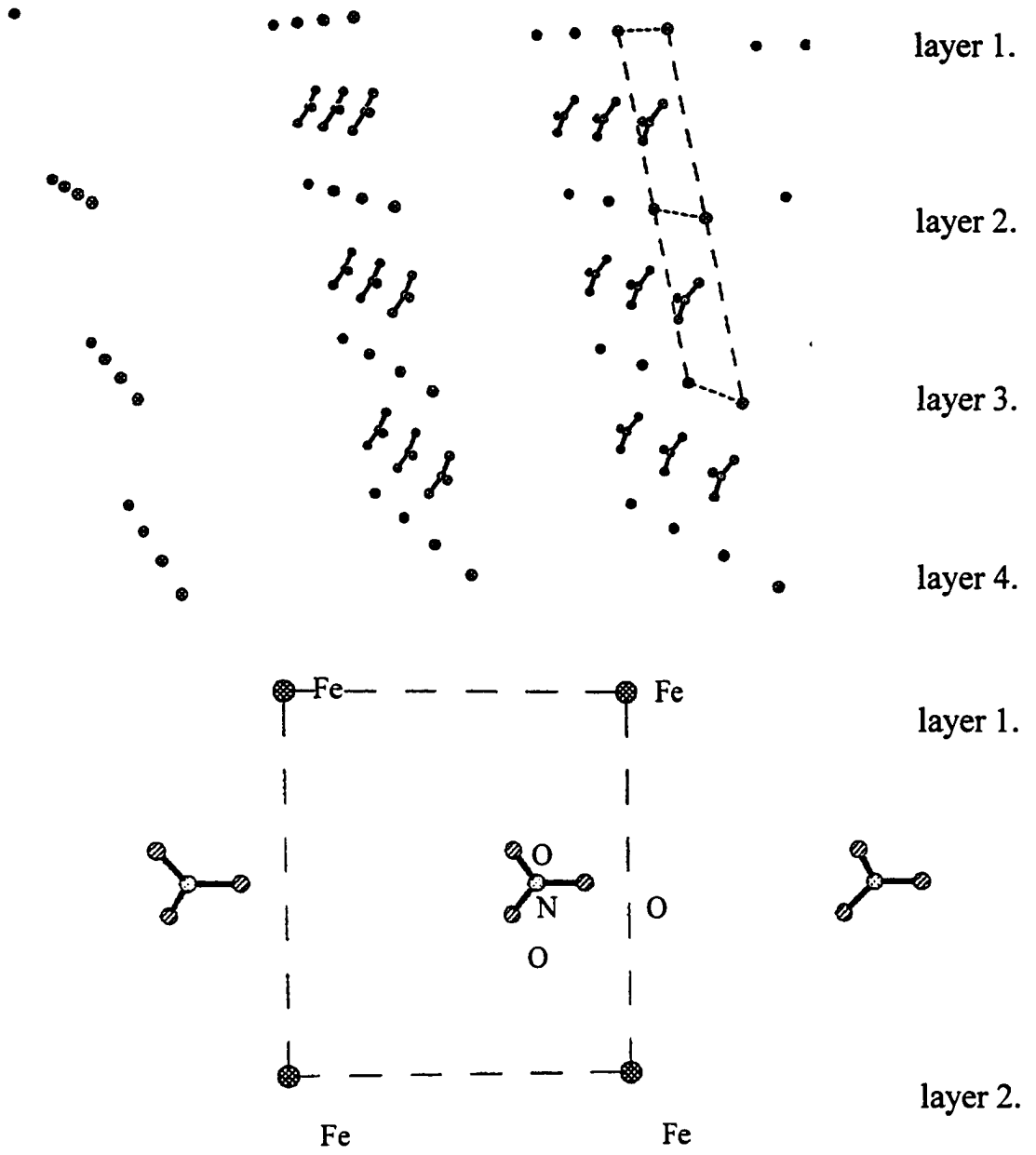

Figure 2.11. Diagrams of the packing arrangement of iron(III) atoms in $DEC^{+}NO_3^{-}$ (top) and the "face on" view of the pseudo-rectangle formed between the iron(III) atoms in the *ab* plane (bottom). Nitrate anions are also shown. The top view is the same as that seen in Figure 2.10 (top) with the hydrogen and carbon atoms omitted for clarity. Dashed lines show atoms in the same plane and do not represent bonding.

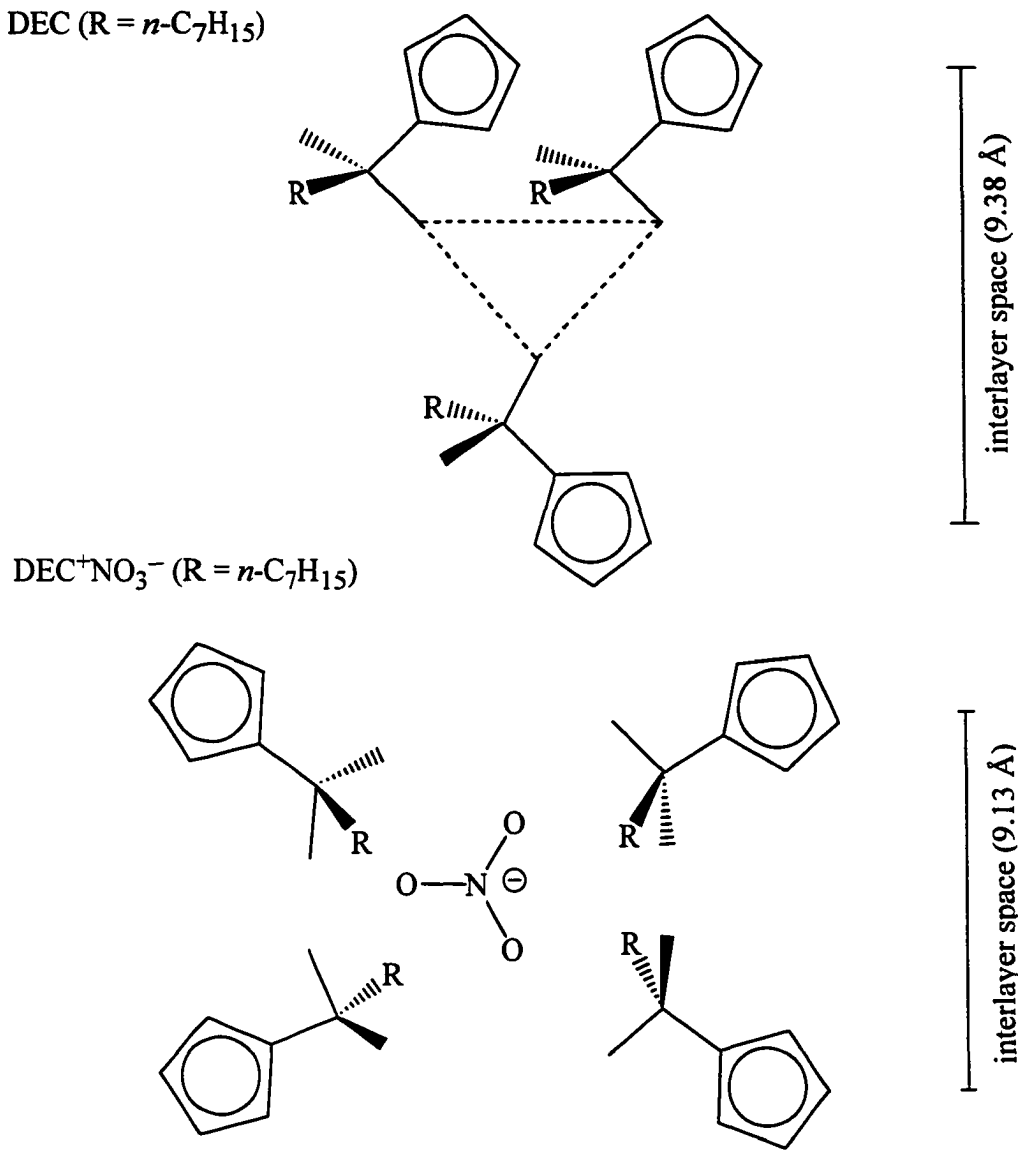

Figure 2.12. A diagram depicting the different orientations of the *t*-alkyl methyl groups in the interlayer spacing for DEC (top) and $DEC^{+}NO_3^{-}$ (bottom). Both views are down a vector bisecting the *a* and *c* axes. In this view, all of the Cp' rings shown are approximately in the plane of the page. For clarity, only Cp' rings and the closest 4 carbon atoms of the *t*-decyl chains are shown. Only one nitrate anion is included in the $DEC^{+}NO_3^{-}$ representation. The dashed lines in the DEC picture shows the alternating pattern of methyl groups (approximately in the same plane) between adjacent layers. The interlayer space shown is the distance between the planes of iron atoms in each layer.

twisted as compared to their counterparts in the neutral DEC structure. Though the packing of the alkyl chains in DEC^+ is less organized, the interdigitation of these alkyl groups still form channels similar to the ones observed in DEC. The channels formed by the interdigitation of alkyl chains of the cations are approximately 7.95 x 0.31 Å. The different channel size for DEC^+ is another result of the rotated alkyl chain and disordered methylene groups.

The closest approach of two layers in the DEC^+ structures is 0.20 Å between a hydrogen atom of a *t*-decyl methyl group and a methylene hydrogen atom in an alkyl chain. (Despite the other two shorter distances between layers discussed above, the closest approach of the layers is now larger due to the different packing arrangements between *t*-decyl methyl groups.) In a single layer, the closest approach of iron(II) centers is 8.68 Å.

Electronic Properties. Electrochemical and UV-visible data can be seen in Table 2.9. Data for $Fe(Cp)_2$ and $Fe(Cp^*)_2$ and their nitrate salts have also been included for comparison. As expected, the tetraalkylated ferrocenes are much easier to oxidize than ferrocene due to the presence of the four electron-donating alkyl groups, but they are not as easy to oxidize as decamethylferrocene. Furthermore, the number of carbon atoms in the tertiary alkyl chain does not seem to influence the half-wave potential of the ferrocene for chains containing 5 or more carbons. As can be seen, the half-wave potentials for PENT, HEX, HEP, and DEC, 5 to 10 carbons respectively, are all approximately –263 mV vs. vs. $Fe(Cp)_2^+/Fe(Cp)_2$. BUT is slightly harder to oxidize by approximately 20 mV, but there is not a large influence on the half-wave potential of the ferrocene by the number of carbons in the tertiary alkyl chain beyond the 4 carbons closest to the Cp' ring in the *t*-alkyl conformation. The positions of the alkyl groups on the Cp' rings, however, does appear to have an effect on the half-wave potential. BUT2, which is alkylated in the 1,1',2,2' positions of the Cp rings, is 54 mV harder to oxidize than BUT, which is alkylated in the 1,1',3,3' positions of the Cp rings. The reason for this is not fully

Table 2.9. Electronic properties of polyalkylated ferrocenes and ferrocenium cations.[a]

$Fe(Cp')_2$	$\lambda_{max}(Fe(Cp')_2)$ (nm)	$\varepsilon(Fe(Cp')_2)$ ($M^{-1}cm^{-1}$)[c]	$\lambda_{max}(Fe(Cp')_2^+)$ (nm)[b]	$\varepsilon(Fe(Cp')_2^+)$ ($M^{-1}cm^{-1}$)[c]	$E_{1/2}$ (V vs. $Fe(Cp)_2^+/Fe(Cp)_2$
$Fe(Cp)_2$	440 (red/orange)	97(3)	622 (blue)	—	0.000
BUT2	442 (yellow)	104(1)	674 (blue)	453(2)	–0.190
BUT	466 (orange)	158(4)	682 (green)	450(1)	–0.244
PENT	466 (orange)	166(5)	686 (green)	467(2)	–0.265
HEX	466 (orange)	171(1)	686 (green)	455(1)	–0.263
HEP	466 (orange)	174(1)	687 (green)	466(3)	–0.263
DEC	466 (orange)	179(2)	687 (green)	471(2)	–0.262
$Fe(Cp^*)_2$	424 (orange)	125(1)	778 (green)	577(2)	–0.548

[a] All $E_{1/2}$ values were determined in a dichloromethane solution of 0.1 M TBAP supporting electrolyte, 0.001 M ferrocene, and 0.001 M polyalkylated ferrocene at a scan rate of 50 mV/s with a platinum disk electrode, platinum mesh counter electrode, and a silver wire quasi-reference electrode. All UV-vis spectra were taken in a 0.001 M dichloromethane solution. [b] Spectra were taken of the nitrate salts. [c] The numbers in parentheses represent the standard deviation for three separate measurements.

understood, but may be due to less inductive electron donation from the *t*-butyl groups due to their close proximity on the Cp' ring. Since they are on adjacent carbons for BUT2, the electron donating effects may be less due to increased electron repulsion. The 1,1',3,3' substituted ferrocenes maximize the separation possible between the alkyl groups on a Cp' ring, thus minimizing electron repulsion and maximizing the amount of inductive electron donation. As a result, we see more negative half-wave potentials for 1,1',3,3' substituted ferrocenes.

UV-visible spectra of both reduced and oxidized tetraalkylated ferrocenes show similar electronic trends. All reduced ferrocenes are orange with a wavelength of maximum absorbance (λ_{max}) of approximately 466 nm, except BUT2 which has a λ_{max} of 442 nm. The nitrate salts all have $\lambda_{max}(+)$ values at about 686 nm, except $BUT2^{+}NO_3^{-}$ which has a $\lambda_{max}(+)$ of 674 nm. This red shift in λ_{max} for both oxidized and reduced BUT2 can be qualitatively explained by understanding the source of the d-d transition energies for alkyl substituted ferrocenes observed in the visible spectrum. Any perturbation to the molecular orbital energies by ring substituents will be observed in the energy of the HOMO (highest occupied molecular orbital) for each substituted ferrocene. The energies of the other unoccupied molecular orbitals do not change to any appreciable extent for alkyl substitution of a Cp ring.[25] As the electron donating ability of the substituent increases, the energy of the HOMO increases.[26] Similarly, as the electron withdrawing ability of the substituent increases, the energy of the HOMO decreases. The absorption transition of a substituted ferrocene observed in the visible spectrum arises from a d-d transition from the HOMO to an unfilled orbital. The energy gap arising from this d-d transition is smaller for ferrocenes with electron donating substituents than for ferrocenes with electron withdrawing substituents due to the relative level of the HOMO's in each case, again assuming that the energy of the unfilled orbital does not change with ferrocene substituent.

The apparent dependence of half-wave potential and λ_{max} on the substitution

pattern of the Cp' rings as well as the number of substituents on the Cp rings is further demonstrated in a plot of half-wave potential vs. $\lambda_{max}(+)$, shown in Figure 2.13. It has been confirmed that the electron donating ability of Cp ring substituents is directly related to the reduction potential of the ferrocenium salt.[27] Electron donating substituents decrease the reduction potential, while electron withdrawing substituents increase the reduction potential. During reduction of ferrocenium, an electron is much more likely to go into a low energy HOMO (e.g. a ferrocene with electron withdrawing substituents) than into a high energy HOMO (e.g. a ferrocene with electron donating substituents). The linear relationship ($R^2 = 0.99$) between reduction potential and d-d transition energy for the ferrocenium salts shown in Figure 2.13 is expected, based on the correlation between HOMO energy with both the reduction potential and d-d transition energy for the various ferrocenium salts.[28] Both ferrocene and $Fe(Cp^*)_2$ also fit well with the trends seen for the tetra-*t*-alkylated ferrocenes, demonstrating the effect that the number of Cp ring substituents has on both half-wave potential and $\lambda_{max}(+)$. Ferrocene, with no additional substituents, has the least negative reduction potential and lowest $\lambda_{max}(+)$, while $Fe(Cp^*)_2$, with the maximum number of substituents, has the most negative half-wave potential and highest $\lambda_{max}(+)$. The tetraalkylated ferrocenes prepared in this study fall between these two extremes due to the presence of four alkyl groups.

Conclusions

Tetraalkylated ferrocenes can be made in high yields and isomeric purity by Friedel-Crafts alkylation of ferrocene with tertiary chloroalkanes. The corresponding cationic ferrocenium salts are easily produced in high purity by oxidation of the neutral tetraalkylated ferrocene with silver(I) salts of NO_3^- and ReO_4^-. Despite the presence of long alkyl chains, both the tetraalkylated ferrocenes and ferrocenium salts are readily crystallized from a variety of solvents.

X-ray crystallographic structures were obtained from suitable crystals for six new tetraalkylated ferrocenes and ferrocenium salts. Several similarities were noted between

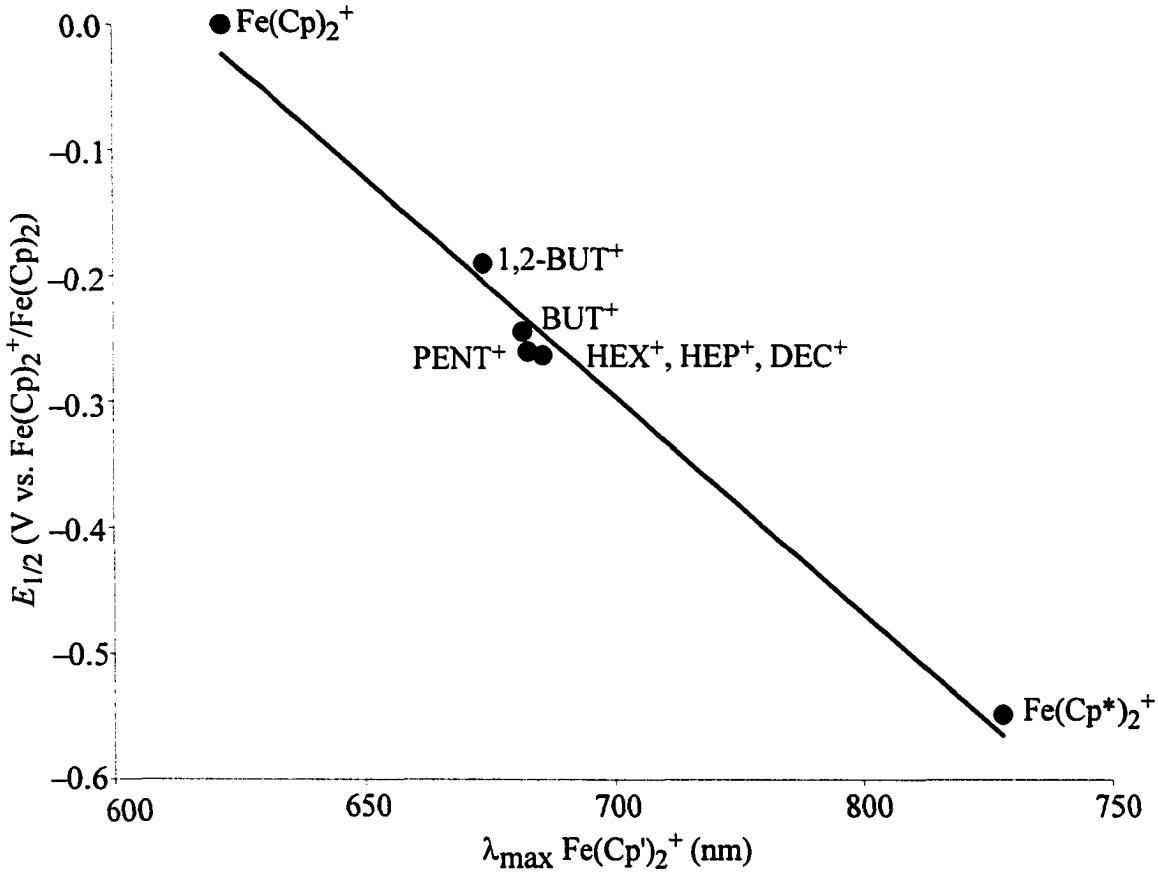

Figure 2.13. The linear relationship between the reduction potential and wavelength of maximum absorption ($\lambda_{max}(+)$) for the tetraalkylated ferrocenium nitrate salts. All $E_{1/2}$ values were determined in a dichloromethane solution of 0.1 M TBAP supporting electrolyte, 0.001 M ferrocene, and 0.001 M tetraalkylated ferrocene at a scan rate of 50 mV/s with a platinum disk electrode, platinum mesh counter electrode, and a silver wire quasi-reference electrode. All UV-vis spectra were taken in a 0.001 M dichloromethane solution. Ferrocene and decamethylferrocene have been included for comparison.

the structures of the 1,1',3,3'-alkylated ferrocenes and ferrocenium salts. All had Cp' interplane angles > than 8° and demonstrated ring-slippage from the Cp' ring centroid. Furthermore, the degree of ring slippage observed in the tetraalkylated ferrocenium cations correlated well with the Fe–C distances. These properties were in contrast with those observed for the 1,1',2,2'-tetra-*tert*-butyl ferrocene prepared previously and the 1,1',2,2'-tetra-*tert*-butyl ferrocenium perrhenate salt prepared in our laboratory. These molecules displayed interplane angles < 1° with no apparent ring-slippage. The difference in the two substitution patterns is apparently due to the 1,1',2,2'-alkylated Cp' rings to orient in a manner that prevents interaction between *t*-butyl groups of the two Cp' rings.

Finally, unique layered packing structures were observed for the two novel ferrocenyl compounds DEC and $DEC^{+}NO_3^{-}$. The packing structure of $DEC^{+}NO_3^{-}$ was similar to that seen for DEC with the NO_3^{-} anions crystallizing in the interlayer spaces. Despite the presence of NO_3^{-} anions, however, the interlayer spacing in $DEC^{+}NO_3^{-}$ was actually smaller than that observed for DEC. The smaller interlayer space appears to be the result of the alkyl chains orientation in the interlayer spacing.

References

1. Togni, A.; Hayashi, T. *Ferrocenes: Homogeneous Catalysis, Organic Synthesis, Materials Science*; VCH: New York, 1995 and references therein.
2. Geiger, W. E. *J. Organomet. Chem. Libr.* **1990**, *22*, 142.
3. King, R. B.; Bisnette, M. B. *J. Organomet. Chem.* **1967**, *8*, 287.
4. Robbins, J. L.; Edelstein, N.; Spencer, B.; Smart, J. C. *J. Am. Chem. Soc.* **1982**, *104*, 1882.
5. Clark, J. F.; Clark, D. L.; Whitener, G. D.; Schroeder, N. C.; Strauss, S. H. *Environ. Sci. Technol.* **1996**, *30*, 3124.
6. Strauss, S. H.; Odom, M. A.; Hebert, G. N.; Clapsaddle, B. J., 2001 *ATR-FTIR Detection and Quantification of Anionic Pollutants in Water.*
7. Chambliss, C. K.; Odom, M. A.; Morales, C. M. L.; Martin, C. R.; Strauss, S. H. *Anal. Chem.* **1998**, *70*, 757.
8. Chambliss, C. K.; Odom, M. A.; Martin, C. A.; Moyer, B. A.; Strauss, S. H. *Inorg. Chem. Commun.* **1998**, *1*, 435.
9. Rosenblum, M. *Chemistry of the Iron Group Metallocenes: Ferrocene, Ruthenocene, Osmocene*; John Wiley: New York, 1965.
10. Bublitz, D. E.; Rinehart, K. L., Jr. In *Organic Reactions*; John Wiley: New York, 1969; Vol. 17, pp pp23 - 32 and references therein.
11. Nesmeyanov, A. N.; Kchetkova, N. S. *Doklady Akad. Nauk SSSR* **1956**, *109*, 543.
12. Vogel, M.; Rausch, M.; Rosenberg, H. *J. Org. Chem.* **1957**.
13. Bhattacharya, S. *J. Org. Chem.* **1998**, *68*, 7101.
14. Hughes, R. P.; Kowalski, A. S.; Lomprey, J. R.; Rheingold, A. L. *Organometallics* **1994**, *13*, 2691.
15. Leigh, T. *J. Chem. Soc.* **1964**, 3294.
16. Shriver, D. F.; Drezdzon, M. A. *The Manipulation of Air-Sensitive Compounds*; Wiley-Interscience: New York, 1986.

17. Gansle, K. M. Investigation and Development of Liquid-Liquid Extraction Systems for the Removal of Pertechnetate from Aqueous Nuclear Waste-Stream Simulants. Ph.D. Dissertation, Colorado State University, Fort Collins, CO, 1998.
18. Clark, J. F. Design, Synthesis, and Evaluation of Redox-Recyclable Organometallic Extractants for the Recovery of Ionic Radionuclides From Aqueous Waste Streams. Ph.D. Dissertation, Colorado State University, Fort Collins, CO, 1999.
19. Sheldrick, G., M., 1995 SHELXTL, v. 5.03; Bruker AXS: Madison, WI.
20. Sheldrick, G. M., SADABS - a program for area detector absorption corrections.
21. Kalushi, Z. L.; Gusev, A. I.; Kalinin, A. E.; Struchkov, Y. T. *Zh. Struckt. Khim.* **1972**, *13*.
22. Boese, R.; Bläser, D.; Kuhn, N.; S., S. *Z. Kristallogr.* **1993**, *205*, 282.
23. Rogers, R. D.; Cook, W. J.; Atwood, J. L. *Inorg. Chem.* **1979**, *18*, 279.
24. Henning, H.; Gürtler, O. *J. Organomet. Chem.* **1968**, *11*, 307.
25. Ritsko, J. J.; Nielsen, P.; Miller, J. S. *J. Chem. Phys.* **1977**, *67*, 687.
26. Dowben, P. A.; Driscoll, D. C.; Tate, R. S.; Boag, N. M. *Organometallics* **1988**, *7*, 305.
27. Silva, M.; Pombeiro, A. J. L.; Frausto da Silva, J. J. R. F.; Herrmann, R.; Deus, N.; Castilho, T. J.; Silva, M. F. C. G. *J. Organomet. Chem.* **1991**, *421*, 75.
28. Okuda, J.; Albach, R. W.; Herdtweck, E.; Wagner, F. E. *Polyhedron* **1991**, *10*, 1741.

Chapter 3

Synthesis and Characterization of Novel Functionalized Polyalkylated Ferrocenes and Ferrocenium Salts

Introduction

The preparation of new polyalkylated ferrocenes and new functionalized polyalkylated ferrocenes and their salts for use as ion-exchange materials in the Redox-Recyclable Extraction and Recovery (R^2ER) Paradigm is a vital part of advancing this new technology. The original R^2ER extractant, 1,1',3,3'-tetra(2-methyl-2-hexyl)ferrocene (HEP) was synthesized by Clark *et. al.* by Friedel-Crafts alkylation of ferrocene using 2-chloro-2-methylhexane as an alkylating agent.[1] The resulting tetraalkylated, lipophilic ferrocene, in its cationic ferrocenium form, has since been used as a selective anion-exchange material for a variety of anion extraction and detection projects.[2-4] It has since been shown that polyalkylated ferrocene ion-exchange materials are governed by the same principles that govern tetraalkylammonium ion-exchange materials.[5,6] More specifically, the size of the extractant ferrocene greatly influences its selectivity towards weakly hydrated anions.[5-7] Towards this end, the synthesis of the larger, more lipophilic tetraalkylated ferrocene 1,1',3,3'-tetra(2-methyl-2-nonyl)ferrocene (DEC), has been accomplished to take advantage of this increased selectivity.[8]

Several extraction techniques have been employed using the anion-exchange material HEP. Bi-phasic liquid-liquid extraction has been demonstrated for the remediation and recovery of the radioactive anion $^{99}TcO_4^-$ in high salt solutions.[2] Similarly, solid supported anion-exchange materials have been developed by physisorption of the highly lipophilic HEP onto solid supports such as silica gel or polymer beads.[3,6,7] These materials have been successfully used in the biphasic solid-

liquid remediation of $^{99}TcO_4^-$, as well as the remediation and recovery of ClO_4^- and perfluorooctylsulfonate ($C_8F_{17}SO_3^-$, PFOS), a fluorinated surfactant that has been shown to be persistent in the environment. Finally, it has been shown that by modifying the surface of an attenuated total reflectance FTIR (ATR-FTIR) sensing crystal with DEC^+ that a variety of IR-active anions can be preconcentrated at the surface of the ATR-FTIR sensing crystal and subsequently detected by FTIR in water at ppb levels.[4]

Though surface modification by physisorption of the lipophilic polyalkylated ferrocenes has resulted in the production of highly selective ion-exchange materials and sensing devices, it is still desirable to synthesize functionalized polyalkylated ferrocenes which can be covalently attached to surfaces or included in their own polymer matrix. Though robust ion-exchange materials have been made without covalent modification of surfaces, applications such as ion-exchange from organic media or studies of extractants that are water soluble make the covalent attachment of these tetraalkylated ferrocenes to surfaces necessary. It has also been shown that the HEP^+ cation physisorbed on to the surface of silica gel is mobile on the surface, thus resulting in a decreased capacity of the material over time.[6,9] It is also suspected that the physisorbed films used for the ATR-FTIR detection of anions flake off of the sensing surface over the duration of a detection experiment.[10] The surface modification of conducting substrates is also desirable since such materials may eliminate the need for chemical oxidants and reductants for the recycling of the tetraalkylated ferrocene ion-exchange materials. Electrochemically mediated ion-exchange of modified conducting solid supports has been previously demonstrated and may prove useful to the recycling and ion-exchange processes of redox-active polyalkylated ferrocene ion-exchange materials.[11,12] For these reasons, the synthesis of tetraalkylated ferrocenes with a variety of functional groups used for covalent attachment to surfaces or inclusion in polymeric materials is desirable. These types of functionality may also result in methodology for the inclusion of tetraalkylated ferrocenes in surface coating media, such as sol-gel or polymer coatings, or possibly be

used for the synthesis of novel ion-exchange resins.

Several challenges and strategies must be considered in the design of synthetic strategies for the functionalization of the tetraalkylated ferrocenes before attempting their syntheses. (1) The properties that make polyalkylated ferrocenes attractive redox-recyclable anion-exchange materials, such as size, lipophilicity, and redox potential, must not be changed by the type of functionalization introduced to the molecules. (2) The tetraalkylated ferrocenes are sterically hindered to further functionalization due to the size of the four tertiary alkyl substituents on the alkylated cyclopentadienyl (Cp') rings. Synthetic methodology must be developed to overcome this steric hindrance as well as extend functionalities beyond the steric influence of the tertiary alkyl groups. (3) Synthesis schemes should first be developed for less sterically hindered polyalkylated ferrocenes. Ferrocenes with fewer alkyl chains or shorter alkyl chains, such as 1,1',3-tri(2-methyl-2-propyl)ferrocene (tri-BUT) and 1,1',3,3'-tetra(2-methyl-2-propyl)ferrocene (BUT)[13] respectively, may provide insight into functionalization of the larger tetraalkylated ferrocenes HEP and DEC. (4) Functional groups that can undergo further reaction for linkage to surfaces, inclusion in bulk materials, and further functionalization should be the goal.

Functionalization of tetraalkylated ferrocenes using the strategies outlined above has been explored and the results presented herein. The goal of surface modification and materials development has been demonstrated for some of the novel functionalized polyalkylated ferrocenes synthesized. Both surface modification and polymer inclusion of the larger tetraalkylated ferrocenes HEP and DEC have been achieved. Many novel compounds are discussed in this chapter. Table 1.1 in Chapter 1 shows structures, compound names, and the abbreviations used for the compounds discussed in this chapter as well as the entire dissertation and should be referred to as needed.

Experimental

General Procedures. All synthesized compounds appear to be stable to air and

moisture, but some reagents were moisture sensitive. Therefore, unless otherwise indicated, all reactions were performed in an inert atmosphere using standard Schlenk and glovebox techniques, with purified nitrogen used as the inert atmosphere.[14] All nuclear magnetic resonance spectroscopy (NMR) was performed on a Varian VXR, 300 MHz spectrometer at 25 °C. Liquid secondary ion mass spectrometry (LSIMS) was performed on a Fisons Instruments VG autospec mass spectrometer using a cesium ion gun. Fourier transform infrared spectroscopy (FTIR) was performed on a Nicolet Model 5PC at a resolution of 2 cm^{-1}, obtaining 100 scans for each spectrum and background. An orbital shaker bath model 3545 from Lab-Line Instruments, Inc. was used in some reactions. Reactions requiring sonication used a Branson model 3210 sonicator with variable temperature water bath. Solvent removal was done under vacuum with a Buchi R-124 rotary evaporator.

Reagents and Solvents. All reagents were Reagent Grade or better unless otherwise indicated. All reagents and solvent were used as received unless purified as noted:[15] 1,2-dichloroethane (Fisher, pre-dried and distilled from P_2O_5); dichloromethane (Fisher, pre-dried and distilled from P_2O_5); ethyl ether (Fisher, anhydrous, pre-dried and distilled over sodium metal); acetone (Fisher, pre-dried and distilled from anhydrous calcium sulfate); tetrahydrofuran (THF, Fisher, pre-dried and distilled from sodium metal); acetonitrile (Fisher); methanol (Fisher); *n*-heptane (Fisher); petroleum ether (Fisher); pyridine (Fisher); *N,N*-dimethyl formamide (Fisher; stored over Lynde type 4A molecular sieves (Fisher)); water (distilled deionized to 18Ω on a Barnstead NANOpure H_2O purification system); anhydrous potassium bromide (Aldrich); ferrocene (Lancaster, sublimed under vacuum at room temperature and stored in a glovebox); 1,1',3-tri(tmethyl-2-propyl)ferrocene (tri-BUT, prepared by Kevin Chambliss at Oak Ridge National Laboratory according to literature procedures[13]); 3-ethyl-3-pentanol (Aldrich); acetyl chloride (Aldrich); ethyl acetate (Fisher); thionyl chloride (ACROS); zinc chloride (Fisher, dried with $SOCl_2$ and stored in a glovebox); lithium aluminum hydride (Alpha

AESAR, purified by dissolving in ether, filtering gray solids, removing ether, and heating at 65 °C under vacuum for 16 hrs, stored in a glovebox); zinc metal (Fisher), anhydrous sodium sulfate (Fisher); ammonium chloride (J.T. Baker); sodium hydroxide (Fisher); hydrochloric acid (Mallinckrodt);silica gel (J.T. Baker, 60-200 mesh); activated aluminum oxide powder (activity grade I; M. Woelm Eschwege); acetone-d_6 (Cambridge Isotopes Laboratories); methylene chloride-d_2 (Cambridge Isotopes Laboratories); benzene-d_6 (Cambridge Isotopes Laboratories); poly(vinylbenzyl chloride) (Aldrich); methyllithium (1.4 M in diethyl ether, hexanes, or THF, Aldrich); butyllithium (2.5 M in hexanes, Aldrich); allylmagnesium bromide (1.0 M solution in diethyl ether, Aldrich); titanocene dichloride (Boulder Scientific); methyltriphenylphosphonium iodide (Aldrich); styrene (Aldrich; passed through columns of alumina (J. T. Baker) and De-hibit 100 (Polysciences, Inc.) before use); methyl methacrylate (Aldrich; passed through columns of alumina and De-hibit 100 before use); 2,2'-azobisisobutyronitrile (AIBN, Aldrich); chloroplatinic acid (Aldrich); Karstedt's catalyst (*rac*-tris(divinyltetramethyldisiloxane) diplatinum(0); 2.1-2.4% platinum concentration in xylenes; Gelest Inc.); triethoxysilane (Gelest Inc.); trimethoxysilane (Gelest Inc.); trichlorosilane (Gelest Inc.); dimethylethoxysilane (Gelest Inc.); methanesulfonyl chloride (mesyl chloride; Aldrich); thiolacetic acid (Aldrich); tetrabutylammonium hexafluorophosphate (Aldrich); 11-bromoundecanoic acid (Aldrich), 4-(dimethylamino)pyridine (Aldrich), 4-nitrophenyl chloroformate (Aldrich); *N,N*-diisopropylamine (Aldrich); sodium iodide (Fisher); sodium methylate(Fisher); acrolyl chloride (Aldrich).

Preparation of 3-chloro-3-ethylpentane. In a Schlenk flask, 3-ethyl-3-pentanol (6.0 g, 52 mmol) was cooled in an ice bath for 30 minutes. Thionyl chloride (6.2 g, 52 mmol) was added slowly by syringe and HCl was allowed to evolve for 2 hours. The reaction mixture turned faint blue in color due to some polymerized species. The mixture was then passed over a column of dry silica gel yielding 3-chloro-3-ethylpentane as a colorless liquid in a 56% yield. The light sensitive liquid was stored in the dark until

used. ^{1}H-NMR (acetone-d_6, 300 MHz, 25 °C) δ 1.75 (q, 6H), 0.91 (t, 9H). LSIMS m/z = 135.1 (135.7 calc.).

Preparation of 1,1',3-Tri(3-ethyl-3-pentyl)ferrocene (tri-HEP2). In a glovebox, ferrocene (0.54 g, 2.9 mmol) was weighed into a Schlenk flask. Also in a glovebox, dry zinc chloride (1.1 g, 7.8 mmol) was weighed into a three neck round-bottom flask equipped with a stir bar. Both flasks were then removed from the glovebox and connected to a Schlenk line. Under nitrogen purge, 3-chloro-3-ethylpentane (3.8 g, 29 mmol) was added to the zinc chloride, and the round-bottom flask was then equipped with a condenser and addition funnel. In the other Schlenk flask, the ferrocene was dissolved in dichloromethane (200 mL) and then transferred via cannula into the addition funnel attached to the round-bottom flask containing the 3-chloro-3-ethylpentane and zinc chloride. The ferrocene solution was then added drop wise over 1 hour to the zinc chloride/3-chloro-3-ethylpentane slurry while heating and stirring. The reaction mixture gradually turned greenish/brown due to the presence of oxidized alkylated ferrocenes. After refluxing for 96 hours, the reaction mixture was opened to air and washed with an equal volume of 10 vol% concentrated HCl in water. After separation, the organic layer was stirred under mild heat with granular zinc metal until the solution turned bright orange. The organic layer was then filtered and washed with an equal volume of 1M NaOH followed by two washings with water. The solvent was then removed under vacuum, leaving a red orange oil composed of a mixture of mono-, di-, tri-, and tetraalkylated ferrocenes. The oil was separated by fractional column chromatography on silica gel with *n*-heptane or petroleum ether eluant. The fractions were tested by thin layer chromatography (TLC) using petroleum ether as the solvent (tri-HEP2 R_f = 0.048). Concentration of the appropriate fractions gave slightly impure tri-HEP2 as an orange oil in a 30% yield. Attempts to crystallize the oil from ethanol or a dichloromethane/acetonitrile co-solvent system were unsuccessful. For ^{1}H-NMR and LSIMS data, see Figure 3.2.

Acylation of Polyalkylated Ferrocenes. The polyalkylated ferrocenes tri-BUT, tri-HEP2, and BUT were all acylated in the manner described below. A mixture of acetyl chloride (0.089 g, 1.1 mmol) and zinc chloride (0.10 g, 0.76 mmol) was prepared under an N_2 atmosphere in a three neck flask equipped with an addition funnel, condenser, and stir bar. In a separate Schlenk flask also under a N_2 atmosphere, the polyalkylated ferrocene (0.10 g, 0.28 mmol) was dissolved in 25 ml of dichloromethane and cannulated into the addition funnel attached to the flask containing the zinc chloride/acetyl chloride mixture. The polyalkylated ferrocene was then added drop wise to the zinc chloride/acetyl chloride mixture while stirring and heating. The resulting solution gradually turned a deep purple. While refluxing, the reaction was monitored by TLC in dichloromethane. When TLC showed side products beginning to form, the reaction was stopped. Typical reactions times were between 3 and 5 hours. After opening the reaction to air, the reaction mixture was washed three times with water, turning the organic layer a deep red/pink color. After separation, the organic layer was dried by stirring with anhydrous sodium sulfate and filtering. Removal of the solvent under vacuum gave a rose colored oil. The oil was further purified with column chromatography on silica gel with a dichloromethane eluant. Products were obtained as either red oils or red solids upon evaporation of solvent in 88 to 96% yields. For ^{1}H-NMR and LSIMS data, see Figures 3.3, 3.4 and Table 3.1.

Conversion of Acylferrocenes to α-Hydroxyethylferrocenes. The compounds tri-BUT-Ac, tri-HEP2-Ac, and BUT-Ac were converted to the α-hydroxyethyl functionalized trialkylated ferrocenes in the manner described below. Under an N_2 atmosphere, the acylated ferrocene (0.092 g, 0.23 mmol) was dissolved and stirred in anhydrous diethyl ether in a Schlenk flask equipped with an addition funnel. In a separate Schlenk flask also under an N_2 atmosphere, lithium aluminum hydride (0.018 g, 0.49 mmol) was dissolved in anhydrous diethyl ether and cannulated into the addition funnel attached to the flask containing the acylferrocene solution. The lithium aluminum

hydride solution was added drop wise to the acylferrocene solution over 1 hour. The addition of lithium aluminum hydride was accompanied by a solution color change from red/pink to yellow. After refluxing for ~10 hours, the mixture was opened to air and cooled in an ice bath. While cooling, ~5 mL of ethyl acetate were added to destroy excess lithium aluminum hydride. The resulting reaction mixture was then treated with 10 mL of a 0.12 M aqueous solution of ammonium chloride and allowed to sit in an ice bath for a half hour. The mixture was then filtered, the two phases separated, and the organic layer washed twice with water. After separation, the organic layer was dried by stirring with anhydrous sodium sulfate, filtered, and solvent was removed under vacuum. The resulting α-hydroxyethyl polyalkylated ferrocenes were obtained as orange oils or orange solids in 95 to 99% yields. For ^{1}H-NMR and LSIMS data, see Figures 3.5, 3.6, and Table 3.1.

Pyrolysis of α-Hydroxyethylferrocenes. Pyrolysis of tri-BUT-OH and BUT-OH to the vinyl functionalized ferrocenes was performed in the manner described below. A small amount (~1 g) of aluminum oxide powder was added to a solution of α-hydroxyethylferrocene dissolved in dichloromethane. Using a rotary evaporator, the α-hydroxyethylferrocene was deposited on the surface of the alumina by gently removing the solvent under vacuum. The resulting alumina powder had a red/pink color. The powder was placed in a sublimator equipped with a cold finger to ~5 °C and heated under vacuum (0.003 torr) in an oil bath at 120 to 150 °C for 16 hours. After cooling, the product was abstracted from the coldfinger using dichloromethane. After removal of the solvent under vacuum, vinylated polyalkylated ferrocenes were isolated as orange powders in 12 to 18 % yields. For ^{1}H-NMR and LSIMS data, see Figures 3.7, 3.8, and Table 3.1.

Wittig Reactions of Acylated Polyalkylated Ferrocenes. Wittig reactions of tri-BUT-Ac were performed in the manner described below. In a glovebox, methyltriphenylphosphonium iodide (0.072 g, 0.19 mmol) was placed in a Schlenk flask

equipped with a stir bar. After transferring the flask to a Schlenk line, THF was cannulated into the flask and the resulting suspension was cooled to 0 °C in an ice bath while stirring. Butyllithium (2.5 M in hexanes, 0.071 mL, 0.18 mmol) was added by syringe turning the solution pale yellow and dissolving all remaining solid. After stirring for 30 minutes, the acylferrocene (0.054 g, 0.12 mmol) was added to the reaction mixture under an N_2 purge, turning the reaction mixture red. After stirring for 3 hours at 0 °C, the ice bath was removed and the reaction mixture stirred for 12 hours at room temperature. At this time, the reaction mixture was opened to air and *n*-pentane added to precipitate triphenylphosphine oxide. Following filtering, the reaction mixture was washed with water, the organic phase separated and dried with anhydrous sodium sulfate, filtered, and the solvent removed under vacuum yielding a red/orange oil. The oil was purified by column chromatography on silica gel with dichloromethane, yielding the final product as a yellow/orange oil in a 30% yield. For ^{1}H-NMR and LSIMS data, see Figures 3.9 and 3.10.

Covalent Attachment of 1,1',3-Tri(2-methyl-2-propyl)ferrocene (tri-BUT) to Poly(Vinylbenzyl Chloride) by Friedel-Crafts Alkylation. In a glovebox, anhydrous zinc chloride (0.57 g, 4.2 mmol) was placed in a Schlenk flask equipped with a stir bar and condenser. After transferring the flask to a Schlenk line, dichloromethane was cannulated into the flask and the resulting suspension was stirred vigorously. Poly(vinylbenzyl chloride) (0.25 g, 1.6 mmol active sites) and tri-BUT (0.58 g, 1.6 mmol) were added to the reaction mixture under a N_2 purge. This mixture was refluxed and after five hours, the solution had turned gelatinous. After opening the reaction to air, the solid was washed with 10 vol% HCl, 0.1 M NaOH, and twice with water. Excess oxidized tri-BUT was removed during the washings as indicated by the blue/green color of the aqueous phase. The excess tri-BUT was recovered and quantified for determination of the loading onto the polymer. The extent of tri-t-butyl ferrocene inclusion was estimated to be 8 ± 3% by weight. Following washing, the resulting

yellow/green gel was dried under vacuum on a Schlenk line for 12 hours, yielding an insoluble yellow powder. The solid was ground with KBr(s) to form a pellet and analyzed by FTIR.

Preparation of 1,1',3,3'-tetra(2-methyl-2-propyl)-4-(2-propenyl)ferrocene (BUT-Pr) Using the Petasis Reagent. In a glovebox, titanocene dichloride (0.34 g, 1.4 mmol) was placed in a 250 mL Kontes tube equipped with a stir bar, teflon cap, and sidearm for attachment to a Schlenk line or high vacuum line. After transferring the Kontes tube to a Schlenk line, the titanocene dichloride was dissolved in dry distilled toluene (75 mL) and cooled to 0 °C with an ice bath while stirring. Methyllithium (1.4 M in diethyl ether, 2.0 mL, 2.7 mmol) was then added by syringe to generate dimethyltitanocene, which turned the solution from red to yellow/orange. CAUTION: dimethyltitanocene is extremely shock sensitive and light sensitive and should be generated *in situ* only. This mixture was wrapped in tin foil to avoid exposure to light and a toluene solution (75 mL) of BUT-Ac (0.25 g, 0.55 mmol) from a separate Schlenk flask was cannulated into the reaction mixture. After the addition of BUT-Ac was complete the Kontes tube was transferred to a high vacuum line. The solution was then freeze-pump-thawed, left under vacuum (~10^{-5} torr) in the sealed Kontes tube, and removed from the high vacuum line. The sealed tube was again wrapped in tin foil and heated with stirring to between 60 and 65 °C for 48 hours. The reaction mixture was then allowed to cool to room temperature, opened to air, and poured into 100 mL of petroleum ether, which caused a brown precipitate to form. The mixture was filtered and the solvent removed under vacuum, producing an orange oil. Column chromatography on silica gel in dichloromethane followed by removal of the solvent gave the product, BUT-Pr, as a red/orange solid in a 68% yield. For ^{1}H-NMR and LSIMS data, see Figures 3.12 and 3.13.

Preparation of 1,1',3,3'-tetra(2-methyl-2-propyl)-4-(4-hydroxy-4-(pentenyl))ferrocene (BUT-PtOH). To a dry Schlenk flask under an N_2 atmosphere

equipped with a stir bar was added BUT-Ac (0.25 g, 0.55 mmol) under an N_2 purge and dissolved in dry distilled diethyl ether. The solution was then cooled to 0 °C in an ice bath while stirring. To the resulting red solution was added allylmagnesium bromide (1.0 M in diethyl ether, 0.55 mL, 0.55 mmol) by syringe. The reaction mixture immediately turned orange and a white precipitate formed. This mixture was stirred for 1 hour at which time the ice bath was removed and the mixture allowed to warm to room temperature over 1 hour. The reaction mixture was then opened to air and ice was slowly added while continuing to stir. After the ice had melted, the organic phase was separated and the solvent removed under vacuum yielding the product, BUT-PtOH, as an orange solid in 99% yield. For ^{1}H-NMR and LSIMS data, see Figures 3.14 and 3.15.

Preparation of 1,1',3,3'-tetra(2-methyl-2-propyl)-4-(4-(1,3-dipentenyl)) ferrocene (BUT-diPt). To a dry Schlenk flask under a N_2 atmosphere equipped with a stir bar was added BUT-PtOH (0.20 g, 0.40 mmol) under N_2 purge and dissolved in dry THF. The solution was then cooled to –78 °C in a dry ice/acetone bath while stirring. To the cooled orange solution was added mesyl chloride (0.10 g, 0.88 mmol) and 0.2 mL of pyridine by syringe. This mixture was stirred for 1 hour at which time methyllithium (1.4 M in hexanes, 0.60 mL, 0.84 mmol) was added by syringe. After stirring this mixture for 15 minutes, the dry ice/acetone bath was removed and the mixture allowed to warm to room temperature while stirring. During this time, the solution slowly turned from orange to red. After 2 hours, the reaction mixture was then opened to air and ice was slowly added while continuing to stir. As the ice melted, the solution turned green/brown. After the ice had melted, the organic phase was separated and stirred with zinc metal to reduce any oxidized product, turning the solution red/orange again. The solvent was then removed under vacuum yielding a the product, BUT-diPt, as an orange oil in 87% yield. For ^{1}H-NMR and LSIMS data, see Figures 3.16 and 3.17.

Hydrosilation Reactions of Olefinic Ferrocenes. To a dry Schlenk flask under a N_2 atmosphere equipped with a stir bar was added vinylferrocene or olefinic

polyalkylated ferrocene (0.70 mmol) under N_2 purge and dissolved in dry distilled toluene. The desired amount of hydrosilation catalyst, either Karstedt's catalyst or Speier's catalyst, was then added by syringe to the reaction mixture. The amount of catalyst was typically between 0.2 and 0.4 mol% platinum relative to the starting amount of olefinic ferrocene. (Karstedt's catalyst was purchased as a 2-3% platinum solution (by weight) in xylenes from United Chemical Technologies, Inc. and was assumed to be 2.5% platinum with a solution density of 0.88 g/mL; A solution of Speier's catalyst (chloroplatinic acid) in 2-propanol was made in our laboratory as a 0.01 M solution.) After addition of the catalyst solution, dried air was bubbled through the reaction mixture for 30 seconds to a minute to introduce a catalytic amount of oxygen into the reaction. After stirring this solution for 1 hour, the desired silane (0.70 mmol) was added by syringe. The reactions usually turned brown over time and were generally stirred at room temperature for 24 hours. After removal of the solvent, some silated ferrocenes were purified by column chromatography on silica with a 2:1 (v:v) dichloromethane:hexanes eluant, though as may be expected, this greatly diminished the yields. Yields varied between 10 and 70% depending on the olefinic ferrocene as well as the silane used. Products were typically obtained as yellow or orange oils and stored under N_2 to avoid condensation reactions. For ^{1}H-NMR and LSIMS data, see Figures 3.18, 3.19, 3.21, and 3.22.

Preparation 11-Bromoundecanoyl Chloride.[16] 11-bromoundecanoic acid was dissolved in dichloromethane under a N_2 atmosphere. An equal molar amount of thionyl chloride was then added by syringe to the 11-bromoundecanoic acid solution and the mixture refluxed for 4 hours. Distillation under vacuum (105 °C at 0.003 torr) gave 11-bromoundecanoyl chloride in an 85% yield which was stored at 0 °C. ^{1}H-NMR (benzene-d_6, 300 MHz, 25 °C): δ 3.01 (t, 2H), 2.25 (t, 2H), 1.53 (m, 2H), 1.25 (m, 1H), 0.80 – 1.2 (m, 12H). LSIMS m/z 282.1, 282.0 calculated.

Preparation of 1,1',3,3'-Tetra(2-methyl-2-alkyl)-4-(11-bromoundecanoyl) ferrocene. Anhydrous zinc chloride (4.8 g; 35 mmol) was added to three-necked round-bottom flask equipped with a condenser and an addition funnel under N_2 purge. A dichloromethane solution of 11-bromoundecanoyl chloride (10 g; 35 mmol) was cannulated over the zinc chloride from a separate Schlenk flask and the resulting mixture stirred vigorously. A dichloromethane solution of tetra-*t*-alkylferrocene (17 mmol) was then cannulated into the addition funnel and slowly added drop wise to the round-bottom flask while heating the mixture. The resulting solution turned a deep purple and was refluxed for 12 to 16 hours. The mixture was then washed twice with water. The organic layer turned a red-pink color upon washing with water. After separation, the organic phase was dried by stirring with anhydrous sodium sulfate, filtered, and the solvent removed under vacuum. Column chromatography on silica gel with petroleum ether removed unreacted polyalkylated ferrocene. Separation of the desired monoacylated product from the diacylated product was then accomplished by repeated chromatographic separations with a dichloromethane/hexane eluant. (Ratios of dichloromethane:hexane varied from 0:1 to 3:1 as the size of the tertiary alkyl chains of the polyalkylated ferrocene increased.) The resulting red oils were obtained in yields between 60 and 80% depending on the size of the tertiary alkyl chains on the polyalkylated ferrocenes. For ^{1}H-NMR and LSIMS data, see Figure 3.23 and Table 3.3.

Preparation of 1,1',3,3'-Tetra(2-methyl-2-alkyl)-4-(11-iodoundecanoyl) ferrocene. To a dry Schlenk flask under a N_2 atmosphere equipped with a stir bar was added 11-bromoundecanoyl polyalkylated ferrocene (1.0 mmol) and an excess of sodium iodide (0.75 g, 5.0 mmol). Dry distilled acetone (100 mL) was cannulated into the flask and the reaction stirred for 16 hours. The reaction mixture was then filtered, the solvent removed under vacuum, redissolved in hexanes, filtered, and again the solvent was removed under vacuum to yield the desired product as oily, tacky red crystals in 99% yield. ^{1}H-NMR spectroscopic data for the representative compound DEC-I (benzene-d_6,

300 MHz, 25 °C): δ 4.54 (br m, 1H), 4.39 (d, 1H), 4.32 (br t, 1H), 4.05 (br m, 1H), 3.98 (q, 2H), 3.85 (br m, 1H), 3.36 (m, 4H), 2.73 (m, 2H), 2.15 (t, 2H), 2.03 (br m, 2H), 1.81 (m, 2H) 0.60 – 1.70 (m, 90H). LSIMS see Table 3.4.

Preparation of 1,1',3,3'-Tetra(2-methyl-2-alkyl)-4-(11-hydroxyundecanoyl)ferrocene. In a round-bottom flask equipped with a condenser, 11-bromoundecanoyl polyalkylated ferrocene was dissolved in dimethyl formamide. For longer chain 11-bromoundecanoyl polyalkylated ferrocenes (HEP and DEC), some oil droplets were observable in the DMF solution due to the lower solubility of the polyalkylated ferrocene. A large excess (> 100 times) of sodium hydroxide was added to this mixture and the mixture refluxed for 16 hours. During this time a brown precipitate formed. After cooling, the reaction mixture was filtered, dried under vacuum, and redissolved in dichloromethane. The dichloromethane solution was stirred vigorously with water, separated, dried with anhydrous sodium sulfate, filtered, and the solvent removed under vacuum. The final product was obtained as a viscous red oil in a 99% yield. ^{1}H-NMR spectroscopic data for the representative compound HEP-OH (benzene-d_6, 300 MHz, 25 °C): δ 4.47 (br m, 1H), 4.35 (d, 1H), 4.27 (br t, 1H), 3.98 (br m, 1H), 3.79 (br m, 1H), 3.36 (t, 2H), 2.69 (m, 2H), 2.00 (br t, 2H), 1.77 (m, 2H), 0.50 – 1.60 (m, 73H). LSIMS see Table 3.4.

Preparation of 1,1',3,3'-Tetra(2-methyl-2-alkyl)-4-(11-acrolylundecanoyl) ferrocene. A Schlenk flask equipped with a stir bar and containing 11-hydroxyundecanoyl polyalkylated ferrocene (0.16 mmol) was connected to a Schlenk line and evacuated and backfilled with N_2. Dry/distilled dichloromethane (125 mL) was then cannulated into the flask, dissolving the 11-hydroxyundecanoyl polyalkylated ferrocene. To this stirred solution was added acrolyl chloride (0.10 mL, 1.2 mmol) and pyridine (0.5 mL) by syringe. Upon addition of the pyridine, a gray/brown precipitate formed. This mixture was stirred for four hours at room temperature, at which time it was opened to air, filtered, and solvent removed under vacuum. The product was then purified by

column chromatography on silica gel with dichloromethane. Upon removal of solvent, the product was obtained as a red oil (0.059 mmol) in a 37% yield. ^{1}H-NMR spectroscopic data for the representative compound HEP-acr (benzene-d_6, 300 MHz, 25 °C): δ 6.33 (dd, 1H), 6.02 (m, 1H), 5.26 (dd, 1H), 4.50 (br m, 1H), 4.35 (br m, 1H), 4.27 (br m, 1H), 4.05 (t, 2H), 3.98 (br m, 1H), 3.81 (br m, 1H), 2.69 (m, 2H), 2.00 (br t, 2H), 1.77 (m, 2H), 0.50 – 1.60 (m, 72H). LSIMS see Table 3.4.

Preparation of 1,1',3,3'-Tetra(2-methyl-2-alkyl)-4-(11-thiolundecanoyl) ferrocene. In a round-bottom flask, 11-bromoundecanoyl polyalkylated ferrocene (2.0 g, 2.4 mmol) was combined with NaOMe (0.16 g, 3.0 mmol) and thiolacetic acid (0.46 g, 4.0 mmol) in methanol and refluxed for 24 hours. The product was then dried under vacuum to a viscous red oil and checked for unreacted starting material by TLC in dichloromethane. When all the starting material was reacted, the oil was redissolved in degassed ethanol and added to 1.5 mL of concentrated HCl. This mixture was refluxed for 4 to 8 hours. The solution was then rotovapped to dryness and purified by column chromatography on silica gel with 1:1 (v:v) dichloromethane:hexanes eluant. The final product was obtained as a red oil with the characteristic odor of a thiol. Yields varied from 30 to 70 % depending on the length of the alkyl chains on the polyalkylated ferrocene unit. ^{1}H-NMR spectroscopic data for the representative compound HEP-SH (benzene-d_6, 300 MHz, 25 °C): δ 4.49 (br m, 1H), 4.37 (d, 1H), 4.29 (br t, 1H), 4.01 (br m, 1H), 3.84 (br m, 1H), 2.71 (m, 2H), 2.17 (q, 2H), 1.65 (br t, 2H), 1.79 (m, 2H), 0.60 – 1.60 (m, 73H). LSIMS see Table 3.4.

Co-Polymerization of Olefinic Ferrocenes. Co-polymerization of all polyalkylated olefinic ferrocenes was performed as described below. The desired amount of styrene or methyl methacrylate was weighed into a glass scintillation vial. The desired amount of olefinic polyalkylated ferrocene (typically 5 to 10 mol% with respect to the co-monomer) was then added. In most cases the ferrocene was soluble in the liquid co-monomer. At this point, 1 mol% 2,2'-azobisisobutyronitrile (AIBN) was added, the vial

purged for 30 seconds under nitrogen, capped and sealed with parafilm. The solution was then heated and sonicated at 60 – 70 °C for 1 hour. The mixture was further polymerized in an oven at 100 °C for 1 hour or placed under a long-wave UV lamp overnight. Successful polymerizations yielded a variety of tacky or rigid solids upon cooling.

Surface Modification of Indium-Tin Oxide (ITO) Electrodes. Indium-tin oxide coated glass slides (Delta Technologies, Stillwater Minnesota) were cut into 1 x 2 cm pieces and cleaned by sonicating in both acetone and deionized water and then dried under a stream of nitrogen. Prior to surface modification, the ITO was soaked for 1 hour in an 0.5 M aqueous solution of potassium hydroxide. The ITO was then rinsed thoroughly with ethanol and dried under N_2. The ITO was then placed in an ethanolic solution containing a siloxy functionalized ferrocene (see hydrosilation *vide supra*) under an N_2 atmosphere and soaked for 24 hours. The ITO was then removed from the solution and rinsed thoroughly with water, ethanol, and dichloromethane and allowed to dry. After drying, tin-coated copper tape was attached to the electrode surface for an electrical contact to the potentiostat and the ITO surface was then masked with Teflon tape to limit the exposed surface area to 1 cm^2.

Surface Modification of Hydroxymethylpolystyrene with HEP-OH. Hydroxymethylpolystyrene (Advanced Chemtech, 1% DVB crosslinked 100 – 200 mesh beads, 1.6 mmol/g, 1.0 g, 1.6 mmol active sites), 4-nitrophenyl chloroformate (0.65 g, 3.2 mmol), and dimethylaminopyridine (DMAP, 0.098 g, 0.80 mmol) were mixed and suspended in dichloromethane and shaken at room temperature for 2 hours. The beads were then filtered and rinsed with dichloromethane followed by drying under vacuum to yield colorless beads. To a suspension of this material in DMF, HEP-OH (0.56 g, 0.74 mmol), DMAP (0.098 g, 0.80 mmol), and *N,N*-diisoproplyethylamine (0.21 g, 1.6 mmol) was added and the resulting red suspension was shaken at room temperature for 3 hours. The product was then filtered and thoroughly rinsed sequentially with DMF, CH_2Cl_2, MeOH, and CH_2Cl_2 followed by drying under vacuum to yield red beads. The filtrate

was dried under vacuum and purified by column chromatography on silica gel with dichloromethane in order to quantify the amount of unreacted HEP-OH. Based on this analysis, the final loading of the polymer beads was determined to be 0.066 mmol/g.

Electrochemical Analysis of Modified Electrodes. All electrochemical experiments were performed with an EG&G model 263A potentiostat/galvanostat from Princeton Applied Research using a standard three electrode configuration. All analyses performed in organic electrolyte solutions were referenced to a silver wire electrode (Aldrich). All analyses performed in aqueous electrolyte solutions were referenced to a silver/silver chloride electrode (Bioanalytical Systems, Inc.). Supporting electrolytes and scan rates were chosen as appropriate. The auxiliary electrode was platinum mesh in all cases. Electrolyte solutions were purged with N_2 for at least thirty minutes prior to analysis and all experiments performed under a flush of N_2.

Results and Discussion

Preparation and Functionalization of Trialkylated Ferrocenes. The preparation of a trialkylated ferrocene similar to the tetraalkylated ferrocenes previously used by the Strauss research group for ion-exchange applications is desirable for further functionalization. The preparation of 1,1',3-tri(2-methyl-2-propyl)ferrocene (tri-BUT) was performed by literature methods via the incomplete Friedel-Crafts tetraalkylation of the ferrocene cyclopentadienyl (Cp) rings with *tert*-butyl chloride in the presence of zinc chloride.[13] By using an excess of *tert*-butyl chloride, but not enough to promote tetraalkylation of ferrocene, the tri-*t*-butylferrocene could then be isolated by using a combination of column chromatography followed by distillation.

The preparation of 1,1',3-tri(3-ethyl-2-pentyl)ferrocene (tri-HEP2), shown in Scheme 3.1, was prepared in a similar manner to tri-BUT using 3-chloro-3-ethylpentane as the alkylating agent. This reaction resulted in a product mixture of mono–, di–, tri–, and tetraalkylated ferrocene in which the dialkylated ferrocene was the major product. The synthesis of the pure, crystalline, tetraalkylated ferrocene as seen with 2-chloro-2-

methylalkanes was not accomplished in an isolable amount with the bulkier 3-chloro-3-ethylpentane alkylating agent; its preparation is apparently hindered by the steric bulk of the alkylchloride. Increased reaction times as well as increased amounts of 3-chloro-3-ethylpentane did not result in the production of the pure, tetraalkylated ferrocene, but did enrich the product mixture with the tri- and tetraalkylated ferrocene product. The tetra-

Scheme 3.1.

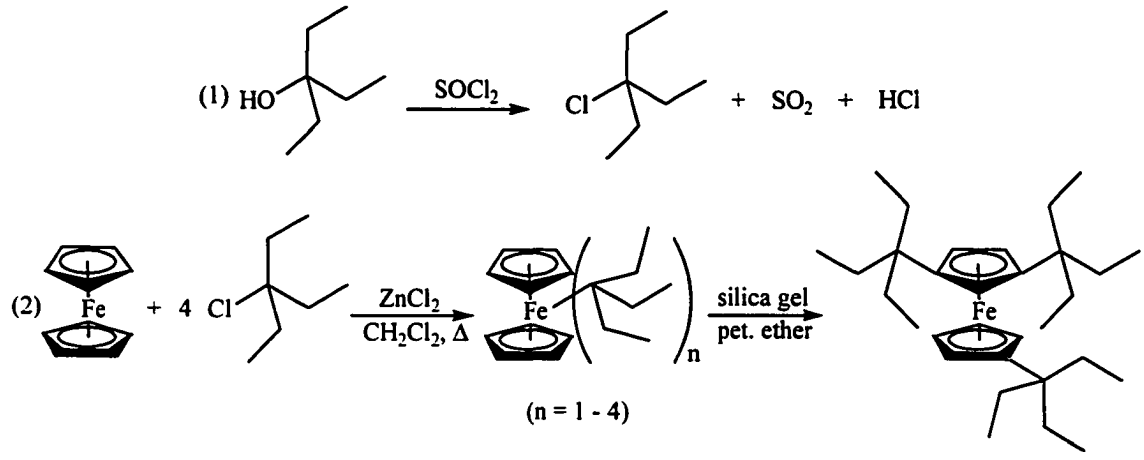

alkylated product, however, was still not present in an isolable amount. Figure 3.1 shows the mass spectrum of the reaction product mixture. As stated above, the dialkylated ferrocene (m/z 382.3) is the major product, followed by tri (m/z 480.4) and monoalkylated (m/z 284.2) ferrocene in a ratio of approximately 5:4:2 respectively. A small fraction of tetraalkylated ferrocene can be seen at m/z 578.5. The isotope pattern for all alkylated ferrocenes is consistent with that expected for the appropriate number of carbons and one iron atom.

The trialkylated ferrocene, tri-HEP2, was isolated from the product mixture by fractional column chromatography on silica-gel using *n*-heptane or petroleum ether as the eluant. Figure 3.2 shows the ^{1}H-NMR spectrum of tri-HEP2 after purification by chromatography. A small amount of the tetraalkylated species can be seen in both spectra. Complete separation of the tetra and tri species was not achieved. The

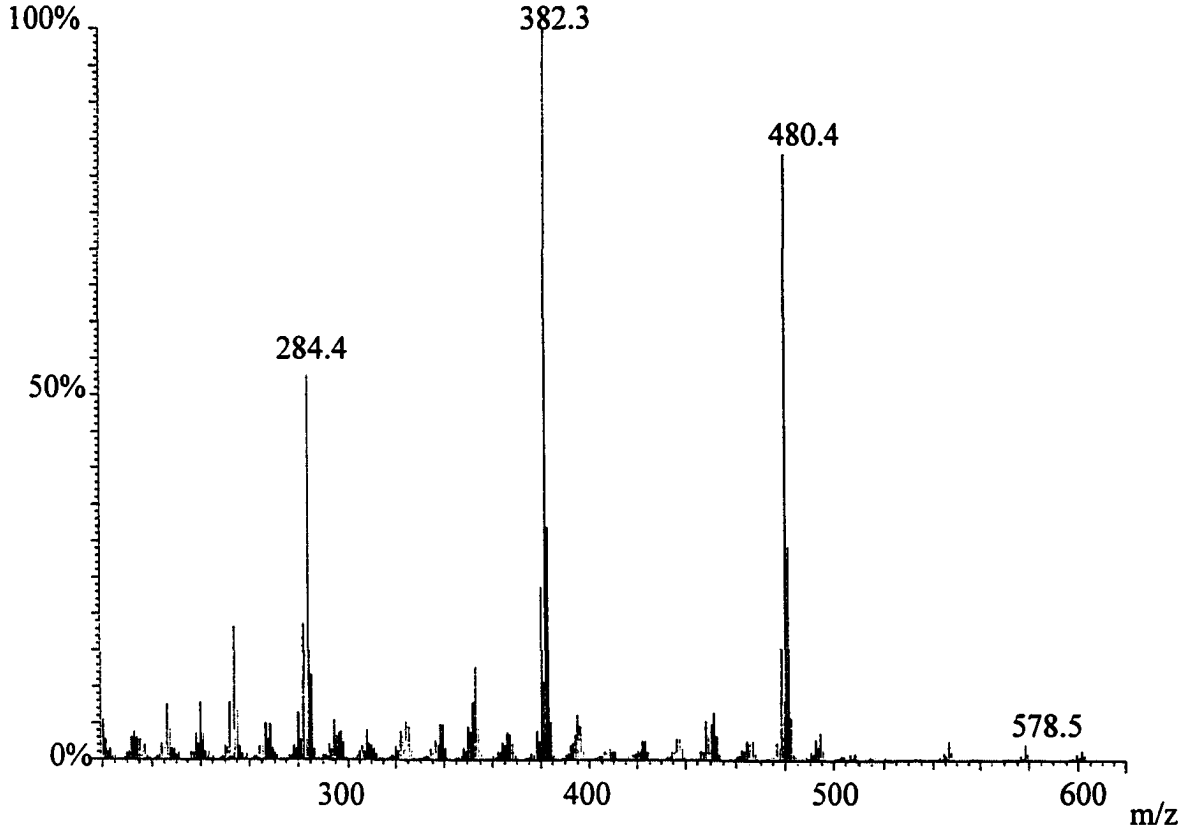

Figure 3.1. The LSIMS mass spectrum of the reaction mixture of 1,1',3,3'-mono- (m/z 284.2), di- (m/z 382.3), tri- (m/z 480.4), and tetra(3-ethyl-3-pentyl)ferrocene (m/z 578.5) obtained in the reaction shown in Scheme 3.1.

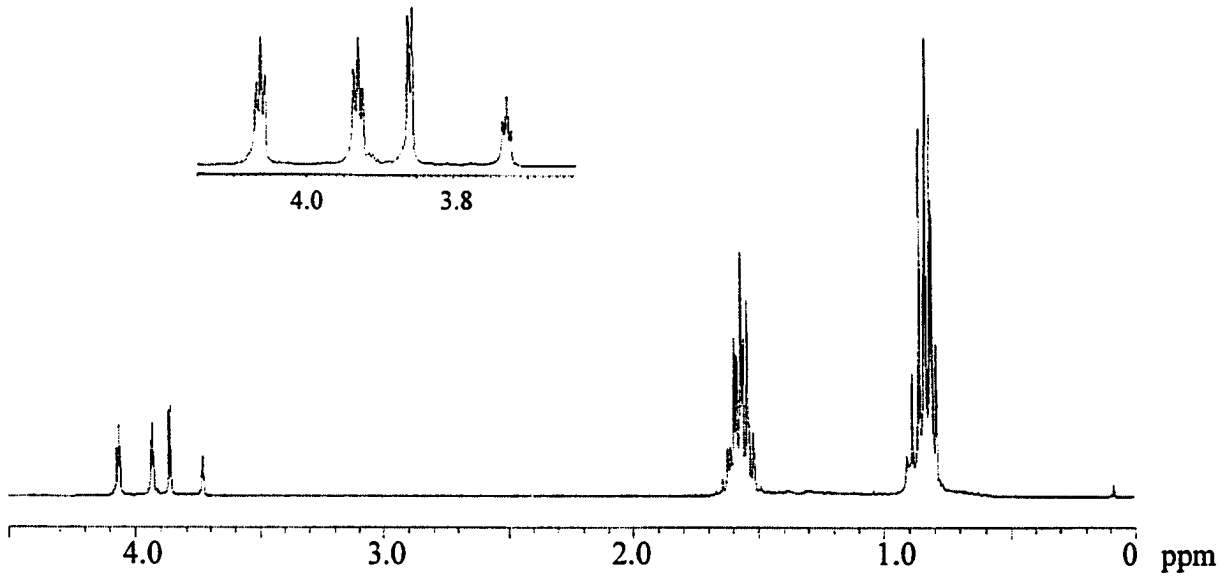

Figure 3.2. The ^{1}H-NMR spectrum of tri-HEP2. A small amount of tetraalkylated impurity can be seen in the spectrum (δ 4.08 (t, 2H), 3.91 (d, 4H)). The peak ratios and splitting patterns for the spectrum agree with the predicted structure. The inset shows the ring proton resonances.

approximate yield of tri-HEP2 after column chromatography was 30%.

Functionalization of Trialkylated Ferrocenes. The functionalization of tri-HEP2 and tri-BUT with three different functional groups can bee seen in Scheme 3.2. Each step of Scheme 3.2 resulted in the production of a novel, functionalized trialkylated ferrocene. The functional groups were chosen based on the variety of further functionalization reactions that could be subsequently carried out. Reaction conditions

Scheme 3.2.

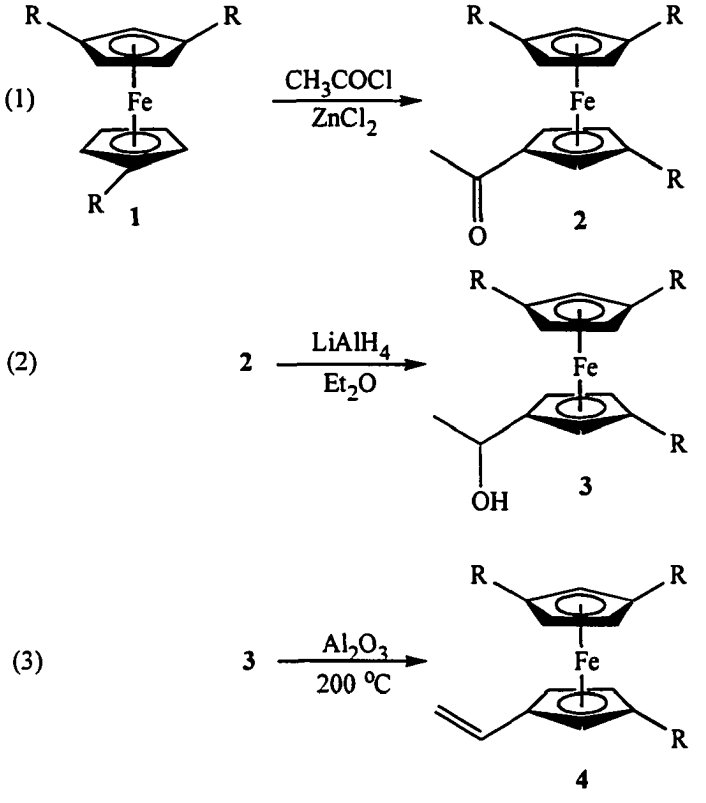

$R = -C(CH_3)_3$ or $-C(C_2H_5)_3$

and procedures were identical for both the tri-HEP2 and tri-BUT starting materials.

Friedel-Crafts acylation of the trialkylated ferrocenes tri-BUT and tri-HEP2 is shown in reaction one of Scheme 3.2. The Friedel-Crafts acylation of ferrocene with one

equivalent of acetyl chloride is known to be a robust reaction producing a mixture of starting material, mono–, and diacylated ferrocene, with the monoacylated ferrocene being the major product.[13,17] Both tri-BUT and tri-HEP2 were acylated in the same manner resulting in an analogous mixture. Separation of the crude reaction mixtures using column chromatography on silica with dichloromethane as the eluant resulted in isolation of the novel compounds 1,1',3-tri(2-methyl-2-propyl)-3'-acylferrocene (tri-BUT-Ac) and 1,1',3-tri(3-ethyl-3-pentyl)-3'-acylferrocene (tri-HEP2-Ac) in 90% and 27% yields respectively.

The ^{1}H-NMR spectrum for tri-BUT-Ac in can be seen in Figure 3.3. As expected for a tetra-substituted ferrocene with C_1 symmetry, the spectrum shows resonances for six nonequivalent ring protons between 3.9 and 4.8 ppm and a single resonance due to the three equivalent acetyl protons at 2.36 ppm. The ^{1}H-NMR spectrum of tri-HEP2-Ac shows the same pattern of resonances with as that described above for tri-BUT-Ac with a slight upfield shift and more methyl and methylene resonances due to the different alkyl substituents. Splitting patterns for the peaks in the ring proton region of tri-HEP2-Ac were obscured, but six distinct peaks for each of the ring protons were discernable. Broadened peaks for the ring proton resonances are a common feature for polyalkylated ferrocenes with bulky alkyl groups.[1,18] The appearance of a singlet at 2.3 ppm in the spectrum of tri-HEP2-Ac due to the three acyl group protons was also observed.

Mass spectra of both tri-HEP2-Ac and tri-BUT-Ac before and after purification by chromatography are shown in Figure 3.4. The major impurities in the crude reaction products were unreacted starting material (m/z 480.5 and m/z 354.3 respectively) and diacylated species (m/z 438.3 for tri-BUT). The isotope patterns for both acylated ferrocenes are consistent with those expected for the appropriate number of carbon atoms with one oxygen atom and one iron atom.

The conversion tri-HEP2-Ac and tri-BUT-Ac to the respective α-hydroxyethyl functionalized trialkylated ferrocenes was done almost quantitatively using lithium

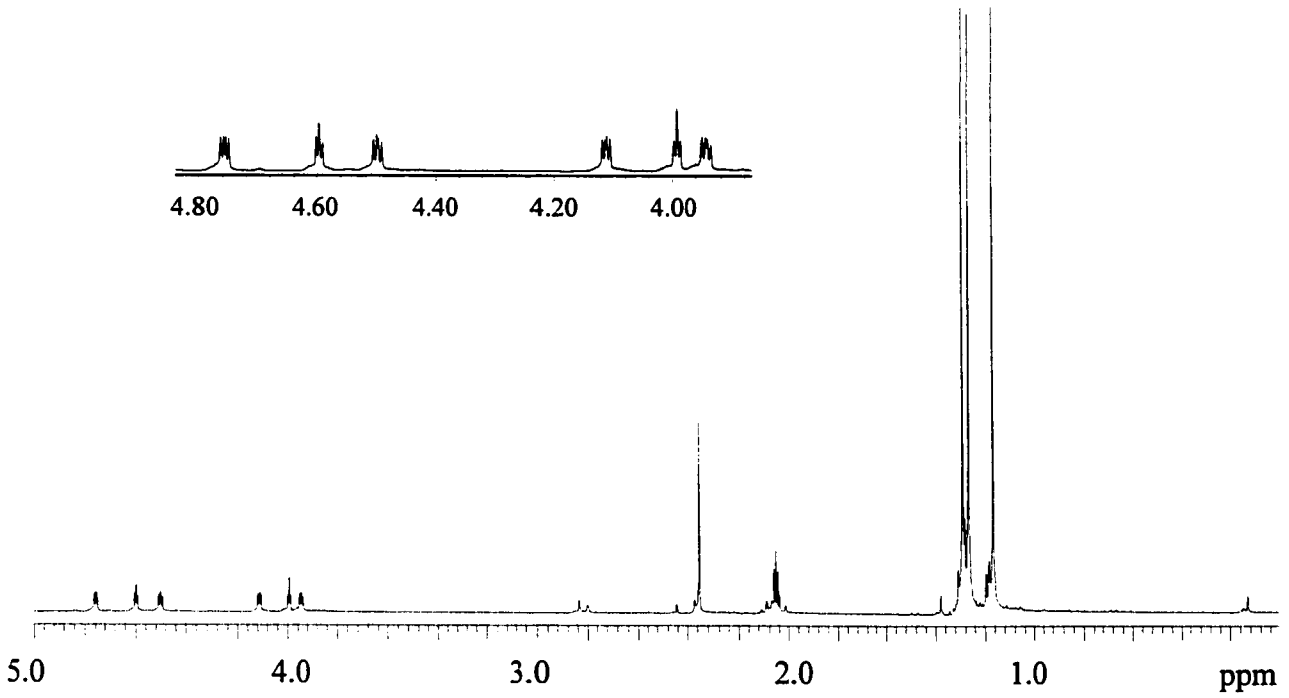

Figure 3.3. The ^{1}H-NMR spectrum of tri-BUT-Ac in acetone-d_6. The inset shows the ring proton resonances.

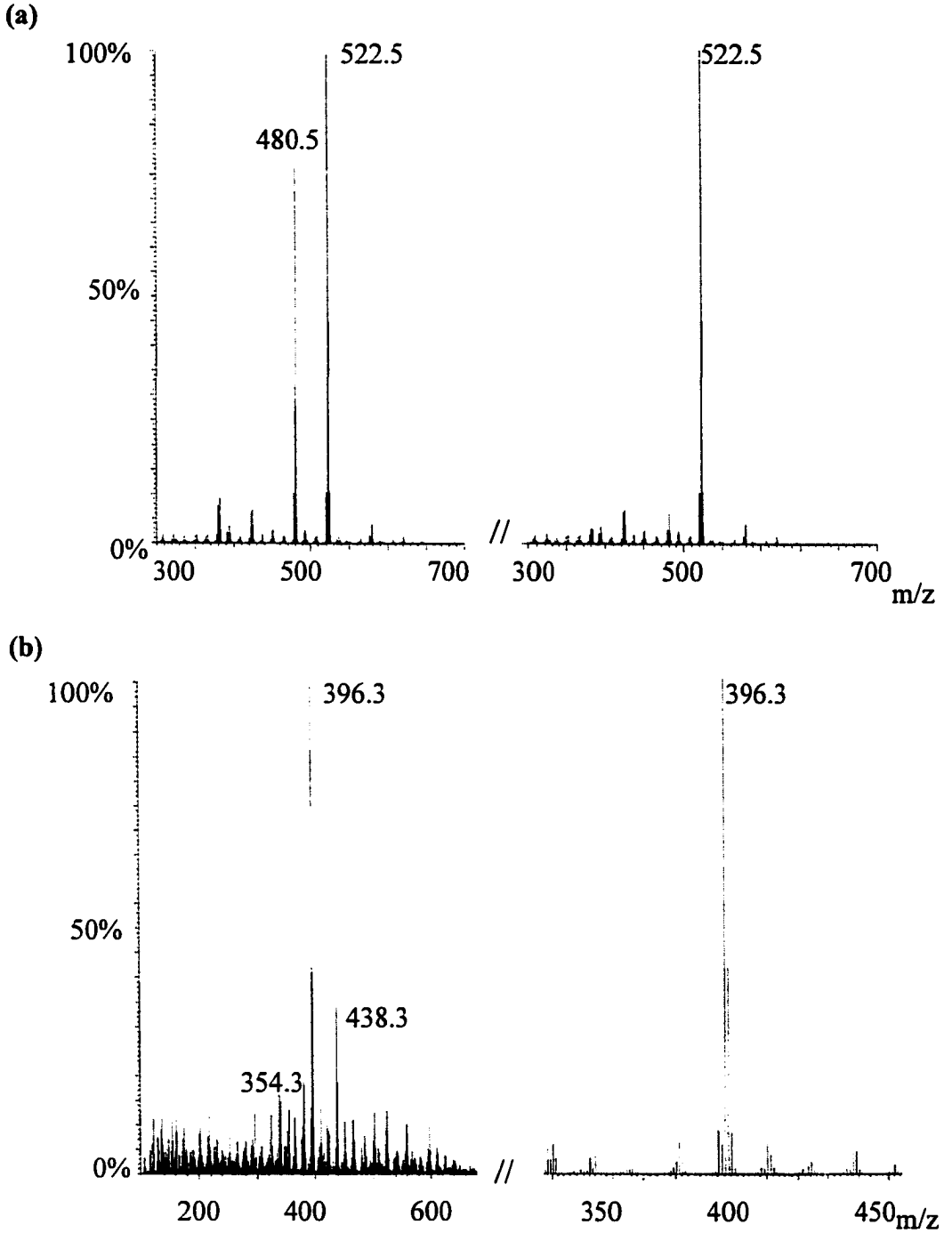

Figure 3.4. The LSIMS mass spectra of crude and purified (a) tri-HEP2-Ac (m/z 522.5; 522.64 calc.) and (b) tri-BUT-Ac (m/z 396.3; 396.40 calc.).

aluminum hydride as shown in step 2 of Scheme 3.2. The compounds 1,1',3-tri(3-ethyl-3-pentyl)-3'-(2-hydroxyethyl) ferrocene (tri-HEP2-Ac) and 1,1',3-tri(2-methyl-2-propyl)-3'-(2-hydroxyethyl) ferrocene (tri-BUT-OH) were obtained in 92% and 96% yields respectively after minor purification by column chromatography in dichloromethane. Analogous to the acyl-functionalized ferrocenes, tri-HEP2-Ac was isolated as a red orange oil and tri-BUT-OH was isolated as an orange solid following solvent evaporation.

Mass spectra of tri-HEP2-Ac and tri-BUT-OH can be seen in Figure 3.5. The isotope patterns for tri-HEP2-Ac and tri-BUT-OH are consistent with those expected for ferrocene derivatives containing the appropriate number of carbon atoms, one oxygen atom, and one iron atom. Both compounds, however, give additional signals that can be seen in the mass spectra at m/z 507.5 for tri-HEP2-Ac and m/z 381.3 for tri-BUT-OH. The signal in both cases is 18 mass units less than the desired product. It is assumed this signal is due to fragmentation in the mass spectrometer due to the dehydration involving the alcohol group. (Fragmentation by dehydration is commonly observed for alcohols.[19]) Thin layer chromatography on silica in several solvents of varying polarity show the presence of only one molecular species in both of the purified α-hydroxyethyl substituted trialkylated ferrocenes.

The ^{1}H-NMR spectra for both compounds also supports the presence of only one molecular species for each of the purified products. The ^{1}H-NMR spectrum of tri-BUT-OH can be seen in Figure 3.6. The spectrum is very similar to that obtained for the acylated starting material, with the exception of a quartet at 4.2 ppm due to the proton on the hydroxy-substituted carbon atom. The number of resonances and the splitting patterns for the Cp' ring protons remain the same as those seen for tri-BUT-Ac, as expected. The resonance for the methyl group protons on the α-hydroxyethyl moiety is seen at 2.34 ppm. As with the acylated compounds, the ^{1}H NMR spectrum of tri-HEP2-Ac (not shown), is similar to that of tri-BUT-OH, but the ring protons and the proton on

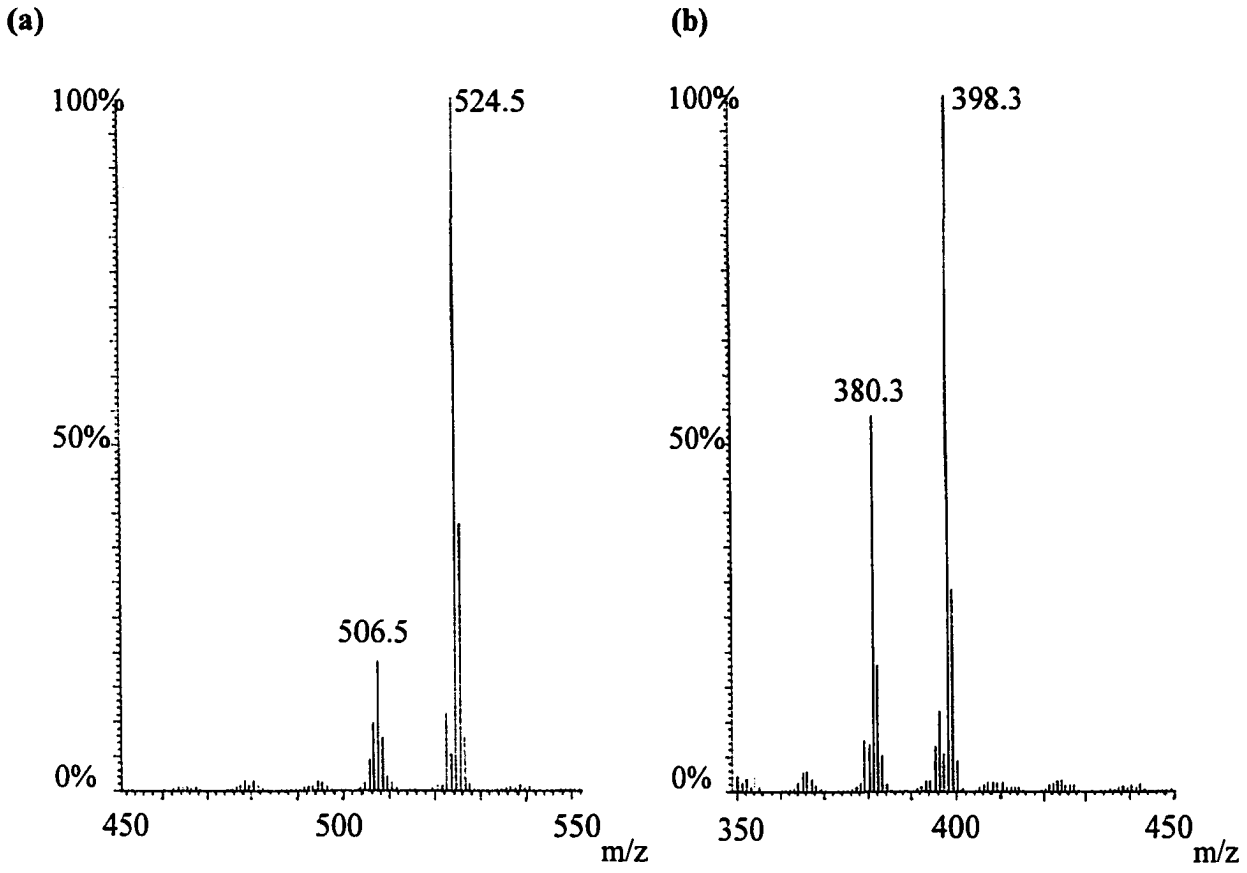

Figure 3.5. The LSIMS mass spectra of (a) tri-HEP2-Ac (m/z 524.5; 524.65 calc.) and (b) tri-BUT-OH (m/z 398.3; 398.41 calc.). Fragmented species due to dehydration of the α-hydroxymethyl substituents can be seen at (a) m/z 507.7 and (b) m/z 380.3.

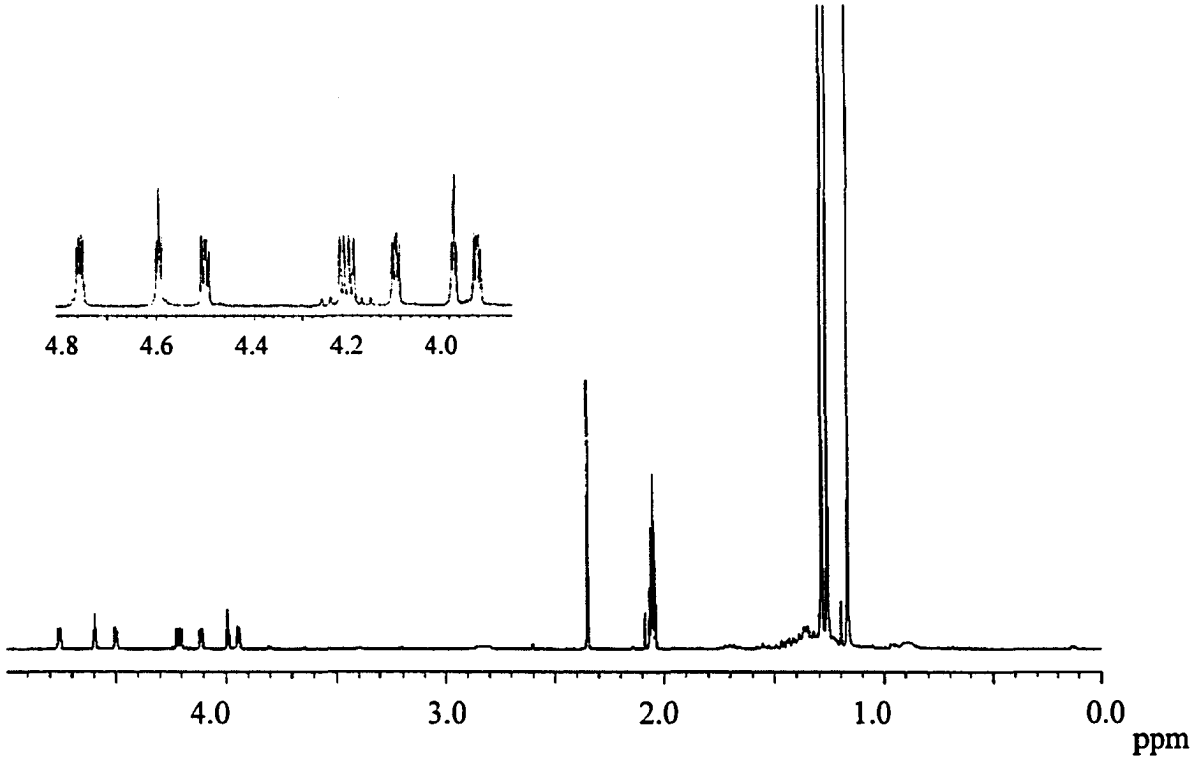

Figure 3.6. The ^{1}H-NMR spectrum of tri-BUT-OH in acetone-d_6. The inset shows the quartet at 4.2 ppm due to the proton on the hydroxy-substituted carbon atom of the α-hydroxyethyl moiety and the ring protons at 3.94, 3.99, 4.11, 4.50, 4.59, and 4.76 ppm.

the hydroxy-substituted carbon atom of the α-hydroxyethyl moiety all appear as one broad resonance from 3.8-4.5 ppm; the integration of this broad peak confirms the presence of 7 protons. The appearance of a singlet at ~2.3 ppm due to the three acyl group protons was also observed.

The final step of Scheme 3.2 shows the dehydration of the α-hydroxyethyl ferrocenes to the vinyl trialkylated ferrocenes by means of pyrolysis on activated alumina. Traditionally, vinylferrocenes are prepared by dehydration of hydroxyalkyl groups attached to the Cp rings with 10-camphorsulfonic acid or sulfuric acid,[20] or by pyrolysis on activated alumina.[17,21,22] Attempts to dehydrate tri-HEP2-Ac and tri-BUT-OH with either 10-camphorsulfonic acid or sulfuric acid were unsuccessful, thus pyrolysis was chosen as a method for the conversion to the vinyl group. Pyrolysis of tri-HEP2-Ac and tri-BUT-OH was attempted on activated alumina at ~130 °C under vacuum. No product was observed for the reaction with tri-HEP2-Ac. For the reaction with tri-BUT-OH, 1,1',3-tri(2-methyl-2-propyl)-3'-vinylferrocene (tri-BUT-Vn) was isolated as a yellow oil on a cold finger in an 18% yield. The low yield is probably a result of the harsh reaction conditions. In comparison, Arimoto *et. al.* observed a 21% yield when preparing vinylferrocene by the same method.[17]

The LSIMS mass spectrum and ^{1}H-NMR spectrum of tri-BUT-Vn are shown in Figure 3.7 and 3.8 respectively. In the mass spectrum, an additional peak can be seen at m/z 354.2. Though this m/z ratio corresponds to that of tri-BUT, it is believed to be due to fragmentation. The ^{1}H-NMR spectrum does not show any evidence of tri-BUT or any other impurity in the oily yellow product. The ^{1}H-NMR spectrum shows the six expected resonances due to the ring protons, as well as three doublet of doublets at 5.0, 5.3, and 6.5 ppm due to the presence of the vinyl group. This is the expected splitting pattern for a vinyl group on a ferrocene moiety and is the same as that seen for vinylferrocene.

Due to the low yield observed for the pyrolysis reaction, another method was tried for formation of an olefinic, trialkylated ferrocene. One popular method for the

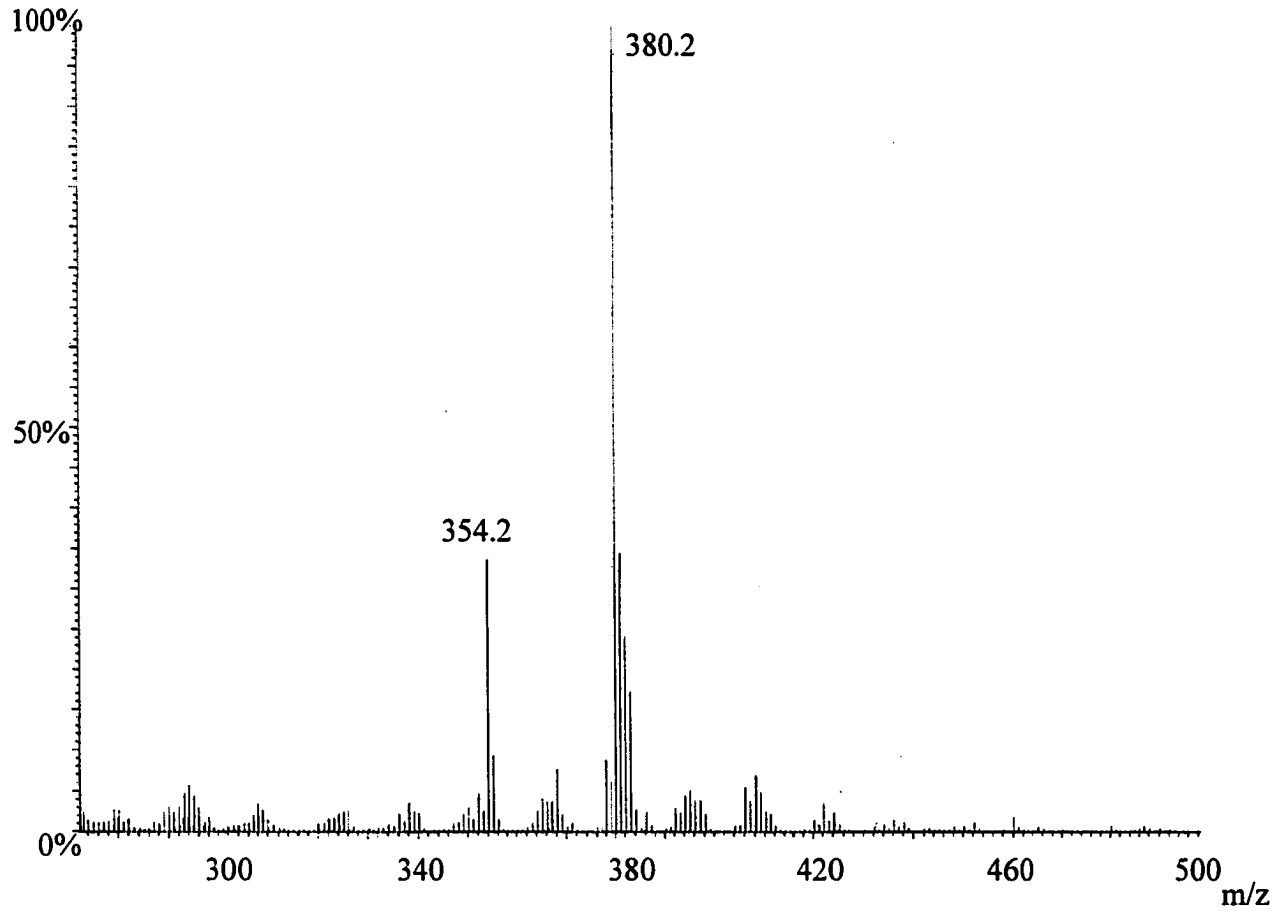

Figure 3.7. The LSIMS mass spectrum of tri-BUT-Vn (m/z 380.2; 380.40 calculated). The peak at m/z 354.2 is due to fragmentation of tri-BUT-Vn to tri-BUT in the spectrometer.

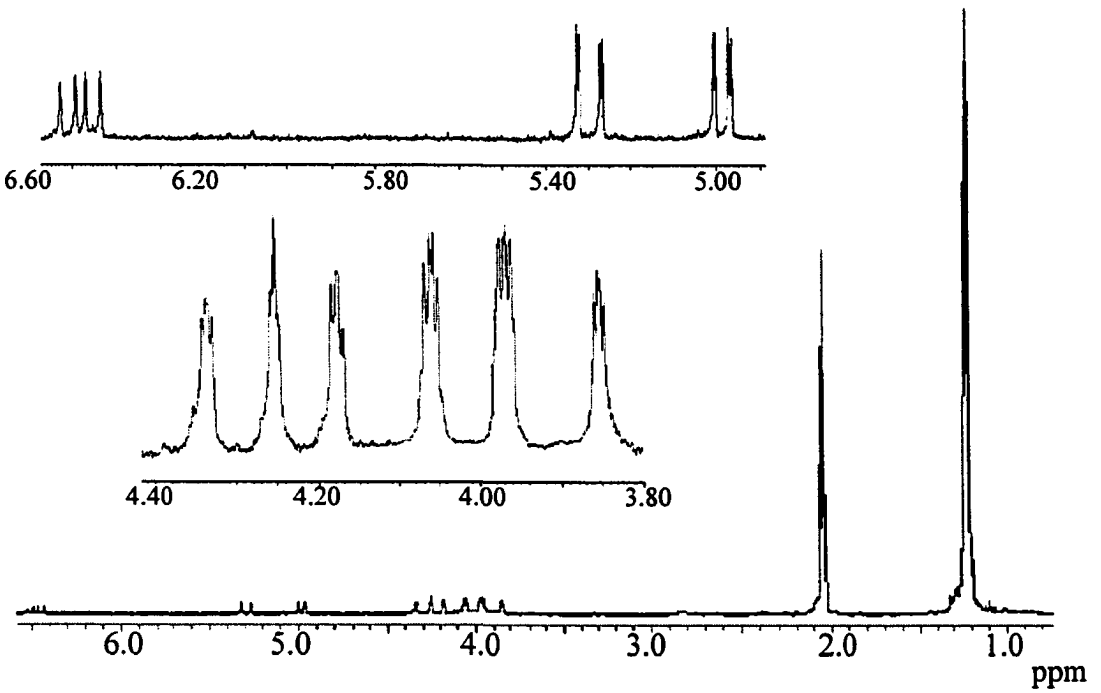

Figure 3.8. The ^{1}H-NMR spectrum of tri-BUT-Vn in acetone-d_6. The insets show the vinyl group proton (top) and rings proton (bottom) resonances.

olefination of ferrocenes has been the conversion of an acyl moiety into an olefin using Wittig reactions.[23-26] This method of olefination was performed with tri-BUT-Ac and methyltriphenylphosphonium iodide as shown in Scheme 3.3. The desired olefinic ferrocene, 1,1',3-tri(2-methyl-2-propyl)-3'-(2-propenyl)ferrocene (tri-BUT-Pr) was obtained as an orange oil in a 30% yield after purification by column chromatography. Though the yield was low, it is better than the 18% yield of olefin observed in the pyrolysis reaction and is performed under much milder conditions. In comparison, Miller

Scheme 3.3.

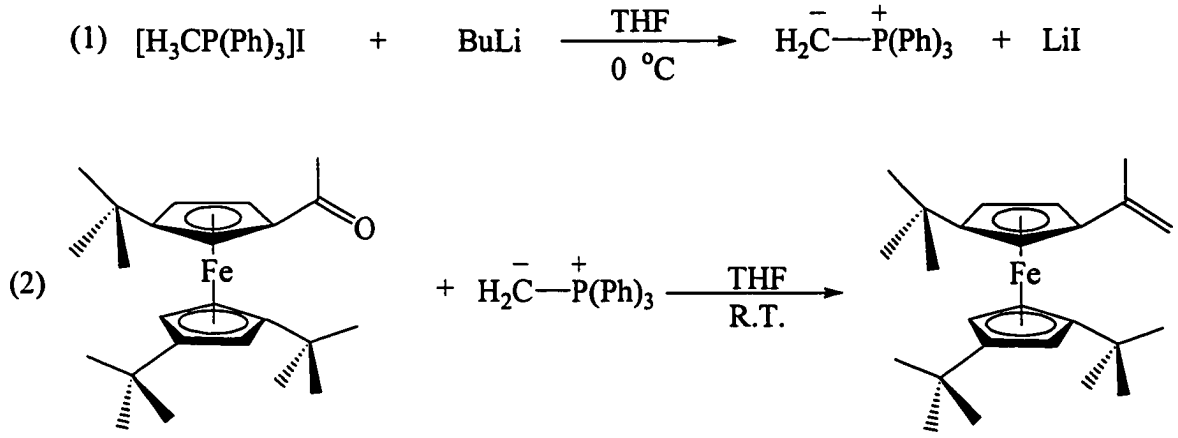

et. al. reported an 81% yield for the same reaction performed with acylferrocene.[23,25]

The mass spectrum and ^{1}H-NMR spectrum of tri-BUT-Pr can be seen in Figure 3.9 and 3.10 respectively. Both show the product to be pure. The mass spectrum gives the expected isotope pattern for a molecule with the appropriate number of carbon atoms and one iron atom. The ^{1}H-NMR spectrum shows the expected splitting pattern for the propenyl protons[25] with resonances at 4.86 and 5.03 ppm for the alkene protons and 2.07 ppm for the three propenyl group methyl protons. Six resonances are observed for the ring protons as expected.

The polymerization of both olefinic trialkylated ferrocenes, tri-BUT-Vn and tri-

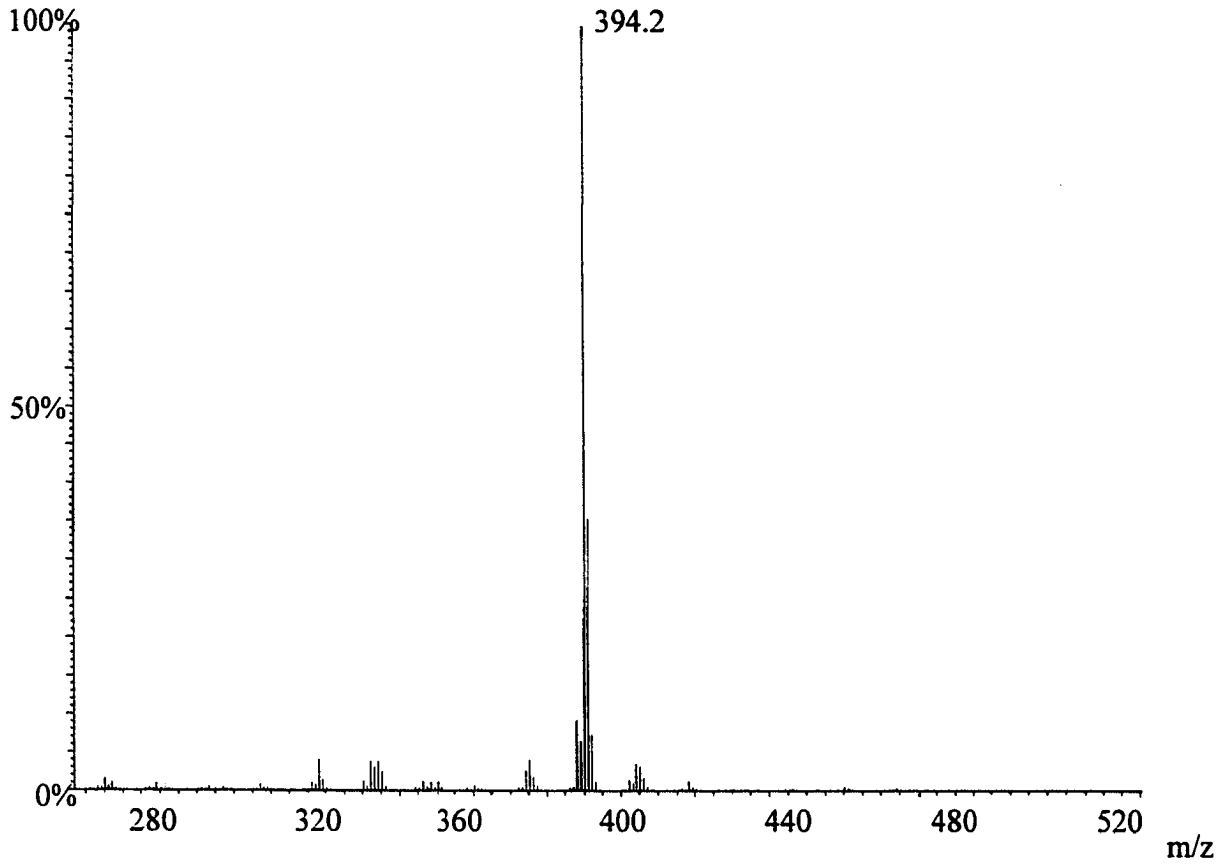

Figure 3.9. The LSIMS mass spectrum of tri-BUT-Pr (m/z 394.2, 394.38 calculated)

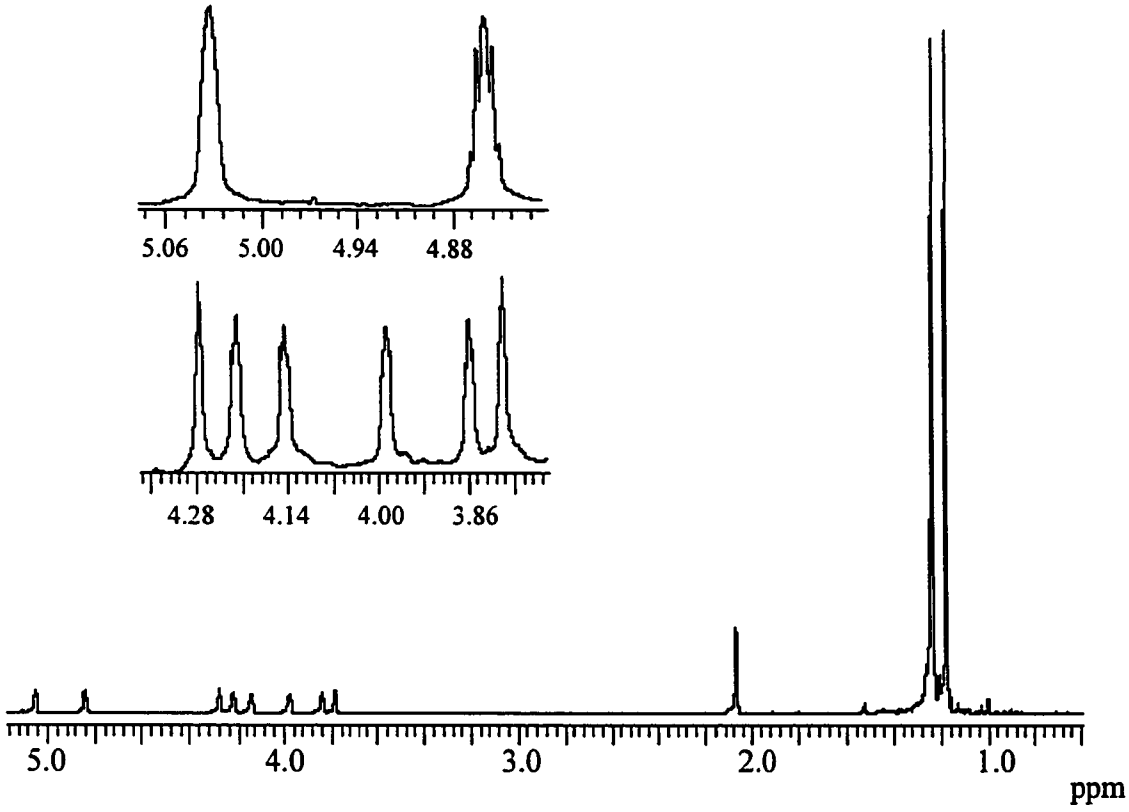

Figure 3.10. The ^{1}H-NMR spectrum of tri-BUT-Pr. The insets show the olefinic proton (top) and ring proton (bottom) resonances.

BUT-Pr, was attempted. The polymerization of vinylferrocene has been accomplished by radical, and cationic polymerization by a variety of methods including electrochemical polymerization.[17,27-29] Vinylferrocene has not been observed to polymerize under anionic conditions.[28] The polymerization of 2-propenylferrocene has been achieved with limited success by cationic polymerization methods.[22,30] Polymerization of 2-propenylferrocene by free radical polymerization has not been observed, but co-polymerization with styrene by free radical methods has had limited success.[22] No polymerization was observed for either tri-BUT-Vn or tri-BUT-Pr by radical or cationic methods. Electrochemical polymerization attempts were also unsuccessful. It is suspected that the presence of the *t*-butyl groups on the Cp rings sterically hinder polymerization by preventing a close enough approach of the polymerizable moieties. Co-polymerizations of both tri-BUT-Vn and tri-BUT-Pr with other monomers were not attempted. The presence of small, sterically unhindered monomers such as methyl methacrylate or styrene may overcome the problems observed during the homopolymerization attempts. Future experiments designed for synthesizing polyalkylated ferrocene polymers should be focused in this direction.

One final reaction was performed with tri-BUT. Since attempts to polymerize functionalized tri-BUT were unsuccessful, a method for covalent attachment to a polymer was devised. Due to the robust alkylation reaction of ferrocene under Friedel-Crafts alkylation conditions,[1,8,13] the covalent attachment of tri-BUT to poly(vinylbenzyl chloride) (PVBC) was attempted using Friedel-Craft alkylation chemistry. This reaction is shown in Scheme 3.4 and was carried out under the same reaction conditions used for the tetraalkylation of ferrocenes described previously[2,8,13]. During the reaction, the reaction mixture becomes gelatinous, presumably due to crosslinking of the polymer. (Under Friedel-Crafts reaction conditions, it is assumed that the chlorobenzyl groups can also react with the aromatic rings present in the polymer chain. Crosslinking of the polymer thus occurs simultaneously with the covalent attachment of the tri-BUT moiety.)

Scheme 3.4.

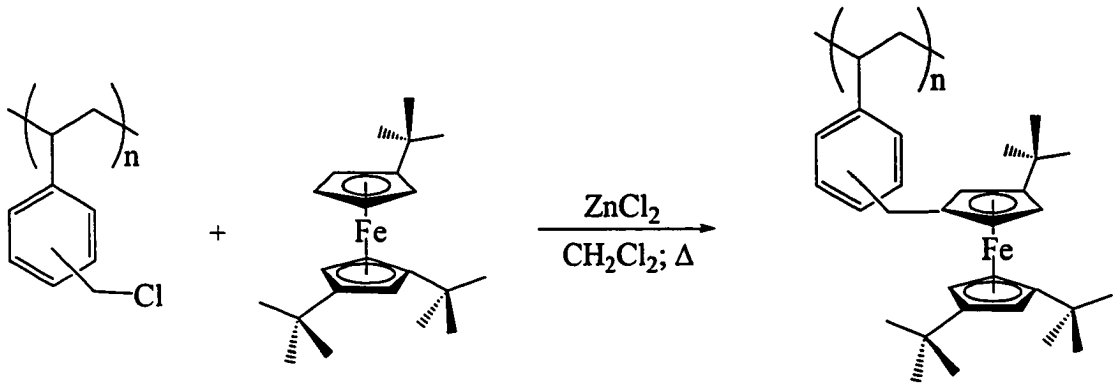

Upon complete solidification, the product was washed and filtered to yield a yellow solid and yellow filtrate. The ^{1}H-NMR spectrum of the yellow filtrate showed no trace of polymer, only unreacted tri-BUT. The yellow solid was washed thoroughly with dichloromethane until no further yellow color was observed in the filtrate. The resulting yellow solid was the ferrocenylated polymer (PVB-triBUT). The extent of covalent attachment was estimated to be 8 ± 3% by weight (0.26 mmol/g) from the amount of recovered tri-BUT in the filtrate from three separate reactions.

The solid isolated was insoluble in organic solvents and water. For this reason, characterization was performed only by FTIR spectroscopy. FTIR spectra of KBr pellets of tri-BUT, PVBC, and PVB-triBUT are shown in Figure 3.11. The spectrum of PVB-triBUT shows features present in both the tri-BUT and PVBC spectra as can be seen in the aromatic ν(CH) region (3000 to 3100 cm^{-1}) and the aliphatic ν(CH) region (2850 to 3000 cm^{-1}). Furthermore, ν(CCl) = 707 and 671 cm^{-1} in the spectrum of PVBC are not present in the spectrum of PVB-triBUT. The combination of ν(CH) stretches and the absence of the ν(CCl) in the spectrum of the final material as well as the fact that no tri-BUT species are washed off of the solid with organic solvents is a good indication of a covalent bond between the tri-BUT moiety and the polymer. Furthermore, the

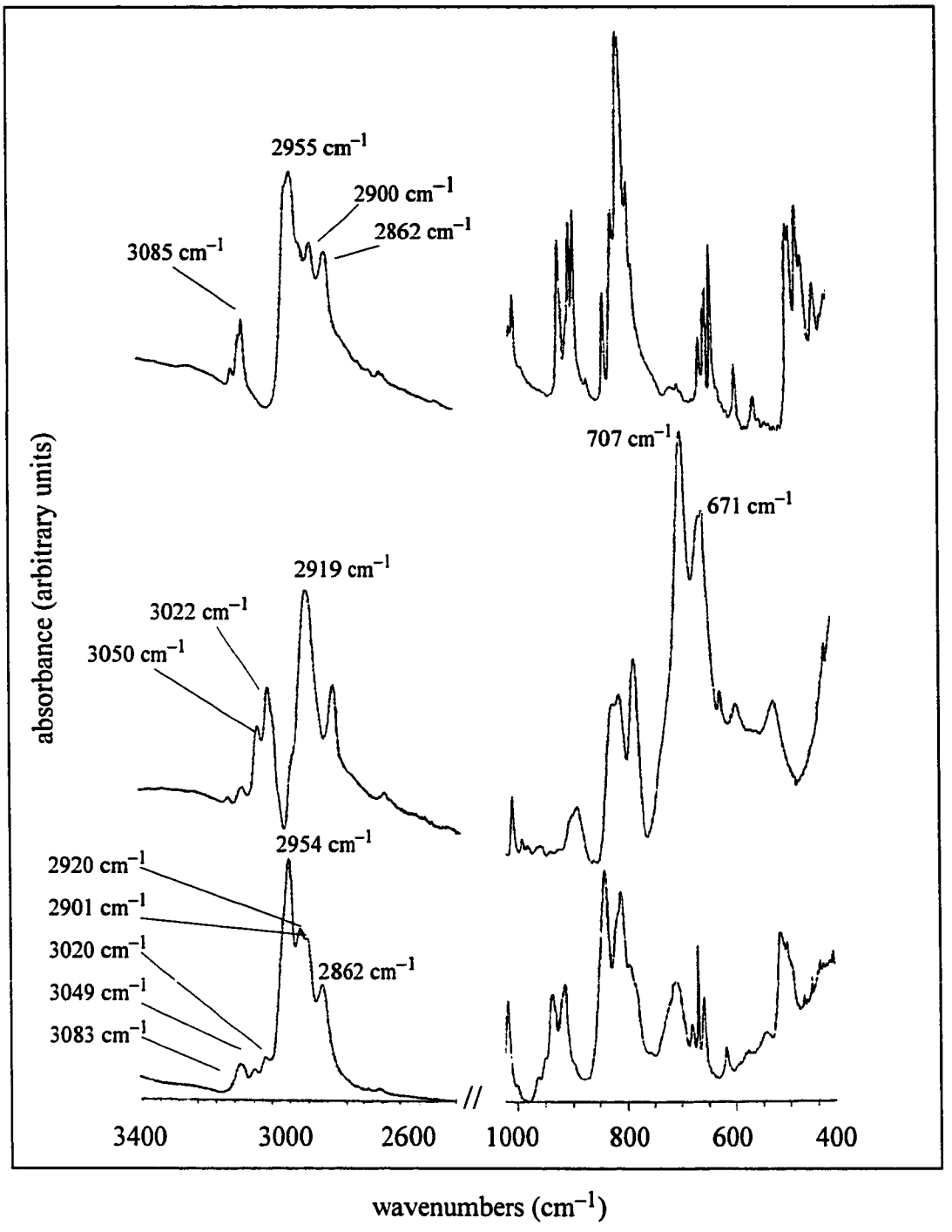

Figure 3.11. FTIR spectra of tri-BUT (top), PVBC (middle), and PVB-triBUT (bottom). The covalent attachment of tri-BUT to the PVBC polymer chain is evidenced by the disappearance of ν(CCl) = 707 and 671 cm^{-1} in the PVBC spectrum and the combination of ν(CH) stretches in the PVB-triBUT spectrum.

insolubility of the polymer suggests crosslinking of the polymer during the reaction.

PVB–triBUT was reacted with aqueous chemical oxidizing and reducing agents to test the recyclability of the new material. When stirred with an aqueous solution of the oxidizing agent $Ce(NH_4)_2(NO_3)_6$, the material changed color from yellow to bright green, indicating the formation of cationic tri-BUT$^+NO_3^-$ moieties in the material. Subsequent treatment of the oxidized material PVB–triBUT$^+NO_3^-$ with the aqueous reducing agent $Na_2S_2O_4$ changed the color from bright green back to yellow, indicating the reduction of the PVB–triBUT$^+NO_3^-$ material to the neutral PVB-triBUT material.

Functionalization of Tetraalkylated Ferrocenes. Due to the effect of extractant size on the selectivity of the ion-exchange process,[5] it was desirable to also functionalize, some larger, tetraalkylated ferrocenes for the attachment to surfaces and inclusion in materials. Strategies for doing this were similar to those mentioned earlier for the trialkylated ferrocenes.

The first tetraalkylated ferrocene modified was 1,1',3,3'-tetra(2-methyl-2-propyl)ferrocene (BUT). BUT was first functionalized in the same manner as tri-BUT as shown in Scheme 3.2, producing the three novel, tetraalkylated ferrocenes 1,1',3,3'-tetra(2-methyl-2-propyl)-4-acylferrocene (BUT-Ac), 1,1',3,3'-tetra(2-methyl-2-propyl)-4-(2-hydroxyethylferrocene (BUT-OH), and 1,1',3,3'-tetra(2-methyl-2-propyl)-4-vinylferrocene (BUT-Vn). Table 3.1 compares the yields between the Scheme 3.2 reactions of tri-BUT with the yields of the same reactions with BUT. In all cases, the yields were slightly lower for BUT, presumably due to steric factors as a result of the presence of the fourth alkyl substituent. Mass spectral data and ^{1}H-NMR data of all the functionalized BUT molecules were consistent with their proposed structures and showed the products to be pure. Mass spectra gave the expected isotope patterns for all products. The ^{1}H-NMR spectra for all functionalized BUT products were similar to those seen for the functionalized tri-*t*-butylferrocenes (*vide supra*) with the exception of the presence of only five distinct ring proton resonances, each due to one proton. The splitting patterns

Table 3.1. Comparison of reaction data for functionalized tri-BUT and BUT prepared by the reactions shown in Scheme 3.2.

functionality	tri-BUT product and yield (%)	BUT product and yield (%)
acyl	tri-BUT-Ac; 90	BUT-Ac; 88
α-hydroxyethyl	tri-BUT-OH; 96	BUT-OH; 94
vinyl	tri-BUT-Vn; 18	BUT-Vn; 12

of the ring proton resonances were not discernible due to peak broadening of the ring proton signals.

The preparation of 1,1',3,3'-tetra(2-methyl-2-propyl)-4-(2-propenyl)ferrocene (BUT-Pr) was also attempted under the same Wittig conditions used for the preparation of tri-BUT-Pr shown in Scheme 3.3, but no reaction was observed. It is known that conversions of acyl groups to olefins under Wittig conditions require the formation of sterically bulky oxaphosphetane intermediates.[31,32] The oxaphosphetane intermediate required for the Wittig reaction of BUT-Ac with $H_2C^-–^+PPh_3$, below, is probably prohibited from forming due to steric hindrance from the four *t*-butyl groups on

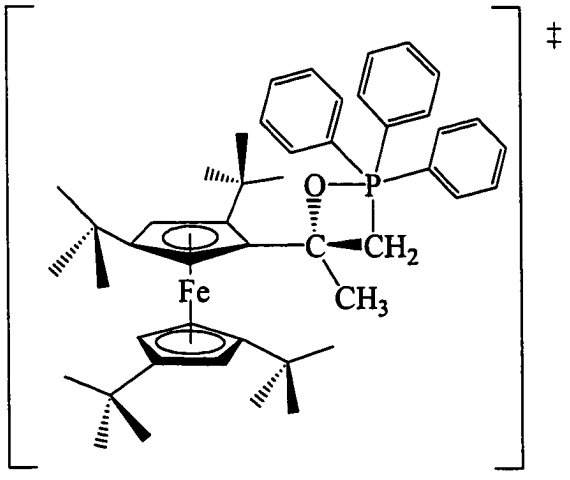

the Cp' rings of BUT-Ac. Unlike the trialkylated ferrocene, partial rotation of the Cp' rings of the tetraalkylated ferrocene can not give an orientation that isolates the starting acyl group from steric interactions of the *t*-butyl groups on the adjacent Cp' ring. The bulky intermediate in the Wittig reaction is therefore unable to form.

Other methods for formation of BUT-Pr were explored including the Takai reagent ($CH_2I–Zn–TiCl_4$)[33] and the Petasis reagent (Cp_2TiMe_2).[34,35] No reaction was observed using the Takai reagent. The Petasis reagent is believed to react through the formation of methylidenetitanocene ($Cp_2Ti{=}CH_2$), like Tebbe's reagent

($Cp_2Ti(Cl)CH_2AlMe$), but the intermediate is generated from dimethyltitanocene.[36,37] The reaction of BUT-Ac with the Petasis reagent is shown in Scheme 3.5.

Scheme 3.5.

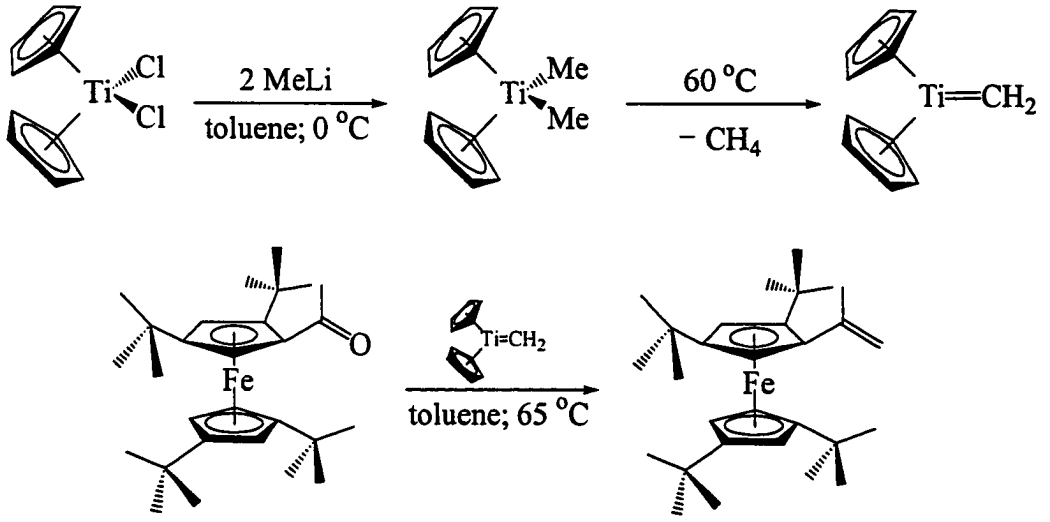

Dimethyltitanocene is generated *in situ* by addition of 2 equivalents of methyl lithium to titanocene dichloride. Addition of BUT-Ac gave the desired product, BUT-Pr in a 68% yield, which is larger than that obtained for tri-BUT-Pr by the Wittig reaction. Preparation of tri-BUT-Pr using the Petasis reagent has not been tried. The mass spectrum and ^{1}H-NMR of BUT-Pr are shown in Figures 3.12 and 3.13 respectively. Both show the product to be pure. The mass spectrum gives the expected isotope pattern for a molecule with the appropriate number of carbons and one iron atom. The ^{1}H-NMR spectrum in benzene-d_6 shows the expected splitting pattern for the propenyl moiety protons[25] with resonances at 5.24 and 5.55 ppm for the alkene protons and 1.97 ppm for the three methyl protons. Five resonances are observed for the ring protons as expected.

The polymerizations of BUT-Vn and BUT-Pr were attempted under similar

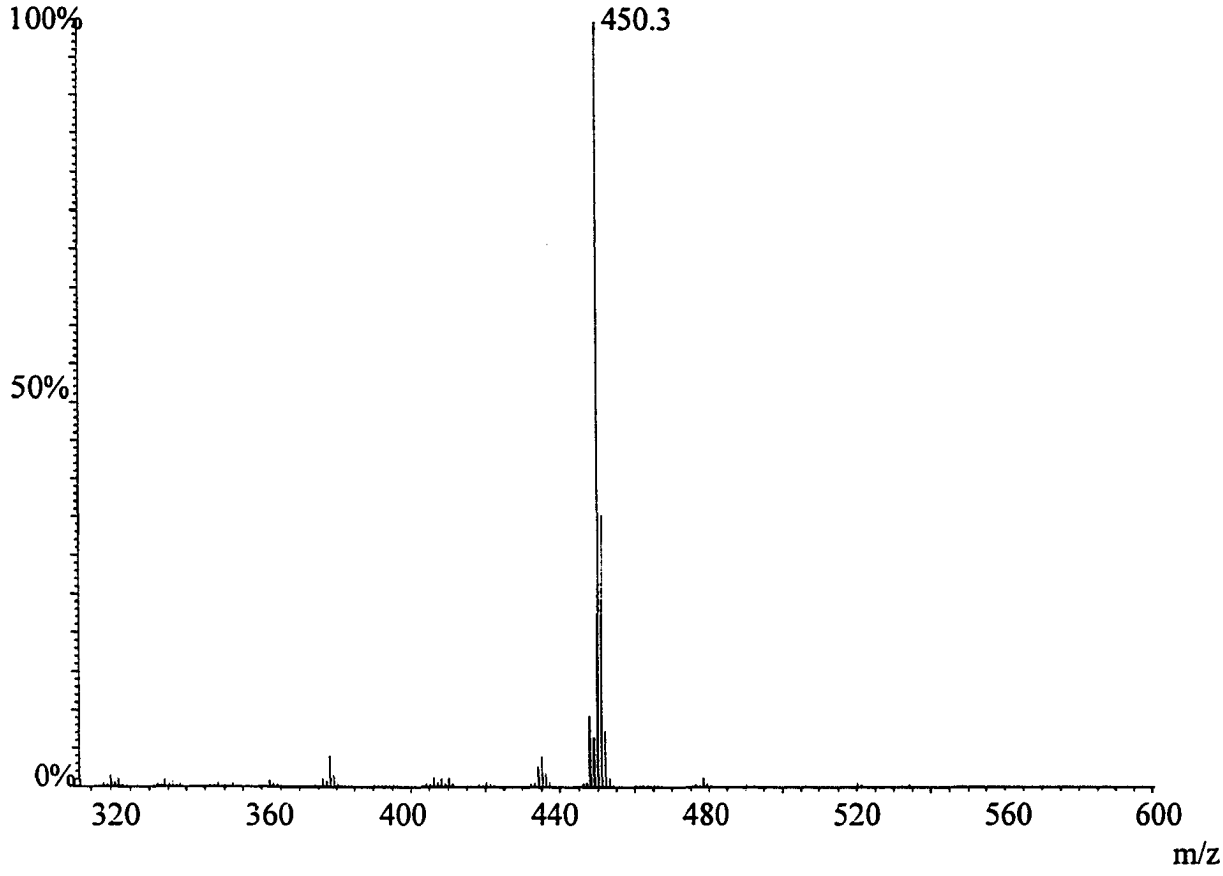

Figure 3.12. The LSIMS mass spectrum of BUT-Pr (m/z 450.3; 450.49 calculated).

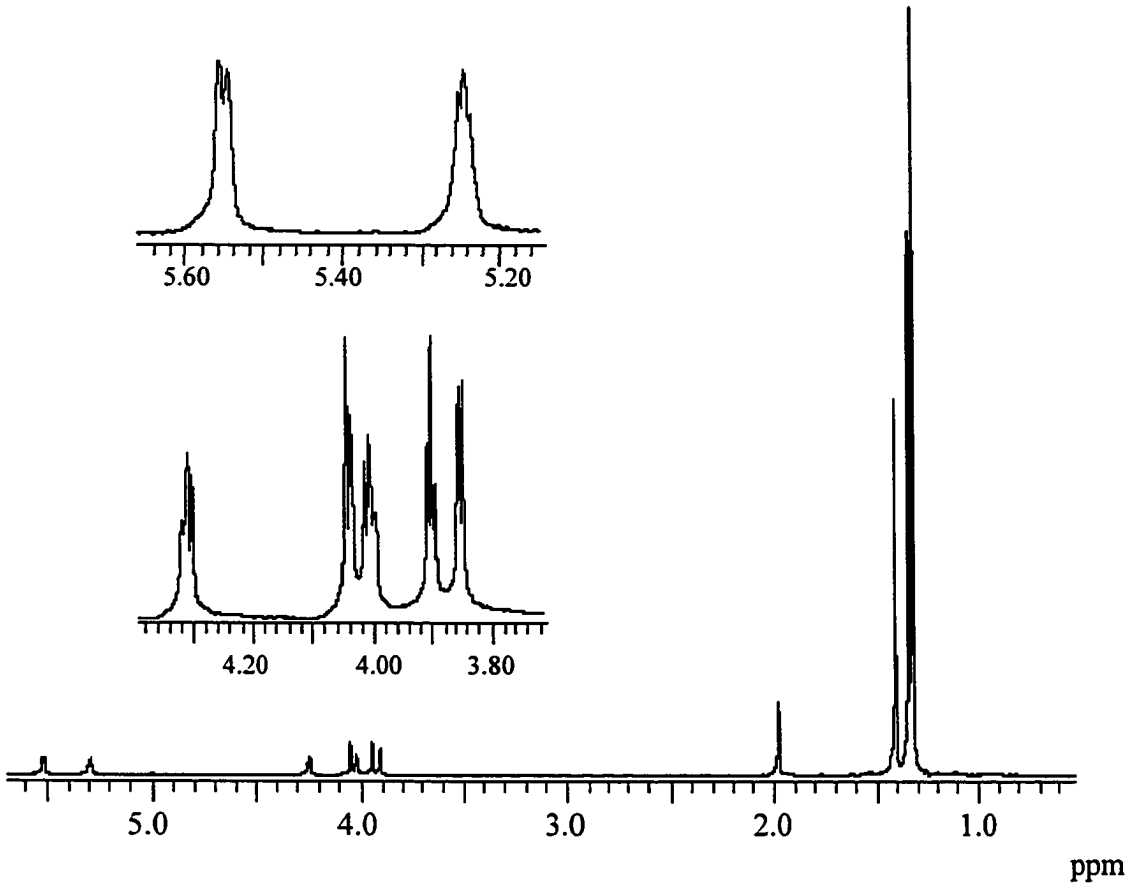

Figure 3.13. The ^{1}H-NMR spectrum of BUT-Pr in benzene-d_6. The insets show the olefinic proton (top) and ring proton (bottom) resonances.

conditions to those described for tri-BUT-Vn and tri-BUT-Pr. Again no polymerization was observed. Attempted co-polymerizations with styrene and methyl methacrylate alsofailed. The Friedel-Crafts modification of PVBC was also attempted with BUT, but no tetraalkylated ferrocene inclusion was observed. It is clear from the attempted polymerization studies and previous success of polymerization of non-alkylated ferrocenes with the same functional groups[28] that the alkyl groups of the polyalkylated ferrocenes greatly influence the preparation of the materials able to be produced from the synthesized monomers. It is assumed that the major influence on the polymerization reactions is steric in nature. Due to the tertiary alkyl groups on both Cp' rings, steric hindrance not only occurs from either side of the olefinic moiety, but also from below. For these reasons, further functionalization reactions designed to extend the polymerizable olefinic groups beyond the steric influence of the alkyl groups were designed.

Scheme 3.6 shows the preparation of two new tetraalkylated ferrocenes with

Scheme 3.6

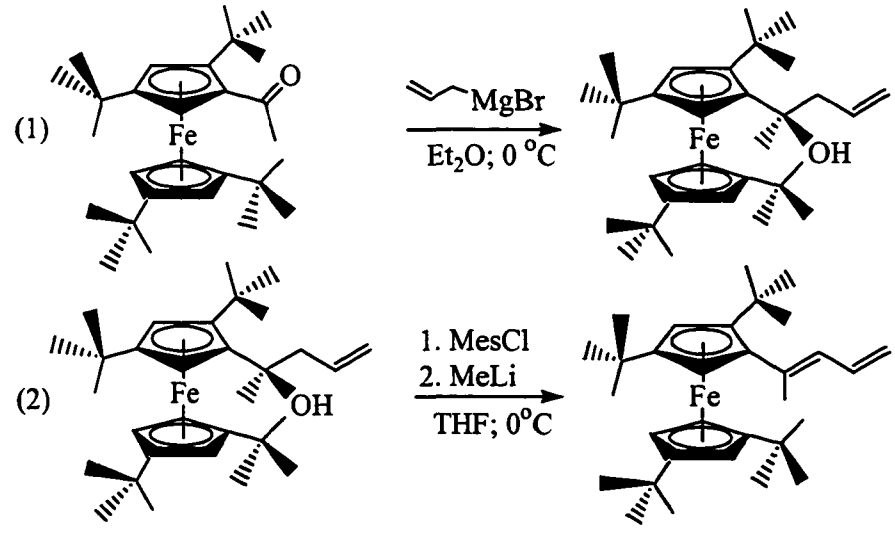

olefinic groups extended beyond the steric scope of the *t*-butyl groups present on the Cp' rings. The reaction of BUT-Ac with allyl Grignard gives 1,1',3,3'-tetra(2-methyl-2-propyl)-4-(2-hydroxy-2-(4-pentenyl))ferrocene (BUT-PtOH) in a 99% yield. The

product BUT-PtOH is isolated as a red-orange solid and the vinyl group extends 2 carbon atoms farther than the *t*-butyl groups on the Cp' ring. The mass spectrum and ^{1}H-NMR spectrum can be seen in Figures 3.14 and 3.15 respectively. Both show the product to be pure. The mass spectrum gives the expected isotope pattern for a molecule with the appropriate number of carbons, one oxygen atom, and one iron atom. The ^{1}H-NMR spectrum shows the expected splitting pattern for the olefinic protons with resonances at 5.03 and 5.75 ppm for the alkene protons and a doublet at 2.55 ppm for the two methylene protons. Four broad resonances due to a total of five protons are observed for the ring protons. In addition, a singlet due to three protons is observed at 1.7 ppm for the methyl group on the hydroxy substituted carbon atom.

The second reaction in Scheme 3.6 was designed for the methylation of the α-carbon atom of the Cp' ring. The original intent of the reaction was to replace the α-hydroxy moiety with a methyl group by first mesylating the α-position with methanesulfonyl chloride (MesCl) followed by nucleophilic attack with a methyl carbanion. The resulting product was not the desired methylated product, but instead the elimination product 1,1',3,3'-tetra(2-methyl-2-propyl)-4-(2-(2,4-dipentenyl))ferrocene (BUT-diPt). The reason for elimination instead of methylation is again believed to be due to sterics, as demonstrated below. Nucleophilic attack at the tertiary α-carbon atom cannot occur due to steric congestion from the methyl, allyl, and tetra-*t*-butylferrocenyl (Fc') moieties. As a result, elimination occurs creating the dienyl moiety observed. Sterics, however, apparently do not prevent the initial mesylation from occurring; the reaction does not proceed as described if the mesylation step is omitted before the addition of methyllithium. The observed elimination product is obtained in an 87% yield. The mass spectrum and ^{1}H-NMR spectrum of BUT-diPt can be seen in Figures 3.16 and 3.17 respectively. Both show the product to be pure. The mass spectrum gives the expected isotope pattern for a molecule with the appropriate number of carbons, one oxygen atom, and one iron atom. The ^{1}H-NMR spectrum shows the expected splitting

nucleophilic attack

side view

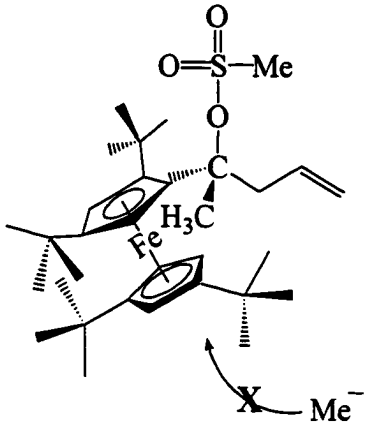

top view

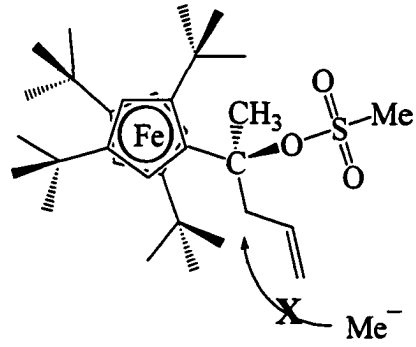

elimination

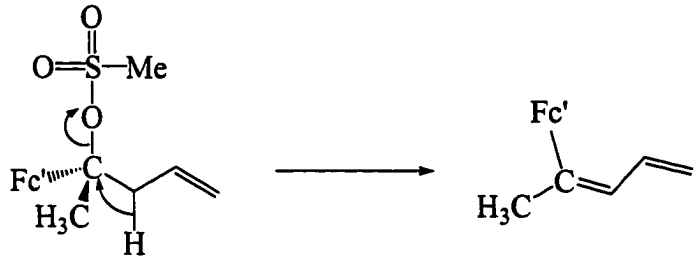

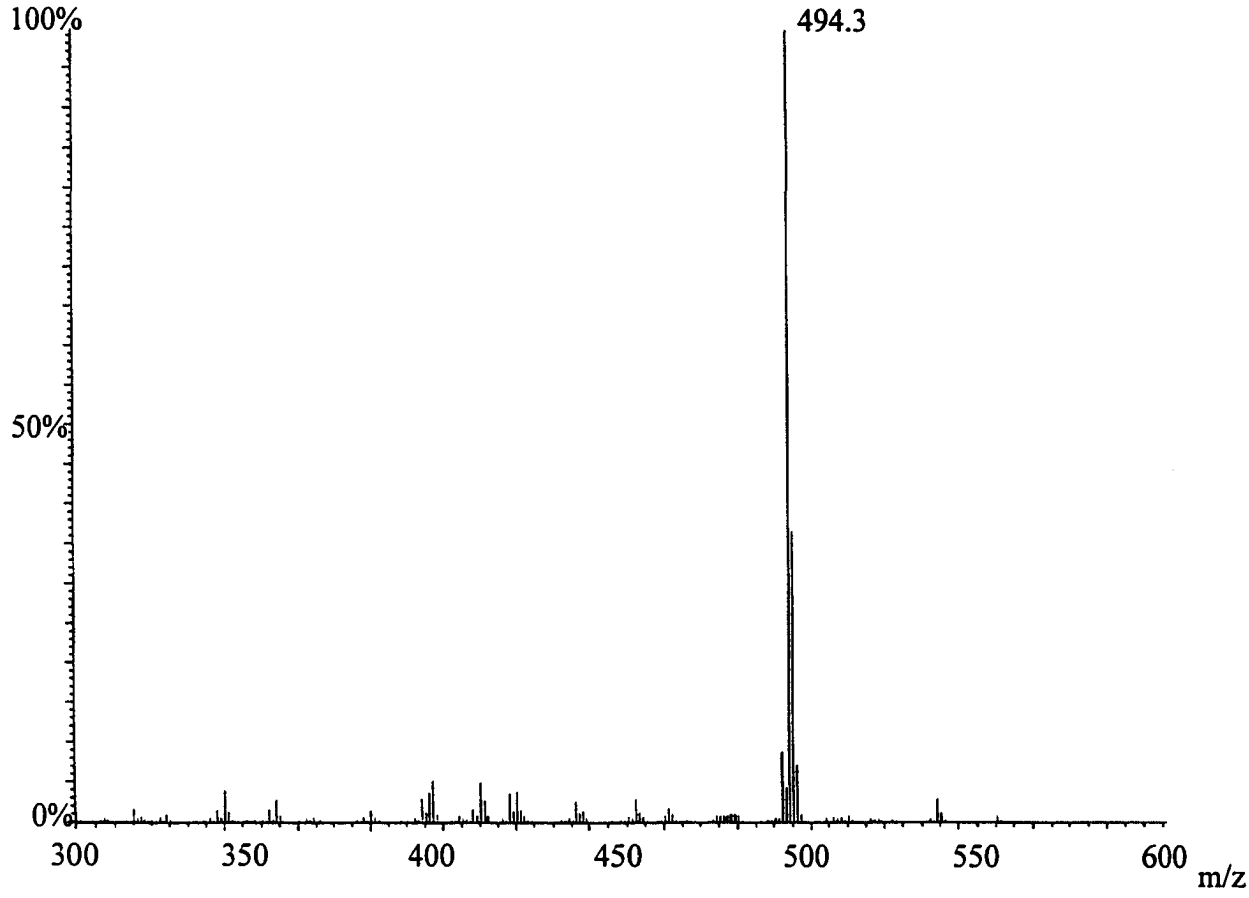

Figure 3.14. The LSIMS mass spectrum of BUT-PtOH (m/z 494.3; 494.59 calculated).

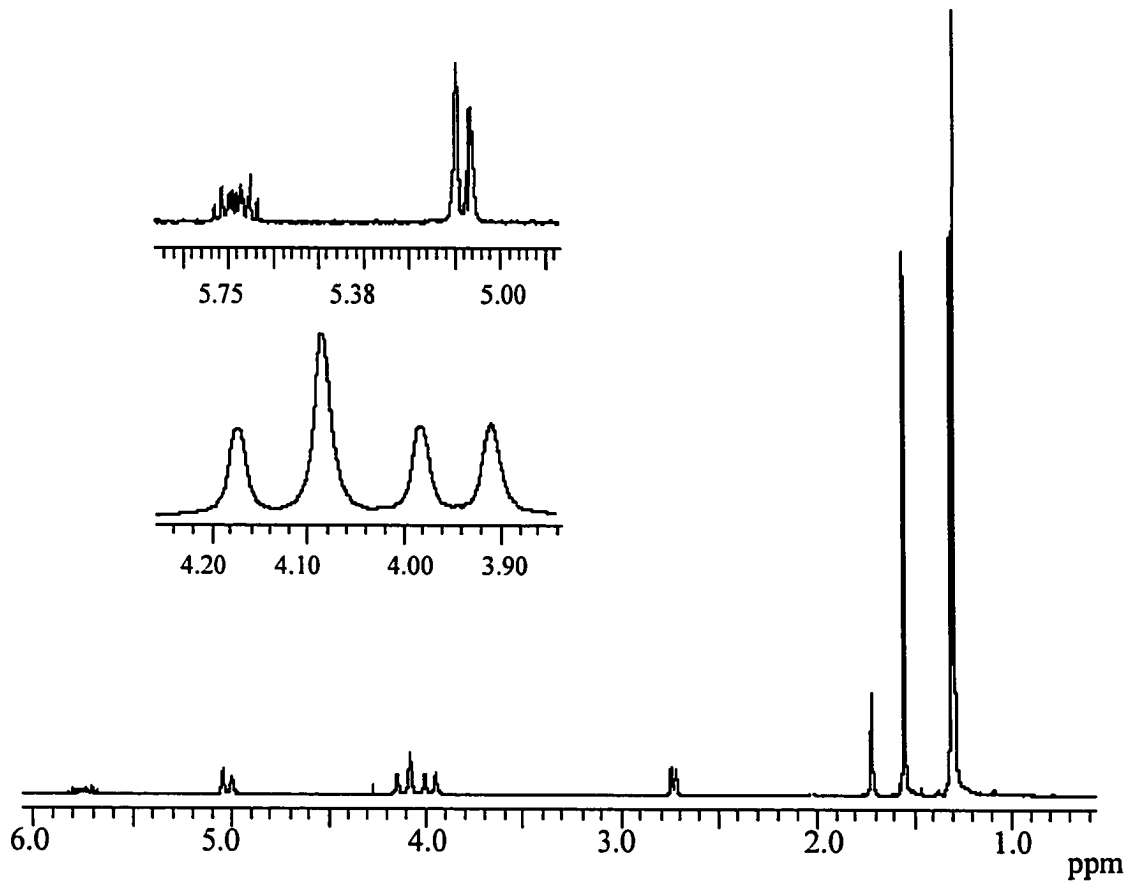

Figure 3.15. The ^{1}H-NMR of BUT-PtOH in benzene-d_6. The insets show the olefinic proton (top) and ring proton (bottom) resonances.

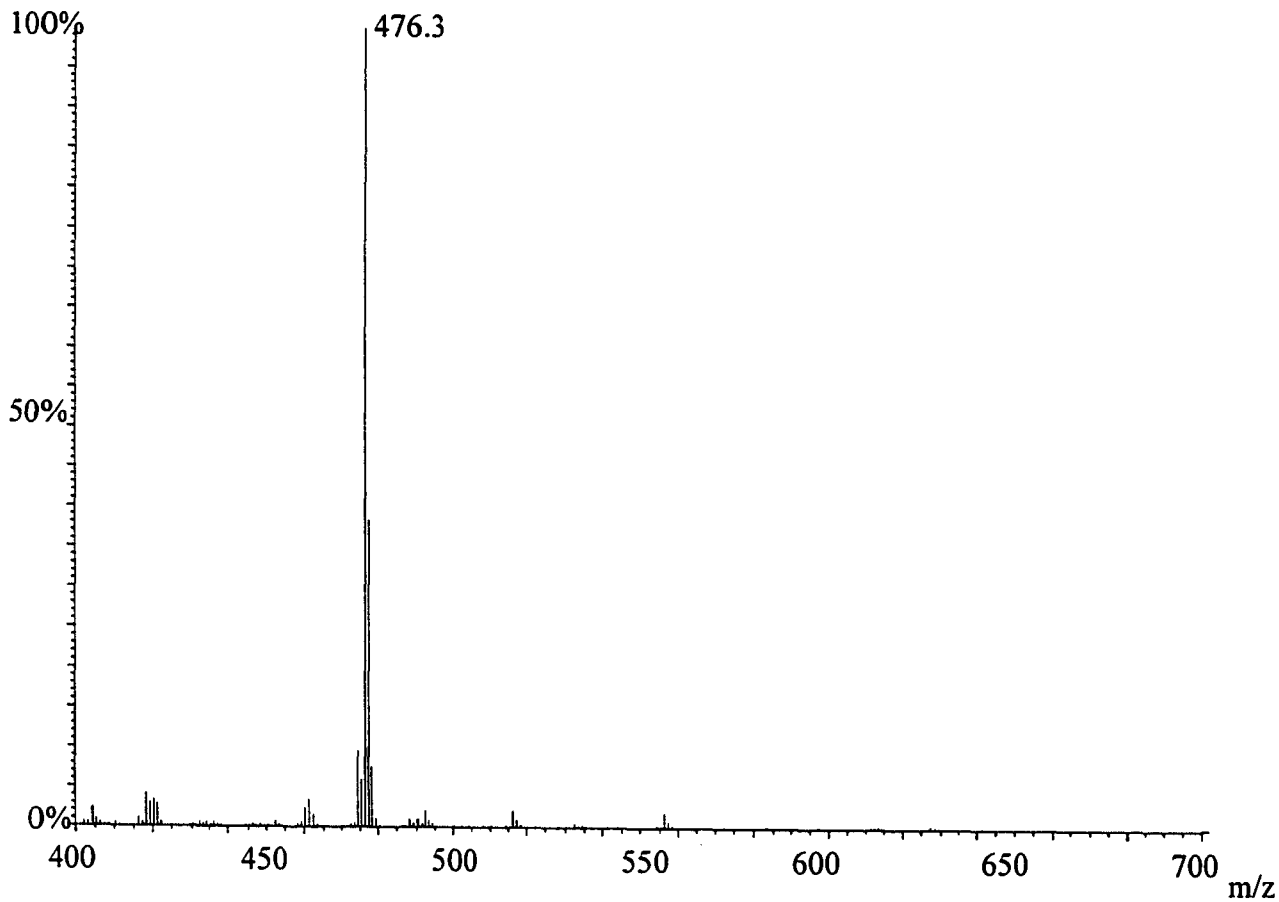

Figure 3.16. The LSIMS mass spectrum of BUT-diPt (m/z 476.3; 476.57 calculated).

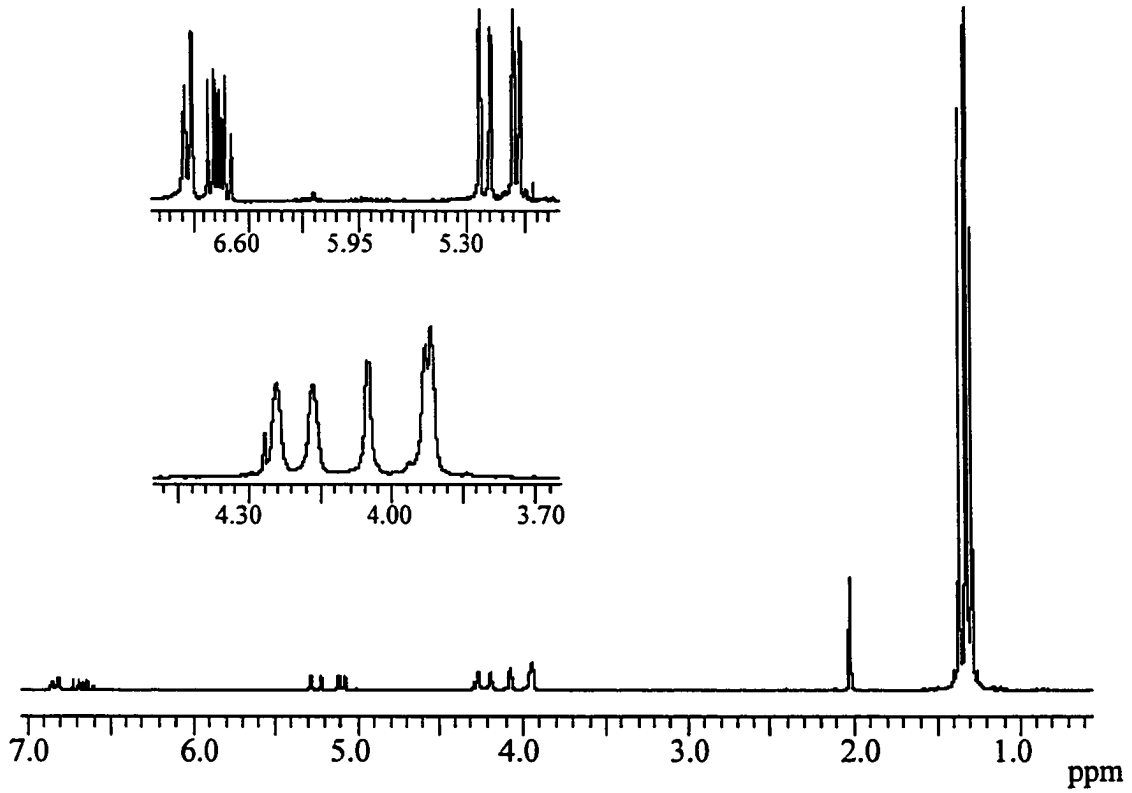

Figure 3.17. The ^{1}H-NMR of BUT-diPt in benzene-d_6. The insets show the olefinic proton (top) and ring proton (bottom) resonances.

pattern for the dienyl protons with resonances at 6.84 (m), 6.65 (m), 5.25 (dd), and 5.10 (dd) ppm for the olefinic protons and a singlet at 2.03 ppm for the methyl group protons. Four broad resonances due to a total of five protons are observed for the ring protons.

Co-polymerization of BUT-PtOH was attempted with both styrene and methyl methacrylate. Co-polymerization of BUT-PtOH with styrene under radical conditions was not successful as indicated by leaching of the ferrocene from the polymerized styrene in a variety of solvents. Furthermore, ^{1}H-NMR of the product clearly shows the resonances due to the olefinic protons of BUT-PtOH. Co-polymerization under radical conditions of BUT-PtOH with methyl methacrylate, however, appears to have been successful. No leaching of ferrocene is observed from the final product and ^{1}H-NMR shows no evidence of olefinic proton resonances. The resulting polymeric material was unable to be oxidized or reduced with aqueous oxidizing or reducing agents, presumably due to the non-wetability of poly(methyl methacrylate). Polymerizations of BUT-diPt were not attempted, but should be explored in the future.

Hydrosilation Reactions of Vinylferrocene and Olefinic Polyalkylated Ferrocenes. As stated above, in addition to inclusion in polymeric materials, the covalent attachment of polyalkylated ferrocenes to metal oxide surfaces is also desirable. Surfaces of particular interest include silica and ITO. The ion-exchange properties of HEP physisorbed onto silica have been reported previously.[3] The physisorbed HEP molecules, however, were observed to migrate on the silica support after extended periods of exposure to water.[9] For this reason, it is desirable to synthesize polyalkylated ferrocenes with functional groups that can be reacted to form covalent bonds to metal oxide surfaces. Such linkages would prevent the migration of the extractant on the surface of the resulting ion-exchange materials. As shown in Scheme 3.7, one such functional group that results in a covalent bond to hydroxylated metal-oxide surfaces is a siloxy moiety (Si–OR).[38] Following hydroxylation of the metal oxide surface with a strong base, the metal oxide surface is then soaked in an alcoholic solution of a

Scheme 3.7.

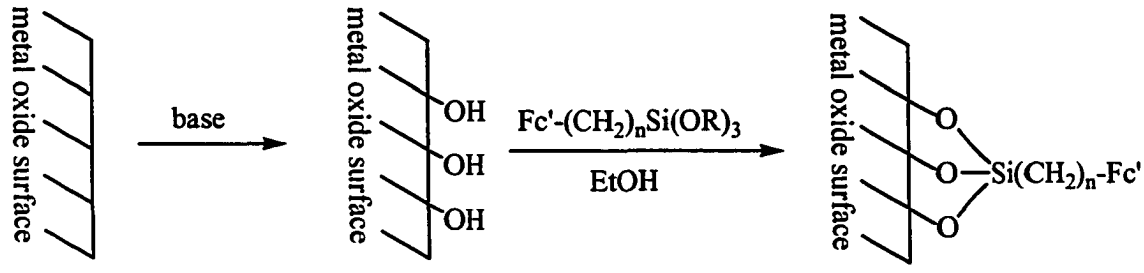

functionalized siloxane ($Fc'\text{-}(CH_2)_nSi(OR)_3$). The siloxy moieties are easily converted to silanols (Si–OH) in alcoholic media that can then undergo a condensation step with the hydroxy groups present on the metal oxide surface. The result is a covalent Si–O–surface linkage.

Synthesis of a siloxy-functionalized ferrocene can be accomplished through the hydrosilation of an olefinic ferrocene with a trialkoxysilane in the presence of a transition metal catalyst. Such a reaction with vinylferrocene is shown in Scheme 3.8. There are

Scheme 3.8.

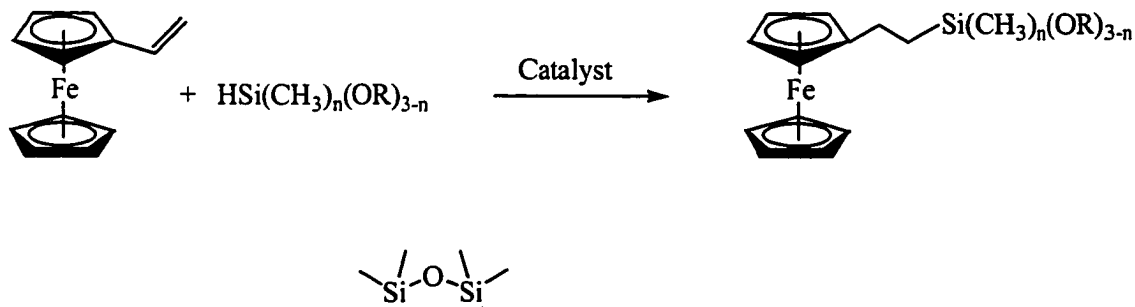

Catalyst = 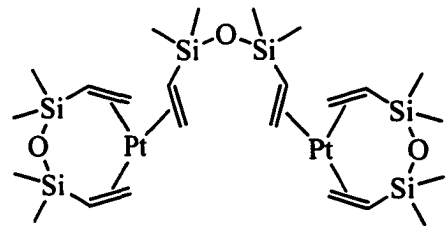

or $H_2PtCl_6 \cdot x\,H_2O$ (x = 2, 4, 6)

Karstedt's (Pre)Catalyst

Speier's (Pre)Catalyst

many catalysts known to catalyze this reaction, but the two most common hydrosilation catalysts are Speier's catalyst (hydrogen hexachloroplatinate(IV)) and Karstedt's catalyst (*rac*-tris(divinyltetramethyldisiloxane)diplatinum(0)[39]). The hydrosilation of olefinic ferrocenes has been performed for a variety of applications including dendrimer growth,[40,41] silsesquioxane functionalization,[42,43] and preparation of ferrocenyltrialkylsilanes.[44,45] All of these applications, with the exception of silsesquioxane functionalization, have used alkylsilanes as substrates. The only known example of hydrosilation of an olefinic ferrocene using alkoxysilanes is the hydrosilation of decaallylferrocene, which has been hydrosilated at all ten olefinic sites in a 90% yield using triethoxysilane and Karstedt's catalyst.[40]

Before attempting hydrosilation reactions of olefinic polyalkylated ferrocenes, several hydrosilations were performed first with vinylferrocene and a variety of silanes as shown in Scheme 3.8. The result was the production of several novel ferrocenyl-alkoxysilanes. Reactants, products, and yields of these hydrosilations are summarized in Table 3.2. The data suggest that the presence of electron withdrawing or donating groups on the silane has an effect on the hydrosilation reaction. The presence of electron withdrawing or donating groups on the silicon atom affects the Si–H bond strength and also the resulting Pt(0)–Si bond in the catalytic complex formed.[46] A strong Si–H bond will slow or prevent coordination of the silane to the Pt(0) catalyst. In a subsequent catalytic step, a strong Pt(0)–Si bond will slow or prevent dissociation of the final complex. The effect of strong Si–H and Pt(0)–Si bonds on the hydrosilation reaction is shown below. The silane with the most electron withdrawing groups will have the strongest Si–H bond due to inductive electron withdrawing effects from the electropositive silicon atom. The same effect should be seen for a Pt(0)–Si bond. It is therefore predicted that hydrosilations performed with silanes that have electron withdrawing groups should have smaller yields than those performed with silanes containing no or fewer electron withdrawing groups.

Table 3.2. Summary of hydrosilation reactions with vinylferrocene.

silane	catalyst	product	amt. of catalyst[a]	yield[b]
$HSi(CH_3)_2(OEt)$	Karstedt's	Fc-DMES	0.30%	67%
$HSi(OEt)_3$	Karstedt's; Speier's	Fc-TES	0.30%; 0.30%	27%; 17%
$HSi(OMe)_3$	Karstedt's	Fc-TMS	0.16% to 1.6%	<1%[c]
$HSiCl_3$	Karstedt's	no rxn.	0.08% to 1.6%	—

[a] Values are expressed as mole percent platinum relative to the starting amount of vinylferrocene. [b] Percent yields given are approximate. Final products still contain minor amounts of impurities. [c] Only observed by mass spectrometry.

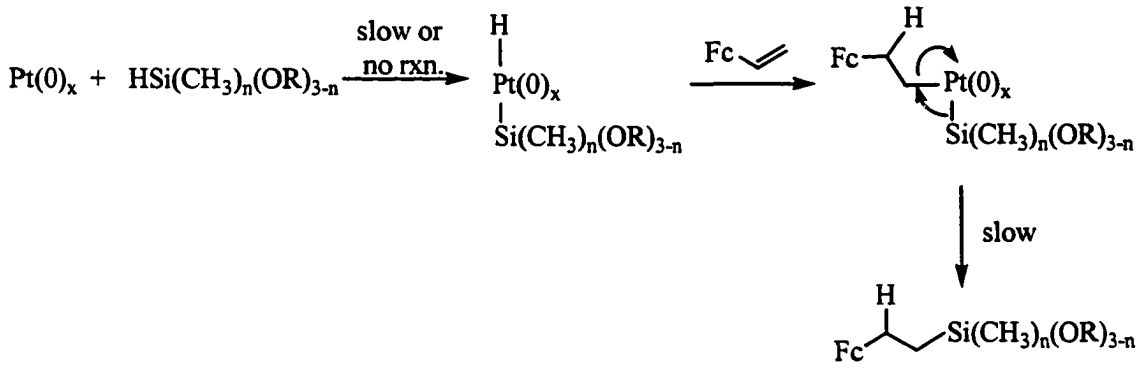

The data in Table 3.2 support this hypothesis. For example, no silated ferrocene was obtained for the reaction with $HSiCl_3$. This silane has three electron withdrawing chlorine atoms bonded to the silicon atom, thus increasing the Si–H bond strength. This trend can also be seen in the lower yields obtained for the trialkoxysilanes compared to the monoalkoxysilane. The hydrosilation reaction with dimethylethoxysilane produced a greater yield of hydrosilated product (67%) than triethoxysilane (27%) or trimethoxysilane (1%). The electron withdrawing alkoxy substituents strengthen the Si–H bond while electron donating alkyl groups weaken it. Furthermore, the effect of the alkyl substituent of the alkoxy group also appears to play a role. Very little product was observed for hydrosilation with trimethoxysilane, but a 27% yield was observed for hydrosilation with triethoxysilane. The difference in yields can be explained by the added electron donating ability of an ethyl group versus a methyl group. The more electron density the oxygen atom can receive from the alkyl group, the less electron density it will take from the silicon atom, therefore the overall effect of substituting OEt for OMe groups would be to weaken the Si–H bond and make the hydrosilation reaction more favorable.

The two novel silated ferrocenes, ferrocenylethyldimethylethoxysilane (Fc-DMES) and ferrocenylethyltriethoxysilane (Fc-TES), were isolated as yellow/orange oils and the ^{1}H-NMR spectra and mass spectra can be seen in Figures 3.18 and 3.19 respectively. The mass spectra show the expected isotope patterns for molecules with the

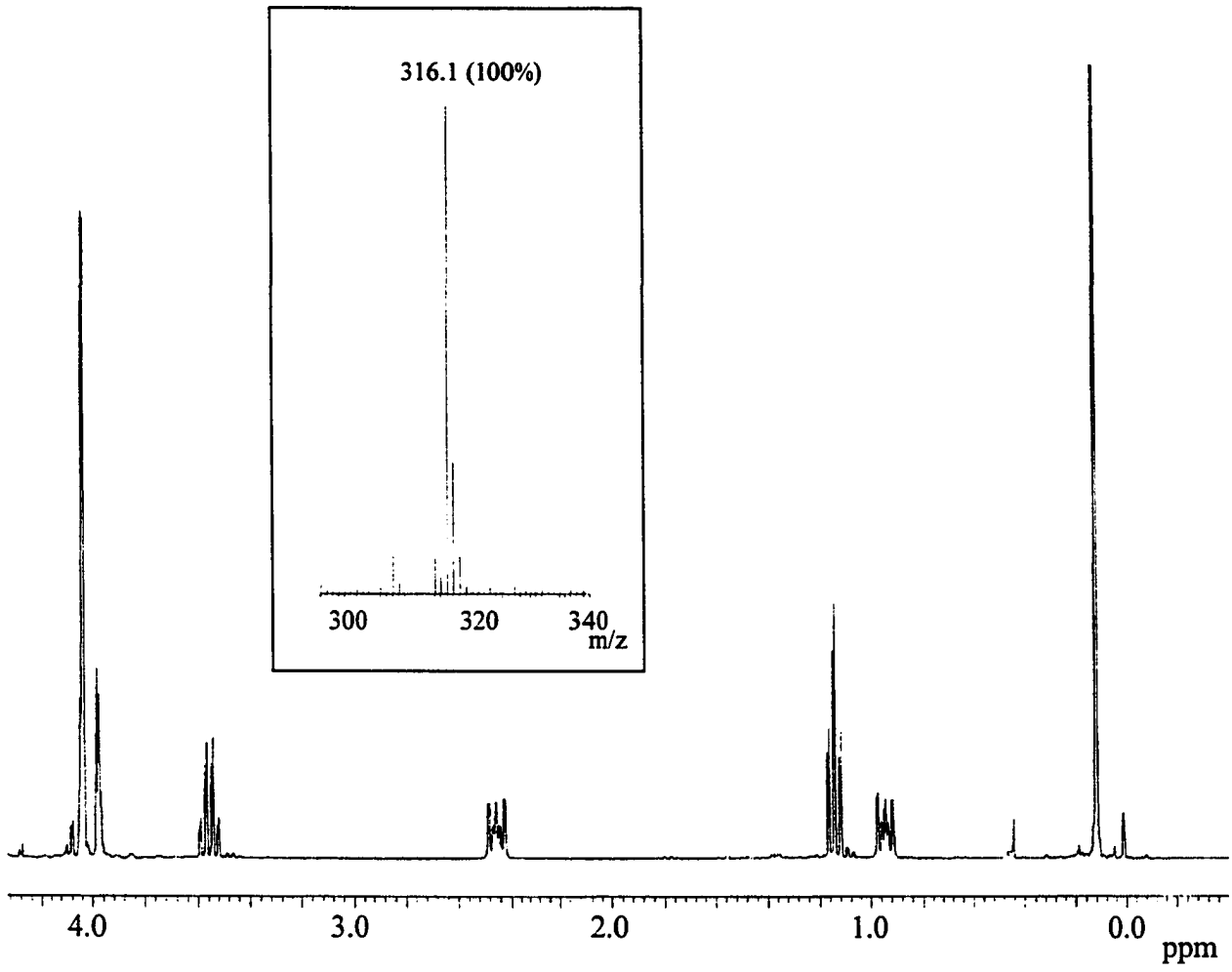

Figure 3.18. ^{1}H-NMR spectrum (benzene-d_6) and the LSIMS mass spectrum (inset) of Fc-DMES (m/z 316.1; 316.29 calculated). The relative peak height is shown in parentheses in the mass spectrum. The ^{1}H-NMR spectrum shows resonances for the ethoxy protons at 3.56 (q, 2H) and 1.14 (t, 3H) ppm, ring protons at 4.03 (s, 5H) and 3.99 (m, 4H) ppm, methyl protons at 0.12 (s, 6H) ppm, and methylene protons at 2.46 (m, 2H) and 0.94 (m, 2H) ppm.

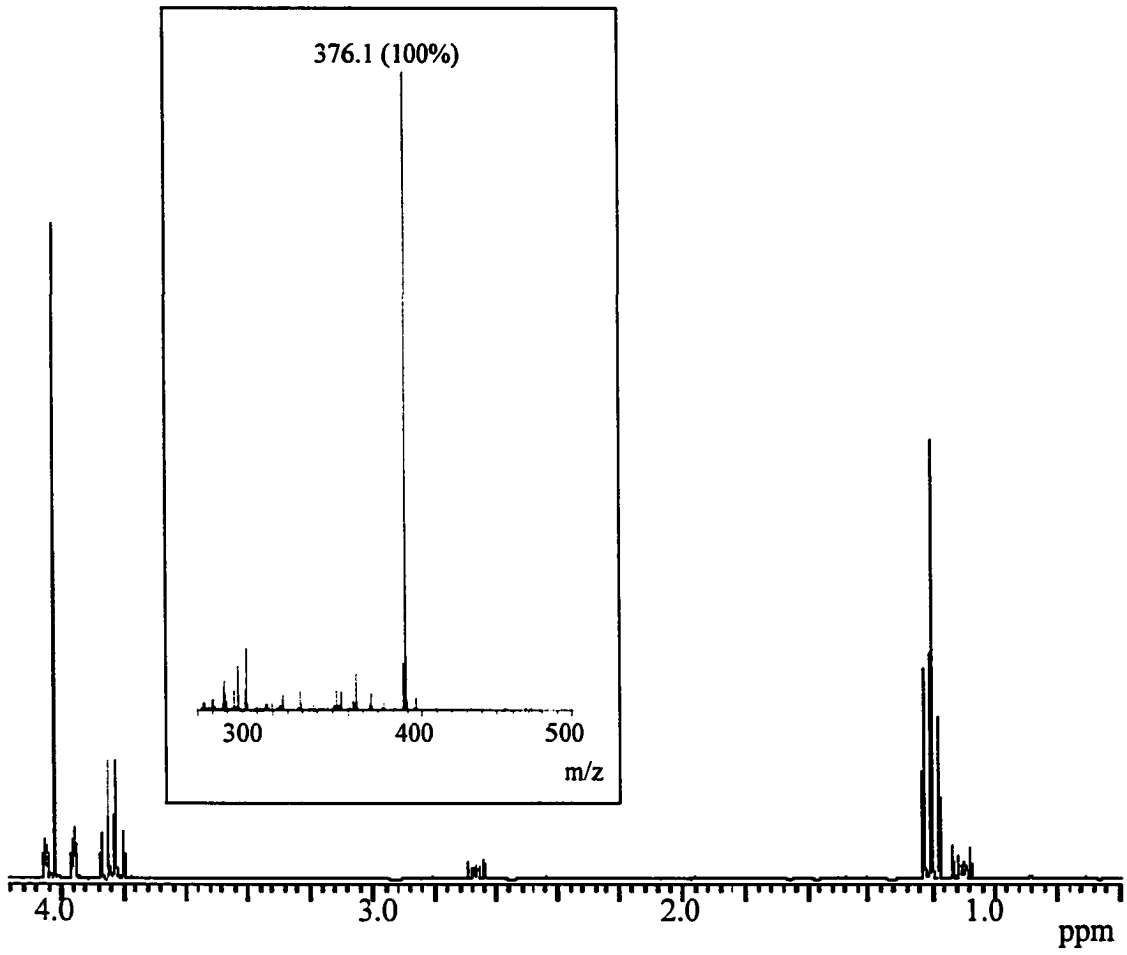

Figure 3.19. ^{1}H-NMR spectrum (benzene-d_6) and the LSIMS mass spectrum (inset) of Fc-TES (m/z 376.1; 376.35 calculated). The relative peak height is shown in parentheses in the mass spectrum. The ^{1}H-NMR spectrum shows resonances for the ethoxy protons at 3.84 (q, 6H) and 1.21 (t, 9H) ppm, ring protons at 4.05 (t, 2H), 4.02 (s, 5H), and 3.96 (t, 2H) ppm, and methylene protons at 2.67 (m, 2H) and 1.11 (m, 2H) ppm.

appropriate number of carbon and oxygen atoms with one iron and one silicon atom. The ^{1}H-NMR spectrum of Fc-DMES (Figure 3.18) shows the expected resonances and splitting patterns. The ^{1}H-NMR spectrum of Fc-TES (Figure 3.19) also shows the expected resonances and splitting patterns.

Surface modification of ITO with both Fc-DMES and Fc-TES was attempted in the manner described above (see Scheme 3.7). Following the attempted surface reaction, ITO substrates were analyzed electrochemically by cyclic voltammetry in a 0.1M acetonitrile solution of [TBA][PF_6] for surface attachment. For a cyclic voltammetric experiment, the electrochemical response of a surface confined, redox active species will be a reversible symmetric wave on a current vs. voltage voltammogram with a peak separation < 0.059 V for a one electron redox process. In addition, the current will scale linearly with the scan rate, thus creating a means for confirming the surface confinement of a redox active species to an electrically conducting surface.[47] Electrochemical analysis of the ITO electrode reacted with Fc-DMES revealed no surface attachment of the ferrocenyl moiety by reaction of the ethoxysilane functional group. The absence of any observable surface attachment may be in part due to the presence of only one siloxy moiety in Fc-DMES and as a result, perhaps longer reaction times are necessary for surface modification. Electrochemical analysis of the ITO electrode reacted with Fc-TES, however, did confirm surface attachment. Figure 3.20 shows the cyclic voltammogram of an ITO electrode modified with Fc-TES along with a plot of current vs. scan rate for the same electrode. The half-wave potential ($E_{1/2}$) was 0.485 V vs. Ag/Ag^+ with a peak separation (ΔE_{pk}) of 0.020 V. As can be seen in the plot, the current scales linearly with the scan rate with an R^2 value of 0.99. The current vs. scan rate plot, the ΔE_{pk} < 0.059V, and the symmetric peak shapes all confirm the presence of the surface confined ferrocenyl species. Finally, the electrochemical signal is still present after thorough washings of the modified electrode with several organic solvents in which Fc-TES is soluble.

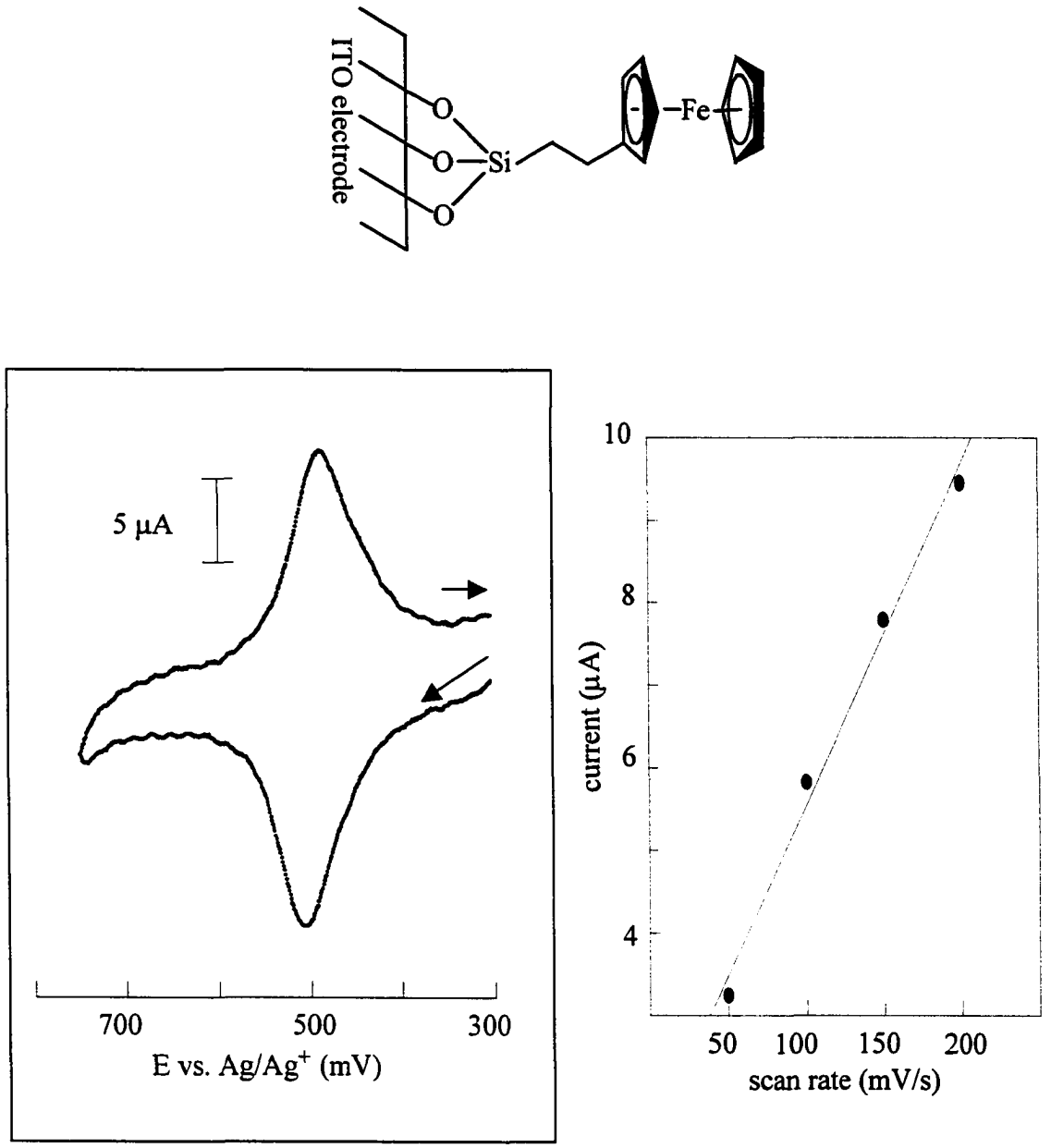

Figure 3.20. Cyclic voltammogram of Fc-TES covalently attached to an ITO coated glass electrode. The plot of current vs. scan rate is linear with an R^2 value of 0.99. Scan rate = 200 mV/s; Ag/Ag^+ reference electrode; 0.1 M $TBA^+PF_6^-$ in acetonitrile supporting electrolyte; platinum mesh counter electrode.

Hydrosilation reactions were also performed on the olefinic polyalkylated ferrocene BUT-diPt using Karstedt's catalyst with trimethoxysilane and triethoxysilane under the same reaction conditions as those used for the hydrosilation of vinylferrocene. It was found for BUT-diPt that the formation of the hydrogenation product 1,1',3,3'-tetra(2-methyl-2-propyl)-4-(2-(2-pentenyl))ferrocene (BUT-2Pt) was favored over the desired hydrosilation reaction, as shown below. Some desired hydrosilation product was

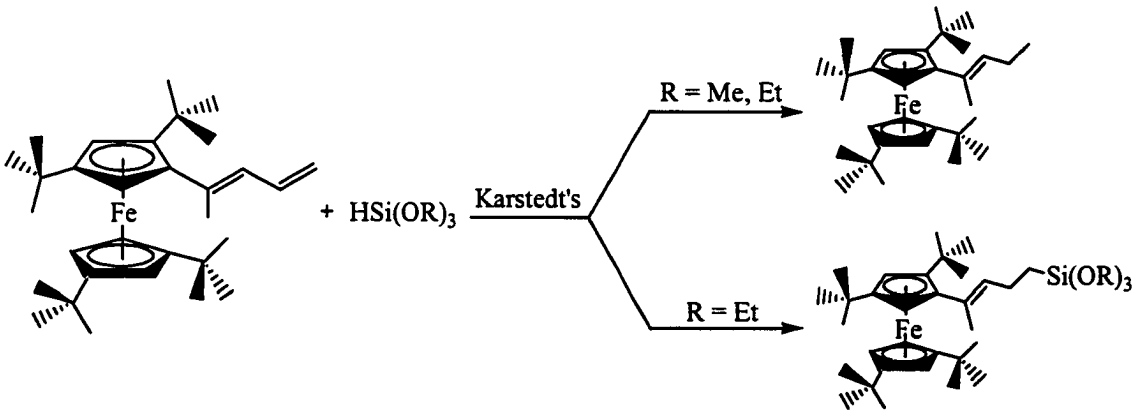

observed for the reaction with triethoxysilane, as can be seen in the mass spectrum of the resulting product mixture shown in Figure 3.21. The desired product, 1,1',3,3'-tetra(2-methyl-2-propyl)-4-(2-(5-triethoxysilyl-2-pentenyl))ferrocene (BUT-PtTES) can be seen at m/z 640.4 and the hydrogenation product BUT-2Pt at m/z 478.3.

The hydrosilated product BUT-PtTES was not able to be isolated from the reaction mixture, and subsequently, no surface attachment to a metal oxide surface was attempted. Other means of synthesizing a siloxy functionalized polyalkylated ferrocene should be explored to achieve this end. The hydrosilation route may be an effective means to this end, however a better olefinic ferrocene substrate may be needed.

In an attempt to determine why the hydrogenation product was formed, the hydrosilation of BUT-diPt with trimethoxysilane was repeated and monitored by mass spectrometry for 24 hours. The mass spectra of this reaction mixture at 2, 16 and 24

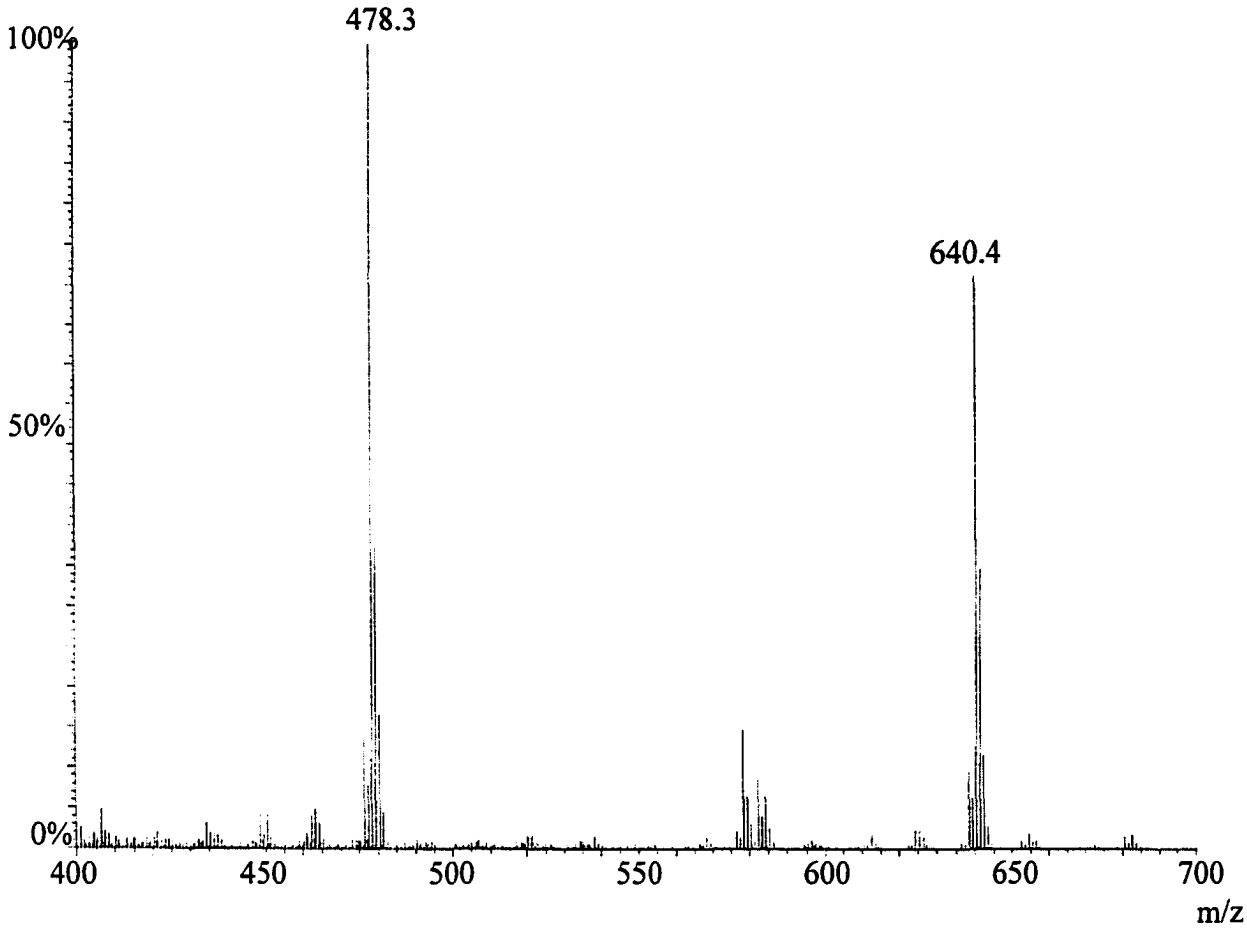

Figure 3.21. The LSIMS mass spectrum of the product mixture obtained from the hydrosilation of BUT-diPt with triethoxysilane. The desired product BUT-PtTES can be seen at m/z 640.4 (640.85 calculated) and the hydrogenation product BUT-2Pt at m/z 478.3 (478.59 calculated).

hours can be seen in Figure 3.22. The hydrogenation was still not complete after 48 hours, at which time the reaction was stopped. The desired product, 1,1',3,3'-tetra(2-methyl-2-propyl)-4-(2-(5-trimethoxysilyl-2-pentenyl))ferrocene (F.W. 598.77) was not observed in any of the spectra. It is not known at this time why the hydrogenated ferrocene is formed. The proton source is assumed to be the silane used, but no further investigation into this reaction was explored. Perhaps the presence of a diene moiety rather than a vinyl moiety affects the reaction. Due to the formation of hydrosilated product when triethoxysilane is used, it is suspected that the Si–H bond strength again plays a role. Furthermore, since a hydrogenated product is formed, the formation of platinum nanoclusters from the catalyst during the reaction may also play a role.

Functionalization of Longer Alkyl Chain Polyalkylated Ferrocenes. Due to the increased selectivity of the larger alkylated ferrocenes HEP and DEC in an ion-exchange process,[5] it was desirable to explore synthesis schemes for functionalization of these molecules as well. Surface attachment and materials inclusion were again the main goals for functionalization. Functional groups large enough to extend beyond the reach of the alkyl groups and discovering reactions robust enough to overcome the even more sterically hindered environment around the Cp' rings was again a major factor in choosing reaction schemes. Due to the robust nature of the Friedel-Crafts acylation reaction discovered for functionalization of BUT, this method of attaching a fifth group to the Cp ring was chosen. The acid chloride used for this reaction was 11-bromoundecanoyl chloride. It has been previously shown that under Friedel-Crafts conditions, the bromo moiety is left in tact while the acid chloride functionality undergoes the desired Friedel-Crafts acylation reaction.[16,48] The reaction shown in Scheme 3.9 is the basis for all functionalization reactions for polyalkylated ferrocenes with tertiary alkyl groups larger than four carbon atoms, though the reaction has been performed with BUT. As might be expected, the yield of 11-bromoundecanoyl ferrocene decreased as the tertiary alkyl chains became larger, though yields were still between 60

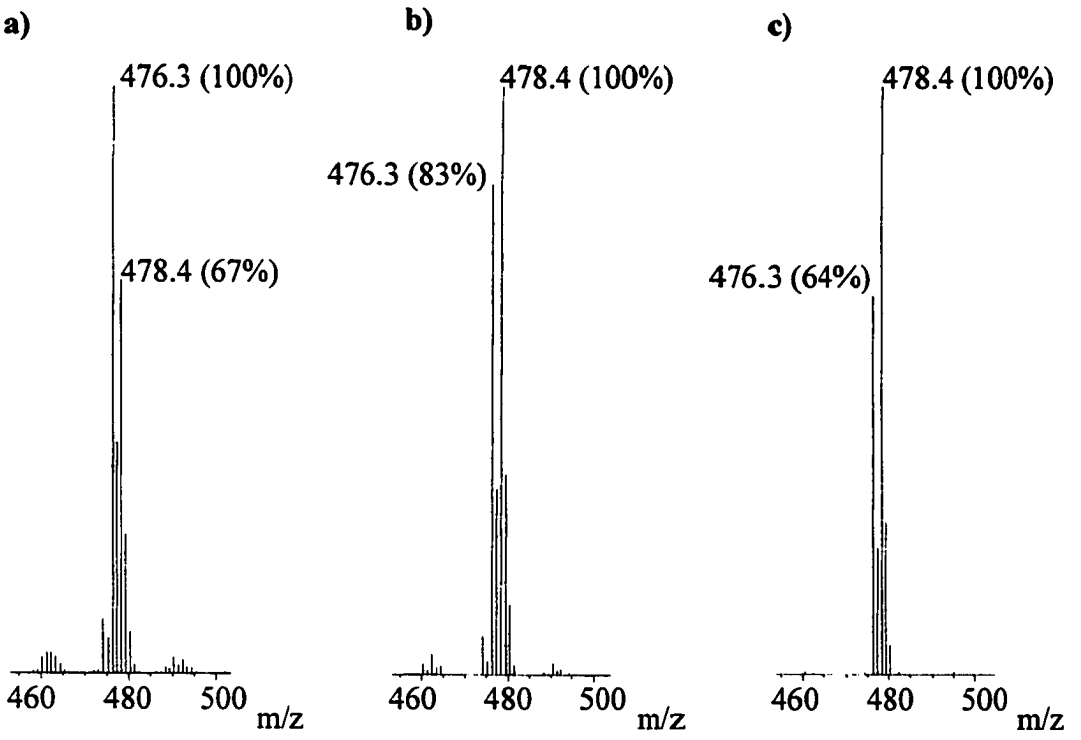

Figure 3.22. The LSIMS mass spectra of the hydrosilation reaction of BUT-diPt (m/z 476.3) with trimethoxysilane at time intervals of (a) 2 hours; (b) 16 hours; and (c) 24 hours. The peak at m/z 478.4 is due to the hydrogenated product BUT-2Pt. Relative peak heights are shown in parentheses.

Scheme 3.9.

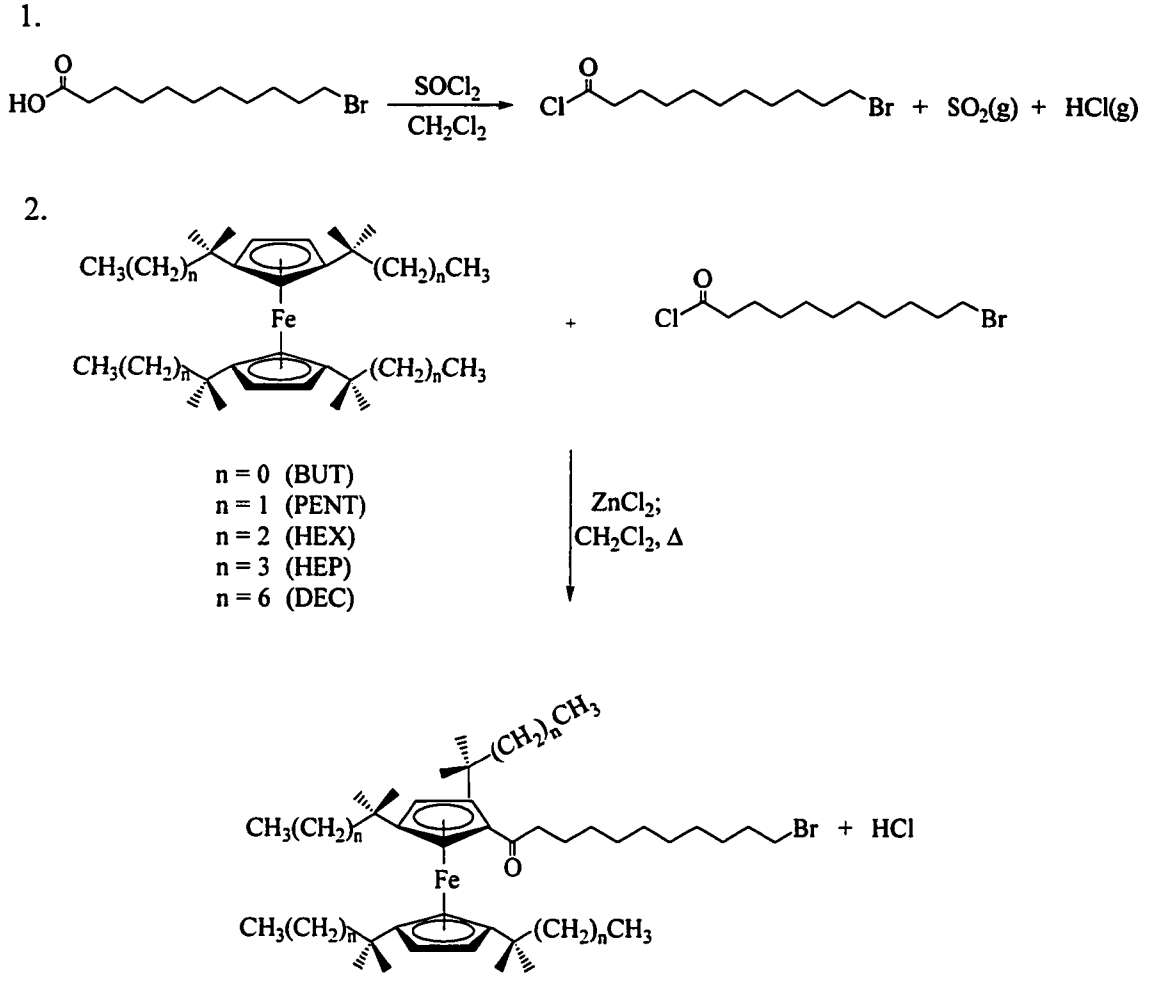

and 70% for HEP and DEC.

Products were characterized by LSIMS mass spectrometry and ^{1}H-NMR spectroscopy. Table 3.3 shows a summary of mass spectral data for all five novel 11-bromoundecanoyl polyalkylated ferrocenes. The spectra showed all compounds to be pure and all spectra gave the expected isotope patterns for molecules with the appropriate number of carbon atoms, one oxygen atom, one bromine atom, and one iron atom. The ^{1}H-NMR spectrum of 1,1',3,3'-tetra(2-methyl-2-nonyl)-4-(11-bromoundecanoyl) ferrocene (DEC-Br) is shown in Figure 3.23 as a representative spectrum. The five expected ring proton resonances are broad, but can be seen at 4.56, 4.40, 4.32, 4.06, and

Table 3.3. Mass spectral data for 11-bromoundecanoyl polyalkylated ferrocenes.

product	mass to charge ratio (m/z)[a]	m/z (calc.)
BUT-Br	656.3	656.33
PENT-Br	712.7	712.39
HEX-Br	768.9	768.45
HEP-Br	824.8	824.51
DEC-Br	993.7	993.72

[a] All relative peak heights were 100%.

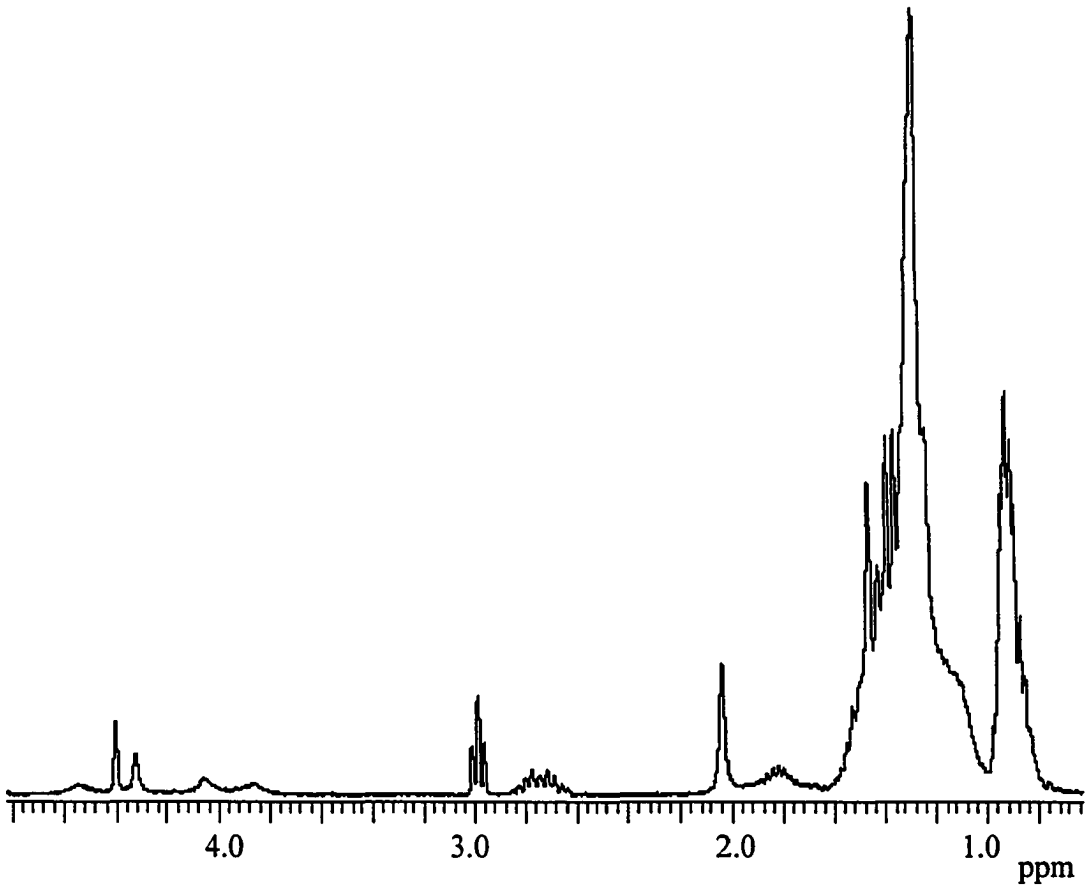

Figure 3.23. The ^{1}H-NMR spectrum of DEC-Br in benzene-d_6.

3.86 ppm. The proton resonances due to the two methylene groups closest to the bromine atom can be seen at 2.98 (t, 2H) and 2.74 (m, 2H) ppm. The proton resonances due to the two methylene groups closest to the carbonyl moiety can be seen at 2.03 (br t, 2H) and 1.82 (m, 2H) ppm. The remaining proton resonances can be seen as two multiplets between 0.8 and 1.6 ppm. The ^{1}H-NMR spectra of all of the 11-bromoundecanoyl polyalkylated ferrocenes are similar with the exception of a varying number of resonances in the methyl and methylene region of the spectrum (~0.05 to 1.7 ppm).

As can be seen in Scheme 3.10, the 11-bromoundecanoyl ferrocenes can be reacted further to yield a variety of functional groups that are useful for both surface modification as well as materials synthesis. The reactions shown in Scheme 3.10 are assumed to be general for all the 11-bromoundecanoyl polyalkylated ferrocenes presented in Table 1.1. Table 3.4 summarizes mass spectral data and purity data for representative compounds that have been used for subsequent reactions (*vide infra*). All compounds in Table 3.4 displayed the expected isotope patterns for their respective molecular formulas. The compounds from Table 3.4 have also been characterized by ^{1}H-NMR spectroscopy and their spectra described in the experimental section (*vide supra*).

By reacting the 11-bromoundecanoyl ferrocenes with sodium iodide in anhydrous acetone, the novel 1,1',3,3'-tetra(2-methyl-2-alkyl)-4-(11-iodoundecanoyl) ferrocenes were able to be synthesized. These iodo-functionalized ferrocenes were intended to be reacted further with olefinic Grignard reagents in the presence of copper(I) iodide, as shown below, to form olefinic ferrocenes,[49-52] especially for the larger ferrocenes HEP and DEC. The reactions of the iodo-functionalized ferrocenes with allylmagnesium bromide instead reacted with the carbonyl carbon in the alpha position to the Cp' rings. Small amounts of the desired products were observed in the mass spectrum of the product, but were not able to be isolated. Interestingly, neither reaction was observed without the addition copper(I) iodide, suggesting the alkyl copper reagent formed is reactive enough to overcome the sterics around the carbonyl carbon atom. No further

Scheme 3.10.

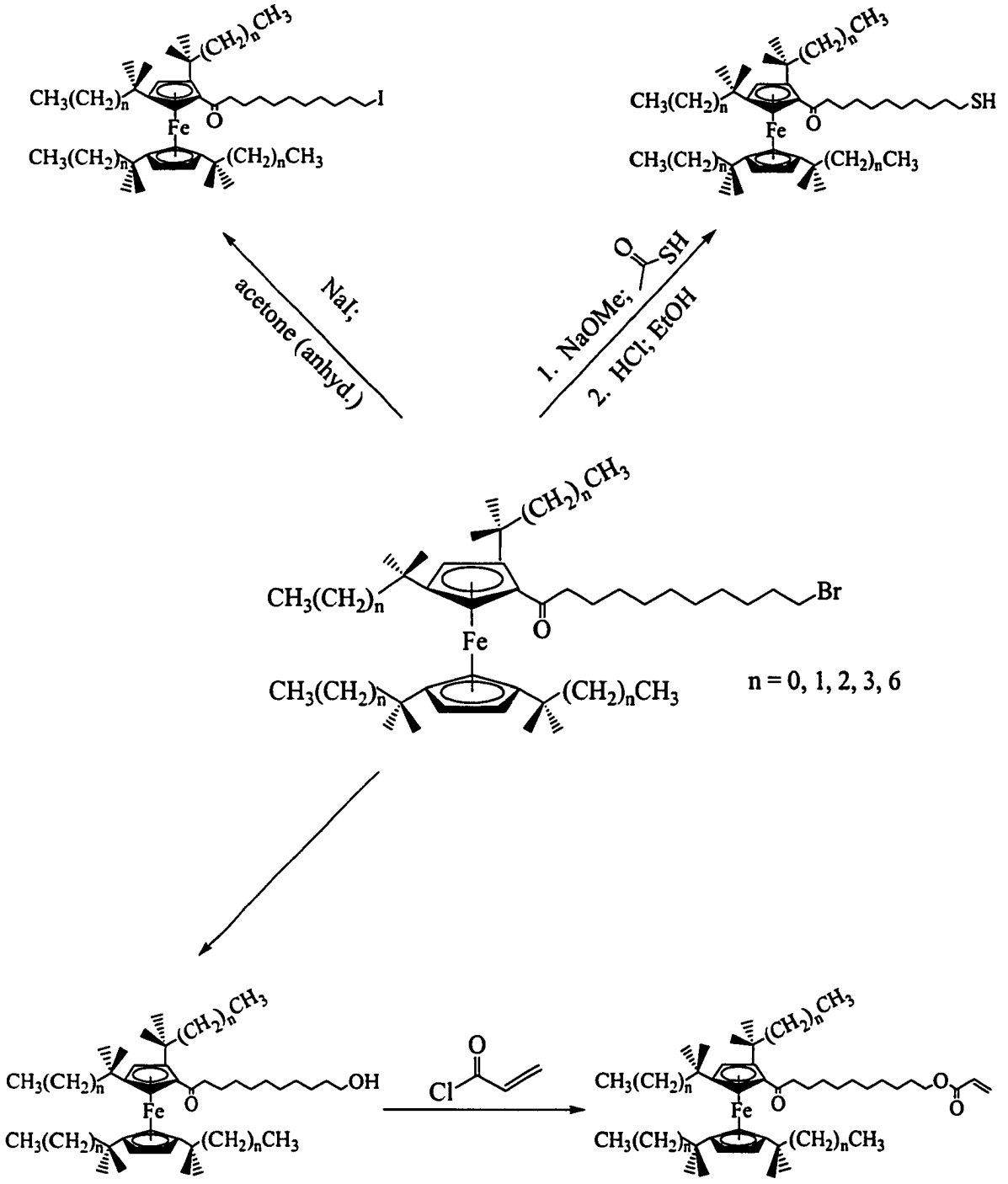

Table 3.4. Summary of mass spectral data for compounds prepared in Scheme 3.10.

func. ferrocene	m/z	m/z (calc.)	estimated purity[a.]
BUT–SH	610.3	610.39	99%
PENT–SH	666.6	666.45	98%
HEX–SH	722.8	722.51	98%
HEP–SH	778.8	778.58	97%
DEC–SH	946.4	946.76	95%
HEP–OH	762.8	762.60	99%
DEC–I	1039.2	1040.69	95%
HEP–acr	817.1	817.10	98%

[a.] Estimated from the LSIMS mass spectrum peak heights of desired product, starting material, identified fragmentation peaks and/or impurities. Purification estimates from mass spectra taken after purification by column chromatography.

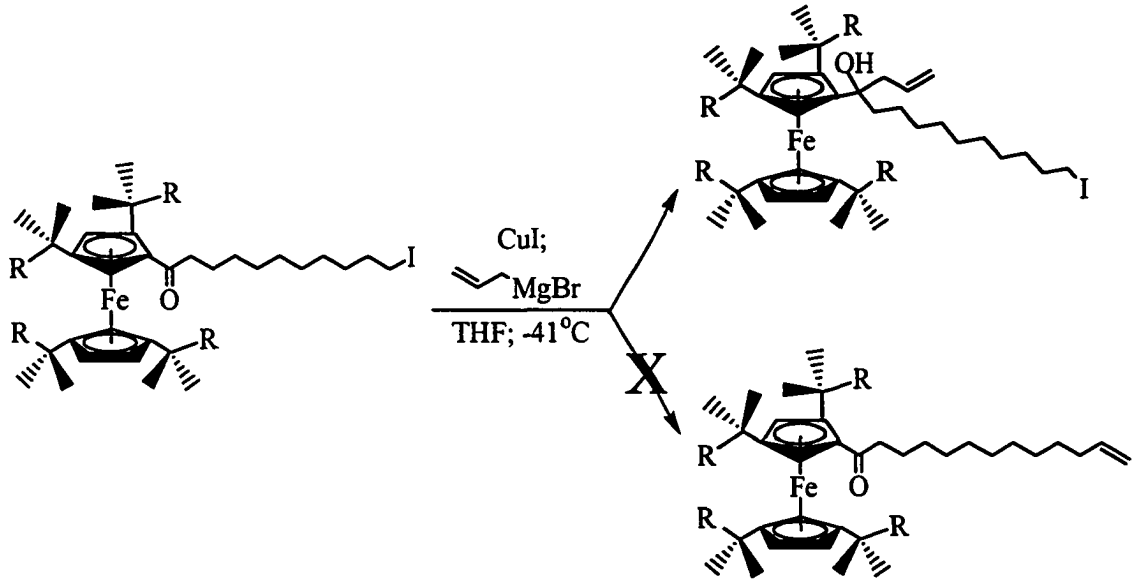

reactions were performed with the iodo-functionalized ferrocenes.

An olefinic ferrocene was synthesized from a different method illustrated in Scheme 3.10 (bottom). Using the two products formed in this step, two novel polymeric materials have been synthesized. The first material was made by a surface reaction of hydroxymethylpolystyrene polymer beads with 1,1',3,3'-tetra(2-methyl-2-hexyl)-4-(11-hydroxyundecanoyl))ferrocene (HEP-OH) by the method described by Annis *et. al.* for synthesis of surface supported heterogeneous catalysts.[53] This surface modification reaction can be seen in Scheme 3.11. The final material was obtained as brown/red beads with a powdery appearance. The amount of HEP covalently attached was determined to be 0.071 mmol based on the amount of HEP-OH recovered after the surface linkage reaction. Based on this number, the HEP content of the final material was determined to be 0.066 mmol/g.

This material was subsequently oxidized with an acetone solution of $Ce(NH_4)_2(NO_3)_6$, yielding beads with a yellow/green color. The color change is indicative of HEP^+ sites on the bead surface. The polymer beads were not able to be oxidized and reduced using aqueous oxidizing or reducing solutions. Furthermore,

Scheme 3.11.

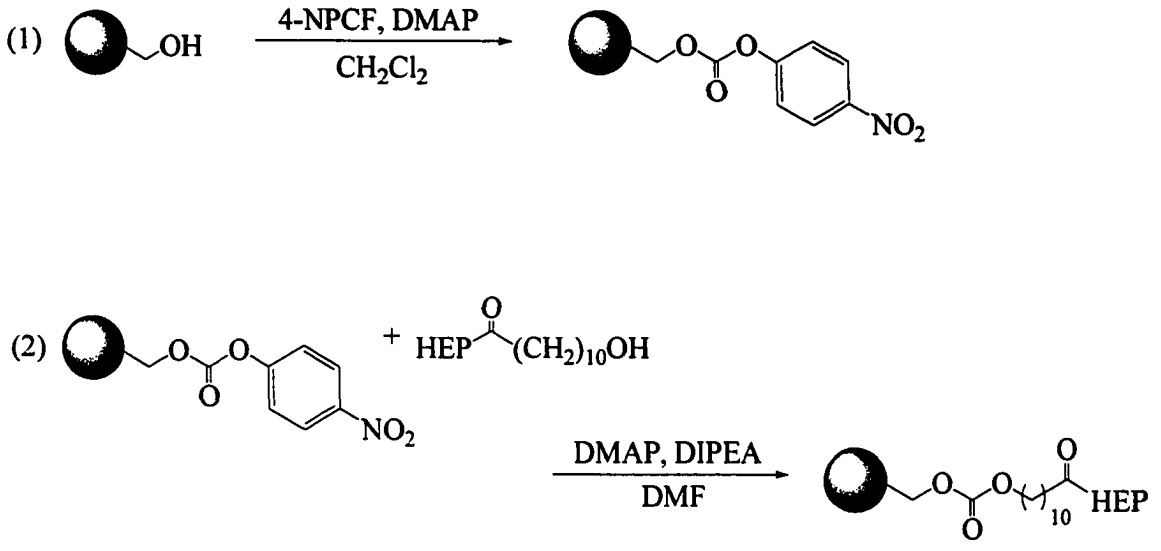

= 100-200 mesh hydroxymethylpolystyrene

4-NPCF = 4-nitrophenyl chloroformate

DMAP = 4-(dimethylamino)pyridine

DIPEA = *N,N*-diisopropylethylamine

acetone solutions of reducing agents such as $K_4Fe(CN)_6$ or NaS_2O_4 did not reduce theoxidized material. It is assumed that the inability to oxidize and reduce this material with aqueous solutions is due to the wetability of the material. This problem will have to be addressed before using this material as an ion-exchange material for aqueous anions. This reaction does, however, demonstrate a useful means of covalent attachment to hydroxylated polymeric surfaces. Other hydroxylated polymer beads with better wetability properties may prove to yield a more robust ion-exchange material.

The second polymeric material was made by first reacting HEP-OH with acrolyl

chloride to yield 1,1',3,3'-tetra(2-methyl-2-hexyl)-4-(11-acrolylundecanoyl)ferrocene (HEP-acr) as shown in Scheme 3.10. The product was isolated as a red oily residue in a 37% yield. HEP-acr was subsequently co-polymerization with methyl methacrylate under radical conditions. The product was a red, rigid, translucent material. Leaching of the HEP was not observed in hexanes, a solvent which dissolves HEP-acr but only swells poly(methyl methacrylate), after swelling of the polymer for at least 24 hours. This material was not able to be oxidized and reduced with aqueous oxidizing and reducing agents, again due to the hydrophobicity of poly(methyl methacrylate). It did, however, demonstrate a functional group that can be polymerized for inclusion of polyalkylated ferrocenes in polymeric materials. It is suggested that similar materials be made with polymers that are more wetable than those described here. One starting monomer that may prove useful is hydroxyethyl methacrylate, which is known for its ability to swell in water.

The most useful functionality has proved to be an 11-thiolundecanoyl moiety. This functionalization reaction has been performed on all of the polyalkylated ferrocenes used in our laboratory. Self assembled monolayers (SAMs) of all the thiol functionalized tetraalkylated ferrocenes listed in Table 3.4 have formed on the surfaces of gold electrodes. Cyclic voltammograms and electrochemical properties of all these SAMs on gold electrodes can be seen in Chapter 4. Briefly, like the voltammogram described earlier for Fc-TES, all the voltammograms for thiolated polyalkylated ferrocene SAMs show the characteristics of a surface confined, redox active species. The ion-exchange properties of these SAMs are also discussed in detail in Chapter 4.

Conclusions

A variety of novel functionalized polyalkylated ferrocenes based on the 1,1',3,3'-tetra(2-methyl-2-alkyl)ferrocene moiety has been synthesized. Though the presence of the four tertiary alkyl groups on the Cp rings of the ferrocenes create steric hindrance for further substitution, reactions such as Friedel-Crafts acylation have been found to be

robust enough to overcome these challenges. After the successful extension of functional groups beyond the steric influence of the tertiary alkyl substituents, a variety of useful reactions have been performed that resulted in functional groups useful for both surface modification and materials synthesis. In the case of 11-bromoundecanoyl functionalized polyalkylated ferrocenes with four tertiary alkyl chains up to 10 carbon atoms in size, further functionalization reactions have been shown to be possible independent of the size of the tertiary alkyl group substituents. Yields of these functionalized ferrocenes, however, do sometimes diminish as the alkyl chains become longer. Most of the functionalized polyalkylated ferrocenes can be made readily and in decent yields. Surface modification and co-polymerization with functionalized polyalkylated ferrocenes have been demonstrated. Although not all materials synthesized may be useful for ion-exchange applications, techniques and methodology for synthesis of ion-exchange materials that will work have been developed.

References

1. Clark, J. F. Design, Synthesis, and Evaluation of Redox-Recyclable Organometallic Extractants for the Recovery of Ionic Radionuclides From Aqueous Waste Streams. Ph.D. Dissertation, Colorado State University, Fort Collins, CO, 1999.
2. Clark, J. F.; Clark, D. L.; Whitener, G. D.; Schroeder, N. C.; Strauss, S. H. *Environ. Sci. Technol.* **1996**, *30*, 3124.
3. Chambliss, C. K.; Odom, M. A.; Morales, C. M. L.; Martin, C. R.; Strauss, S. H. *Anal. Chem.* **1998**, *70*, 757.
4. Strauss, S. H.; Odom, M. A.; Hebert, G. N.; Clapsaddle, B. J., 2001 *ATR-FTIR Detection and Quantification of Anionic Pollutants in Water.*
5. Moyer, B. A.; Bonnesen, P. V. In *Supramolecular Chemistry of Anions*; Bianchi, A., Bowman-James, K., Garcia-Espana, E., Eds.; VCH: New York, 1997.
6. Chambliss, C. K.; Odom, M. A.; Martin, C. A.; Moyer, B. A.; Strauss, S. H. *Inorg. Chem. Commun.* **1998**, *1*, 435.
7. Odom, M. A. Development of Strategies for the Detection, Extraction, and Recovery of Aqueous Anions Using Highly Selective Redox-Recyclable Materials. Ph.D. Dissertation, Colorado State University, Fort Collins, CO, 2001.
8. Clapsaddle, B. J.; Clark, J. F.; Clark, D. L.; Gansle, K. M.; Gash, A. E.; Miller, S. M.; Anderson, O. P.; Hughes, R. P.; Strauss, S. H., 2002 *Synthesis and Characterization of Polyalkylated Ferrocenes and Ferrocenium Salts.*
9. Chambliss, C. K. Redox-Recyclable Extraction and Recovery. A New Strategy for the Separation and Recovery of Aqueous Ions. Ph.D. Dissertation, Colorado State University, Fort Collins, CO, 1998.
10. Hebert, G. N.; Strauss, S. H., Colorado State University, Fort Collins, CO. Unpublished results, 2001.
11. Ghatak-Roy, A. R.; Martin, C. R. *Anal. Chem.* **1986**, *58*, 1574.
12. Deinhammer, R. S.; Ting, E. Y.; Porter, M. D. *Anal. Chem.* **1995**, *67*, 237.

13. Leigh, T. J. *J. Chem. Soc.* **1964**, 3294.

14. Shriver, D. F.; Drezdzon, M. A. *The Manipulation of Air-Sensitive Compounds*; Wiley-Interscience: New York, 1986.

15. Perrin, D. D.; Armarego, W. L. F. *Purification of Laboratory Chemicals*; 3 ed.; Pergamon Press: New York, 1988.

16. Gardner, T. J.; Frisbie, C. D.; Wrighton, M. S. *J. Am. Chem. Soc.* **1995**, *117*, 6927.

17. Arimoto, F. S.; Haven, A. C. *J. Am. Chem. Soc.* **1955**, *77*, 6295.

18. Gansle, K. M. Investigation and Development of Liquid-Liquid Extraction Systems for the Removal of Pertechnetate from Aqueous Nuclear Waste-Stream Simulants. Ph.D. Dissertation, Colorado State University, Fort Collins, CO, 1998.

19. McMurry, J. *Organic Chemistry*; 2 ed.; Brooks/Cole: Pacific Grove, CA, 1988.

20. Heo, R. W.; Somoza, F. B.; Lee, T. R. *J. Am. Chem. Soc.* **1998**, *120*, 1621.

21. Rausch, M., D.; Siegel, A. *J. Organomet. Chem.* **1968**, *11*, 317.

22. Gonsalves, K.; Lin, Z.; Lenz, R. W.; Rausch, M. D. *J. Polym. Sci., Polym. Chem. Ed.* **1985**, *23*, 1707.

23. Miller, E. J.; Weigelt, C. A.; Serth, J. A.; Rusyid, R.; Brenner, J.; Luck, L. A.; Godlewski, M. *J. Organomet. Chem.* **1992**, *440*, 91.

24. Liu, W.; Xu, Q.; Ma, Y.; Liang, Y.; Dong, N.; Guan, D. *J. Organomet. Chem.* **2001**, *625*, 128.

25. Horspool, W. M.; Sutherland, R. G. *Can. J. Chem.* **1968**, *46*, 3453.

26. Boev, V. I.; Dombrovskii, A. V. *Zh. Obshch. Khim.* **1980**, *50*, 121.

27. Pittman, C. U. In *Organometallic Polymers*; Carraher, C. E., Sheats, J. E., Pittman, C. U., Eds.; Academic: New York, 1977.

28. Gonsalves, K.; Chen, X. In *Ferrocenes: Homogenous Catalysis; Organic Synthesis; Materials Science*; Togni, A., Hayashi, T., Eds.; VCH: New York, 1995.

29. Ju, H.; Leech, D. *J. Chem. Soc., Faraday Trans.* **1997**, *93*, 1371.

30. Howard, M.; Reed, S. F. *J. Polym. Sci. A-1* **1971**, *9*, 2085.

31. Vedejs, E.; Marth, C. F. *J. Am. Chem. Soc.* **1988**, *110*, 3948.

32. March, J. *Advanced Organic Chemistry: Reactions, Mechanisms, and Structure*; 4 ed.; John Wiley and Sons: New York, 1992.

33. Hibino, J.; Okazoe, T.; Takai, K.; Nozaki, H. *Tetrahedron Lett.* **1985**, *26*, 5579.

34. Petasis, N. A.; Patane, M. A. *Tetrahedron Lett.* **1990**, *31*, 6799.

35. Petasis, N. A.; Bzowej, E. I. *J. Am. Chem. Soc.* **1990**, *112*, 6392.

36. Tebbe, F. N.; Parshall, G. W.; Reddy, G. S. *J. Am. Chem. Soc.* **1978**, *100*, 3611.

37. Petasis, N. A.; Dian-Kui, F. *Organometallics* **1993**, *12*, 3776.

38. Arkles, B. *Chemtech* **1977**, *7*, 766.

39. Hitchcock, P. B.; Lappert, M. F.; Warhurst, N. J. W. *Angew. Chem. Int. Ed. Eng.* **1991**, *30*, 438.

40. Jutzi, P.; Batz, C.; Neumann, B.; Stammler, H. G. *Angew. Chem. Int. Ed. Eng.* **1996**, *35*, 2118.

41. Cuadrado, I.; Casado, C. M.; Alonso, B.; Moran, M.; Losada, J.; Belsky, V. *J. Am. Chem. Soc.* **1997**, *119*, 7613.

42. Calzaferri, G.; Imhof, R. *J. Chem. Soc. Dalton Trans.* **1992**, 3391.

43. Moran, M.; Casado, C. M.; Cuadrado, I.; Losada, J. *Organometallics* **1993**, *12*, 4327.

44. Massarskaya, S. M.; Sokolova, E. B.; Cherepakhina, G. V.; Karableva, A. V. *Tr. Mosk. Khim.-Tekhnol. Inst.* **1969**, *61*, 170.

45. Asatiani, L. P.; Zurabishvili, D. S.; Gverdtsiteli, I. M. *Zh. Obshch. Khim.* **1979**, *49*, 788.

46. Finke, R. G., Colorado State University, Fort Collins, CO. Personal communication, 1999.

47. Bard, A. J.; Faulkner, L. R. *Electrochemical Methods: Fundamentals and Applications*; John Wiley & Sons: New York, 1980.

48. Okahata, Y.; Enna, G.; Takenouchi, K. *J. Chem. Soc., Perkin Trans. 2* **1989**, 835.

49. Tamura, M.; Kochi, J. K. *J. Organomet. Chem.* **1972**, *42*, 205.

50. Tamura, M.; Kochi, J. *J. Am. Chem. Soc.* **1971**, *93*, 1485.

51. Derguini-Boumechal, F.; Linstrumelle, G. *Tetrahedron Lett.* **1976**, *36*, 3225.

52. Mirviss, S. B. *J. Org. Chem.* **1989**, *54*, 1948.

53. Annis, D. A.; Jacobsen, E. N. *J. Am. Chem. Soc.* **1999**, *121*, 4147.

Chapter 4

Selectivity Studies and Sensor Applications of Tetraalkylated Ferrocene Ion-Exchange Materials Confined to Electrically Conducting Substrates

Introduction

Electrochemical sensing and molecular recognition is a fast expanding research area in both electrochemistry and supramolecular chemistry.[1,2] Anion recognition is of particular interest due to the small number of reliable techniques in contrast to the large number of techniques developed for cation recognition.[3] Three strategies have typically been applied to electrochemical anion detection: 1) extraction of the anion into a membrane by a host molecule followed by measurement of the membrane potential (ion-selective electrodes), 2) detection of a current/potential perturbation to a redox-active host molecule (voltammetric or amperometric sensors), and 3) chemically modified electrodes with a redox-active matrix and anion selective binding sites.[3] The most common involves current/potential perturbation of a redox-active host in an aqueous or organic solution containing the target anion.[2,3] A large variety of organometallic functionalized, redox-active host molecules exist, including cobaltocene and ferrocene modified calixarenes,[4,5] macrocycles,[2,3] guanidines,[6] dendrimers,[7,8] and a variety of other anion specific functionalities.[3,9] These hosts "complex" the target anions by a variety of methods including electrostatic interactions, hydrogen bonding, hydrophobicity and combinations of these interactions. Cathodic potential shifts between 30 – 250 mV for various redox-active hosts have been observed upon complexing of target anions such as halides, acetate, SO_4^{2-}, and $H_2PO_4^-$. Anion recognition and sensing have not, however, been explored to the same extent with chemically modified electrodes, despite the observation of large potential shifts for surface confined redox-active species due to

variation of anions in electrolytes.

Modifying electrically conducting surfaces with redox active functionalities is a well established, useful area of research in the fields of electrochemistry and materials science.[10] Methods of surface modification vary depending on the proposed application. These methods include, but are not limited to, coating techniques,[11-16] covalent bond formation to the substrate,[17-20] Langmuir-Blodgett thin films,[21,22] and self-assembly.[23-26] Some applications of surface modified electrodes include the study of electron transfer,[27,28] ion-selective electrodes,[29,30] corrosion inhibition,[23,31-33] electrochemically modulated chromatography,[9,34] and electrochemical sensing.[24,35-37]

Surface modifications with ferrocene are of particular interest. Ferrocene offers a well characterized, reversible, one electron couple at reasonable potentials and is easily functionalized for a variety of surface confinement methods. Surface modification with ferrocene has been performed by all of the techniques mentioned above for a variety of conducting substrates.[14,15,19,20,22,25,38] Ferrocenyl modified conducting substrates have been used to study electron transfer reactions,[27,28] electromodulated ion-exchange chromatography,[34] and several possible sensor applications.[24,37]

One of the most popular surface modification methods is the formation of self-assembled monolayers (SAMs) on gold (111) surfaces with functionalized thiols.[23,39,40] This is also a popular method for electrode surface modification with ferrocenes. Ferrocenylhexadecanethiol has been used in mixed monolayer systems to measure glucose concentrations amperometrically.[37] The compound 11-thiolundecanoylferrocene has been used as a surface confined internal reference in mixed monolayers for sensor applications in media of varying pH.[24] Mixed monolayers of ferrocenylalkanethiols and *n*-alkanethiols are the most popular surfaces for the study of electron transfer mechanisms.[26,27,41-43]

With the creation of several new polyalkylated ferrocenyl ion-exchange compounds,[44] surface modification of electronically conducting surfaces with these

compounds has become of interest. The idea of an electroactive ion-exchange system for the R^2ER process, similar to that previously described,[9,34] is attractive since the ion-exchange materials could then be electrochemically recycled. Due to their electrochemical properties, the polyalkylated ferrocene ion-exchange materials present this unique recycling method not possible for many common ion-exchange materials, such as tetraalkylammonium salts. The resulting elimination of chemical oxidizing and reducing agents would further reduce the volume of secondary chemical waste in the remediation process.

In addition to remediation applications, the selectivity exhibited by these tetraalkylated ferrocene ion-exchange materials for weakly hydrated anions suggests that they may be suitable for electrochemical sensing devices. The formation of tetraalkylated ferrocenyl monolayers on gold electrodes would also present a unique evaluation method of ion-exchange selectivity. It is well established that surface confined ferrocenes in all of the previously mentioned applications exhibit a variation in the apparent formal potential of the ferrocenyl group. The formal potential of surface confined redox groups has been shown to depend on properties such as surface coverage, electrolyte content and concentration, surface dielectric, and other factors.[25-27,45-47]

To date, two models have been used to explain the variances in formal potential. The first considers a simple Born model in which changes in ion solvation at the monolayer/electrolyte interface are attributed to the change in the local dielectric of the medium relative to that in bulk solution.[27,28] These changes are responsible for the observed potential variations. The second model considers an electrical double-layer effect in which the ion spatial distribution, and not the energetics of ion solvation, is responsible for the potential variations.[27,48] Experimental data give support to both models; each model, however, appears inadequate for explaining all the data and it seems likely that both models need to be invoked for a complete explanation.[27,28] The Born model described above, however, is similar to the modified Born model presented in

Chapter 1 for describing the selectivity of tetraalkylated ferrocene ion-exchange materials. Though the use of the double-layer model should not be ignored, a Born treatment of the observed potential variations is very useful for a semi-quantitative evaluation of ion-exchange properties.

This study focuses on the electrochemical characterization of the functionalized tetraalkylated ferrocenes confined to electrode surfaces. The electrochemical characterization of tetraalkylated ferrocene thin films and monolayers has been evaluated in order to test their ion-exchange properties in a common electrochemical cell. Due to predictions based on the modified Born model for ion-exchange, as discussed above, it is hypothesized that "electrochemical selectivity" could be determined and directly related to ion-exchange extraction selectivity data previously collected for the tetraalkylated ferrocenes used in this study. The potential shifts observed for tetraalkylated ferrocenyl monolayers on gold in various electrolytes have been used to evaluate the electrochemical selectivity of the tetraalkylated ferrocene monolayers. Since selectivity is important for detection applications and electrochemical modulated ion-exchange chromatography, a correlation between the electrochemical selectivity the ion-exchange extraction selectivity could be useful for developing these tetraalkylated ferrocenes into electrochemical sensors or electrochemically modulated extractants for aqueous anions. The use of electrode-confined tetraalkylated ferrocenes and their use in electrochemical anion sensing applications as well as their possible use in electrochemical modulated ion-exchange chromatography will be demonstrated.

Experimental

General Procedures. All tetraalkylated and functionalized tetraalkylated ferrocenes and ferrocenium salts appear to be stable to air and moisture. As such, experimental procedures were performed in an inert atmosphere only when noted. Fluorine-19 nuclear magnetic resonance spectroscopy (^{19}F-NMR) was performed on a Varian VXR, 300 MHz spectrometer at 25 °C. The ^{19}F frequency was 282 MHz and the

chemical shift was referenced to an external $CFCl_3$ standard (0.0 ppm). Negative ion electrospray mass spectrometry (N.I.E.,M.S.)was performed on a Fisons VG Quattro single quadrupole mass spectrometer. An orbital shaker bath model 3545 from Lab-Line Instruments, Inc. was used for all batch extractions. Reactions requiring sonication used a Branson model 3210 sonicator with a variable temperature water bath. Solvent removal was done under vacuum with a Buchi R-124 rotary evaporator. Spin coating was performed on a Photoresist Spinner, Model 1201 spin coater from Macronetics, Inc. Ellipsometry of thin films on ITO was performed on a VB-250 VASE ellipsometer from J. A. Woollam Co., Inc. and was operated by WVASE 32™ software. Calibration curves for quantitation of tetraalkylated ferrocenium nitrate salts were constructed using a Perkin-Elmer, Lambda-40 ultraviolet-visible spectrometer operated by UV-Winlab™ software.

Reagents and Solvents. All reagents were Reagent Grade or better unless otherwise indicated. All reagents and solvents were used as received unless purified as noted: acetone (Fisher); dichloromethane (Fisher); absolute ethanol (Pharmco); water (distilled deionized to 18Ω on a Barnstead NANOpure H_2O purification system); acetonitrile-d_3 (Cambridge Isotope Laboratories, Inc.); H_2SO_4 (Mallinckrodt); $HClO_4$ (Mallinckrodt); H_3PO_4 (Mallinckrodt); NaOH (Fisher); KOH (Fisher); KNO_3 (Fisher); KCl (Fisher); $KClO_4$ (Fisher); NH_4PF_6 (Aldrich); $CsCB_{11}H_{12}$ (prepared in our laboratories according to literature procedures[49,50]); $KReO_4$ (Aldrich); perfluorooctylsulfonyl fluoride ($C_8F_{17}S(O)OF$ (FX-8™), 3M corporation); perfluorooctylcarboxylic acid ($C_7F_{15}C(O)OH$ (HPFC-8), Aldrich); perfluorododecylcarboxylic acid ($C_{11}F_{23}C(O)OH$ (HPFC-12); Aldrich); XAD-7 polymer beads (Supelco; polymer beads were dried under vacuum (0.003 torr) at 24 °C until a constant weight was obtained).

Preparation of Potassium Perfluorooctylsulfonate ($K[C_8F_{17}SO_3]$; K^+PFOS^-). The potassium salt of $PFOS^-$ was prepared by adding FX-8™ (a mixture of

perfluoroalkylsulfonyl fluorides with the major constituent being perfluorooctylsulfonyl fluoride) to an aqueous solution of excess KOH and isolating the precipitate by filtration. CAUTION: hydrofluoric acid is a side product of this reaction. Skin contact should be avoided and the remaining aqueous solution neutralized with $CaCO_3$. The major product in this reaction is K^+PFOS^-, but other perfluorinated chain lengths, C7 and C6, are also precipitated due to impurities in the starting material FX-8™. To minimize the amounts of these impurities, K^+PFOS^- was recrystallized three times from boiling water to take advantage of the lower solubility of K^+PFOS^- relative to the shorter chain perfluoroalkylsulfonates. The purity of the K^+PFOS^- was determined to be > 99% by N.I.E.,M.S. and by ^{19}F-NMR spectroscopy. ^{19}F-NMR (acetonitrile-d_3, 300 MHz, 25 °C): δ –80.3 (t, 3F), –114.2 (m, 4F), –120.0 (m, 2F), –121.1 (m, 4F), 121.9 (m, 2F), –125.3 (t, 2F). N.I.E.,M.S. m/z 499.0, 499.11 calculated.

Preparation of Tetraalkylated and Functionalized Tetraalkylated Ferrocenes and Ferrocenium Salts. The preparation of all tetraalkylated and functionalized tetraalkylated ferrocenes and ferrocenium salts used in this study has been described previously as well as in detail in Chapter 2 and Chapter 3.[44,51-53] The abbreviations used for all compounds are defined in Table 1.1 in Chapter 1.

Physisorption of $HEP^+NO_3^-$ onto Indium-Tin Oxide (ITO). Indium-tin oxide coated glass slides (Delta Technologies, Stillwater Minnesota) were cut into 1 × 2 cm pieces and then cleaned by sonicating in both acetone and deionized water followed by drying under a stream of nitrogen. Prior to physisorption of $HEP^+NO_3^-$, the ITO was soaked for 1 hour in a 0.5 M aqueous solution of potassium hydroxide. The ITO was then rinsed thoroughly with ethanol and dried under nitrogen. The ITO was then soaked for at least 30 minutes in a 1 mM dichloromethane solution of $HEP^+NO_3^-$. Following physisorption of $HEP^+NO_3^-$, the ITO slide was rinsed thoroughly with water and again dried under nitrogen. After drying, tin-coated copper tape was attached to the electrode surface for an electrical contact and the ITO surface masked with teflon tape to limit the

exposed surface area to 1 cm^2.

Spin-coating of HEP onto Indium-Tin Oxide (ITO). Indium-tin oxide was first cleaned and prepared as described previously (*vide supra*). Prior to spin-coating, the ITO was soaked for 1 hour in a 0.5 M aqueous solution of potassium hydroxide. The ITO was then rinsed thoroughly with ethanol and dried under nitrogen. The ITO was spin-coated at 1000 rpm by slowly dripping 75 μL of a 1 mM dichloromethane solution of neutral HEP onto the ITO surface over 1 minute. The electrode was allowed to spin for an additional 30 seconds and excess dichloromethane left in the thin film was allowed to evaporate by standing in air for at least 30 minutes. Tin-coated copper tape was attached to the electrode surface for an electrical contact and the ITO surface masked with teflon tape to limit the exposed surface area to 1 cm^2.

Surface Modification of Gold Electrodes. The gold disk electrodes (Bioanalytical Systems, Inc.) had a diameter of 1.6 mm and were encased in a solvent resistant CTFE plastic casing. Prior to modification, the electrodes were polished to a mirror finish on a polishing wheel using 1.0 μm alumina micropolish® (Buehler). Gold electrodes were then placed in soapy deionized water and sonicated for 15 minutes to remove any excess alumina, followed by thorough rinsing with deionized water and further sonication for 15 minutes in pain deionized water.

The microscopic surface area of the gold disk electrodes after cleaning in the above manner was determined by the method of Oesch *et. al.*[54] Briefly, using cyclic voltammetry, a monolayer of gold oxide is formed on the gold electrode surface by cycling the bare electrode surface between 0 and 1.84 V (vs. SCE, scan rate = 100 mV/s, platinum mesh counter electrode) in a 0.5 M H_3PO_4 solution that was adjusted to pH 7 with NaOH. The resulting cathodic peak area was integrated to determine the charge passed by the reduction of the gold oxide layer. The amount of charge passed was then compared to a previously prepared graph[54] of cathodic reduction charge vs. surface roughness factor (r = ratio of microscopic to geometric area) to determine the

microscopic surface area. The average microscopic surface area of the gold disk electrodes after polishing and cleaning as described above was determined to be 0.044(5) cm^2 ($r = 2.2$).

Monolayers of 11-thiolundecanoyl tetraalkylated ferrocenes were deposited electrochemically as described by Weisshaar *et. al.*[55] Deposition of monolayers was accomplished by placing the gold disk electrode in an ethanolic solution containing 500 mM KOH and 10 mM 11-thiolundecanoyl tetraalkylated ferrocene and holding the potential at –600 mV vs. Ag/AgCl for one to five minutes. The larger 11-thiolundecanoyl tetraalkylated ferrocenes, such as HEP-SH and DEC-SH, were not soluble in ethanol to 10 mM at room temperature. Ethanolic 0.5 M KOH solutions of HEP-SH or DEC-SH were instead prepared by saturation using heat and sonication and then allowed to cool to room temperature before monolayer deposition. Partial monolayers were also formed electrochemically by holding the electrodes at potentials more negative than –600 mV vs. Ag/AgCl (–1,200 to –600 mV) or by varying the concentrations of the 11-thiolundecanoyl tetraalkylated ferrocenes between 1 mM and 10 mM until the desired surface coverage was achieved. The resulting modified electrodes were then removed from the deposition solution and rinsed thoroughly with ethanol and water before further analysis.

Electrochemical Analysis of Modified Electrodes. All electrochemical experiments were performed at room temperature (23.2 °C) with an EG&G model 263A potentiostat/galvanostat from Princeton Applied Research using a standard three electrode configuration. All analyses performed in organic electrolyte solutions were referenced to a silver wire electrode (Bioanalytical Systems, Inc.). All analyses performed in aqueous electrolyte solutions were referenced to a silver/silver chloride electrode (Bioanalytical Systems, Inc.). Supporting electrolytes and scan rates were chosen as appropriate. The auxiliary electrode was platinum mesh (Aldrich) in all cases. Electrolyte solutions were purged with nitrogen for at least thirty minutes prior to

analysis and all experiments performed under a flush of nitrogen.

All cyclic voltammetry was performed under the above conditions within appropriate potential ranges. Reductive differential pulse voltammetry of HEP Thin Films on ITO was done under the following conditions in all cases. All electrodes were held at an oxidizing potential (generally > 750 mV) for 1 minute before scanning. The following parameters were used: scan rate = 25 mV/s, pulse amplitude = 50 mV, pulse width = 25 ms, pulse interval = 80 ms.

Electrochemical Determination of Effective Formation Constants (K_{eff}). Effective formation constants were determined using cyclic voltammetry by measuring the anodic peak potential (E_{pa}) of tetraalkylated ferrocenyl partial monolayers in a 1 M H_2SO_4 electrolyte with increasing amounts of $HClO_4$ added. A cyclic voltammogram of the partial monolayer was first taken in 10 mL of the 1 M H_2SO_4 electrolyte with no $HClO_4$ added. Cyclic voltammograms were then taken at a minimum of five different increasing concentrations of $HClO_4$, which were achieved by adding appropriate volumes of a 1 M $HClO_4$ solution to the original 10 mL of H_2SO_4 electrolyte. The 1 M $HClO_4$ solution used was prepared in 1 M H_2SO_4 in order to keep the concentration of H_2SO_4 and ionic strength constant in the electrolyte. Table B.1 in Appendix B shows the volumes of this solution added and the resulting concentration of $HClO_4$ in the electrolyte. The values of K_{eff} were then determined graphically from a plot of E_{pa} vs. $\log[ClO_4^-]$ using the method of Rowe *et. al.* (*vide infra*).[25] It should be noted that formation constants were determined for perchlorate instead of perrhenate due to the lower solubility of perrhenate in aqueous solutions. Potassium perrhenate is not soluble over the range of concentrations necessary for the determination of K_{eff}.

Preparation of Tetraalkylated Ferrocenium Nitrate Ion-Exchange Materials. All tetraalkylated ferrocenium nitrate ion-exchange materials were prepared in our laboratories by Dr. Matthew A. Odom. The preparation of tetraalkylated ferrocenium nitrate ion-exchange materials has been described previously and is summarized

below.[56,57] A known amount of tetraalkylated ferrocenium nitrate was first dissolved in dichloromethane (~30 mL). Highly crosslinked XAD-7 polymer beads (usually 5.0 g), previously dried under vacuum (0.003 torr), were then added to the solution. The solvent was then slowly removed on a rotary evaporator operated at 150 rpm with a water bath temperature of 30 °C. The material was then dried under vacuum for several hours.

The amount of tetraalkylated ferrocenium nitrate adsorbed onto the polymer beads was determined by washing a known amount of material several times with dichloromethane to remove the ferrocenium nitrate salt from the polymer. The collected washings were then diluted to a known volume. The polymer beads returned to their original white color after the tetraalkylated ferrocenium nitrate was desorbed. The ratio mmol tetraalkylated ferrocenium nitrate per gram of material was calculated following concentration determination by UV-visible spectroscopy from a calibration curve of absorption vs. concentration that was linear over the range of 1.0 mM – 0.05 mM tetraalkylated ferrocenium nitrate in CH_2Cl_2. The visible peak at 686 nm, used for quantifying the tetraalkylated ferrocenium nitrate salts, was the maximum peak height for all compounds in CH_2Cl_2 with an extinction coefficient of 455 ± 5 L mol^{-1} cm^{-1}. Surface coverage was then calculated using the manufacturers specified surface area and the cross section areas of the tetraalkylated ferrocenium nitrate salts. All tetraalkylated ferrocenium nitrate ion-exchange materials used in this study contained roughly a monolayer of physisorbed tetraalkylated ferrocenium nitrate.

Batch Extraction Experiments. All batch extraction experiments were performed in our laboratories by Dr. Matthew A. Odom. Procedures for performing batch extractions using tetraalkylated ferrocenium nitrate ion-exchange materials has been described previously and is summarized below.[57] It should be noted that perrhenate was used in extraction experiments instead of perchlorate due to the ease of quantification of rhenium by inductively-coupled plasma atomic emission spectroscopy (ICP-AES). Perchlorate can also be quantified, typically by ion-chromatography (IC),

however no IC apparatus was available to us at the time of this study.

The tetraalkylated ferrocenium nitrate ion-exchange materials (2.0 g) were shaken horizontally at 200 rpm in 20 mL vials with 10 mL of an aqueous solution of 1 mM $KReO_4$ in 1 M $NaNO_3$ for 24 hours. All extractions were done in triplicate for determination of standard deviations. After ion-exchange had reached equilibrium, the beads were separated from the aqueous solution by filtration and the solutions kept for analysis by ICP-AES. The extractions were evaluated by the calculation of the distribution coefficients (*vide infra*) K_d and K_d* for ReO_4^- for all ion-exchange materials. Concentrations of ReO_4^- were determined by measuring total Re concentration before and after the extractions using a Perkin-Elmer P400 inductively-coupled plasma atomic emission spectrometer equipped with a high-salt nebulizer. The emission intensity was monitored at the rhenium line of 221.426 nm. Calibration curves, which were linear over the concentration range of 1.00 to 0.010 mM, were constructed using known concentrations of $KReO_4$ in 1 M $NaNO_3$ aqueous solutions (i.e.,, matrix matching was done for the standards used for the construction of calibration curves). For each sample, five readings of the ICP-AES intensity were recorded and averaged. Triton-X-100 (Mallinckrodt), a non-ionic surfactant, was added (1% total) to all solutions prior to analysis by ICP-AES. The addition of a non-ionic surfactant increases the wettability of the sample introduction system and has been shown to increase reproducibility without affecting the analytical results.[58]

Results and Discussion

Electrochemical Properties of HEP Physisorbed onto Indium-Tin Oxide (ITO) Surfaces. It has been shown that novel ion-exchange materials can be made by physisorbing tetraalkylated ferrocenes (Fc'), such as HEP, onto solid supports.[56,59] Ion-exchange materials have been made on both polymeric[57,60] and silica solid supports. Due to the success of physisorption onto silica gel, the first attempts at making an electroactive ion-exchange material were performed by physisorbing $HEP^+NO_3^-$ onto

ITO, an electrically conducting metal oxide similar to silica. Electromodulated ion-exchange and chromatographic materials have previously been prepared by physisorption of a redox active material to a conducting substrate.[9,34]

Physisorption was performed in a 1 mM dichloromethane solution of $HEP^+NO_3^-$ after the ITO was first soaked in base for at least half an hour. The resulting electrode was then tested by cyclic voltammetry for physisorption of $HEP^+NO_3^-$. The resulting voltammograms in 100 mM $KNO_3(aq)$ can be seen in Figure 4.1. The physisorbed $HEP^+NO_3^-$ had an $E^{\circ\prime}$ ($E^{\circ\prime}$, taken as the average of the anodic and cathodic peak potentials) value of 524 mV vs. Ag/AgCl and a ΔE_{pk} (ΔE_{pk}, taken as the difference of the anodic and cathodic peak potentials) of 180 mV.

The ion-exchange properties of HEP physisorbed on ITO were tested electrochemically by adding anions (A^-) other than nitrate to the electrolyte. Figure 4.1 shows the electrochemical response of the electrode described above in the presence of 2 mM perrhenate anion (ReO_4^-), an ion commonly used for simulated extractions in our laboratories,[53,58,59] and 2 mM *closo*-1-carbaundecaborane anion ($CB_{11}H_{12}^-$), a fairly large, weakly hydrated anion. Both these experiments were run in the 0.1 M $KNO_3(aq)$ electrolyte solution, a 50 times excess of NO_3^- anion. Furthermore, the voltammogram taken in the presence of 2 mM $CB_{11}H_{12}^-$ also contained 2 mM ReO_4^-. The addition of ReO_4^- shifted the half-wave potential ($E^{\circ\prime}$ = 452 mV vs. Ag/AgCl and ΔE_{pk} = 141 mV) by –92 mV. The subsequent addition of $CB_{11}H_{12}^-$ to this electrolyte further shifted the half-wave potential ($E^{\circ\prime}$ = 67 mV vs. Ag/AgCl and ΔE_{pk} = 76 mV) by –385 mV from $E^{\circ\prime}(ReO_4^-)$ and –457 mV from $E^{\circ\prime}(NO_3^-)$. As indicated by the negative half-wave potential shifts ($\Delta E^{\circ\prime} = E^{\circ\prime}(A^-) - E^{\circ\prime}(NO_3^-)$) upon addition of both ReO_4^- and $CB_{11}H_{12}^-$ to the electrolyte solution, the physisorbed HEP became easier to oxidize in the presence of ReO_4^- and $CB_{11}H_{12}^-$.

The above experiment demonstrates three important factors that govern the ion-exchange process of $HEP^+NO_3^-$ as described by Moyer *et. al.* and demonstrated for the

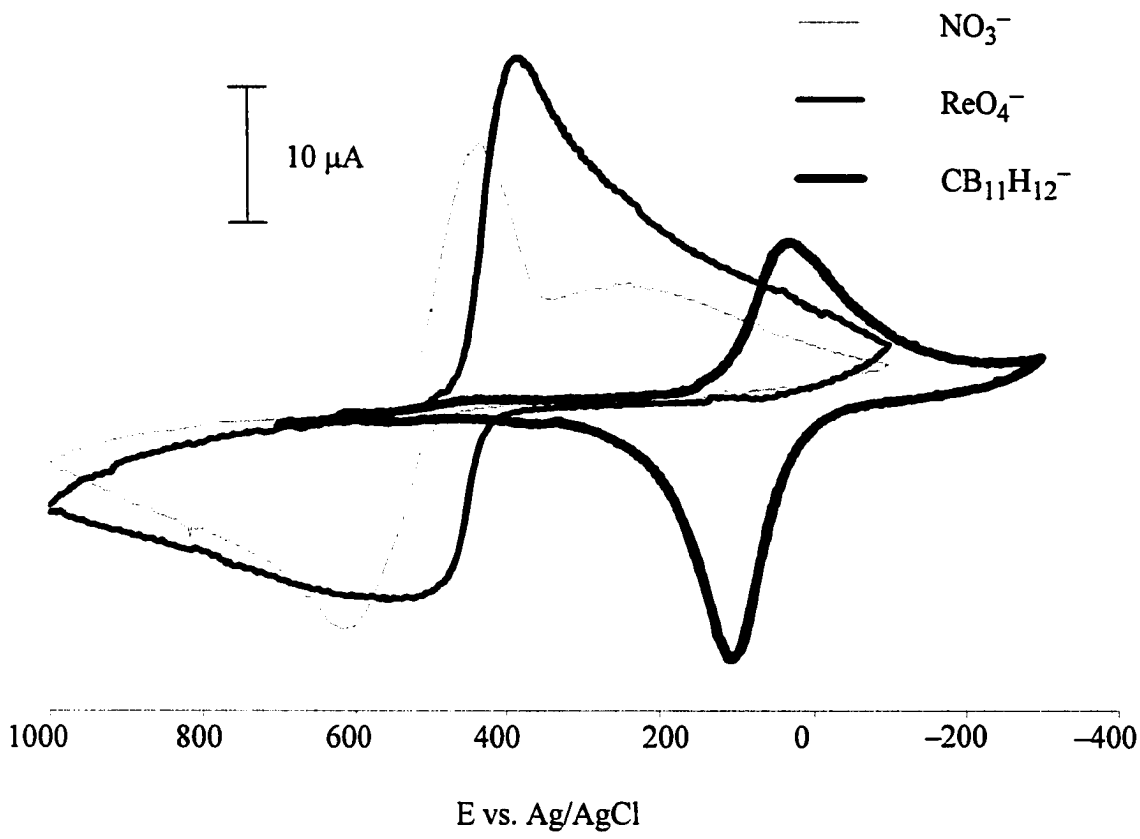

Figure 4.1. Cyclic voltammograms of $HEP^+NO_3^-$ physisorbed onto an ITO electrode. Physisorption was done from a 1 mM dichloromethane solution of $HEP^+NO_3^-$. The three voltammograms from left to right are of the electrode in a 0.1 M $KNO_3(aq)$ electrolyte, the same electrolyte solution with < 1 mM $KReO_4$, and the same electrolyte solution with < 1 mM $KReO_4$ and < 1 mM $CsCB_{11}H_{12}$. Scan rate = 50 mV/s; Pt^0 mesh counter electrode.

polyalkylated ferrocene ion-exchange materials prepared in our laboratories.[57,59,61] First, anion ion-pairing with tetraalkylated ferrocenium cations (Fc^{++}) is dependant on the hydration energy ($\Delta G°_{hyd}$) of the anions in solution; the most weakly hydrated anion will be preferentially ion-paired with the oxidized HEP^+ cation. This property is reflected in the negative potential shifts, $-\Delta E°'$, of the HEP/HEP^+ redox couple when anions with $\Delta G°_{hyd}$ less negative than that of the starting NO_3^- anion ($\Delta G°_{hyd} = -314$ kJ/mol), such as ReO_4^- ($\Delta G°_{hyd} = -240$ kJ/mol) and $CB_{11}H_{12}^-$, are introduced into the electrolyte. (All values of $\Delta G°_{hyd}$ were taken form reference 61 when available.) The smaller the hydration energy of an anion, the larger the $\Delta E°'$ of the HEP/HEP^+ redox couple when that anion is introduced into the electrolyte solution. Anion hydration has been used to describe similar anion effects for ferrocenylalkanethiol/*n*-alkanethiol mixed monolayers on gold electrodes.[25,26,62]

Secondly, the $\Delta E°'$ value also demonstrates the selectivity of the HEP^+ cation to ion-pair with the most weakly hydrated anion in solution. The potential shifts for ReO_4^- and $CB_{11}H_{12}^-$ were observed in the presence of a 50 times excess of NO_3^- present in the supporting electrolyte. Furthermore, the $\Delta E°'$ observed for $CB_{11}H_{12}^-$ was also done in the presence of an equimolar amount of ReO_4^-. The latter observation also demonstrates the difference between anion bias and recognition, which was initially discussed in Chapter 1. Though ReO_4^- was present in the electrolyte solution during the $CB_{11}H_{12}^-$ experiment, $CB_{11}H_{12}^-$ was still preferentially ion-paired with HEP^+, even though both anions are more weakly hydrated than NO_3^-. Since $CB_{11}H_{12}^-$ was preferentially ion-paired with HEP^+, a bias for ion-pairing with the most weakly hydrated anion in solution is observed rather than a specific recognition of an anion.

The final factor demonstrated by the large $\Delta E°'$ is the ability to electroactively control ion-pairing based on $\Delta G°_{hyd}$ of the desired anion. Due to the large $\Delta E°'$ observed, it can be rationalized that different anions will be ion-paired with HEP^+ at different potentials, dependant on the $\Delta G°_{hyd}$ of the anion of interest and thus the

magnitude of $\Delta E^{\circ\prime}$ for that anion If the ITO electrode with physisorbed HEP is held at a potential negative enough of the $E^{\circ\prime}$ observed for 0.1 M NO_3^-, HEP will only oxidize if that anion is present in the electrolyte. For example, in the system used for the data collected in Figure 4.1, if the electrode is held at 67 mV, $E^{\circ\prime}(CB_{11}H_{12}^-)$, in an aqueous electrolyte containing only NO_3^- anions, no oxidation of the HEP to HEP^+ will be observed unless $CB_{11}H_{12}^-$ (or an anion with ΔG°_{hyd} less negative than $\Delta G^\circ_{hyd}(CB_{11}H_{12}^-)$) is added to the electrolyte at a concentration of $\geq$ 2 mM. This "electrochemical modulation" also has important implications for electrochemical anion sensing and extraction chromatography and will be discussed later.

HEP/ITO Electrode Materials Prepared by Spin-Coating. In order to further study these effects and their applications in ion-exchange or sensor materials, deposition of HEP onto the ITO surface needed to be more reproducible. Physisorption of $HEP^+NO_3^-$ onto ITO surfaces in the manner described above did not give reproducible surface coverages and thus quantification of anion potential shifts was difficult. Furthermore, HEP has to be physisorbed onto ITO as a salt. Neutral HEP was not observed to physisorb onto oxidized ITO surfaces. By starting with neutral HEP on the electrode, $\Delta E^{\circ\prime}$ values could be referenced to anions other than NO_3^-. For these reasons, a new method of immobilizing HEP onto ITO was desirable.

The method chosen was spin coating. It was found that an ITO surface spin coated with 30 μL of a 1 mM dichloromethane solution of HEP resulted in electrodes with reproducible amounts of neutral HEP deposited on the surface. The resulting thin films of HEP were shown to be electroactive. Reductive differential pulse voltammograms for 3 separate 1 cm^2 electrodes prepared in this manner can be seen in Figure 4.2. The voltammograms were obtained in a 0.1 M KCl(*aq*) electrolyte not previously used due to the presence of the NO_3^- salt of HEP on the ITO surface. The cathodic reduction peak maximum (E_{pc}) for the three electrodes was 600 ± 10 mV. The amount of HEP in the thin film was determined from the total amount of charge passed

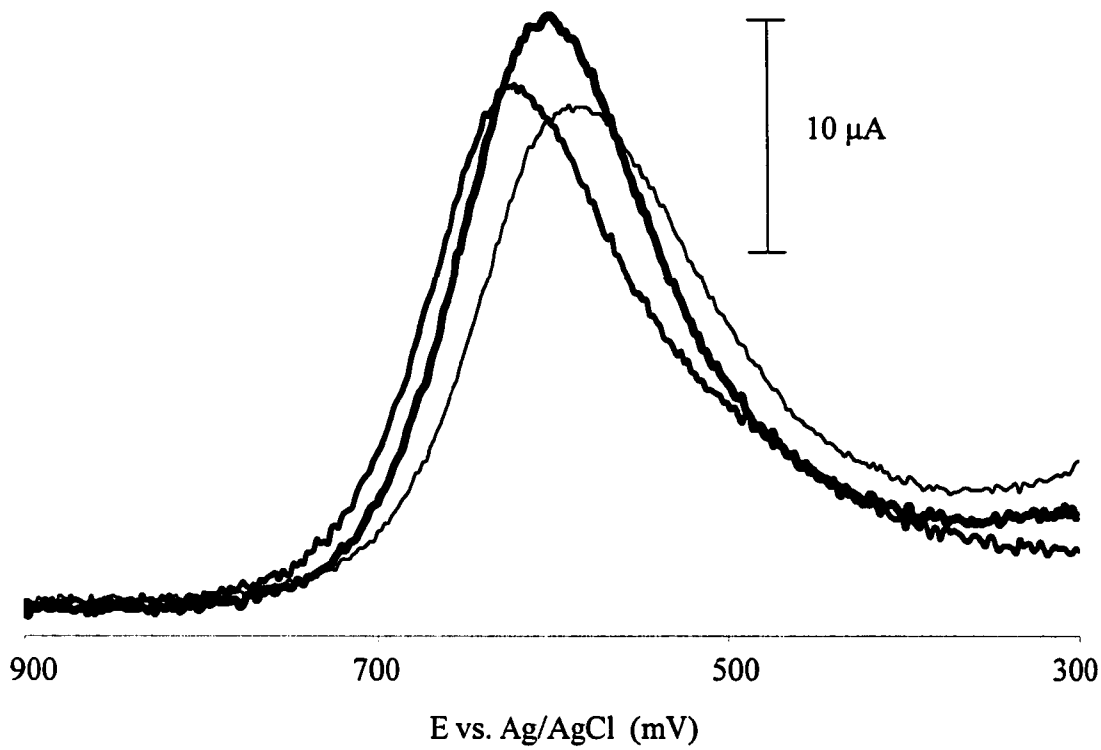

Figure 4.2. Reductive differential pulse voltammograms for three different ITO electrodes spin coated with 30 μL of a 1 mM dichloromethane solution of HEP. The average E_{pc} is 600 ± 10 mV. The amount of HEP in the thin film was determined by peak integration and was calculated to be 5.0(3) x 10^{-9} mol/cm^2. The electrode was held at an oxidizing potential of 900 mV for one minute before scanning. Scan rate = 25 mV/s, pulse amplitude = 50 mV, pulse width = 25 ms, pulse interval = 80 ms, Pt^0 mesh counter electrode, 0.1 M KNO_3 (*aq*) electrolyte.

calculated from peak integration and was $5.0 \times 10^{-9} \pm 0.3 \times 10^{-9}$ mol/cm^2. The film thickness was measured by ellipsometry at three different places on the electrode. As can be expected for a spin-coated surface, the film became thicker towards the edges of the electrode. Thin film thickness varied from 50 ± 1 Å at the center of the electrode to 120 ± 3 Å at the edges of the electrode.

Anion exchange experiments similar to those performed with $HEP^+NO_3^-$ physisorbed onto ITO (Figure 4.1) were performed with the spin-coated ITO electrodes (HEP/ITO). Figure 4.3 shows reductive differential pulse voltammograms of HEP/ITO in a 0.1 M KCl(*aq*) electrolyte with other weakly hydrated anions concentrated to 1 mM sequentially. Again, large potential shifts are seen as $\Delta G°_{hyd}$ of the anion added to the electrolyte becomes less negative. In this particular study, it is possible to observe a potential shift for the NO_3^- anion since the experiment can now be done in a Cl^- electrolyte. The $\Delta G°_{hyd}$ for Cl^- ($\Delta G°_{hyd}$ = –338 kJ/mol) is more negative than that for NO_3^-, and hence, when nitrate is added to the electrolyte solution, a potential shift is observed. Table 4.1 shows peak potential shifts (ΔE_{pc}) for various anions. All ΔE_{pc} are relative to the cathodic peak potential maximum of HEP/HEP^+ in 0.1 M KCl(*aq*) and are referenced to a Ag/AgCl electrode. Values shown represent the average of three measurements each done with separate electrodes prepared by spin coating. Values for $\Delta G°_{hyd}$ are given when available. The data follow the predicted trend of increasing ΔE_{pc} as $\Delta G°_{hyd}$ becomes less negative.

An interesting trend can be seen in the ΔE_{pc} data for the perfluorinated surfactants and qualitative assumptions can be made about their $\Delta G°_{hyd}$. As stated previously, a major factor in the magnitude $\Delta G°_{hyd}$ is the size of the anion; in general, as the size of the anion increases, $\Delta G°_{hyd}$ becomes less negative. Both the perfluorooctylsulfonate anion ($PFOS^-$) and perfluoroctylcarboxylate anion ($PFC\text{-}8^-$) contain 8 carbon atom chains and are assumed to be similar in size. The $PFC\text{-}8^-$ anion, however, has a much larger potential shift (ΔE_{pc} = –414 mV) than $PFOS^-$ (ΔE_{pc} = –293 mV) and therefore is

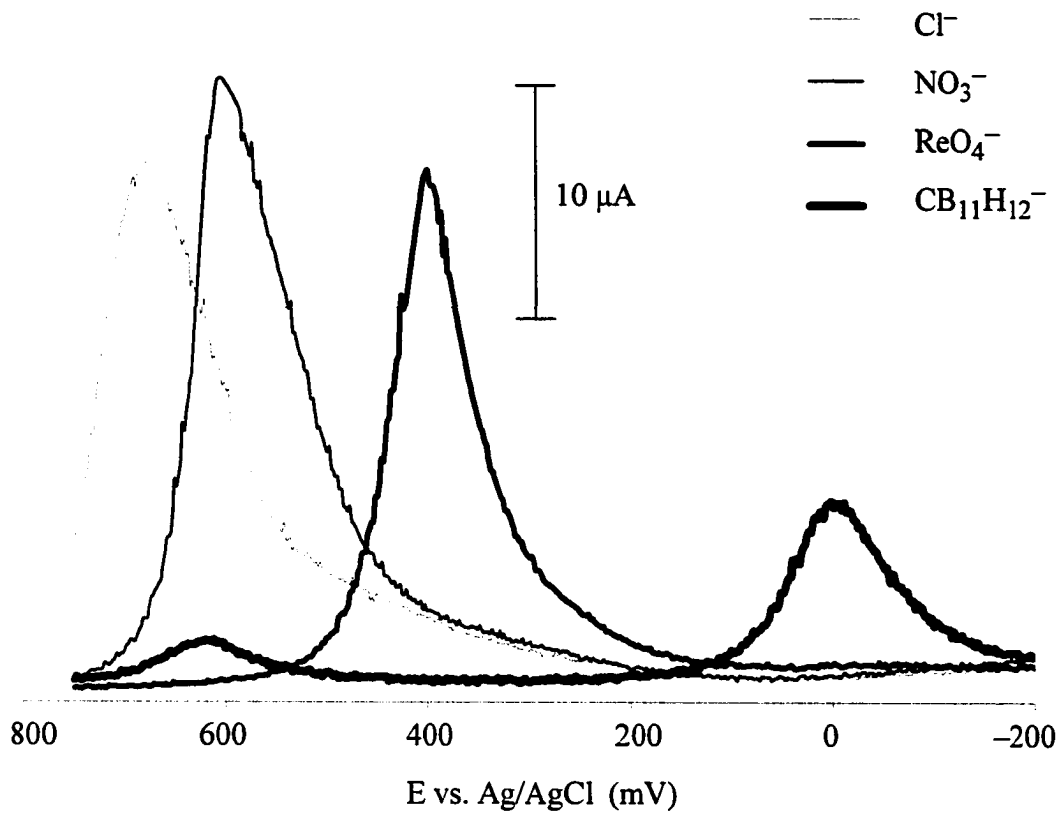

Figure 4.3. Differential pulse voltammograms of HEP/ITO in a 0.1 M KCl(*aq*) electrolyte with NO_3^-, ReO_4^-, and $CB_{11}H_{12}^-$ anion added sequentially. The anions were all added as potassium salts except for $CB_{11}H_{12}^-$, which was added as the cesium salt and concentrated in the KCl electrolyte to 1 mM. The electrode was held at an oxidizing potential of 800 mV for one minute before scanning. Scan rate = 25 mV/s, pulse amplitude = 50 mV, pulse width = 25 ms, pulse interval = 80 ms, Pt^0 mesh counter electrode.

Table 4.1. The HEP/ITO peak potential shifts (ΔE_{pc})[a] obtained from reductive differential pulse voltammograms for various anions (A^-) in a 0.1 M KCl(*aq*) electrolyte.

A^- (1 mM)[b]	$\Delta G°_{hyd}$ (kJ/mol)[d]	$E_{pc}(A^-)$ (mV)[e]	ΔE_{pc} (mV)[e]
Cl^- [c]	–338	678	0
NO_3^-	–314	606	–72
ClO_4^-	–259	529	–149
ReO_4^-	–240	400	–278
$C_8F_{17}SO_3^-$ ($PFOS^-$)	—	385	–293
$C_7F_{15}COO^-$ ($PFC\text{-}8^-$)	—	264	–414
$C_{11}F_{23}COO^-$ ($PFC\text{-}12^-$)	—	179	–499
$CB_{11}H_{12}^-$	—	–18	–696

a. $\Delta E_{pc} = E_{pc}(Cl^-) - E_{pc}(A^-)$ b. All anions were introduced as potassium salts except ClO_4^- (Na^+), and $CB_{11}H_{12}^-$ (Cs^+). c. The concentration of chloride anion was 100 mM (electrolyte concentration). d. Hydration energy values were taken from reference 61. e. All values are reported vs. a Ag/AgCl reference electrode. The value reported is the average of three measurements done with separate electrodes. The error associated with these measurements is the standard deviation for the three measurements and is $\leq \pm 15$ mV in all cases.

assumed to have a less negative $\Delta G°_{hyd}$. The difference in $\Delta G°_{hyd}$ is assumed to be due to the presence of three oxygen atoms in the $PFOS^-$ anion vs. two in the PFC-8^- anion, thus contributing to better hydration for the $PFOS^-$ anion. The effect of anion size on hydration energy is demonstrated when comparing the ΔE_{pc} values of PFC-8^- and perfluorododecylcarboxylate (PFC-12^-; ΔE_{pc} = –499 mV). Both anions have the same number of oxygen atoms in their structures, but PFC-12^- is larger in size due to its longer perfluorinated chain. The PFC-12^- anion therefore has a larger ΔE_{pc} and a less negative $\Delta G°_{hyd}$.

As with the ITO electrode prepared by physisorption, the anion that displayed the largest ΔE_{pc} for HEP/ITO was the $CB_{11}H_{12}^-$ anion. Its ΔE_{pc} value was almost 700 mV in the presence of 100 times excess Cl^- and equal amounts of NO_3^- and ReO_4^-. To our knowledge, the magnitude of this shift in ΔE_{pc} is unprecedented in the electrochemical literature at these concentrations. Interestingly, the amount of HEP reduced in the presence of the $CB_{11}H_{12}^-$ anion was less than that seen for the other anions. This is evidenced by the smaller amount of current passed in the voltammogram taken in the presence of $CB_{11}H_{12}^-$ anion. One possible reason for the decrease in the current may be a smaller amount of the $CB_{11}H_{12}^-$ anion in the HEP thin film due to the large size of the anion. Figure 4.4 shows microscope pictures of a 6 hour old HEP/ITO electrode before use. As can be seen by the "feathering" at the top of the electrode, the films appear to be at least partially semi-crystalline. As a result, the rate of diffusion into the thin film for a large anion, such as $CB_{11}H_{12}^-$, might be slower than the rate for smaller anions do the rigid nature of the crystalline lattice. The result would be less inclusion of $CB_{11}H_{12}^-$ in the oxidized thin film. In this case, smaller anions may also diffuse into the film to balance charge at a kinetically faster rate than $CB_{11}H_{12}^-$, followed subsequently by ion-exchange with the less hydrated $CB_{11}H_{12}^-$ anion. Evidence for the presence of smaller anions in the thin film can be seen in the voltammogram for HEP/ITO with $CB_{11}H_{12}^-$ in Figure 4.3. A small reduction peak can be seen at 612 mV, a value between the E_{pc}

values observed for Cl^- and NO_3^-. This small peak may be due to reduction of a small amount of HEP^+Cl^- or $HEP^+NO_3^-$ present in the film due to the slow rate of inclusion for the $CB_{11}H_{12}^-$ anion. The total amount of HEP^+ reduced in the two peaks in the voltammogram was calculated to be 4.1×10^{-9} mol, only slightly smaller than the starting amount of 5.0×10^{-9} mol calculated for the thin film.

As discussed previously (*vide* supra), these reproducible potential shifts provide the possibility of "electrochemical modulation" for anion extraction. This modulation could have important impacts on a chromatographic, ion-exchange system for the removal of anions from aqueous media. A conducting material, such as ITO deposited on glass beads or glassy carbon beads, coated with HEP could be packed into an extraction column for anion extraction. While flowing a solution containing the target anion through the extraction column, the material could be held at different potentials. The potential would have drastic effects on both the efficiency of the extraction as well as the anions being extracted. The effects of varying potential on the separation of aromatic sulfonates in an electrochemically modulated chromatographic system have been demonstrated previously.[9] The extraction column could also be easily recycled by holding the material in the column at a significantly reducing potential so that no oxidized ferrocene remained, and all the anions extracted would then be washed away.

Due to the magnitude of the potential shifts observed for various anions and their potential use for electrochemically modulated chromatography and aqueous anion sensing applications, the HEP/ITO material was tested for long term durability. Figure 4.4 shows microscope pictures of a 6 hour old HEP/ITO electrode before and after 100 electrochemical scans between 0 and 1000 mV vs. Ag/AgCl. The cyclic voltammograms for scans 1, 25, 50, 75, and 100 are also shown in Figure 4.4. The amount of current decreases significantly over the 100 cycles, indicating loss of electrochemical activity. The reason for the loss of activity is unknown, but comparison of the microscope pictures before and after 100 scans show obvious damage to the surface of the thin film. One

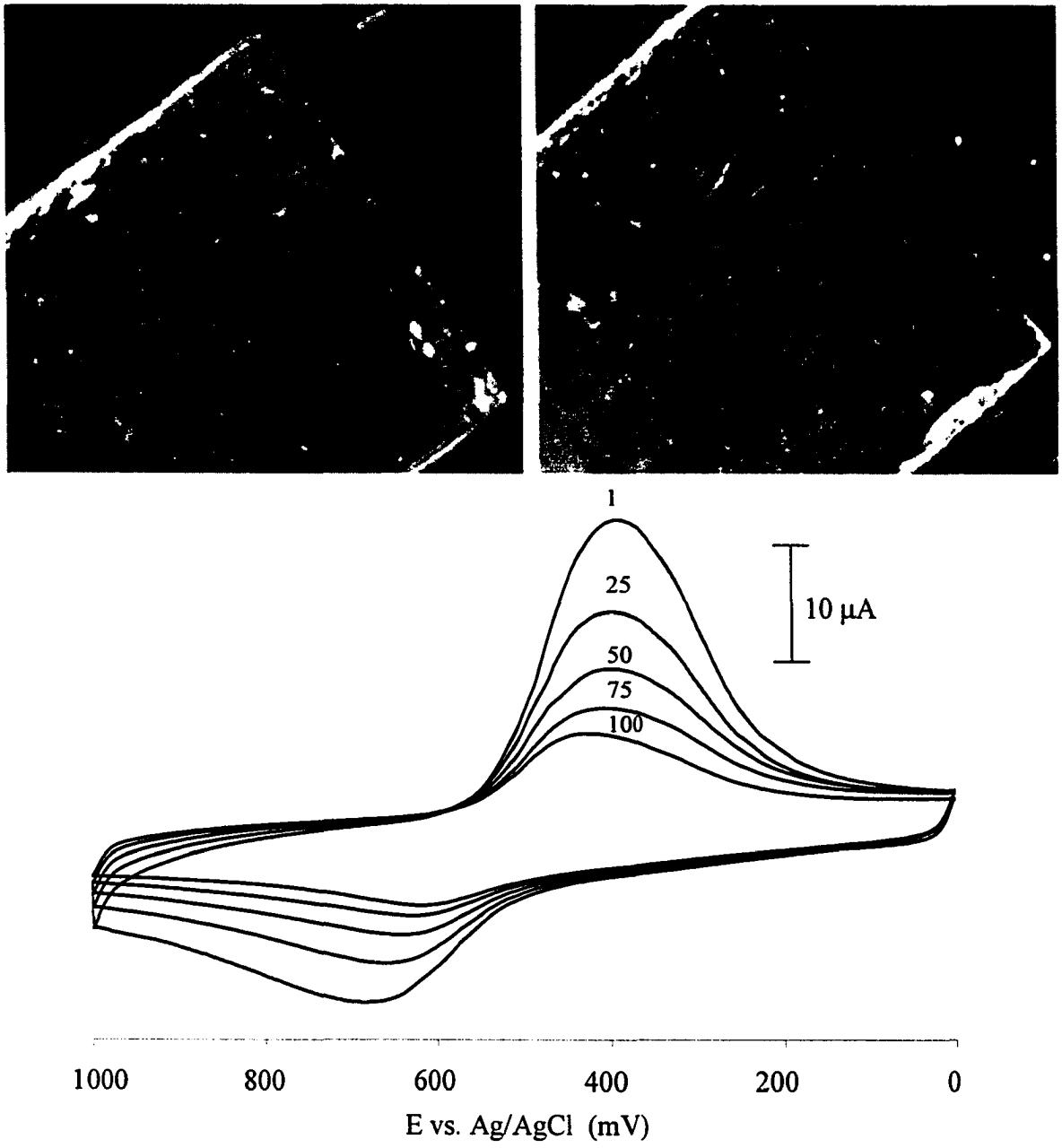

Figure 4.4. Magnified pictures of ITO electrodes spin coated with HEP before (left) and after (right) 100 electrochemical cycles between 0 and 1000 mV. The HEP/ITO electrode was prepared 6 hours before electrochemical cycling. The actual size of the electrodes is 1 cm^2. The cyclic voltammograms (bottom) are for the same electrode at 1, 25, 50, 75, and 100 scans in a 0.1 M KNO_3 aqueous electrolyte (scan rate = 200 mV/s).

possibility is that the film is semi-crystalline and material flakes off of the surface as anions diffuse in and out of the film. Crystallinity has been observed to affect the properties of the film. Figure 4.5 shows a microscope picture of a two week old HEP/ITO electrode. It can clearly be seen that the thin film is more crystalline than electrodes freshly prepared by the appearance of "feathering" and cracking over the entire surface of the thin film. Figure 4.5 also shows cyclic voltammograms of the same electrode in an anion sensing experiment with 1 mM PF_6^- anion and 1 mM $CB_{11}H_{12}^-$ anion. As can be seen, the initial 16 μA of current in the 0.1 M $KNO_3(aq)$ electrolyte is about half the 30 μA observed for freshly prepared electrodes using the same scan rate. Furthermore, the amount of HEP oxidized and reduced in the experiment is 1.6×10^{-10} mol/cm^2, approximately three times less than that observed for the freshly prepared electrodes. Large potential shifts are still observed, however, upon addition of weakly hydrated anions. The potential shifts observed relative to NO_3^- were 99 mV for 1mM PF_6^- and 462 mV for 1 mM $CB_{11}H_{12}^-$. (The magnitudes of the potential shifts are smaller than those reported in Table 4.1 due to reference to the NO_3^- anion instead of the Cl^- anion.) When scanned 100 times in the 0.1 M $KNO_3(aq)$ electrolyte, the current for the crystalline film was also observed to decrease. After 100 scans at 200 mV/s, less than 1μA of current was observed for the cathodic and anodic peaks. Thinner films may solve some of these problems and should be investigated further before pursuing sensor applications for the HEP/ITO material.

11-Thioundecanoyl Tetraalkylated Ferrocene Monolayers on Gold. The synthesis of HEP-SH was performed as described in Chapter 3 and is similar to that described by Hickmann et. al for 11-thiolundecanoylferrocene.[63] Organically modified thiols, including ferrocenylalkanethiols and other organometallic modified thiols, are know to readily form self-assembled monolayers (SAMs) on gold (111) surfaces.[23,38,40,47] A gold disk electrode was placed in a 1 mM THF solution of HEP-SH overnight and the resulting SAM characterized by cyclic voltammetry. Cyclic

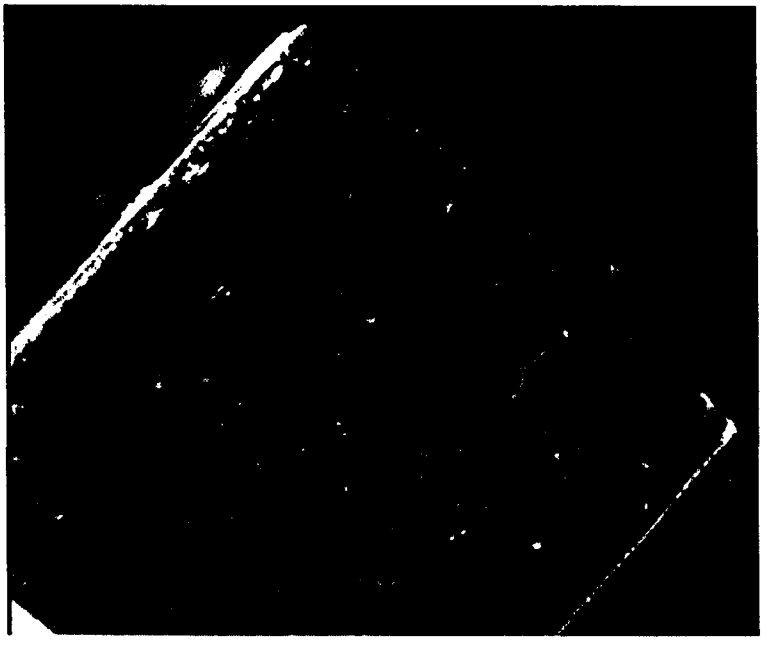

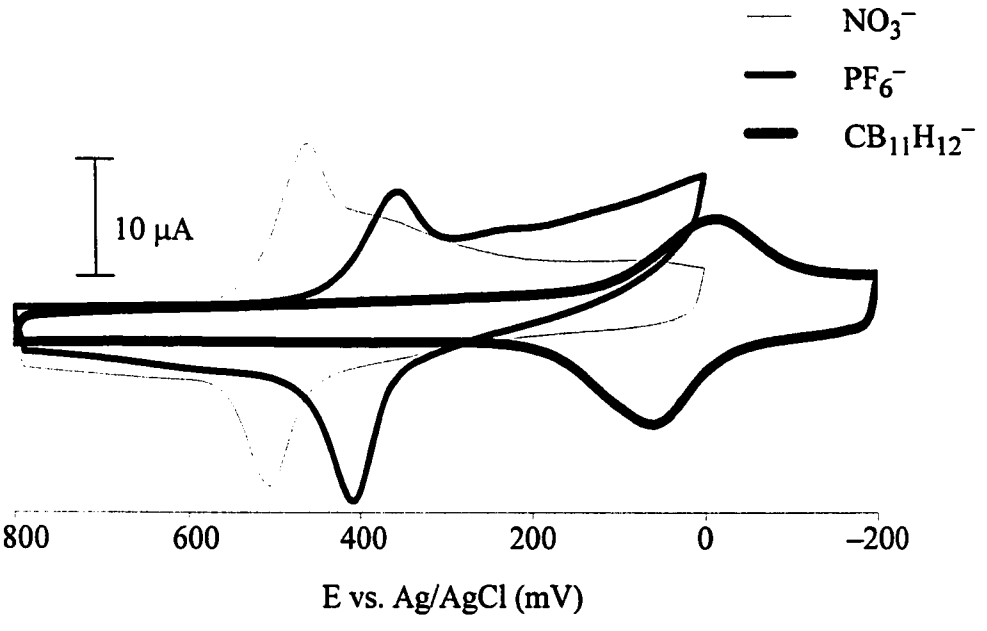

Figure 4.5. A magnified picture of a two-week-old HEP/ITO electrode before electrochemical cycling. The actual size of the electrode is 1 cm^2. The cyclic voltammograms (bottom) are for the same electrode in a 0.1 M $KNO_3(aq)$ electrolyte with PF_6^- and $CB_{11}H_{12}^-$ anion added sequentially to a concentration of 1 mM (scan rate = 200 mV/s, Pt^0 mesh counter electrode).

voltammograms of a HEP-SH SAM can be seen in Figure 4.6. Similar to the HEP/ITO material, when anions with subsequently less negative $\Delta G°_{hyd}$ are added to the electrolyte, there is a potential shift for the SAM. The $E°'$ values for the cyclic voltammograms seen in Figure 4.6 are 681, 455, and 180 mV vs. Ag/AgCl for 0.1 M NO_3^-, 1 mM PF_6^-, and 1 mM $CB_{11}H_{12}^-$ respectively. The $\Delta E°'$ values relative to the 0.1 M KNO_3(aq) electrolyte are –226 mV for PF_6^- and –501 mV for $CB_{11}H_{12}^-$. The peak separations (ΔE_{pk}) for the three voltammograms are 44 ± 2 mV. The inset shows a plot of current (i) vs. scan rate (ν) for the HEP-SH SAM in the pure 0.1 M KNO_3(aq) electrolyte. The linear correlation between i and ν, as well as the $\Delta E_{pk} < 59$ mV, confirm that the HEP-SH redox species is surface confined.[64]

To further investigate the effects of anion hydration energy and other ion-exchange properties of Fc' SAMs, the series of 11-thiolundecanoyl functionalized tetraalkylated ferrocenes containing BUT, PENT, HEX, HEP, and DEC moieties was synthesized and the corresponding SAMs on gold disk electrodes were investigated. Deposition of 11-thiolundecanoyl tetraalkylated ferrocenes (Fc'-SH) with alkyl chains larger than *t*-butyl groups from 1 mM ethanol or THF solutions by soaking for 24 hours proved to be inconsistent for SAM formation. The compounds PENT-SH, HEX-SH, and HEP-SH did not form reproducible SAMs when the monolayers were deposited by soaking in 1 mM ethanol or THF solutions for 24 hours. Full monolayer deposition was accomplished in only a few cases and in others, only small amounts of Fc'-SH were observed to deposit on the gold surface. Little to no self-assembly was observed for DEC-SH by soaking. It was found however, that Fc'-SH monolayers could be deposited reproducibly electrochemically following the method of Weisshaar *et. al.*, who showed that electrochemically deposited monolayers (EAMs) had the same properties as their self-assembled analogs.[55] All experiments involved the following sequence of events: (1) mechanical polishing of gold disk electrodes; (2) electrochemical deposition of Fc'-SH monolayers onto gold disk electrodes from a 10 mM ethanolic solution, also

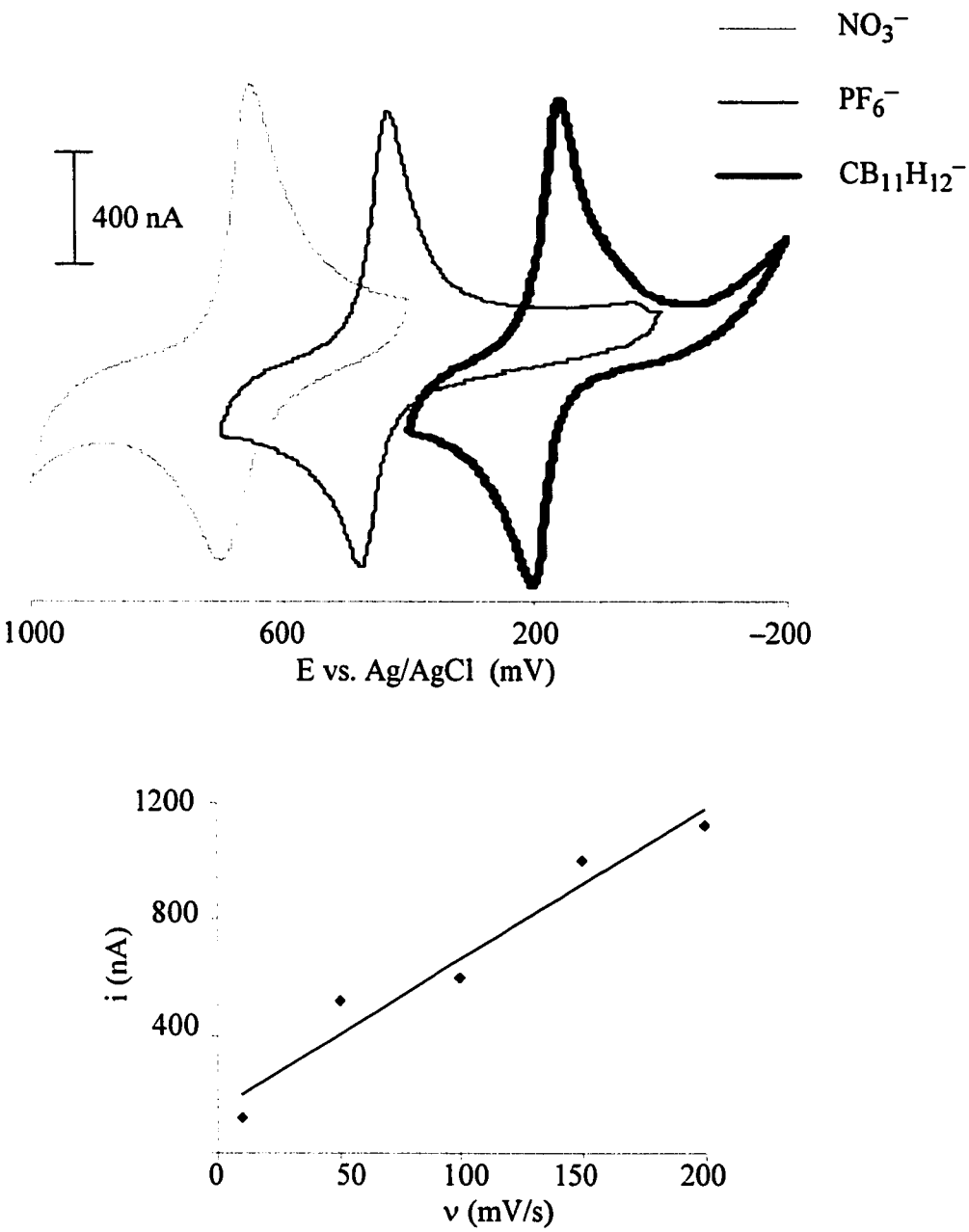

Figure 4.6. Cyclic voltammograms of HEP-SH SAMs on a gold electrode. Similar to the HEP/ITO material, large negative potential shifts are seen as the more weakly hydrated anions, PF_6^- and $CB_{11}H_{12}^-$ are added to the 0.1 M $KNO_3(aq)$ electrolyte (scan rate = 100 mV/s, Pt^0 mesh counter electrode). The plot of i vs. ν,measured in 0.1 M $KNO_3(aq)$, has an $R^2 = 0.96$.

containing 0.5 M KOH, by holding the potential at –600 mV (vs. Ag/AgCl(*aq*)) for > 1 minute; (3) thorough rinsing with ethanol and water; (4) characterization by cyclic voltammetry.

The quantity of immobilized Fc'-SH in an EAM was determined by integration of the voltammetric peaks. The surface coverage (Γ in mols/cm^2) was determined for each of the EAMs using the values obtained from peak integration and the microscopic surface area for the gold disk electrodes (0.044(5) cm^2; *vide supra*). Theoretical monolayer surface coverages for each of the Fc'-SH monolayers were also calculated using two different models, shown in the diagrams below. The first model treats the Fc' moiety as a cylinder, in which the alkyl chains are oriented down into and out above the monolayer, and assumes hexagonal packing of the cylinders. Since the diameter of the Fc'-SH moieties, determined from the crystal structures of the unfunctionalized tetraalkylated ferrocenes,[44] is constant at 11 Å, this model predicts a coverage of 1.6 mols/cm^2 for each Fc'-SH monolayer. The second model assumes that the Fc' moieties lay flat on the surface of the monolayer. Monolayer coverages using this model were calculated using the cross sectional areas of the Fc' moieties, again determined from the crystal structures of the unfunctionalized tetraalkylated ferrocenes. As expected, monolayer coverages calculated using this model decreased as the size of the Fc' moieties increased.

The monolayer coverages calculated from the models discussed above as well as the experimentally observed monolayer coverages are shown in Table 4.2. The experimentally observed monolayers had coverages between the values calculated for the two models. For the BUT and PENT EAMs, which both contain relatively small Fc' moieties, the two calculated monolayer coverages were very similar, and these values were the same as those observed experimentally within experimental error. The HEX, HEP, and DEC EAMs all gave monolayer coverages with values in between those predicted by the two models. It is hard to speculate on the exact method of packing for these EAMs due to the large errors associated with the surface coverage measurements.

theoretical surface coverage models

(R = methyl, ethyl, *n*-propyl, *n*-butyl, and *n*-heptyl)

side view

top view

hexagonal packing model

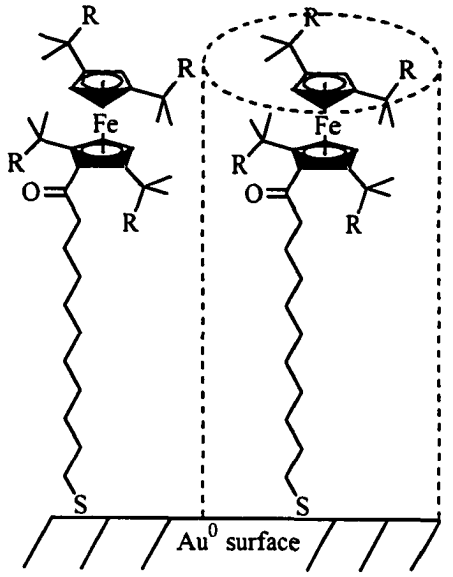

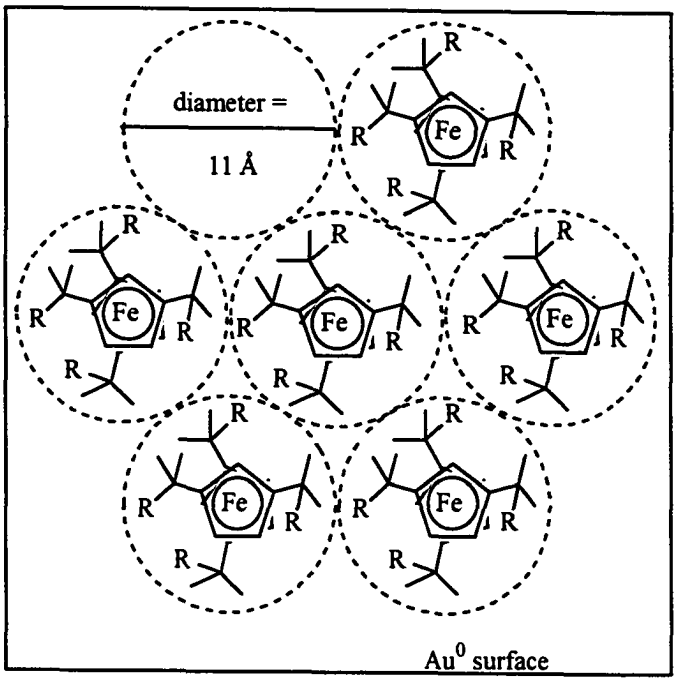

cross section packing model

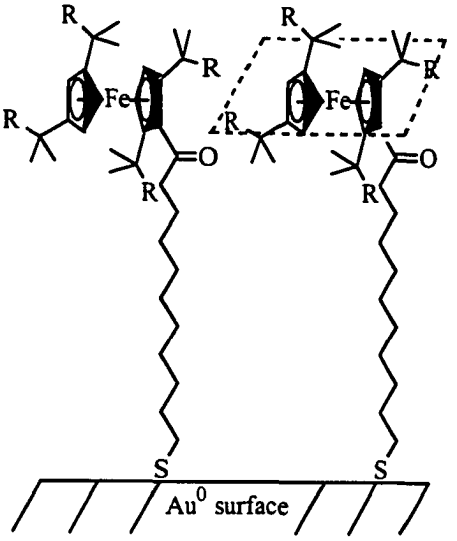

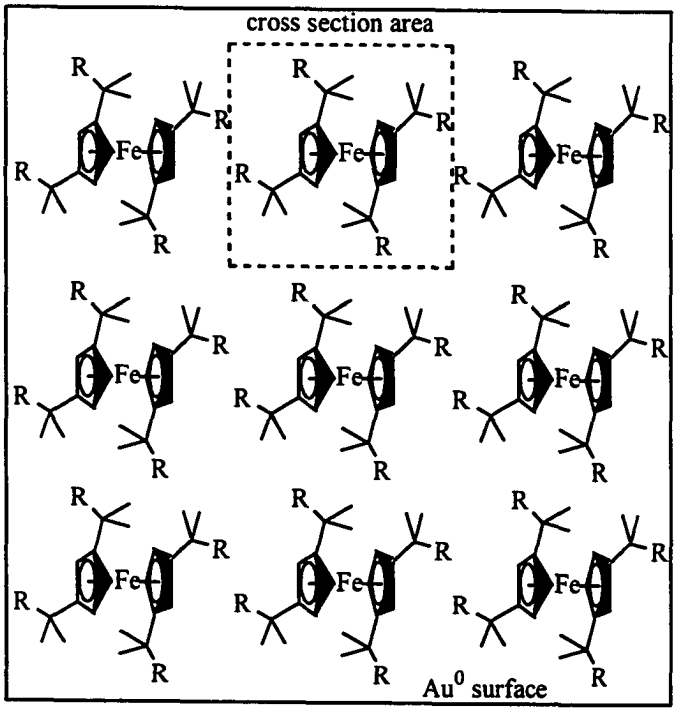

Table 4.2. Theoretical and experimental monolayer surface coverages calculated for 11-thiolundecanoyl tetraalkylated ferrocenes. Values for 11-thiolundecanoyl ferrocene are also included for comparison.

Fc'	diameter of Fc' [a] × 10^8 (cm^2)	Fc' cross section area[a] × 10^8 (cm^2)	monolayer Γ hex. pack[a] × 10^{10} (mol/cm^2)	monolayer Γ x-sect. pack[a] × 10^{10} (mol/cm^2)	experimental monolayer Γ [d] × 10^{10} (mol/cm^2)	partial monolayer Γ [d,e] × 10^{10} ($mols/cm^2$)
FcH[b]	6.6	—	4.5	—	4.6	—
BUT	11	120	1.6	1.4	1.4(5)	0.37(5)
PENT[c]	11	140	1.6	1.2	1.4(5)	0.32(7)
HEX[c]	11	160	1.6	1.0	1.1(4)	0.37(4)
HEP	11	180	1.6	0.92	1.1(4)	0.42(6)
DEC	11	290	1.6	0.57	0.8(6)	0.35(5)

[a.] Calculated from crystal structure data of the unfunctionalized tetraalkylated ferrocenes. [b.] Values were taken from reference 25 for ferrocenylhexanethiol monolayers. [c.] Values estimated from the crystal structure of HEP. [d.] Numbers in parentheses represent one standard deviation of at least three separate determinations. [e.] Surface coverages calculated for the monolayers used in the calculation of K_{eff} values (*vide infra*).

Due to the difficulty of determining microscopic surface areas of disk electrodes, the large error associated with each measurement may be a result of differences in surface roughness for each electrode.[54] Despite the large error in the observed surface coverage measurements, it is believed that the average surface coverage values are indicative of the hexagonal packing model. The hexagonal packing arrangement has been previously observed for *n*-alkanethiols on gold (111) surfaces.[39] The arrangement of atoms on the gold (111) surface contains "hollow" sites arranged in a hexagonal array between the gold atoms and the sulfur atoms sit in these sites. In this hexagonal packing model, defect sites in the monolayer could explain the deviations from the calculated surface coverage value of 1.6×10^{-10} mols/cm^2. A defect site would include sites in which the Fc' moiety is folded over into the monolayer or is just oriented parallel to the electrode surface, as shown below. Similar defects for ferrocenyl monolayers on gold have been

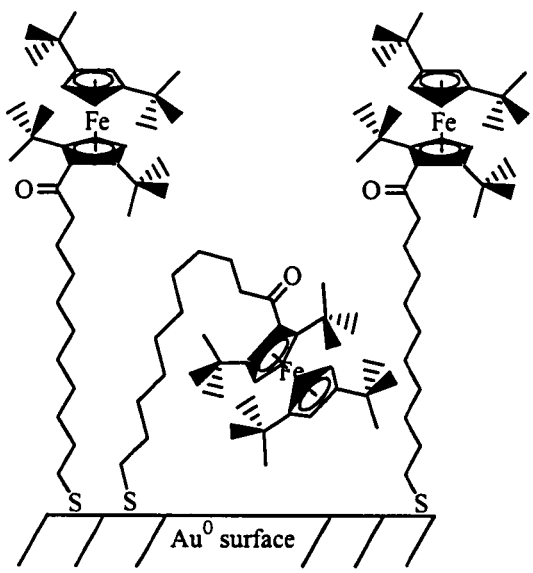

defect site for BUT monolayer

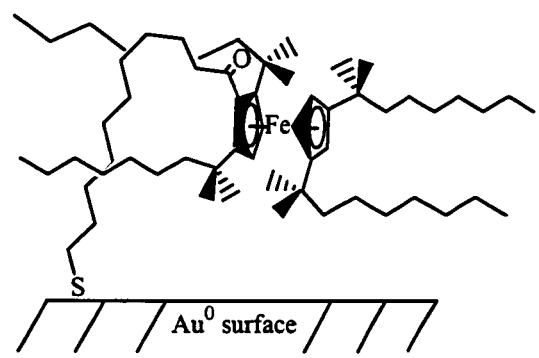

defect site for DEC monolayer

proposed previously.[38,41] Assuming these types of defects, deviations from the predicted hexagonal monolayer coverage of 1.6×10^{-10} mols/cm^2 should be larger for monolayers of the larger Fc' moieties, such as HEP and DEC. As shown above, such a defect would

prevent more chemisorption than a similar defect in a monolayer containing smaller Fc' moieties, such as BUT or PENT.

Figure 4.7 shows cyclic voltammograms of partial Fc'-SH EAMs in 1 M H_2SO_4. The cyclic voltammograms shown are for approximately 50 - 60% of a monolayer, in each case, assuming the hexagonal packing model. Coverages less than a monolayer were chosen to avoid multiple peaks in the voltammetric responses, a common occurrence observed in this work for Fc'-SH monolayers at high surface coverages. The cause of multiple peaks at high surface coverages is not fully understood, but it is proposed that the multiple peaks are caused by the presence of different adsorption domains due to defects or solvent molecules.[25] Similar multiple peak voltammograms have been observed previously for mixed ferrocenylalkanethiol/*n*-alkanethiol monolayers as well as other mixed monolayers containing high concentrations of redox active centers.[28,46,47] The electrochemical potential was scanned from 0 to 1 V vs. Ag/AgCl at 200 mV/s. Minimal loss of Fc'-SH was observed after 25 such cycles, indicating the stability of the Fc'-SH partial monolayers to electrochemical cycling. The peak current scaled with scan rate in all cases as expected for a surface confined redox species. The values of ΔE_{pk} were between 38 and 48 mV for the five cyclic voltammograms. The small peak separation (< 59 mV) at this relatively fast scan rate and the nearly identical anodic and cathodic peaks indicate that the redox couple is rapid and reversible on the time scale of these experiments.

As the size of the Fc' moiety increases from BUT to DEC, the redox potential shifts to more positive values. A positive shift of 100 mV is observed upon going from the partial monolayer of BUT to the partial monolayer of DEC. Potential shifts of this magnitude have also been seen by Rowe *et. al.* with mixed monolayers of ferrocenylalkane- thiols/*n*-alkanethiols as the chain length of the co-adsorbed *n*-alkanethiol increased. The positive potential shift in the presence of the HSO_4^- anion may be explained by the increasingly alkane like environment between BUT and DEC.[25]

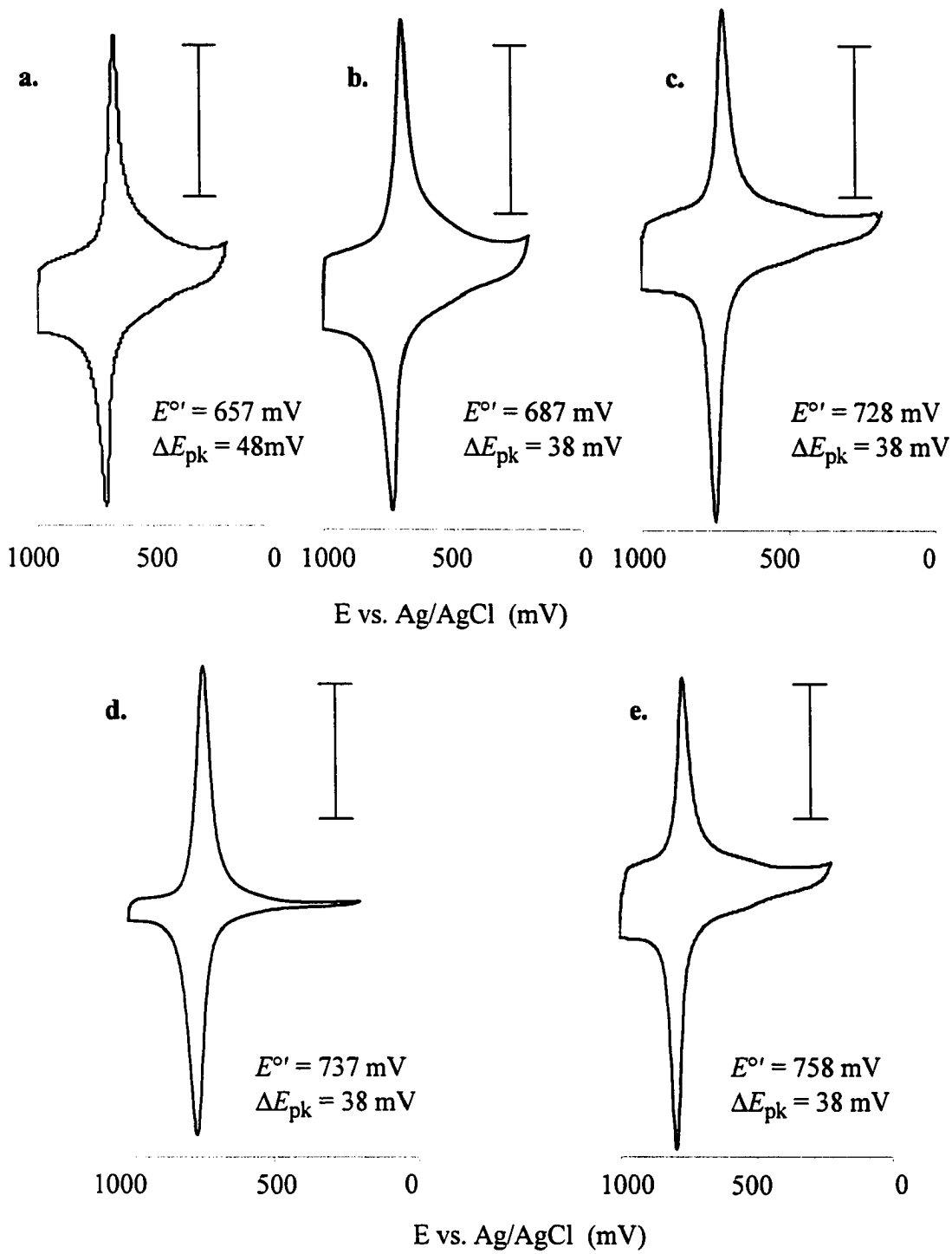

Figure 4.7. Cyclic voltammograms of gold disk electrodes modified with (a) BUT-SH (b) PENT-SH (c) HEX-SH (d) HEP-SH and (e) DEC-SH in a 1.0 M $H_2SO_4(aq)$ electrolyte (scan rate = 200 mV/s). The vertical bars represent 0.5 μA.

As the electrode surface becomes more hydrophobic due to the increased length of the alkyl chains in the Fc' moieties, it becomes more favorable for the the well hydrated bisulfate anion to stay in the aqueous solution. The result therefore is a larger reduction potential as the monolayer becomes more hydrophobic, demonstrating the thermodynamic barrier required for a well hydrated anion to penetrate the monolayer.

Electrochemical Determination of Effective Formation Constants (K_{eff}) of Tetraalkylated Ferrocenium Salts. The ion-exchange selectivity from aqueous media of tetraalkylated ferrocenium (Fc'^{+}) ion-exchange materials has been shown to depend on both the hydration energies of the target anion as well as the size of the Fc'^{+} cation.[59] It has further been shown that the dielectric of the surface of these ion-exchange materials may also play a role in the selectivity.[57] Ion-exchange selectivity based on these properties has been previously described by Moyer *et. al.*[61] and is summarized in Chapter 1. We propose that similar properties control the selectivity of ion-exchange/ion-pair formation in the partial Fc'-SH monolayers described above.

Before making such a comparison, it is necessary to be able to evaluate the electrochemical ion pair formation of Fc'-SH modified gold surfaces with various anions. Such an evaluation can be done by calculation of the "effective" formation constant (K_{eff}) for an ion pair consisting of the Fc'^{+} cation and an anion using the method of Rowe *et. al.*.[25] This method has also been used by Ju *et. al.* for the evaluation of ion-pairing in mixed ferrocenylalkanethiol/*n*-alkanethiol monolayers.[26] This method considers the formation of ion-pairs in the presence of two anions, X^- or Y^-, with different hydration energies and is defined by the following set of equilibria (see Appendix C) and Equation 4.1:

$$Fc' + X^- \rightleftharpoons Fc'^{+}X^- \qquad K_X = \frac{\Gamma_{Fc'^{+}X^-}}{\Gamma_{Fc'^{+}} C_{X^-}}$$

$$Fc' + Y^- \rightleftharpoons Fc'^+Y^- \qquad K_Y = \frac{\Gamma_{Fc'^+Y^-}}{\Gamma_{Fc'^+} C_{Y^-}}$$

(4.1) $$K_{eff} = \frac{K_Y}{1 + K_X C_X}$$

where K_{eff} is an "effective" formation constant for the Fc'^+Y^- ion pair. Electrochemically, simultaneous ion-pairing equilibria of Fc'^+ with X^- or Y^- can be described by

(4.2) $$E_{pk} = E^{\circ\prime} - \frac{RT}{nF} \ln(1 + K_X C_X + K_Y C_Y)$$

where E_{pk} is the peak potential of a symmetrical wave (where half of the bound Fc' has been oxidized) and K_X and K_Y are defined above. (For derivation of Equation 4.2 see Appendix C.) It is reasonably assumed that there is no association of X^- or Y^- with neutral Fc'^+. The problem with direct determination of K_X or K_Y from this expression is that the value of $E^{\circ\prime}$ is not precisely known and cannot be determined without knowing the products of $K_X C_X$ and $K_Y C_Y$.

This problem can be solved by comparing the potentials of the partial monolayers measured in one electrolyte, containing X^-, to the potentials obtained in the same electrolyte with small amounts of the second electrolyte, containing Y^-, added. In this case, the ΔG°_{hyd} for the X^- anion is more negative than the ΔG°_{hyd} for the Y^- anion. In the presence of only X^- (e.g., $C_Y = 0$)

(4.3) $$E'_{pk} = E^{\circ\prime} - \frac{RT}{nF} \ln(1 + K_X C_X)$$

where E'_{pk} is the peak potential with no Y^- present. Combining Equation 4.3 with Equation 4.2 gives

(4.4) $$E_{pk} = E'_{pk} - \frac{RT}{nF}\ln\left[1 + \frac{(K_Y C_Y)}{(1 + K_X C_X)}\right]$$

or

(4.5) $$E_{pk} = E'_{pk} - \frac{RT}{nF}\ln(1 + K_{eff} C_Y)$$

where E_{pk} is the potential with Y^- present and K_{eff} is defined by Equation 4.1. Due to the difference in hydration energies of the anions, X^- would preferentially stay in the aqueous electrolyte while Y^- would preferentially ion pair with the surface confined Fc'^+ cation. The assumption can then be made that a single ion pair, that of Fc'^+Y^-, is formed and thus, $(\Gamma_{Fc'^+})_{tot} \approx \Gamma_{Fc'^+Y^-}$, $K_Y C_Y >> (1 + K_X C_X)$, or $K_{eff} C_Y >> 1$, and Equations 4.4 and 4.5 reduce to

(4.6) $$E_{pk} = E'_{pk} - \frac{RT}{nF}\ln(K_{eff} C_Y)$$

Equation 4.6 predicts a negative shift in E_{pk} as Y^- is added to an electrolyte solution containing only X^- and provides physical meaning to the term K_{eff} due to the assumptions made.

Due to a property of logarithms, Equation 4.6 can be rewritten as

(4.7) $$E_{pk} = E'_{pk} - \frac{RT}{nF}\ln(K_{eff}) - \frac{RT}{nF}\ln(C_Y)$$

and, experimentally, K_{eff} can be determined by creating a plot of E_{pk} vs. $\log C_Y$. These plots can be made by measuring E_{pk} at increasing increments of C_Y in an electrolyte solution containing a large excess of X^-. A large excess of X^- is used to give a constant ionic strength and thus eliminate any complications that may be caused by liquid junction

potentials. Such a plot would have a slope of –59 mV (the value of RT/nF at 25 °C following the conversion of ln to log) if the Fc'^{+} cations form a discreet ion pair (i.e., one-to-one ion pair) with Y^{-}. (The ion-pairing of $Fc'^{+}Y^{-}$ could result from either a "free" Fc'^{+} cation or from a $Fc'^{+}X^{-}$ ion pair which ion exchanges with Y^{-} due to the differences in $\Delta G°_{hyd}$ for X^{-} and Y^{-}.) The y-intercept of the same plot would be equal to the $E'_{pk} - (RT/nF)\ln K_{eff}$ term in Equation 4.7, and thus provides a means of calculating K_{eff} since E'_{pk} is simply the measured potential in the X^{-} electrolyte before any Y^{-} is added.

The above experiment was performed for partial monolayers of all the Fc'-SH compounds synthesized in this study. The surface coverage for each partial monolayer was kept constant at ~3.7×10^{-11} mols/cm^2, about 25% of a complete monolayer. Actual surface coverages for each of the monolayers used are shown in Table 4.2. The K_{eff} of each partial monolayer was evaluated for the perchlorate anion in 1 M sulfuric acid (i.e., $X^{-} = HSO_4^{-}$ and $Y^{-} = ClO_4^{-}$). The value of E_{pk} was taken from the anodic peak of the cyclic voltammogram obtained at each concentration of perchlorate. Figure 4.8 shows a plot of E_{pk} vs. $\log[ClO_4^{-}]$ for each of the Fc'-SH partial monolayers. The average slope for the plot of E_{pk} vs. $\log[ClO_4^{-}]$ for all partial monolayers was –62 ± 2 mV, which is very closed to the expected value of –59 mV, indicating the formation of discreet $Fc'^{+}ClO_4^{-}$ ion pairs as discussed above. One reason for the deviation may be the use of concentrations instead of activities.

Using the values obtained for E'_{pk}, K_{eff} values for the $Fc'^{+}ClO_4^{-}$ ion pairs were calculated. The values of E'_{pk} and K_{eff} for each Fc'-SH partial manolayers are given in Table 4.3. The formation constants increase as the size of the Fc' moieties increase. A similar trend has been seen for ion pairing with ferrocenium in ferrocenehexanethiol/*n*-alkanethiol[25] and ferroceneundecanoylthiol/*n*-alkanethiol[26] mixed monolayers. Values of K_{eff} calculated in the same manner increased as the chain length of the *n*-alkanethiol co-adsorbated increased. Given those results, it is no surprise that the formation constants calculated in this study increase as the length of the four tertiary alkyl chains covalently

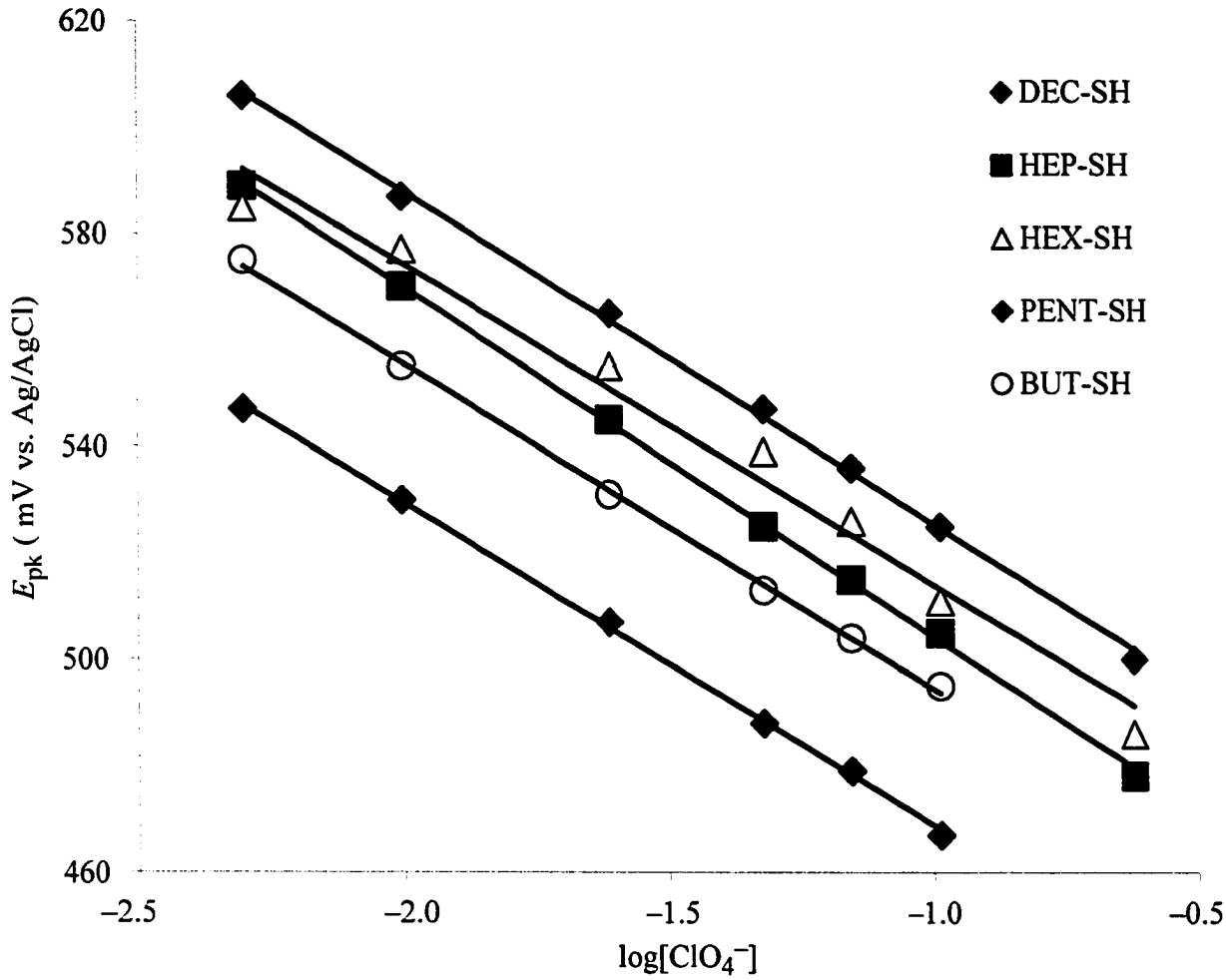

Figure 4.8. Plots of E_{pk} vs. log[ClO_4^-] for partial monolayers ($\Gamma_{Fc'}$ = 3.7 × 10^{-11} mols/cm^2) of the 11-thiolundecanoyl tetraalkylated ferrocenes on gold disk electrodes. The value of E_{pk} was measured using cyclic voltammetry in 1 M sulfuric acid electrolyte with the indicated amount of ClO_4^- achieved by addition of an appropriate volume of a 1M $HClO_4$/1 M H_2SO_4 (*aq*) solution (scan rate = 100 mV/s; platinum mesh counter electrode).

Table 4.3. Electrochemically determined effective formation constants (K_{eff}) for surface-confined $Fc'^{+}ClO_4^-$ ion pairs.

Fc'^{+}	E'_{pk} (mV vs. Ag/AgCl)[a]	$K_{eff} \times 10^{-4}$ (M^{-1})[a]
BUT	681(1)	2(1)
PENT	711(3)	13(1)
HEX	747(5)	15(1)
HEP	756(6)	17(1)
DEC	777(6)	22(2)

a. Numbers in parentheses represent one standard deviation for three separate measurements.

attached to the alkylayted cyclopentadiene (Cp') rings increase. Though the partial monolayers in this study are not part of a mixed monolayer, the effect of lengthening the alkyl chains on the Cp' rings is similar to that of increasing the chain length of an *n*-alkanethiol co-adsorbates in mixed monolayers. It has been proposed that the increase in perchlorate formation constants is caused by the increase in the organic character of the environment surrounding the ferrocenium cation center.[25] As the surface becomes more hydrophobic due to the increasing length of the alkyl chains, the ion pairing of the ferrocenyl moiety with perchlorate becomes more favorable in order to stabilize the electrogenerated cation in an organic environment. The result is the observed increase in formation constants. This trend is opposite that observed for bisulfate above, presumably due to the less negative $\Delta G°_{hyd}$ of perchlorate versus bisulfate ($\Delta G°_{hyd} = -330$).[65] It is much easier to get the less hydrated perchlorate anion to penetrate the monlayer and form ion pairs. It has been shown previously that the perchlorate anion does indeed lose its solvation sphere to form specific ion pairs in organic monolayers,[66] a property which the bisulfate anion almost certainly does not posess.

For the Fc'-SH monolayers, the formation constants are observed to increase by a factor of 13 between BUT and DEC. The trend, however, shows the magnitude of the differences in K_{eff} to become smaller as the length of the tertiary alkyl chains on the Cp' rings becomes larger. Very little thermodynamic advantage may be gained in ion pairing upon further increasing the chain length of the tertiary alkyl chains on the Cp' rings past that of DEC. This effect will be further discussed below.

Comparison of Effective Formation Constants (K_{eff}) and Ion-Exchange Selectivity of Tetraalkylated Ferrocenium Cations. The selectivity of tetraalkylated ferrocenium ion-exchange materials has been studied at length in our laboratories by Dr. Matthew A. Odom using ion-exchange materials which are prepared by confining $Fc'^{+}NO_3^-$ salts on the surface of a polymeric solid support by physisorption.[57] Subsequent contact of these ion-exchange materials with aqueous solutions containing 1

mM potassium perrhenate and 1.0 M $NaNO_3$ resulted in the selective ion exchange of the nitrate anion into the aqueous solution and the perrhenate anion onto the surface of the ion-exchange materials according to the following chemical equation. The concentration

$$Fe(Cp')_2{}^+NO_3{}^-(surf) + ReO_4{}^-(aq) \rightleftharpoons Fe(Cp')_2{}^+ReO_4{}^-(surf) + NO_3{}^-(aq)$$

of perrhenate in the solution after the extraction ($[ReO_4{}^-]_{final}$) was determined by ICP-AES. (It should be noted that the concentrations determined by ICP-AES were really Re concentrations. The assumption is made that all Re is in the form of $ReO_4{}^-$.) The results of these batch extractions were used to evaluate the selectivity of the ion-exchange materials of $BUT^+NO_3{}^-$, $PENT^+NO_3{}^-$, $HEX^+NO_3{}^-$, $HEP^+NO_3{}^-$, and $DEC^+NO_3{}^-$. Evaluations were done by calculating the distribution coefficient, K_d*, which is a figure of merit for expressing ion-exchange selectivity. In general, the larger the K_d* value the more selective the extractant is for the target anion. For the system defined by the preceding ion-exchange equilibrium, K_d* is defined by Equation 4.8,

$$K_d^*(\text{mL mmol}^{-1}) = \frac{([ReO_4^-]_{init.} - [ReO_4^-]_{final})V}{(\text{mmol } Fc'^+_{tot.})[ReO_4^-]_{final}} \quad (4.8)$$

where V is the volume of aqueous solution treated by the resin and $Fc'^+_{tot.}$ is the total amount of Fc'^+ ion-exchange sites on the materials surface.

The K_d* values determined for the five Fc'^+ cations after a twenty four hour contact time with the 1 mM $ReO_4{}^-(aq)$ solution are listed Table 4.4. It can be seen that the selectivity of the $Fc'^+NO_3{}^-$ ion-exchange materials increases as the length of the tertiary alkyl chains increase. As discussed in Chapter 1, one of the factors that influences the selectivity of the ion-exchange process for the $Fc'^+NO_3{}^-$ materials is the size of the ion-exchange site, in this case the Fc'^+ cation. The expected trend as predicted by Moyer *et. al.* from the modified Born model shown in Equation 1.2 is that of increased selectivity with

Table 4.4. K_d* values for the extraction of ReO_4^- from 1.0 M $NaNO_3$ with tetraalkylated ferrocenium nitrate ion-exchange materials.[a]

Fc'^+	K_d* (mL mmol^{-1})[a]
BUT	330
PENT	600
HEX	680
HEP	840
DEC	1000

[a] All values taken from reference 57. All extractions were performed with an initial concentration of ReO_4^- ($[ReO_4^-]_{init.}$) of 1 mM and a contact time of 24 hours. The values shown are the average of 3 separate measurements with an error of ± 5%.

increased size of the extractant.[61] (Equation 1.2 is reproduced here for ease of reference

$$1.2 \qquad \Delta\Delta G^{\circ}_{tr}(\text{kJ/mol}) = B\left\{\frac{1}{\varepsilon_S}\left[\left(\frac{1}{r'_X}-\frac{1}{r'_Y}\right)+2\left(\frac{1}{r_Y+r_R}-\frac{1}{r_X+r_R}\right)\right]+\frac{1}{\varepsilon_W}\left(\frac{1}{r'_Y}-\frac{1}{r'_X}\right)\right\}$$

where B is a temperature independent constant, ε_S and ε_W are the dielectric constants of the material surface and water respectively, r_X and r_Y are ionic radii of the anions, and r_R is the radius of the cationic extractant.) The expected trend for the selectivity of the $Fc^{+}NO_3^-$ materials versus the size of the cation is indeed observed in a plot of K_d* vs. the cross section area of the Fc^{+} cations shown in Figure 4.9. A similar trend has been noted for the extraction of $^{99}TcO_4^-$ from 1 M $NaNO_3$ with ion-exchange materials containing tetraalkyl ammonium ion-exchange sites where the size of the alkyl groups ranged from methyl to *n*-butyl.[60] The data in Table 4.4 and Figure 4.9 also show that the magnitude of the selectivity increase becomes smaller as the size of the cation becomes larger, another principle of ion-exchange predicted by Equation 1.2. It can be seen that if r_R is = ∞ in Equation 1.2, the driving force for the reaction will be primarily dependant on the size of the anions; once a cation reaches an "experimentally infinite size", no further thermodynamic gain can be achieved by further increasing the size of the Fc^{+} cation. This thermodynamic point of "diminishing returns" for selectivity and size of the cation is demonstrated by the leveling off of the curve in Figure 4.9 as the extractant size reaches that of DEC^+. Experimentally, the size of DEC^+ in this extraction system is apparently close to that of a cation of "infinite size"; very little if any increase in selectivity would be gained by increasing the size of the Fc^{+} cation beyond the size of the DEC^+ cation.

The increase in the electrochemically determined formation constants from Table 4.4 also displays the same apparent dependence on the size of the cationic centers as the extraction data. Figure 4.10 shows a plot of K_{eff} vs. cross section area of the

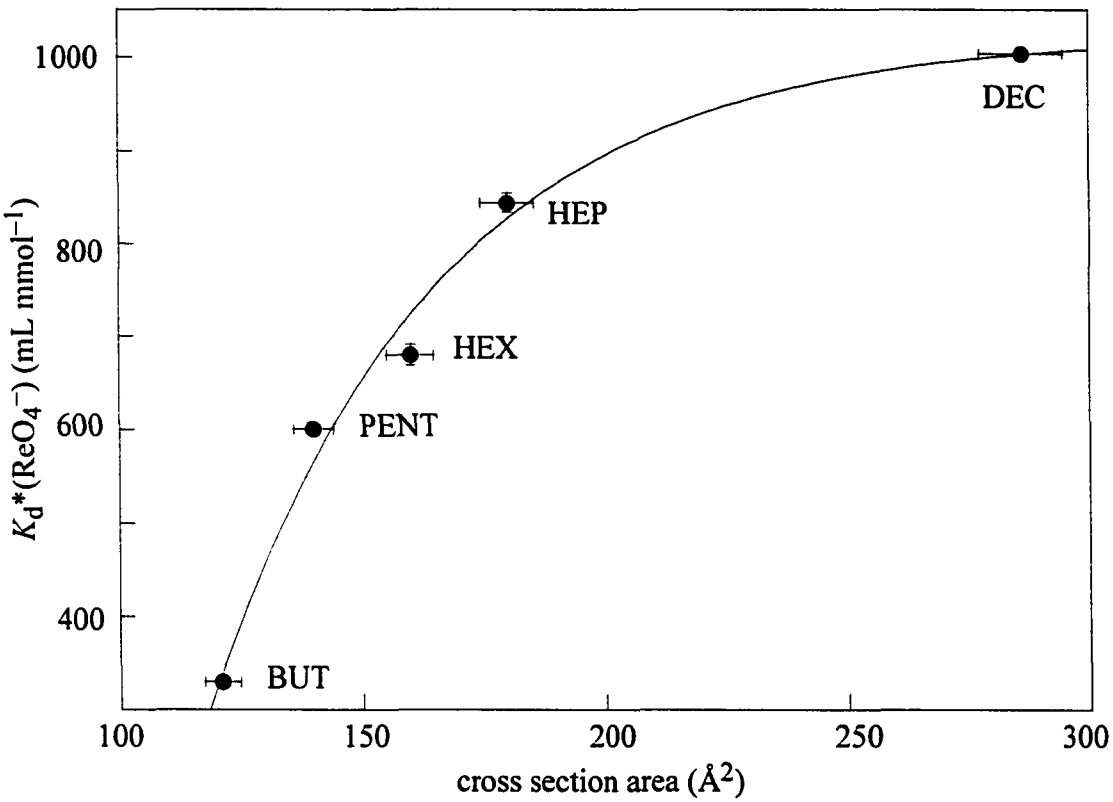

Figure 4.9. Plot of K_d*(ReO_4^-) for the extraction of ReO_4^- from 1.0 M $NaNO_3$ vs. the increasing size of the tetraalkylated ferrocenium cations. Y-error bars represent an average of three samples. Cross section areas (A) were taken from Table 4.2 and the X-error bars represent ±3σ. The curve is a least-squares fit to the empirical exponential equation $K_d^* = c_1 + (c_2 \exp[c_3 A])$ where c_1, c_2, and c_3 are constants. The R^2 value of the fit is 0.99. This figure is reproduced from reference 57.

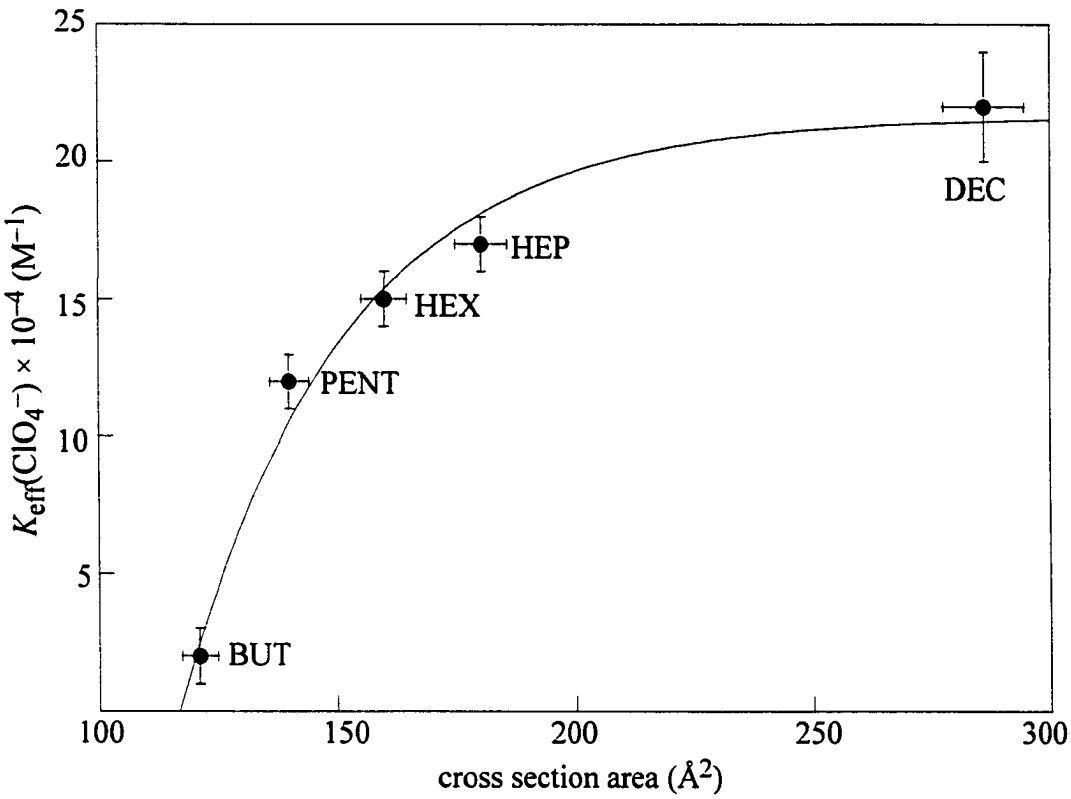

Figure 4.10. Plot of $K_{eff}(ClO_4^-)$ vs. the increasing size of the tetraalkylated ferrocenium cations. Y-error bars represent an average of three samples. Cross section areas (A) were taken from Table 4.2 and the X-error bars represent ±3σ. The curve is a least-squares fit to the empirical exponential equation $K_{eff} = c_1 + (c_2 \exp[c_3 A])$ where c_1, c_2, and c_3 are constants and the R^2 value of the fit is 0.98.

tetraalkylated ferrocenium cations. (Though the monolayers contain Fc'-SH, it is assumed, as it was for the data in Table 4.2, that the size of the cationic center in the monolayer is roughly the same as that for the unfunctionalized Fc'^{+} cations determined by X-ray crystallography.) It can be seen that K_{eff} increases exponentially as the size of the Fc' moiety increases and begins to level off at a value close to that obtained for the DEC monolayer. As discussed briefly above, the electrochemical formation constants also displayed a similar trend of thermodynamic "diminishing returns" as the partial DEC monolayer was approached. The largest increase is observed to take place between BUT and PENT, in which the addition of one extra methyl group to the tertiary alkyl chains increases the formation constant from 17,000 to 117,000 M^{-1}, a factor of almost seven. For comparison, the increase in formation constant between PENT and DEC is only a factor of 1.9 and only a factor of 1.3 between HEP and DEC. It would appear that ion pair formation between the perchlorate anion and the Fc'^{+}-SH cation begins to reach a thermodynamic point of "diminishing returns" close to DEC.

The modified Born model in Equation 1.2 also shows the selectivity of the ion-exchange material to be dependent on the dielectric of the material surface. Almost certainly, the dielectric of the surface of the ion-exchange material and partial monolayer, as discussed in the previous section, changes with adsorption of the larger tetraalkylated ferrocenes. The change in dielectric, according to Equation 1.2, should increase selectivity as the surface dielectric decreases (i.e., becomes more alkane like). More in depth selectivity studies performed on the ion-exchange materials strongly suggest that the selectivity is in fact due to the increasing cation size and not a change in dielectric, however, dielectric effects cannot be ruled out entirely.[57,59,60] Dielectric effects of the monolayers on the magnitude of K_{eff} similarly cannot be ruled out. The issue of dielectric is further clouded for the electroactive monolayers since the monolayer is uncharged until oxidized. Whether due to changes in dielectric or cation size, however, the effect of increasing the size of the tertiary alkyl chains on the Fc' moieties leads to

better selectivity and more favorable ion pairing.

Direct comparison of electrochemical formation constants and ion-exchange selectivity was also performed. Such a comparison is relevant even though ion-exchange and ion pairing were done with different anions due to experimental considerations (*vide supra*). Comparison of perrhenate and perchlorate shows that they have similar sizes (0.260 and 0.240 nm respectively) and therefore similar hydration energies (–240 and–259 kJ mol^{-1} respectively). Given the similarity of the two anions, it would be expected that the ion-exchange data obtained for the two anions be similar and that the electrochemical data for the two anions be similar. Differences in the extraction medium and the electrolyte solution also should not be an issue. Both were done in the presence of a large excess of a competing anion. Though not the same anion, both anions (NO_3^- and HSO_4^-) had more negative hydration energies than that of the target anions (ReO_4^- or ClO_4^-). Due to the similar nature of the driving forces for ion pairing and extraction, it is reasonable to expect that the same trends be exhibited by both systems. The direct comparison of electrochemical ion pairing and ion exchange is shown in a plot of K_{eff} vs. K_d* in Figure 4.11. The plot is linear, indicating that the two properties of ion exchange and ion pairing for the Fc'^+ cations are governed by the same trends. Though the magnitudes of the two sets of values are different (i.e., a line with a slope $\neq 1$), the trends are obviously the same. It is not clear, however, if the trends are only a result of the size of the cationic center or a combination of both cation size and surface dielectric. The above data strongly suggests, however, that the size of the cationic center does in fact play a role in electrochemical ion-pairing.

Finally, Born models have been previously adopted to explain the differences in potentials (and therefore formation constants) observed for ferrocenyl monolayers under various conditions, although in somewhat different manners than that presented here.[27,28,67] The Born model adopted in this study for ion-exchange is very similar to that discussed by Creager *et. al.* for describing the potential shifts observed in mixed

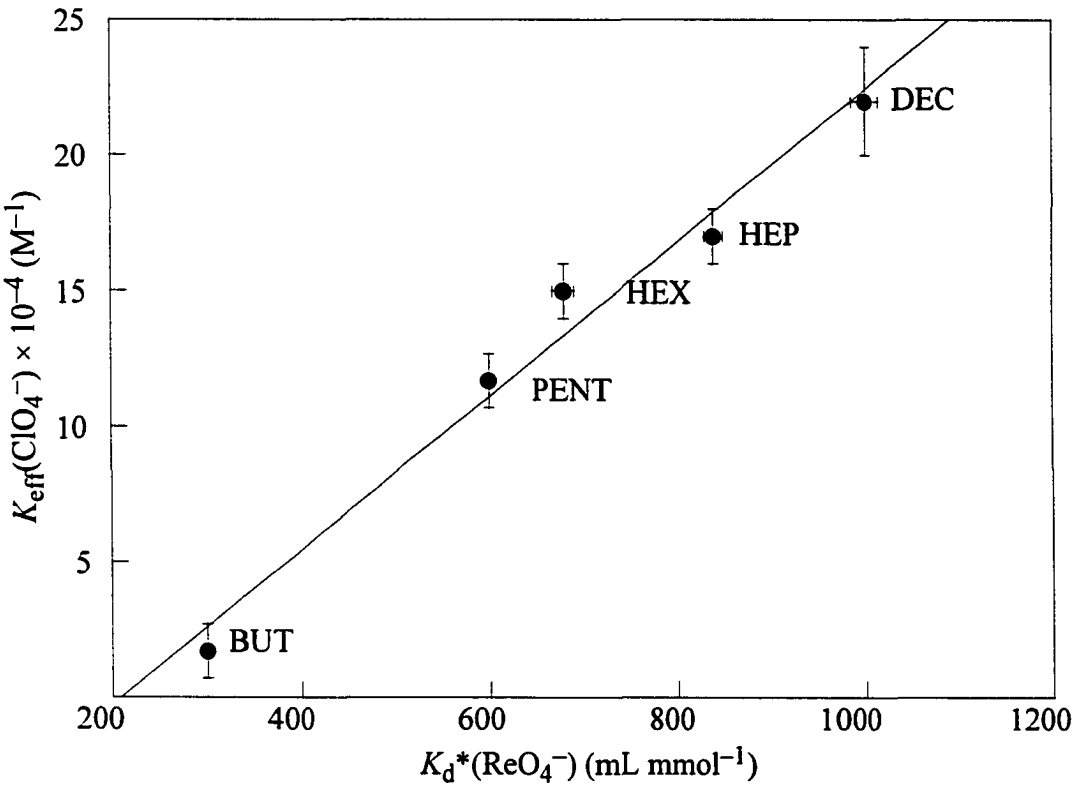

Figure 4.11. Plot of $K_{eff}(ClO_4^-)$ vs. $K_d^*(ReO_4^-)$ for tetraalkylated ferrocenium cations. Both X and Y error bars represent an average of three samples. The line represents a linear regression of the data ($R^2 = 0.98$) with a slope of 284 mmol mL^{-1} M^{-1}.

ferrocenylalkanethiol/*n*-alkanethiol monolayers.[27] It is recognized that a double layer model[48] also exists to explain potential shifts and that a combination of a Born model with this double layer model may provide the best explanation for the physical data.[27,28] Only a modified Born model is considered here, however, since it best explains the similarities between the extraction data and electrochemical data presented above. The goal of this study in comparing the electrochemical data to this particular Born model is not to propose a new model to explain differences in observed potentials, but rather to compare the electrochemical results to those obtained in the batch ion-exchange studies. The usefulness of this correlation is found in the electrochemical evaluation of redox active ion-exchange materials, as those in the R^2ER cycle are. This is a novel approach to the evaluation of ion-exchange materials. Tetraalkylammonium salts, the most common ion-exchange material used for selectivity studies, are not redox active and thus cannot be evaluated in this manner. Other electroactive ion-exchange materials have been developed,[3] however these molecules are tailored to anion recognition and therefore are not governed by the same principles as those considered here for ion-exchange. As explained in Chapter 1, the selectivity in this model represents a "bias" for one anion over another, not recognition of one specific anion.

Amperometric Sensing of Aqueous Anions. As expected, the results of the electrochemical selectivity studies on Fc'-SH monolayers have implications on their use in anionic sensing applications. As seen for both HEP/ITO materials and the partial monolayers on gold, the basis for sensing anions in aqueous media is the potential shift observed for various anions. The magnitude of this shift is based upon the concentration of the anion in the aqueous media, the particular anion in the aqueous media, and the surface environment of the redox-active, surface-confined sensing species, in this case the tetraalkylated ferrocene moieties. Table 4.5 shows the potential shift data used for the determination of K_{eff} values at a ClO_4^- concentration of 5 mM. As can be seen, the magnitude of the potential shift increases as the alkyl chain length of the Fc' moiety

Table 4.5. Potential shifts observed for partial tetraalkylated ferrocenyl monolayers in 1 M H_2SO_4 containing 5 mM $HClO_4$.[a]

	$E^{\circ\prime}$ (mV)		
Fc'	**no ClO_4^-**	**0.005 M ClO_4^-**	**$\Delta E^{\circ\prime}$ (mV)[b]**
BUT	657(1)	551(1)	–106(1)
PENT	687(3)	535(6)	–152(4)
HEX	728(5)	584(5)	–163(1)
HEP	737(6)	574(5)	–163(3)
DEC	758(6)	595(8)	–163(3)

[a] All potentials were referenced to a Ag/AgCl electrode using a platinum mesh counter electrode at a scan rate of 100 mV/s. [b] $\Delta E^{\circ\prime} = \Delta E^{\circ\prime}(ClO_4^-) - \Delta E^{\circ\prime}(HSO_4^-)$

grows longer. Under the specified conditions, this potential shift reaches a maximum at –163 mV, as was observed for partial monolayers of HEX, HEP, and DEC. Since the largest difference in potentials will translate into a more sensitive electrochemical detector, perchlorate sensing applications performed with these monolayers would be most sensitive if we use a monolayer of HEX, HEP, or DEC.

The magnitude of this potential shift has direct implications on sensing applications that are done amperometrically. Amperometric sensing has been performed with thiol monolayers on gold for perchlorate.[24] The usefulness of a large potential shift is further demonstrated by comparing amperometric sensing experiments of ClO_4^- with those of $CB_{11}H_{12}^-$. As was demonstrated for both HEP/ITO and Fc'-SH monolayers on gold, the very weakly hydrated $CB_{11}H_{12}^-$ anion causes much larger potential shifts than ClO_4^- when added to an electrolyte containing a well hydrated anion such as NO_3^-, Cl^-, or HSO_4^-. Given a large enough potential difference for the oxidation of the monolayer in the presence of two different anions, it should be possible to selectively ion pair the Fc'^+ moieties with a target anion by holding the potential at a given value. The larger the potential shift, the more selective this process will be.

Potentiometric controlled ion pairing was demonstrated for a partial monolayer of HEP-SH on gold for both ClO_4^- and $CB_{11}H_{12}^-$. The partial monolayer of HEP, analyzed by cyclic voltammetry, had an $E^{\circ\prime}$ of 720 mV in 1 M $HNO_3(aq)$. The $\Delta E^{\circ\prime}$ value in the same electrolyte when concentrated to 1 mM ClO_4^- was –89 mV. The $\Delta E^{\circ\prime}$ value when concentrated to 1 mM $CB_{11}H_{12}^-$ was > 400 mV. Due to the large potential difference when the $CB_{11}H_{12}^-$ anion was present, the HEP monolayer oxidized at 320 mV with little or no ion pairing with nitrate, even in the presence of 1000 times excess nitrate. No oxidation is observed at these potentials without the presence of $CB_{11}H_{12}^-$ in the electrolyte. The same may also be said for ClO_4^- at 631 mV, but due to its smaller potential shift, quite a bit of oxidation of the monolayer is also observed at 631 mV in the presence of only nitrate.

Using these potential values, two chronoamperometric sensing experiments were performed with 1 mM ClO_4^- and 1 mM $CB_{11}H_{12}^-$ in 1 M $HNO_3(aq)$. In these experiments, the potential was held constant at 631 mV for the ClO_4^- experiment and 320 mV for the $CB_{11}H_{12}^-$ experiment in the 1 M $HNO_3(aq)$ electrolyte solution for 30 seconds, at which time the electrolyte was concentrated to 0.001 M with ClO_4^- or $CB_{11}H_{12}^-$. The resulting current vs. time curves are shown in Figure 4.12. It can be seen for the perchlorate experiment that current is initially passed due to the oxidation of the monolayer in the presence of the nitrate anion. At 30 seconds, more current is passed due to the further oxidation of the monolayer now in the presence of ClO_4^-. For the $CB_{11}H_{12}^-$ sensing experiment, no initial current is passed in the nitrate electrolyte. At 30 seconds, current is passed upon the addition of $CB_{11}H_{12}^-$. Furthermore, it can be seen that much more current is passed for the detection of $CB_{11}H_{12}^-$ than for the detection ClO_4^-.

The above data can be explained by the magnitude of $\Delta E^{\circ\prime}$. At a potential of 631 mV, the monolayer is partially oxidized in the presence of the nitrate anion. As predicted by the Nernst equation, however, the entire monolayer is not oxidized since the potential was held negative of 720 mV, the observed oxidation potential of the monolayer in the presence of only 1 M NO_3^- anion. At 30 seconds, when the ClO_4^- is added to the electrolyte, only a small amount of current is passed due to the already partially oxidized monolayer. (It should be noted that anions that give larger potential shifts than ClO_4^- would also cause the oxidation of the monolayer at this potential. If larger potential shifts exist, however, a constant potential < 631 mV would be used for detection, and less initial oxidation of the monolayer in the presence of nitrate would observed.) The chronoamperometric sensing of the $CB_{11}H_{12}^-$ anion, which has a potential shift > 400 mV, does not show an initial oxidation of the monolayer at 320 mV. Though the Nernst equation predicts some oxidation of the monolayer in the presence of nitrate, the amount is so small that no current is observed upon the initial step to 320 mV. Since no initial

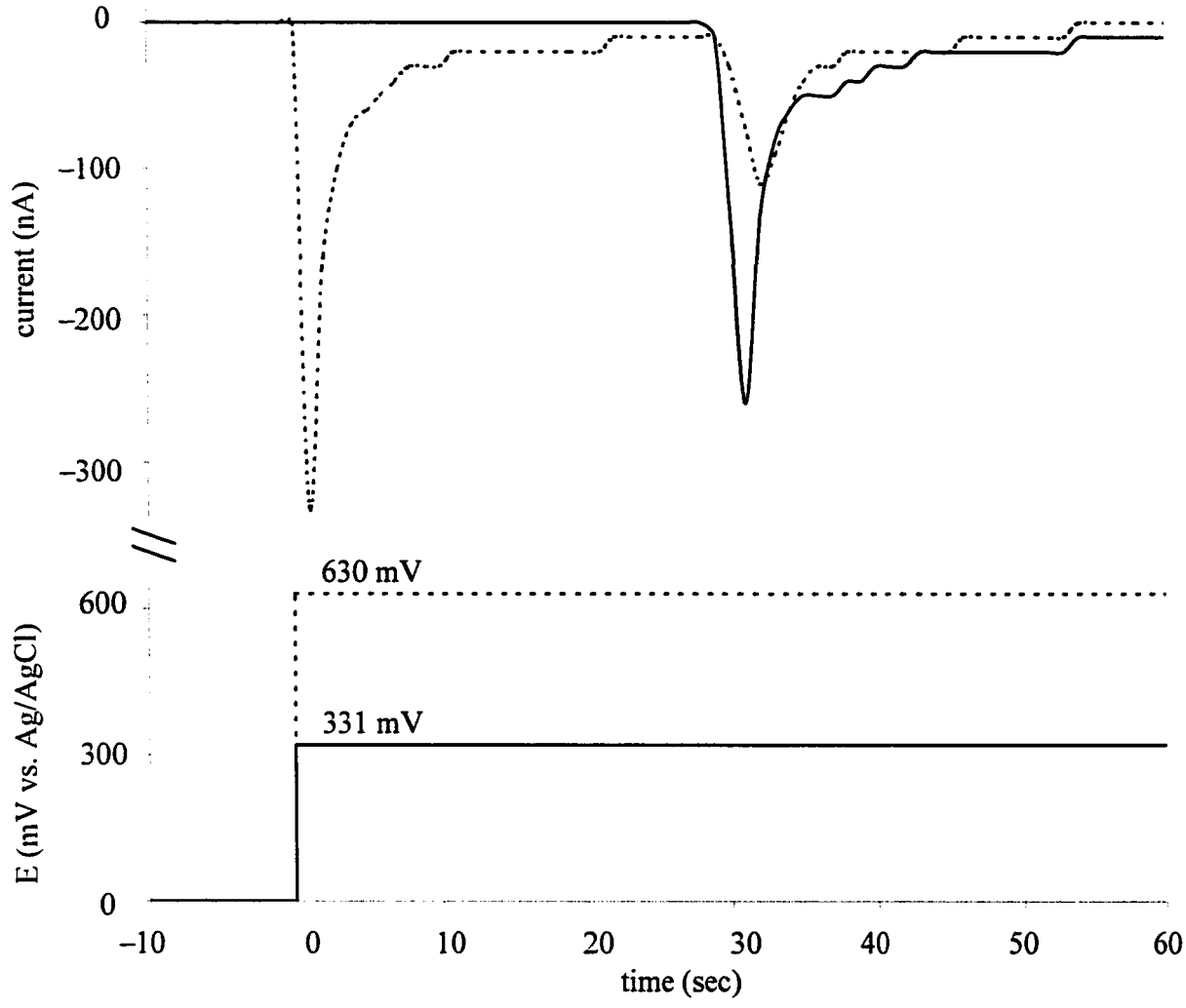

Figure 4.12. Plots of current vs. time for the chronamperometric sensing of 5 mM ClO_4^- (dashed line) and 5 mM $CB_{11}H_{12}^-$ (solid line) in 1 M HNO_3 (*aq*) using a partial monolayer of HEP-SH. The ClO_4^- and $CB_{11}H_{12}^-$ anions were added to the electrolyte solution at ~30 seconds. The potential vs. time profile (bottom) is shown for both experiments.

oxidation of the monolayer occurred, the entire monolayer is left for oxidation when $CB_{11}H_{12}^-$ is added, and thus more current is passed due to the complete oxidation of the monolayer in the presence of $CB_{11}H_{12}^-$. The larger amount of current passed makes the sensing experiment much more sensitive for $CB_{11}H_{12}^-$. For smaller magnitudes of $\Delta E^{\circ\prime}$, more oxidation of the monolayer will occur upon the initial potential step, and the less sensitive the electrochemical sensor will be. By this reasoning, if ways could be found to increase the $\Delta E^{\circ\prime}$ for ClO_4^-, the sensitivity for the detection of ClO_4^- by this method could be increased.

Conclusions

Two methods of confining tetraalkylated ferrocenes to electrically conducting surfaces have been demonstrated. Thin films of the highly lipophilic ion-exchange compound HEP have been deposited on ITO by spin coating techniques. In addition to surface coating techniques, the entire series of Fc' ion-exchange compounds has been functionalized with 11-thiolundecanoyl moieties for formation of monolayers on gold electrode surfaces. Both the thin films and monolayers exhibited robust electrochemical ion-exchange properties, including large potential shifts in presence of various anions. These potential shifts provided a novel method of electrochemically evaluating the selectivity of electroactive ion-exchange materials. A direct correlation between the selectivity of ion-exchange materials and electrochemical ion pairing was demonstrated. Furthermore, it was found that the same properties that make tetraalkylated ferrocenes highly selective ion-exchange materials also make them useful for amperometric sensing applications for aqueous anions. The amperometric sensing of ClO_4^- and $CB_{11}H_{12}^-$ anions has been explored. Overall, these studies demonstrate the potential usefulness of tetraalkylated ferrocenes for use as electrochemical sensors.

References

1. Boulas, P. L.; Gomez-Kaifer, M.; Echegoyen, L. *Angew. Chem. Int. Ed. Eng.* **1998**, *37*, 216.
2. Beer, P. D.; Gale, P. A.; Chen, G. Z. *J. Chem. Soc., Dalton Trans.* **1999**, 1897.
3. Beer, P. D.; Gale, P. A. *Angew. Chem. Int. Ed. Eng.* **2001**, *40*, 486.
4. Beer, P. D.; Drew, M. G. B.; Hesek, D.; Nam, K. C. *Chem. Commun.* **1997**, 107.
5. Beer, P. D.; Hesek, D.; Nam, K. C. *Organometallics* **1999**, *18*, 3933.
6. Beer, P. D.; Drew, M. G. B.; Smith, D. K. *J. Organomet. Chem.* **1997**, *543*, 259.
7. Valerio, C.; Fillaut, J. L.; Ruiz, J.; Guittard, J.; Blais, J. C.; Astruc, D. *J. Am. Chem. Soc.* **1997**, *119*, 2588.
8. Valerio, C.; Alonso, E.; Ruiz, J.; Blais, J. C.; Astruc, D. *Angew. Chem. Int. Ed. Eng.* **1999**, *38*, 1747.
9. Deinhammer, R. S.; Ting, E. Y.; Porter, M. D. *Anal. Chem.* **1995**, *67*, 237.
10. Murray, R. W.; Ewing, A. G.; Durst, R. A. *Anal. Chem.* **1987**, *59*, 379A.
11. Chao, S.; Robbins, J. L.; Wrighton, M. S. *J. Am. Chem. Soc.* **1983**, *105*, 181.
12. Lau, A. N. K.; Miller, L. L. *J. Am. Chem. Soc.* **1983**, *105*, 5271.
13. Guadalupe, A. R.; Abruna, H. D. *Anal. Chem.* **1985**, *57*, 142.
14. Inagaki, T.; Lee, H. S.; Skotheim, T. A.; Okamoto, Y. *J. Chem. Soc., Chem. Commun.* **1989**, 1181.
15. Back, R.; Lennox, R. B. *Langmuir* **1992**, *8*, 959.
16. Sykora, M.; Maxwell, K. A.; Meyer, T. J. *Inorg. Chem.* **1999**, *38*, 3596.
17. Lenhard, J. R.; Rocklin, R.; Abruna, H. D.; William, K.; Kuo, K.; Nowak, R.; Murray, R. W. *J. Am. Chem. Soc.* **1978**, *100*, 7870.
18. Tse, D. C. S.; Kuwana, T. *Anal. Chem.* **1978**, *50*, 1315.
19. Chen, K.; Herr, B. R.; Singewald, E. T.; Mirkin, C. A. *Langmuir* **1992**, *8*, 2585.
20. Herr, B. R.; Mirkin, C. A. *J. Am. Chem. Soc.* **1994**, *116*, 1157.

21. Zawisza, I.; Bilewicz, R.; Luboch, E.; Biernat, J. F. *J. Electroanal. Chem.* **1999**, *471*, 156.
22. Shaowei, C. *Langmuir* **2001**, *17*, 6664.
23. Nuzzo, R. G.; Allara, D. L. *J. Am. Chem. Soc.* **1983**, *105*, 4481.
24. Hickman, J. J.; Ofer, D.; Laibinis, P. E.; Whitesides, G. M.; Wrighton, M. S. *Science* **1991**, *252*, 688.
25. Rowe, G. K.; Creager, S. E. *Langmuir* **1991**, *7*, 2307.
26. Ju, H.; Leech, D. *Phys. Chem. Chem. Phys.* **1999**, *1*, 1549.
27. Rowe, G. K.; Creager, S. E. *J. Phys. Chem.* **1994**, *98*, 5500.
28. Creager, S. E.; Rowe, G. K. *J. Electroanal. Chem.* **1997**, *420*, 291.
29. Lindner, E.; Buck, R. P. *Anal. Chem.* **2000**, *72*, 336A.
30. Buck, R. P.; Lindner, E. *Anal. Chem.* **2001**, *73*, 88A.
31. Porter, M. D.; Bright, T. B.; Allara, D. L.; Chidsey, C. E. D. *J. Am. Chem. Soc.* **1987**, *109*, 3559.
32. Chailapakul, O.; Sun, L.; Xu, C.; Crooks, R. M. *J. Am. Chem. Soc.* **1993**, *115*, 12459.
33. Abbott, N. L.; Whitesides, G. M. *Langmuir* **1994**, *10*, 1493.
34. Ghatak-Roy, A. R.; Martin, C. R. *Anal. Chem.* **1986**, *58*, 1574.
35. Rubinstein, I.; Steinberg, S.; Tor, Y.; Shanzer, A.; Sagiv, J. *Nature* **1988**, *332*, 426.
36. Kepley, L. J.; Crooks, R. M. *Anal. Chem.* **1992**, *64*, 3191.
37. Rubin, S.; Chow, J. T.; Ferraris, J. P.; Zawodzinski, T. A. *Langmuir* **1996**, *12*, 363.
38. Chidsey, C. E. D.; Bertozzi, C. R.; Putvinski, T. M.; Mujsce, A. M. *J. Am. Chem. Soc.* **1990**, *112*, 4301.
39. Ulman, A. *An Introduction toUltrathin Organic Films: From Langmuir-Blodgett to Self-Assembly*; Academic Press, Inc.: San Diego, 1991.
40. Ulman, A. *Chem. Rev.* **1996**, *96*, 1533.
41. Collard, D. M.; Fox, M. A. *Langmuir* **1991**, *7*, 1192.
42. Hockett, L. A.; Creager, S. E. *Langmuir* **1995**, *11*, 2318.

43. Weber, K. S. *J. Electroanal. Chem.* **1998**, *458*, 17.

44. Clapsaddle, B. J.; Clark, J. F.; Clark, D. L.; Gansle, K. M.; Gash, A. E.; Miller, S. M.; Anderson, O. P.; Hughes, R. P.; Strauss, S. H., 2002 *Synthesis and Characterization of Polyalkylated Ferrocenes and Ferrocenium Salts.*

45. Acevedo, D.; Abruna, H. D. *J. Phys. Chem.* **1991**, *95*, 9590.

46. DeLong, H. C.; Buttry, D. A. *Langmuir* **1992**, *8*, 2491.

47. Finklea, H. O.; Hanshew, D. D. *J. Electroanal. Chem.* **1993**, *347*, 327.

48. Smith, C. P.; White, H. S. *Anal. Chem.* **1992**, *64*, 2398.

49. Knoth, W. H. *J. Am. Chem. Soc.* **1967**, *89*, 1274.

50. Plesek, J.; Jelinek, T.; Drdakova, T. E.; Hermanek, S.; Stibr, B. *Collect. Czech. Chem. Commun.* **1984**, *49*, 1559.

51. Leigh, T. J. *J. Chem. Soc.* **1964**, 3294.

52. Clark, J. F.; Clark, D. L.; Whitener, G. D.; Schroeder, N. C.; Strauss, S. H. *Environ. Sci. Technol.* **1996**, *30*, 3124.

53. Clark, J. F. Design, Synthesis, and Evaluation of Redox-Recyclable Organometallic Extractants for the Recovery of Ionic Radionuclides From Aqueous Waste Streams. Ph.D. Dissertation, Colorado State University, Fort Collins, CO, 1999.

54. Oesch, U.; Janata, J. *Electrochim. Acta.* **1983**, *28*, 1237.

55. Weisshaar, D. E.; Lamp, B. D.; Porter, M. D. *J. Am. Chem. Soc.* **1992**, *114*, 5860.

56. Chambliss, C. K.; Odom, M. A.; Morales, C. M. L.; Martin, C. R.; Strauss, S. H. *Anal. Chem.* **1998**, *70*, 757.

57. Odom, M. A. Development of Strategies for the Detection, Extraction, and Recovery of Aqueous Anions Using Highly Selective Redox-Recyclable Materials. Ph.D. Dissertation, Colorado State University, Fort Collins, CO, 2001.

58. Gansle, K. M. Investigation and Development of Liquid-Liquid Extraction Systems for the Removal of Pertechnetate from Aqueous Nuclear Waste-Stream Simulants. Ph.D. Dissertation, Colorado State University, Fort Collins, CO, 1998.

59. Chambliss, C. K. Redox-Recyclable Extraction and Recovery. A New Strategy for the Separation and Recovery of Aqueous Ions. Ph.D. Dissertation, Colorado State University, Fort Collins, CO, 1998.

60. Chambliss, C. K.; Odom, M. A.; Martin, C. A.; Moyer, B. A.; Strauss, S. H. *Inorg. Chem. Commun.* **1998**, *1*, 435.

61. Moyer, B. A.; Bonnesen, P. V. In *Supramolecular Chemistry of Anions*; Bianchi, A., Bowman-James, K., Garcia-Espana, E., Eds.; VCH: New York, 1997.

62. Creager, S. E.; Rowe, G. K. *Anal. Chim. Acta.* **1991**, *246*, 233.

63. Hickmann, J. J.; Ofer, D.; Zou, C.; Wrighton, M. S.; Laibinis, P. E.; Whitesides, G. M. *J. Am. Chem. Soc.* **1991**, *113*, 1128.

64. Bard, A. J.; Faulkner, L. R. *Electrochemical Methods: Fundamentals and Applications*; John Wiley & Sons: New York, 1980.

65. Marcus, Y. In *Liquid-Liquid Interfaces: Theory and Methods*; Volkov, A. G., Deamer, D. W., Eds.; CRC Press, Inc.: New York, 1996, p 39.

66. Buttry, D. A. *Langmuir* **1990**, *6*, 1319.

67. Krishtalik, L. I.; Alpatova, N. M.; Ovsyannikova, E. V. *Electrochim. Acta.* **1991**, *36*, 435.

Chapter 5

Comparison of $HEP^+NO_3^-$ and $DEC^+NO_3^-$ for the Liquid-Liquid Anion Exchange of Aqueous ReO_4^-

Introduction

The R^2ER strategy for the liquid-liquid extraction of aqueous anions has been thoroughly studied using the cationic extractant $HEP^+NO_3^-$.[1-3] The extraction of > 99% of the radioactive $^{99}TcO_4^-$ anion from high ionic-strength acidic and basic media has been demonstrated for $HEP^+NO_3^-$ in a variety of common, environmentally benign, organic solvents.[1] Furthermore, extraction of ReO_4^- (a non-radioactive surrogate for $^{99}TcO_4^-$) and $^{99}TcO_4^-$ by ion-exchange materials prepared by physisorption of $HEP^+NO_3^-$ onto a variety of metal oxide and polymeric solid supports has also been demonstrated.[4-6]

The selectivity of $HEP^+NO_3^-$ towards weakly hydrated aqueous anions has also been demonstrated.[5,6] As described in detail in Chapter 1, the selectivity of $HEP^+NO_3^-$ is based on a bias for the most weakly hydrated anion in an aqueous phase.[7] The selectivity is also controlled by the dielectric of the extraction media as well as the size of the tetraalkylated ferrocenium cationic extractant, with larger extractants being more selective. The dependence of selectivity on extractant size has been demonstrated for $HEP^+NO_3^-$ by comparison to quaternary ammonium extractant resins with varying size ion-exchange sites.[5]

A previous study performed by Chambliss *et. al.* for the extraction of $^{99}TcO_4^-$ compared the liquid-liquid ion-exchange properties of $HEP^+NO_3^-$ with those of tetra-*n*-heptyl ammonium nitrate ($(heptyl)_4N^+NO_3^-$), a commonly used ion-exchange compound.[3] This study showed both extractants to behave primarily as monomeric

species under extraction conditions where the organic phase extractant concentrations were $\leq$ 10 mM. Both extractants were shown to aggregate, however, at higher concentrations, resulting in a drastic reduction of the observed distribution constants for the extraction of $^{99}TcO_4^-$. Aggregation of these extractant species was also shown to be dependent on the amount of $^{99}TcO_4^-$ loading in the organic phase, resulting in aggregation of the extractant species at $^{99}TcO_4^-$ loadings of > 3 mM. Further modeling of this extraction data with the modeling program SXLSQI[8] showed that the selectivity of $HEP^+NO_3^-$ and $(heptyl)_4N^+NO_3^-$ was nearly the same for both extractants. Electrostatic principles also predicted that the selectivity of these large cations reached a point of "diminishing returns" where further selectivity could not be gained by increasing the size of a cationic extractant past that of $HEP^+NO_3^-$ or $(heptyl)_4N^+NO_3^-$ in the same solvent.

Recently, the larger, more lipophilic extractant $DEC^+NO_3^-$ has been synthesized (see Chapter 1).[9] The use of this extractant for the infrared detection of aqueous anions has since been reported.[10] The ion-exchange properties of $DEC^+NO_3^-$ have also been studied by Odom by physisorbing $DEC^+NO_3^-$ onto the surface of the polymeric support XAD-7 and contacting the resulting material with high ionic-strength aqueous media containing ReO_4^-.[6] It was found that under these conditions, $DEC^+NO_3^-$ was more selective for the extraction of ReO_4^- than $HEP^+NO_3^-$. Equilibrium K_d* values for determination of the selectivity of both $HEP^+NO_3^-$and $DEC^+NO_3^-$ ion-exchange materials were 840 and 1000, respectively. Electrochemical studies have also indicated $DEC^+NO_3^-$ to be a more selective extractant than $HEP^+NO_3^-$ (see Chapter 4).

To date, however, no selectivity studies have been performed by liquid-liquid extraction of aqueous anions using $DEC^+NO_3^-$. In this study, therefore, the liquid-liquid ion-exchange properties of $DEC^+NO_3^-$ were determined in dichloromethane and chlorobenzene and compared to the results obtained for $HEP^+NO_3^-$ and previously for $(heptyl)_4N^+NO_3^-$. The extraction of ReO_4^- was performed from a 1 M $NaNO_3(aq)$ in all cases and the concentrations of both ReO_4^- and the organic phase extractant were chosen

as appropriate for the examination of selectivity. Based on the electrostatic and solvation arguments discussed above and in Chapter 1, it would be predicted that the extractant $DEC^+NO_3^-$ should yield a similar, if not slightly better, selectivity than $HEP^+NO_3^-$ and $(heptyl)_4N^+NO_3^-$. Surprisingly, it was found that $DEC^+NO_3^-$ was not as selective for ReO_4^- as $HEP^+NO_3^-$ in dichloromethane and chlorobenzene, despite the results of the selectivity studies done for $DEC^+NO_3^-$ on XAD-7.

According to the results obtained by Chambliss,[3] the selectivity of the larger DEC^+ extractant should be comparable, not lower. One possible reason for the lower selectivity observed for $DEC^+NO_3^-$ may be aggregation of the extractant in the organic phase. In order to determine if aggregation could be the cause for the anomalous selectivity data for $DEC^+NO_3^-$, the aggregation properties of both $DEC^+NO_3^-$ and $HEP^+NO_3^-$ have been investigated by a slope analysis method developed by van Dalen *et. al.* and also used by Chambliss for the study of aggregation of $HEP^+NO_3^-$and $(heptyl)_4N^+NO_3^-$ in chlorobenzene. Attempts to further characterize the aggregation effects observed for $HEP^+NO_3^-$and $(heptyl)_4N^+NO_3^-$, however, were not performed.[3,11] For this reason, the use of dynamic light scattering techniques to determine aggregate size in chlorobenzene solutions of both $DEC^+NO_3^-$ and $HEP^+NO_3^-$ has also been performed. The results of all extraction data, as well as the aggregation properties of both $DEC^+NO_3^-$ and $HEP^+NO_3^-$, determined by slope analysis and dynamic light scattering, will be discussed in order to explain the unusually low selectivity observed for $DEC^+NO_3^-$ in the liquid-liquid extraction of ReO_4^- from aqueous media.

Experimental Section

General Procedures. All synthesized compounds appear to be stable to air and moisture. An orbital shaker bath model 3545 from Lab-Line Instruments, Inc. was used for all liquid-liquid extractions. Inductively-coupled plasma atomic emission spectroscopy (ICP-AES) was performed on a P400 spectrometer from Perkin-Elmer equipped with a high-salt nebulizer.

Reagents and Solvents. All reagents were Reagent Grade or better unless otherwise indicated. All reagents and solvents were used as received unless purified as noted. Dichloromethane (Fisher Scientific); anhydrous chlorobenzene (Aldrich); water was distilled and deionized (Barnstead NANOpure) and had a resistivity of 18 MΩ cm; sodium nitrate (Fisher Scientific); $KReO_4$ (Aldrich).

Preparation of Tetraalkylated and Functionalized Tetraalkylated Ferrocenes and Ferrocenium Salts. The preparation of all tetraalkylated ferrocenes and ferrocenium nitrate salts used in this study has been described previously as well as in detail in Chapter 2.[1,9,12] The abbreviations used for all compounds are defined in Table 1.1 in Chapter 1.

Liquid-Liquid Extraction Experiments. All liquid-liquid extractions were performed as described below. Organic phase solvents were either dichloromethane or chlorobenzene. All extractions were done for perrhenate (ReO_4^-) from a 1 M $NaNO_3$ aqueous solution. Each extraction was performed three times for determination of experimental error.

In a 125 mL Erhlenmeyer flask, 25 mL of a 1 M $NaNO_3$ aqueous solution containing the desired concentration of ReO_4^- was pipetted onto 25 mL of an organic solution containing the desired concentration of $HEP^+NO_3^-$ or $DEC^+NO_3^-$. This bi-phasic mixture was then shaken at 300 rpm in an orbital shaker bath for 1 hour at 25 °C. Following shaking, the two phases were separated in 125 mL separation funnels and saved for further analysis. The aqueous phase was then centrifuged for 2 minutes at 1000 rpm to ensure complete separation of any remaining organic solvent. The aqueous samples were analyzed by ICP-AES for ReO_4^- concentration determination and the organic samples analyzed by dynamic light scattering analysis for aggregation.

Several concentrations of extractant were used in the present investigation. The organic phase consisted of concentrations of 1 mM, 10 mM, and 100 mM $HEP^+NO_3^-$ or $DEC^+NO_3^-$. Aqueous solutions consisted of varying concentrations of ReO_4^- between

0.1 mM and 30 mM to achieve the desired loadings of ReO_4^- in the organic phase upon ion exchange. Perrhenate loading experiments were done by extraction as described above. Loading of ReO_4^- into the organic phase was performed up to 30% based on the initial concentration of extractant in the organic phase.

Determination of Perrhenate Distribution Ratios. The concentration of ReO_4^- in the aqueous phase was determined by measuring the total Re concentration before and after the extractions using ICP-AES. The emission intensity was monitored at the rhenium line of 221.426 nm. Calibration curves, which were linear over the concentration range of 1.00 – 0.010 mM, were constructed using known concentrations of $KReO_4$ in 1 M $NaNO_3(aq)$ (i.e., matrix matching was done for all experiments). For each sample, five readings of the ICP-AES intensity were recorded and averaged. Triton-X-100 (Mallinckrodt), a non-ionic surfactant, was added (1% total) to all solutions before analysis. The addition of a non-ionic surfactant increases the wettability of the sample introduction system and has been shown to increase reproducibility without affecting the analytical results.[2]

The extent of ReO_4^- extraction from the aqueous phase to the organic phase was evaluated by the calculation of the distribution ratio, $D(ReO_4^-)$. The distribution ratio is based on the following equilibria:

(5.1) $$Fc'^+NO_3^-(org) + K^+ReO_4^-(aq) \rightleftharpoons Fc'^+ReO_4^-(org) + K^+NO_3^-(aq)$$

where Fc'^+ is the HEP or DEC cationic extractant. The distribution ratio is defined as

(5.2) $$D(ReO_4^-) = \frac{[ReO_4^-]_{org,final}}{[ReO_4^-]_{aq,final}}$$

when both the organic and aqueous phases are equal in volume. Since quantification of

ReO_4^- (total Re concentration) by ICP-AES is only determined for the final aqueous aliquot, the distribution ratio is alternatively defined as

$$D(ReO_4^-) = \frac{[ReO_4^-]_{aq,initial} - [ReO_4^-]_{aq,final}}{[ReO_4^-]_{aq,final}} \quad (5.3)$$

In all experiments, three separate determinations of $D(ReO_4^-)$ were made and the average reported. The error associated with each measurement was estimated by calculating the standard deviation.

Aggregation Analysis Using Dynamic Light Scattering. Organic solutions of $HEP^+NO_3^-$ and $DEC^+NO_3^-$ were analyzed both before and after extraction of ReO_4^- for aggregates. The average size and range of aggregate sizes for 1.0 mM solutions of $HEP^+NO_3^-$ and $DEC^+NO_3^-$ was determined by dynamic light scattering using 100 μL samples thermostated to 22 °C. Test-runs were performed with solutions of 19 ± 1.5 nm Nanosphere™ polystyrene bead standards (Duke Scientific Corp.) that were diluted by placing one drop of the standard solution in 5 mL of water. Before measurement, laboratory samples were filtered through a 0.1 μm Anodisc-13 filter (Whatman®) to remove dust particles. Samples that had previously undergone liquid-liquid extraction were centrifuged at 3000 rpm for 5 minutes to ensure complete phase separation.

Particle size analysis was performed on a DynaPro MSTC Dynamic Light Scattering Instrument from Protein Solutions, Inc. operated with DYNAMICS software. This system analyzes the time scale of the scattered light intensity fluctuations by an autocorrelation method. Particle size is then determined by first calculating the translational diffusion coefficient of the molecules in the sample. The hydrodynamic radius of the molecules is then derived from the translational diffusion coefficient using the Stokes-Einstein equation. Determination of size uniformity is done using a monomodal curve fit analysis.

Organic solutions with concentrations greater than 10 mM could not be analyzed by this method. Due to the intense green color of $HEP^+NO_3^-$ and $DEC^+NO_3^-$ (molar absorptivity $\geq$ 460 $M^{-1}cm^{-1}$), concentrated solutions of these molecules are extremely opaque. It is assumed that the high opacity observed for these concentrated solutions do not allow light to pass through the solution, and therefore measurements could not be performed on solutions of these concentrations.

Results and Discussion

Preliminary Extraction Studies. In initial extraction experiments, dichloromethane solutions of varying concentrations of $HEP^+NO_3^-$ and $DEC^+NO_3^-$ were equilibrated with aqueous solutions containing 1 M $NaNO_3^-$ and varying concentrations of $KReO_4$. Ion-exchange equilibration took place according to Equation 5.1. The $D(ReO_4^-)$ values for various extraction conditions are shown in Table 5.1. The two extractants exhibit comparable extraction ability under the extraction conditions. In a previous study of liquid-liquid extraction with tetraalkylated ferrocenes (Fc'), solutions of neutral HEP in water-immiscible organic solvents did not remove anions from aqueous waste simulants.[1] Furthermore, no anions could be detected in the organic phase when pure organic solvent was equilibrated with 1 M $NaNO_3$ containing target anions.[3,13] Previous studies have also ruled out the possibility of ion-pair extraction for $Fc'^+NO_3^-$ ion-exchange compounds.[3] It is justifiable, therefore, to consider only the charged (oxidized) form of the Fc' complex as the active extractant in the present investigation.

The data in Table 5.1 show HEP^+ to be slightly more efficient than DEC^+ for liquid-liquid ion-exchange under the various conditions of extraction demonstrated in Table 5.1. For extractions done with 10 mM $Fc'^+NO_3^-$ and 1 mM ReO_4^-, it can be seen that the $D(ReO_4^-)$ values for the HEP^+ and DEC^+ cations are the same within experimental error. For extractions done with 1 mM $Fc'^+NO_3^-$ and 0.1 mM ReO_4^-, it can be seen that the $D(ReO_4^-)$ value for HEP^+ is slightly larger than the $D(ReO_4^-)$ value for DEC^+. These results were somewhat unexpected considering the Born model for ion-

Table 5.1. Results from preliminary liquid-liquid extractions of $ReO_4^-(aq)$ using $HEP^+NO_3^-$ and $DEC^+NO_3^-$ in dichloromethane.[a]

$Fc'^+NO_3^-$	$[Fc']_{org.}$ (mM)	$[ReO_4^-]_{aq,initial}$ (mM)	$[ReO_4^-]_{aq,final}$ (mM)	$D(ReO_4^-)$
$HEP^+NO_3^-$	10	1.0	0.21(1)	4.2(4)
$DEC^+NO_3^-$	10	1.0	0.19(2)	3.2(2)
$HEP^+NO_3^-$	1.0	0.10	0.028(2)	2.2(2)
$DEC^+NO_3^-$	1.0	0.10	0.038(1)	1.9(2)

a. All aqueous solutions also contained 1 M $NaNO_3$. The numbers in parentheses represent the standard deviation of five separate measurements.

exchange presented in Chapter 1 and the results obtained by Chambliss *et. al.*[3,7] According to Equation 1.2, a larger cationic extractant, such as DEC^+, should be more selective for ReO_4^- than a smaller one, such as HEP^+. The $D(ReO_4^-)$ values for the extractions done in dichloromethane indicate an equivalent extraction, if not slightly better for the HEP^+ cation. Increased selectivity for anion ion exchange with large cations has been demonstrated previously for tetraalkylated ammonium salts for liquid-liquid extraction systems.[7] The DEC^+ cation has been shown to be more selective than HEP^+ when immobilized on solid supports and used in ion-exchange chromatography for the extraction of a variety of anions from aqueous solutions.[6] Furthermore, it was shown in Chapter 3 that the electrochemical ion pairing with perchlorate is even more selective using the DEC^+ moiety versus smaller, tetraalkylated ferrocenium cationic moieties, including HEP^+. For these reasons, the results of the liquid-liquid extraction experiments for the DEC^+ and HEP^+ cations seem somewhat anomalous.

One possible explanation for the results may be the thermodynamic point of "diminishing returns", as discussed in Chapter 1 and demonstrated for ion chromatography[6] and electrochemical ion pairing in Chapter 3. Briefly, as the size of the cationic extractant reaches an "experimentally infinite" size, no further selectivity can be gained in an extraction by making the cationic extractant larger. Equilibrium modeling by Chambliss has in fact predicted that this point of diminishing returns has already been reached with the size of the HEP^+ cation.[3] Considering this model, if the experimentally infinite size of the cationic extractant in this system is close to that of the HEP^+ cation, the increased size of the DEC^+ cation should not exhibit any increase in the observed $D(ReO_4^-)$ values, but should yield comparable values. The extractions performed at 1 mM Fc'^+, which yielded equivalent $D(ReO_4^-)$ values, would indeed support this notion. Extractions done with 10 mM Fc'^+ extractant, however, did display a difference in $D(ReO_4^-)$ values, with extractions using HEP^+ being slightly better. As a result, it seems unlikely that the similarity in $D(ReO_4^-)$ values is due to an "experimentally infinite"

sized cationic extractant.

Another possible explanation for the observed data could be aggregation of the extractant in the organic phase. It has been previously suggested that for high concentrations of HEP^+ ($\geq$ 30 mM) in chlorobenzene, aggregation occurs, resulting in a large drop off in selectivity for the extraction of $^{99}TcO_4^-$ from water.[3] Aggregation of quaternary ammonium cationic extractants in organic solvents has been well documented and specifically, $(heptyl)_4N^+NO_3^+$ has been shown to aggregate in chlorobenzene and benzene.[3,14,15] As discussed at length in a recent review by Moyer and Bonnesen and discussed in Chapter 1,[7] the origins of selectivity in anion exchange relate to the change in solvation of the anion on transfer from the aqueous phase to the organic solvent, especially as influenced by hydrogen-bonding interactions. In the present case, decreased selectivity may be interpreted in terms of increased anion solvation due to hydrogen bonding in the organic solvent. This is consistent with the formation of an inverted micelle, which is normally considered to have a core of water molecules. Thus, greater hydration of the anion in the solvent phase favors the smaller anion, nitrate, relative to the larger perrhenate anion. By this reasoning and as inferred in Chapter 1, in the limit that the environment afforded the anion in the solvent phase becomes essentially aqueous, selectivity should disappear altogether. Given the nature of the highly lipophilic cations HEP^+ and DEC^+, it seems likely that an aggregate displaying these micellular type properties is reasonable in an organic phase, and thus, investigation of aggregation effects of these extractants was performed.

Aggregation of HEP^+ and DEC^+ Cations in Chlorobenzene. Aggregation analysis was performed using the method of van Dalen, originally used to investigate the aggregation of dinonyl napthalene sulfonic acid.[11,16] In the present case, an initial organic phase aggregate $Fc^{+}{}_nNO_3^-{}_n$ which incorporates a ReO_4^- anion by ion exchange to form $Fc^{+}{}_mNO_3^-{}_{m-1}ReO_4^-$ is postulated according to Equation 5.4,

(5.4) $m/n\ Fc'^{+}{}_{n}NO_3^{-}{}_{n}(org) + ReO_4^{-}(aq) \rightleftharpoons Fc'^{+}{}_{m}NO_3^{-}{}_{m-1}ReO_4^{-}(org) + NO_3^{-}(aq)$

where the aggregation numbers n and m are not necessarily identical. Such an analysis provides a convenient method for the determination of the aggregation number n of organic phase extractant species. The basis for this determination rests in the mass-action lowering of the distribution coefficient as the extractant species is loaded with ReO_4^-. Based on Equation 5.4 as the predominant equilibrium, the loading experiment may be described in terms of a linear dependence of the distribution coefficient $D(ReO_4^-)$ on the organic-phase concentration of pertechnetate $[ReO_4^-]_{org}$ provided that the concentration of aqueous NO_3^- and the concentration of extractant are held constant and that the aggregation number n does not change upon incorporation of ReO_4^- (i.e.,, $n = m$). For convenience, we express the relationship in slightly rearranged form:

(5.5) $$\frac{D(ReO_4^-)}{[Fc'^{+}\,NO_3^-]_{tot}} = \frac{-Q}{[NO_3^-]_{aq}}\left(\frac{[ReO_4^-]_{org}}{[Fc'^{+}\,NO_3^-]_{tot}}\right) + \frac{Q}{n[NO_3^-]_{aq}}$$

where Q is the equilibrium quotient corresponding to Equation 5.4. It follows that the aggregation number n is given by Equation 5.6

(5.6) $$n = -\left(\frac{\text{slope}}{\text{intercept}}\right)$$

as the negative ratio of the slope to the intercept in plots of $D(ReO_4^-)/[Fc'^{+}NO_3^-]_{tot}$ vs. $[ReO_4^-]_{org}/[Fc'^{+}NO_3^-]_{tot}$.

Distribution data were collected for several chlorobenzene solutions of $HEP^{+}NO_3^-$ and $DEC^{+}NO_3^-$ ranging in concentration from 1 mM to 100 mM. The solvent used for these experiments was switched to chlorobenzene due to the limited

solubility of $DEC^+NO_3^-$ in dichloromethane (< 100 mM). For a given solution, the extractant loading was varied by increasing the initial aqueous concentration of ReO_4^- (see Experimental Section). The initial aqueous concentration of $NaNO_3$ was held constant at 1 M in all experiments. Plots of $D(ReO_4^-)/[Fc'^+NO_3^-]_{tot}$ vs. $[ReO_4^-]_{org}/[Fc'^+NO_3^-]_{tot}$ are shown in Figure 5.1. The solid lines represent linear least-squares fits and dashed lines are merely to guide the eye. The calculated values of the slope, intercept, and aggregation number *n* according to Equation 5.6 are given in Table 5.2. The aggregation number, *n*, was not calculated for plots that gave linear regression results with R^2 values < 0.98. The actual values of $D(ReO_4^-)$ are given in Appendix D.

The data indicate that $DEC^+NO_3^-$ also extracts less ReO_4^- than $HEP^+NO_3^-$ in chlorobenzene as well as dichloromethane. Regression analysis based on Equation 5.5 revealed that $HEP^+NO_3^-$ at concentrations of 1 mM and 10 mM is predominantly monomeric in chlorobenzene. Plots of $D(ReO_4^-)/[Fc'^+NO_3^-]_{tot}$ vs. $[ReO_4^-]_{org}/[Fc'^+NO_3^-]_{tot}$ were linear over the entire loading range and the aggregation numbers determined from Equation 5.6 were all 1 within experimental error. The aggregation numbers calculated were 1.3 ± 0.2 and 0.94 ± 0.2 for $HEP^+NO_3^-$ concentrations of 1 mM and 10 mM, respectively. Aggregation numbers of 1 indicate that $HEP^+NO_3^-$ at these concentrations is monomeric up to 30% anion loading in the organic phase. The highest concentration of ReO_4^- obtained in the organic phase for these two studies was approximately 3 mM, at which point no aggregation for $HEP^+NO_3^-$ was observed. In contrast, the plot of $D(ReO_4^-)/[Fc'^+NO_3^-]_{tot}$ vs. $[ReO_4^-]_{org}/[Fc'^+NO_3^-]_{tot}$ was not observed to be linear for 100 mM $HEP^+NO_3^-$, indicating a change in aggregation number upon extraction (i.e., $n \neq m$ in Equation 5.4).

Similar trends in the extraction of $^{99}TcO_4^-$ by $HEP^+NO_3^-$ have been observed in work performed by Chambliss *et. al.*[3] Though the anion and absolute magnitude of the *D* values obtained were different, the same trends were observed. For the extraction of $^{99}TcO_4^-$ by $HEP^+NO_3^-$, plots of $D(^{99}TcO_4^-)/[Fc'^+NO_3^-]_{tot}$ vs.

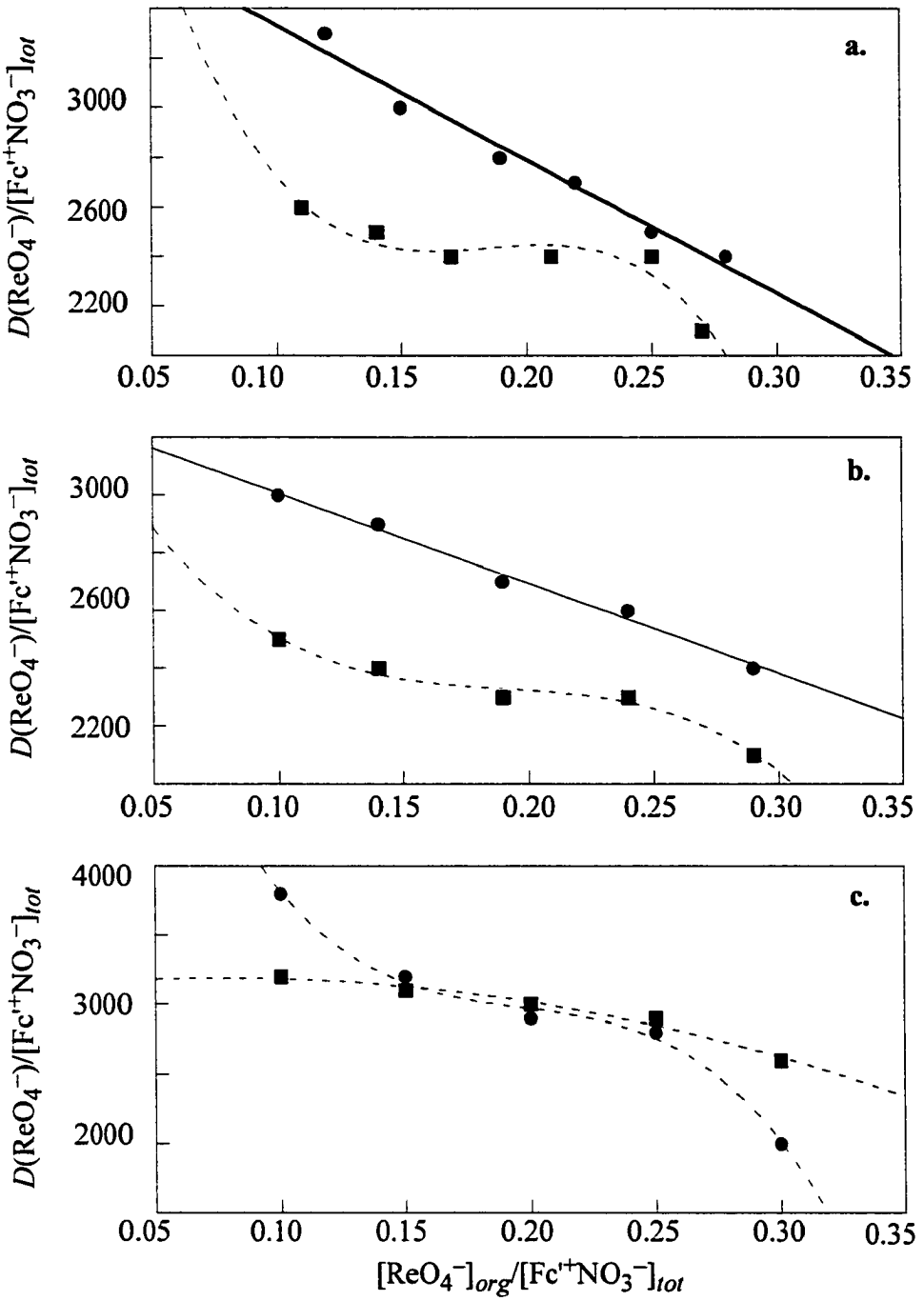

Figure 5.1. Plots of $D(ReO_4^-)/[Fc'^+NO_3^-]_{tot}$ vs. $[ReO_4^-]_{org}/[Fc'^+NO_3^-]_{tot}$ for (a) 1 mM, (b) 10 mM, and (c) 100 mM $HEP^+NO_3^-$ (●) and $DEC^+NO_3^-$ (■) in chlorobenzene at 25 °C. The solid lines denote a linear least-squares fit (see Table 5.1) and dashed lines are merely to guide the eye. The errors on all measurements are < ±5%.

Table 5.2. Least squares analysis and aggregation numbers, *n*, of partial ReO_4^- loading data for $HEP^+NO_3^-$ and $DEC^+NO_3^-$ in chlorobenzene.[a]

Results for $DEC^+NO_3^-$

$[DEC^+NO_3^-]_{tot}$[b] (M)	R^2	slope	y-intercept	*n*
0.001	0.73	—	—	—
0.010	0.92	—	—	—
0.100	0.92	—	—	—

Results for $HEP^+NO_3^-$

$[HEP^+NO_3^-]_{tot}$[b] (M)	R^2	slope	intercept	*n*
0.001	0.98	-5300(400)	3850(90)	1.3(2)
0.010	0.99	-3100(200)	3320(40)	0.9(2)
0.100	0.93	—	—	—

[a.] Data and experimental conditions are given in Figure 5.1 and their captions. Linear least squares analysis was based on Equation 5.5. Numbers in parentheses represent the errors calculated from the linear regression. The aggregation number, *n*, was calculated using Equation 5.6. [b.] Represents the initial organic phase concentration.

$[^{99}TcO_4^-]_{org}/[Fc'^+NO_3^-]_{tot}$ were linear for $HEP^+NO_3^-$ concentrations of 1 mM and 10 mM and loading concentrations of $^{99}TcO_4^-$ up to 3 mM. A sharp drop in the slope of plots of $D(^{99}TcO_4^-)/[Fc'^+NO_3^-]_{tot}$ vs. $[^{99}TcO_4^-]_{org}/[Fc'^+NO_3^-]_{tot}$ was also observed in these studies at a $HEP^+NO_3^-$ concentration of 100 mM or $^{99}TcO_4^-$ loadings of greater than 3 mM. The dependence of aggregation on the loading of $^{99}TcO_4^-$ in the organic phase, however, was much more drastic due to the concentration range studied. Due to the methods used for ReO_4^- quantitation in this study, the broad range of concentrations studied for $^{99}TcO_4^-$ could not be performed in our laboratories. As such, the plot of $D(ReO_4^-)/[Fc'^+NO_3^-]_{tot}$ vs. $[ReO_4^-]_{org}/[Fc'^+NO_3^-]_{tot}$ for 100 mM $HEP^+NO_3^-$ appears to have reached a value at which the slope levels off, indicating that the drastic drop-off in $D(ReO_4^-)$ observed occurs at much lower loadings of ReO_4^- in the organic phase. The significant decrease in $D(^{99}TcO_4^-)$ observed by Chambliss did in fact occur for 100 mM $HEP^+NO_3^-$ extractions between $^{99}TcO_4^-$ loadings of 2% to 10%, concentration ranges which would be beyond our ability to quantify using ReO_4^-. For these reason, reliable slope analysis was not able to be performed for 100 mM $HEP^+NO_3^-$ extractions, but the non-linear curve is highly suggestive of an aggregated species.

Non-linear curves were also obtained for plots of $D(ReO_4^-)/[Fc'^+NO_3^-]_{tot}$ vs. $[ReO_4^-]_{org}/[Fc'^+NO_3^-]_{tot}$ over the entire concentration range of $DEC^+NO_3^-$. Due to the reasons described above for $HEP^+NO_3^-$, reliable slope analysis was not able to be performed for the $DEC^+NO_3^-$ extractions, however, the plots indicate a significant amount of aggregation of $DEC^+NO_3^-$ in chlorobenzene, even at low concentrations of 10 and 1 mM. The aggregation of $DEC^+NO_3^-$ at these lower concentrations may be due to the longer, more lipophilic alkyl chains present in the $DEC^+NO_3^-$ molecule. Aggregation may be responsible for the lower $D(ReO_4^-)$ values observed for $DEC^+NO_3^-$ compared to $HEP^+NO_3^-$ as discussed above. Furthermore, the $D(ReO_4^-)$ values for $HEP^+NO_3^-$ and $DEC^+NO_3^-$ are most similar at concentrations of 100 mM, the only concentration where both extractant species exhibit aggregation behavior. Given this

observation, $DEC^+NO_3^-$ may actually be more selective than $HEP^+NO_3^-$ if aggregation effects could be eliminated. At the very least, $DEC^+NO_3^-$ would be predicted to be equally efficient in the absence of aggregation based on the results of Chambliss, which predict a point of maximum selectivity for extractants equal in size or larger than HEP^+.[3]

Particle Size Analysis of Extraction Media. To further study the effects of aggregation, dynamic light scattering analysis of the organic extractant solutions were analyzed for the formation of aggregates for organic solutions of $DEC^+NO_3^-$ and $HEP^+NO_3^-$. Light scattering techniques have been previously used to monitor the aggregation of quaternary ammonium cations in benzene and toluene.[14] A plot showing the particle size distribution of 10 mM $DEC^+NO_3^-$ and $HEP^+NO_3^-$ in dichloromethane obtained by dynamic light scattering is shown in Figure 5.2. As can be seen, $DEC^+NO_3^-$ shows signs of aggregation whereas no aggregation is observed for the $HEP^+NO_3^-$ solution. The particle distributions observed for $DEC^+NO_3^-$ and $HEP^+NO_3^-$ have radii of 9 ± 5 nm and 0.5 ± 0.1 nm, respectively. If indeed aggregation is the cause, the observation of aggregation for $DEC^+NO_3^-$ and not for $HEP^+NO_3^-$ correlates well with the lower $D(ReO_4^-)$ observed in the 10 mM extractions done in dichloromethane (see Table 5.1).

It should be noted that the deviation reported in the average value is the distribution of sizes observed in the solution and not a calculated error. For example, the average particle size value for the 10 mM $DEC^+NO_3^-$ solution had an average value of 9 nm with a particle size range between 4 nm and 13 nm. As such, the values reported for particle size in this case are distributions of sizes rather than actual size. The idea of size distribution is important for understanding the aggregation phenomenon. Given the large observed deviations from the average particle value, the particles in the $DEC^+NO_3^-$ solution are undoubtedly due to non-uniform aggregates as opposed to uniform structures such as micelles. A more uniform micellular structure would have a much narrower size distribution, usually less than one nanometer. Given the structure of the tetraalkylated

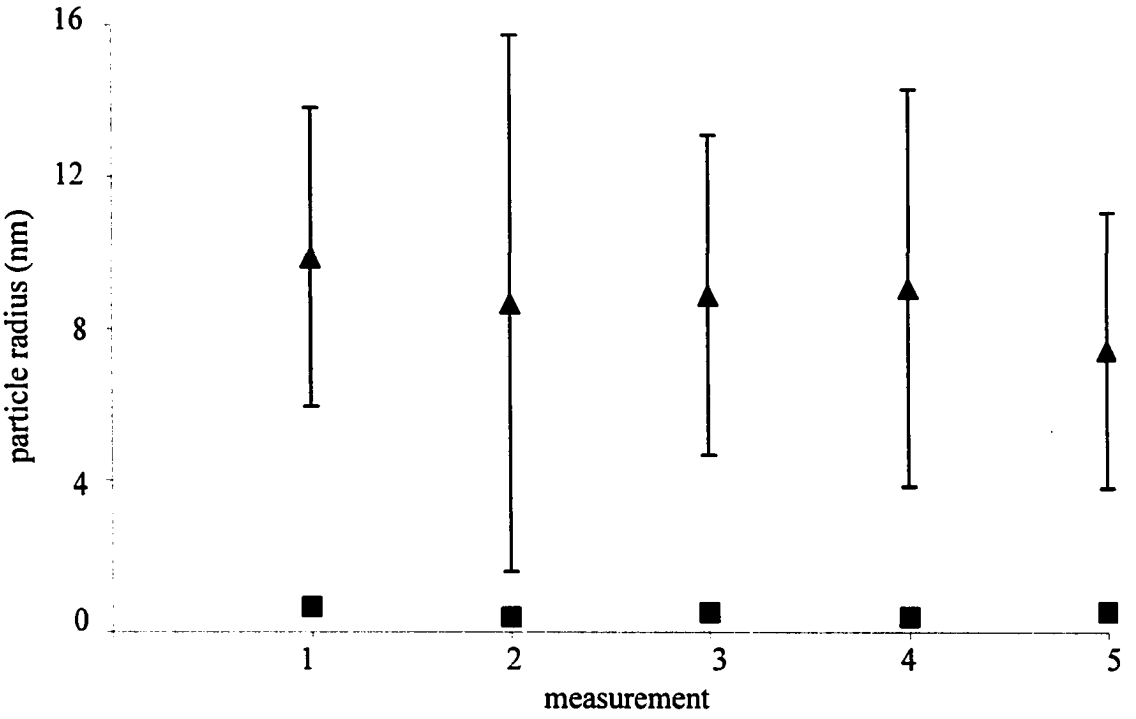

Figure 5.2. Particle size distribution of 10 mM dichloromethane solutions of $DEC^+NO_3^-$ (▲) and $HEP^+NO_3^-$ (■) measured by dynamic light scattering. The lines shown represent the particle size distribution and the markers indicate the average value. The average size measured for the 1 mM $DEC^+NO_3^-$ solution is 9 nm with an average distribution of ± 5 nm. The average size measured for the $HEP^+NO_3^-$ solution is 1 nm with an average distribution of ± 0.1 nm.

ferrocenium cations, which contain a ionic center surrounded by four long aliphatic chains, it seems likely that formation of an aggregate is more likely to occur instead of formation of an ordered structure like those seen with typical surfactant molecules containing a polar head-group and one long aliphatic tail.

To further explore the aggregation of $DEC^+NO_3^-$ and $HEP^+NO_3^-$, dynamic light scattering analysis was also performed on the 1 mM and 10 mM chlorobenzene extractant solutions. Analysis was unable to be performed on the 100 mM chlorobenzene extractant solutions. It is assumed that the light scattering analysis could not be performed at this concentration due to the extremely opaque, dark green solutions obtained for $DEC^+NO_3^-$ and $HEP^+NO_3^-$. Plots of the particle size distributions for the 1 mM and 10 mM chlorobenzene solutions are shown in Figure 5.3. As was seen in the 10 mM dichloromethane solutions, aggregation is observed for $DEC^+NO_3^-$, but little to no aggregation is observed for $HEP^+NO_3^-$. This observation correlates well with the aggregation results obtained by slope analysis in the previous section. The particle distributions observed in 1 mM chlorobenzene solutions of $DEC^+NO_3^-$ and $HEP^+NO_3^-$ have radii of 31 ± 10 nm and 0.5 ± 0.1 nm, respectively. The particle distributions observed in 10 mM chlorobenzene solutions of $DEC^+NO_3^-$ and $HEP^+NO_3^-$ have radii of 44 ± 30 nm and 0.7 ± 0.2 nm, respectively.

The particle size distributions obtained for 10 mM $DEC^+NO_3^-$ in chlorobenzene are much larger than those obtained in dichloromethane. One possible reason for the variation in aggregate size distribution could be the dielectric constant of the two solvents. The dielectric constants for dichloromethane and chlorobenzene at 25 °C are 8.93 and 5.62, respectively.[17] A high dielectric constant solvent is better able to support ionic species than a low dielectric constant solvent, as discussed in Chapter 1. As a result, the aggregation of ions in a low permitivity solvent may be a result of the solvent's inability to adequately solvate the ion. A higher permitivity solvent would be better able to solvate ions, and thus aggregation would decrease due to increased solvation. Though

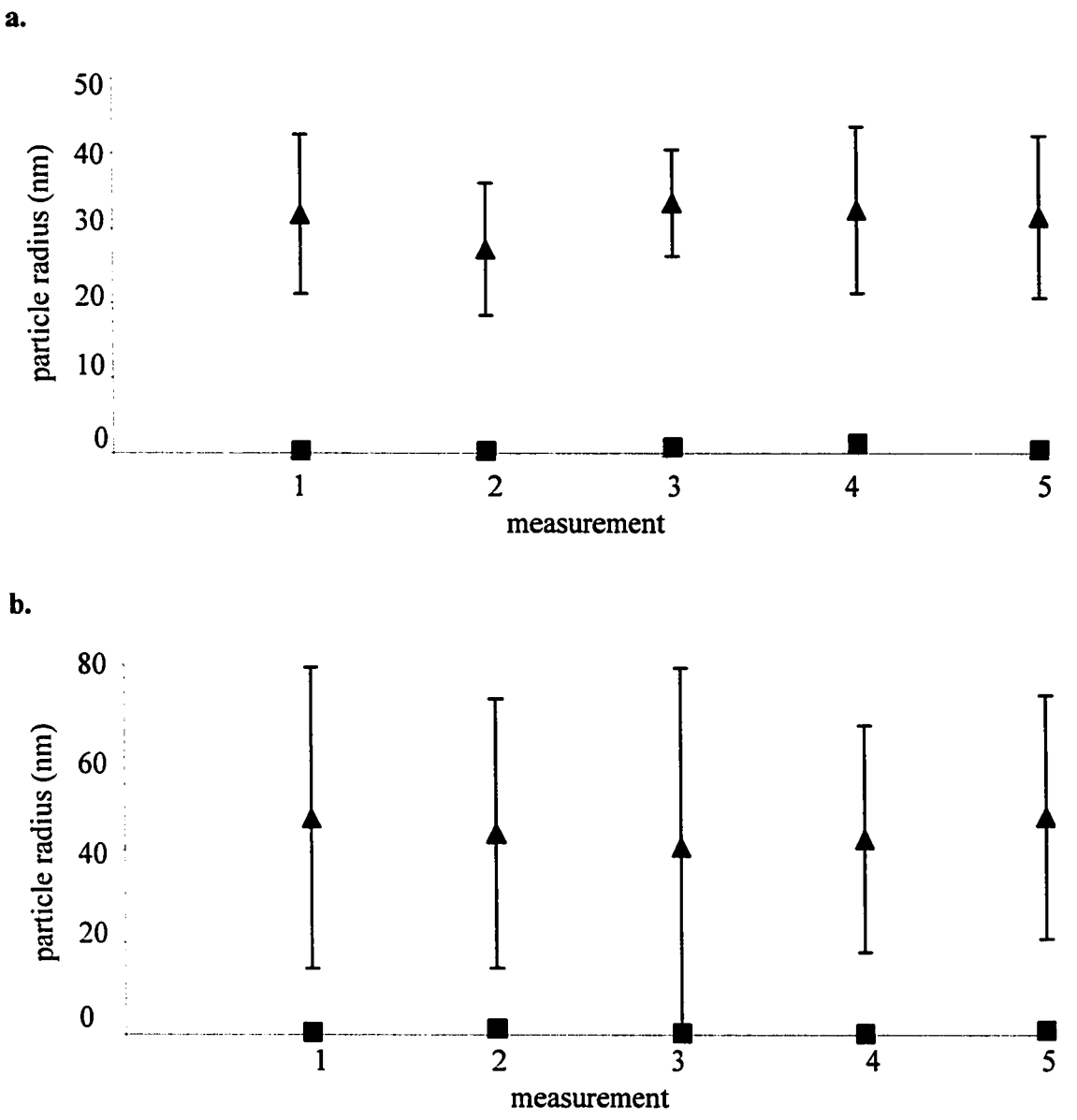

Figure 5.3. Particle size distribution of (a) 1 mM and (b) 10 mM chlorobenzene solutions of $DEC^+NO_3^-$ (▲) and $HEP^+NO_3^-$ (■) measured by dynamic light scattering. The lines shown represent the particle size distribution and the markers indicate the average value. The average particle size and distributions measured for the 1 mM solutions were 31 ± 10 nm for $DEC^+NO_3^-$ and 1 ± 0.1 nm for $HEP^+NO_3^-$. The average particle size and distributions measured for the 10 mM solutions were 44 ± 30 nm for $DEC^+NO_3^-$ and 1 ± 0.2 nm for $HEP^+NO_3^-$.

both dichloromethane and chlorobenzene display aggregation of $DEC^+NO_3^-$, the aggregate size distribution is much smaller in dichloromethane, the solvent with the higher dielectric constant.

Using crystallographic data to estimate the size of both $DEC^+NO_3^-$ and $HEP^+NO_3^-$, it is possible to estimate the number of cations in an aggregate. Assuming that the tetraalkylated ferrocenes are approximately spherical in solution with a diameter equal to the length of the cation in the solid state structure (see Chapter 2 and Chapter 4), values of 1.3 nm and 0.9 nm were calculated for the radii of the DEC^+ and HEP^+ cations, respectively. Using these values and the average particle size for the various concentrations of $DEC^+NO_3^-$ and $HEP^+NO_3^-$ in organic solvents, the aggregation numbers, *n*, have been calculated. The resulting aggregation numbers for $DEC^+NO_3^-$ and $HEP^+NO_3^-$, respectively, are approximately 7 ± 4 and 1 ± 0.1 for 10 mM dichloromethane solutions, 23 ± 8 and 1 ± 0.1 for 1 mM chlorobenzene solutions, and 34 ± 23 and 1 ± 0.2 for 10 mM chlorobenzene solutions. As can be seen, the aggregation numbers obtained for $HEP^+NO_3^-$ by light scattering techniques agree extremely well with those calculated by slope analysis. Particle size analysis using dynamic light scattering techniques shows the extractant $HEP^+NO_3^-$ to be monomeric in organic solutions at concentrations ≤ 10 mM. The observation of monomeric $HEP^+NO_3^-$ at these concentrations in chlorobenzene also agrees well with slope analysis data collected for the $HEP^+NO_3^-$ extraction of $^{99}TcO_4^-$.[3] Though aggregation numbers could not be calculated for $DEC^+NO_3^-$ by slope analysis due to the concentration range studied, the observation of aggregation by dynamic light scattering analysis is consistent with the proposal of aggregation from the slope analysis data. Furthermore, in addition to the apparent dependence of aggregation on the length and/or lipophilicity of the tertiary alkyl chains, the aggregation of $DEC^+NO_3^-$ appears to also be dependent on both concentration and the solvent dielectric constant.

Finally, particle size analysis was also performed on several of the chlorobenzene

solutions after ReO_4^- loading. The results of these analyses are shown in Table 5.3. It can bee seen that $HEP^+NO_3^-$ remains monomeric at concentrations of 1 mM and 10 mM throughout the entire range of ReO_4^- loading. (The average particle size value reported is sometimes smaller than the radius of $HEP^+NO_3^-$ as calculated by crystallography. The correct value, however, is always within the distribution range reported. Smaller values may be the result of the flexible nature of the tertiary alkyl chains when in solution.) As would be predicted from $^{99}TcO_4^-$ loading experiments previously performed for $HEP^+NO_3^-$,[3] the average aggregate size of $DEC^+NO_3^-$ increases slightly as the loading of ReO_4^- increases, however, all aggregates are in the same particle size distribution range for a given concentration of $DEC^+NO_3^-$. In general for the aggregation of $DEC^+NO_3^-$, for similar loadings of ReO_4^-, the average particle size is larger for the 10 mM chlorobenzene solutions, further supporting the effect of larger aggregates with increased concentration.

It should be noted that though the dynamic light scattering data for $DEC^+NO_3^-$ confirm the presence of aggregation, the overall aggregate size determined in these studies is probably not entirely accurate. Dynamic light scattering analyses of polydisperse systems, as is obviously the case for $DEC^+NO_3^-$ given the large particle size distributions, are known to contain large errors when the data is fit by a monomodal curve analysis as was done in this case. For more accurate size distributions, a bimodal data analysis method should be used. Nevertheless, the method does confirm the presence of significant aggregation for the $DEC^+NO_3^-$ extraction solutions. Even if the distributions contained an error of 50%, a large aggregate would still be observed in all of the solutions studied with a significant polydispersity. The conclusion that aggregation is the cause of the lower selectivities observed for $DEC^+NO_3^-$ extractions is still confirmed by this method. The light scattering data obtained for $HEP^+NO_3^-$ is reliable since it is a monodisperse system as discussed above.

Table 5.3. Particle size analysis of partial ReO_4^- loading in chlorobenzene.

Particle Size Analysis for $DEC^+NO_3^-$			
$[DEC^+NO_3^-]_{tot}$ (mM)	ReO_4^- loading (%)[a]	avg. particle size (nm)[b]	particle size distrib. (nm)[b]
1.0	27	40	40 ± 13
1.0	25	41	41 ± 16
1.0	21	30	30 ± 14
1.0	17	35	35 ± 12
1.0	14	27	27 ± 15
1.0	11	19	19 ± 10
10	29	50	50 ± 13
10	10	36	36 ± 7

Particle Size Analysis for $HEP^+NO_3^-$			
$[HEP^+NO_3^-]_{tot}$ (mM)	ReO_4^- loading (%)[a]	avg. particle size (nm)[b]	particle size distrib. (nm)[b]
1.0	28	1	1 ± 1
1.0	25	0.8	0.8 ± 0.5
1.0	22	0.7	± 0.2
1.0	19	1	1 ± 0.1
1.0	15	0.9	0.9 ± 0.1
1.0	12	1	1 ± 0.1
10	29	0.9	0.9 ± 0.6
10	14	0.6	0.6 ± 0.4

[a.] The percent of ReO_4^- in the organic phase with respect to the extractant after partial loading (ie. $[ReO_4^-]_{org}/[Fc'^+NO_3^-]_{tot}$). [b.] The average of five separate measurements.

Conclusions

The liquid-liquid extraction properties of the extractant $DEC^+NO_3^-$ for the extraction of the ReO_4^- anion from aqueous media has been determined and compared to the extractant $HEP^+NO_3^-$. Despite findings in previous studies,[6] $HEP^+NO_3^-$ has been shown to be more selective for the extraction of ReO_4^- than $DEC^+NO_3^-$ in both dichloromethane and chlorobenzene.

The better selectivity observed for $HEP^+NO_3^-$ is believed to be due to the aggregation of the larger, more lipophilic $DEC^+NO_3^-$ in low to moderate dielectric constant organic solvents. Slope analysis of partial ReO_4^- loading experiments shows aggregation of $DEC^+NO_3^-$ at extractant concentrations of 1 mM to 100 mM, whereas aggregation of $HEP^+NO_3^-$ is not observed until concentrated to 100 mM. The aggregation number, *n*, was calculated for $HEP^+NO_3^-$ at concentrations of 1 and 10 mM and was shown to be 1.3 ± 0.2 and 0.94 ± 0.2, respectively, indicating that $HEP^+NO_3^-$ is monomeric at these concentrations. The aggregation numbers of approximately 1 and the onset of aggregation of $HEP^+NO_3^-$ at concentrations > 10 mM are in good agreement with aggregation studies performed previously for the extraction of $^{99}TcO_4^-$ by $HEP^+NO_3^-$.[3]

The effects of aggregation were also studied by dynamic light scattering particle analysis. The particle size distributions obtained for dichloromethane and chlorobenzene solutions of $DEC^+NO_3^-$ and $HEP^+NO_3^-$ at concentrations of 1 mM and 10 mM supported the findings of the slope analysis for aggregation. By using crystallographic data to determine the size of the DEC^+ and HEP^+ cations, the number of molecules in an aggregate measured by dynamic light scattering was approximated. $DEC^+NO_3^-$ was shown to contain up to 34 ± 23 molecules in an aggregate for concentrations of 10 mM in chlorobenzene. The particle sizes measured for the $HEP^+NO_3^-$ solutions in both dichloromethane and chlorobenzene showed no aggregation and were in good agreement

with the crystallographically calculated radius of the HEP^+ cation.

From the results of this study, it is highly probable that aggregation is the reason for lower selectivity of $DEC^+NO_3^-$ as compared to $HEP^+NO_3^-$ in the liquid-liquid extraction of ReO_4^-. It is assumed that in the absence of aggregation, $DEC^+NO_3^-$ would exhibit equal if not better selectivity than $HEP^+NO_3^-$.

References

1. Clark, J. F.; Clark, D. L.; Whitener, G. D.; Schroeder, N. C.; Strauss, S. H. *Environ. Sci. Technol.* **1996**, *30*, 3124.
2. Gansle, K. M. Investigation and Development of Liquid-Liquid Extraction Systems for the Removal of Pertechnetate from Aqueous Nuclear Waste-Stream Simulants. Ph.D. Dissertation, Colorado State University, Fort Collins, CO, 1998.
3. Chambliss, C. K.; Martin, C. A.; Strauss, S. H.; Moyer, B. A. *Solvent Extr. Ion Exch.* **1999**, *17*, 553.
4. Chambliss, C. K.; Odom, M. A.; Morales, C. M. L.; Martin, C. R.; Strauss, S. H. *Anal. Chem.* **1998**, *70*, 757.
5. Chambliss, C. K.; Odom, M. A.; Martin, C. A.; Moyer, B. A.; Strauss, S. H. *Inorg. Chem. Commun.* **1998**, *1*, 435.
6. Odom, M. A. Development of Strategies for the Detection, Extraction, and Recovery of Aqueous Anions Using Highly Selective Redox-Recyclable Materials. Ph.D. Dissertation, Colorado State University, Fort Collins, CO, 2001.
7. Moyer, B. A.; Bonnesen, P. V. In *Supramolecular Chemistry of Anions*; Bianchi, A., Bowman-James, K., Garcia-Espana, E., Eds.; VCH: New York, 1997.
8. Baes, C. F., Jr.; Moyer, B. A.; Case, G. N.; Case, F. I. *Sep. Sci. Technol.* **1990**, *25*, 1675.
9. Clapsaddle, B. J.; Clark, J. F.; Clark, D. L.; Gansle, K. M.; Gash, A. E.; Miller, S. M.; Anderson, O. P.; Hughes, R. P.; Strauss, S. H., 2002 *Synthesis and Characterization of Polyalkylated Ferrocenes and Ferrocenium Salts.*
10. Strauss, S. H.; Odom, M. A.; Hebert, G. N.; Clapsaddle, B. J., 2001 *ATR-FTIR Detection and Quantification of Anionic Pollutants in Water.*
11. van Dalen, A.; Gerritsma, K. W.; Wijkstra, J. *J. Colloid Interface Sci.* **1974**, *48*, 122.

12. Clark, J. F. Design, Synthesis, and Evaluation of Redox-Recyclable Organometallic Extractants for the Recovery of Ionic Radionuclides From Aqueous Waste Streams. Ph.D. Dissertation, Colorado State University, Fort Collins, CO, 1999.
13. Chambliss, C. K. Redox-Recyclable Extraction and Recovery. A New Strategy for the Separation and Recovery of Aqueous Ions. Ph.D. Dissertation, Colorado State University, Fort Collins, CO, 1998.
14. Danesi, P. R.; Magini, M.; Scibona, G. In *Solvent Extraction Research*; Kertes, A. S., Marcus, Y., Eds.; Wiley Interscience: New York, 1969.
15. Scibona, G.; Danesi, P. R.; Conte, A.; Scuppa, B. J. *J. Colloid Interface Sci.* **1971**, *35*, 631.
16. van Dalen, A. *Solvent Extraction and Inclusion Comound Formation with Dinonyl Naphthalene Sulphonic Acid*; RCN 141; Reactor Centrum Nederland, 1970.
17. Lide, D. R. *Handbook of Organic Solvents*; CRC Press: Boca Raton, 1995.

Chapter 6

Results, Conclusions, and Future Work

Introduction

Several new tetraalkylated ferrocenes have recently been synthesized and used for the selective ion exchange and detection of aqueous anions.[1,2] The resulting materials have applications in both the remediation and detection of pollutant anions in aqueous media.[1,3-5] The system used for the remediation and detection of anions using these tetraalkylated ferrocenes is called Redox-Recyclable Extraction and Recovery (R^2ER) and is described in detail in Chapter 1. The scope of this dissertation is the advancement of the R^2ER process in three major areas: 1) synthesis and evaluation of new tetraalkylated ferrocenes for anion-exchange processes, 2) further functionalization of tetraalkylated ferrocenes for use as surface modifying reagents or materials precursors, and 3) electrochemical characterization of the functionalized tetraalkylated ferrocenes in terms of ion-exchange selectivity and their potential uses as aqueous anion sensors.

Important Results and Conclusions

Increased Ion-Exchange Selectivity and Aqueous Anion Detection. To date, the most used tetraalkylated ferrocenium salt in the R^2ER system for ion exchange was $HEP^+NO_3^-$. This tetraalkylated ferrocenium cation has been shown to be robust and selective in both liquid-liquid and solid-liquid ion-exchange processes.[1,3] Due to predictions by the Born model for ion-exchange (see Chapter 1),[6] it was predicted that the selectivity of ion-exchange using tetraalkylated ferrocenium salts could be improved upon by lengthening the alkyl chains attached to the Cp rings to make a larger cationic extractant. Towards this end, the new tetraalkylated ferrocene, DEC, was synthesized. Use of the corresponding $DEC^+NO_3^-$ salt in solid-liquid ion-exchange processes resulted

in a 25% increase in selectivity over the most selective tetraalkylated ferrocenium ion-exchange cation before the current work, $HEP^+NO_3^-$.[4] The liquid-liquid ion-exchange selectivity for $DEC^+NO_3^-$ was also tested; however, the increased selectivity observed for the solid-liquid extraction experiments was not observed for the liquid-liquid methodology. Due to aggregation in the organic solvent, $HEP^+NO_3^-$ was more selective than $DEC^+NO_3^-$ despite predictions made by the Born model for ion exchange. For reasons of selectivity, it was therefore concluded that for bulk extraction processes, $HEP^+NO_3^-$ is the most selective tetraalkylated ferrocenium extractant for liquid-liquid processes, but $DEC^+NO_3^-$ should be used for solid-liquid extraction systems.

The increased lipophilicity of the DEC^+ cation has also been useful. In addition to extraction processes, $DEC^+NO_3^-$ has also been used for the infrared detection of aqueous anions (see Chapter 1).[5] Detection is accomplished by using a thin film of the ion-exchange compound to concentrate the analyte anion at the surface of the infrared detector, and thus reduce the detection limit of various anions in aqueous media. Previously, HEP^+ films were used for this process, but were shown to degrade or desorb from the detector surface before complete detection was achieved.[7] The more lipophilic DEC^+ cation still has some stability issues, but does not desorb from the detectors surface, thus enabling longer detection times and ultimately lowering detection limits for most anions. The synthesis of the DEC molecule has thus advanced the methodology used for the infrared detection of aqueous anions.

Functionalization, Surface Modification, and Electrochemical Sensing Applications. When this work was started, functionalization of tetraalkylated ferrocenes had previously never been attempted due to the assumption that the presence of the four tertiary alkyl groups on the Cp rings created an environment too sterically hindered for further functionalization. However, it was found in this work that Friedel-Crafts acylation is a robust enough reaction to overcome these steric challenges. The successful extension of a functional group beyond the steric influence of the tertiary alkyl

substituents was accomplished by the addition of an 11-bromoundecanoyl moiety by Friedel-Crafts acylation. The presence of the bromo moiety has allowed for the addition of other functional groups in high yields (80 – 99%) using common organic chemistry reactions. This functionalization method should prove useful in the synthesis of new, more selective, and more robust ion-exchange materials (*vide infra*).

In the current study, the functionalized tetraalkylated ferrocenes have allowed for the modification of several substrates, representing the first successful attempts for covalent surface modification using tetraalkylated ferrocenes. Several methodologies for the synthesis of ion-exchange materials with the tetraalkylated ferrocene moieties covalently bound in the materials have been demonstrated.

More importantly, the functionalization allowed the modification of electrically conducting substrates with tetraalkylated ferrocenes. Through the use of a thiol functionality, the electrochemical properties of tetraalkylated ferrocenyl monolayers on gold surfaces were characterized. The studies of the monolayers herein are the first major studies of the electrochemical properties of tetraalkylated ferrocenes, and have applications in both electrochemical extraction and detection of anions. Previously, neither application was possible due to the lack of a reproducible surface modification agent using tetraalkylated ferrocenes.

The electrochemical studies resulted in a novel method of electrochemically determining ion-exchange selectivity. It was shown that a DEC monolayer was 30% more selective for ion-pair formation with anions in the electrolyte solution than a HEP monolayer, results which were almost exactly the same as those observed for the increase in selectivity observed for solid-liquid ion-exchange (*vide supra*). The electrochemical selectivity studies represent the first time a direct correlation has ever been made between electrochemical ion-pair formation and ion-exchange properties, suggesting that the properties that govern ion exchange also govern the ion-pair formation process. Such a conclusion has implications for both the ion-exchange literature and the electroactive

monolayer literature as far as sensing applications and discerning the mechanisms of large electrochemical potential shifts.[8,9]

These monolayers were also found to be good electrochemical anion sensors. It was found that the same properties that make tetraalkylated ferrocenes highly selective ion-exchange materials also make them useful for amperometric sensing applications for aqueous anions. Since selectivity is also desirable in detection schemes, it was concluded that DEC monolayers would be the most selective, and therefore the most sensitive for the electrochemical detection of anions. The DEC monolayers exhibited robust electrochemical ion-exchange properties, including large potential shifts in the presence of various anions. These electrochemical anion sensors were the very first sensors used for aqueous anion detection in our laboratories and first demonstrated the advantages of using tetraalkylated ferrocenes for anion detection. The selectivity demonstrated for the electrochemical sensors developed in this work was later used as the basis of an infrared detection scheme for anions in aqueous media using tetraalkylated ferrocenes.

Future Work

Liquid-Liquid Extractions. In order to confirm that aggregation is the cause of the lower selectivity of $DEC^+NO_3^-$ in liquid-liquid extractions, extractions using $DEC^+NO_3^-$ at concentrations where aggregation is not observed will be necessary. From the current work, $DEC^+NO_3^-$ is known to aggregate at concentrations as low as 1 mM in chlorobenzene. By lowering the concentration of $DEC^+NO_3^-$ further and performing extractions, aggregation may be avoided and the full selectivity of $DEC^+NO_3^-$ may be demonstrated. However, in order to perform these experiments, a different method of quantification for the extracted anion, in this case ReO_4^-, needs to be used. The current research used ICP-AES to quantify ReO_4^- in the final aqueous phase, but the detection limit of rhenium using this technique is only 0.01 mM. Extractions using less than 1 mM $DEC^+NO_3^-$ would leave amounts of ReO_4^- in the final solution which would be well below this detection limit. Quantification techniques such as ion-chromatography or

radiometric methods would therefore have to be employed to perform these low-level extraction experiments.

Alternatively, a higher dielectric solvent could be used as the extractant media. Presumably, the large tetraalkylated ferrocenium cation would be better solvated in a more polar solvent, and thus less aggregation would occur. One such solvent may be 1-octanol. This solvent, though polar ($\varepsilon \cong 10$ at 25 °C), is still immiscible in water. The higher dielectric would certainly result in lower overall selectivity due to solvation effects; however, these effects should be equal for $DEC^{+}NO_3^{-}$ and $HEP^{+}NO_3^{-}$. Thus, if no aggregation is observed in 1-octanol, the true selectivities of each extractant could be compared at concentrations similar to those reported herein for chlorobenzene. Though 1-octanol is a suggested solvent, any moderately polar solvent ($\varepsilon \geq 10$) may work provided it is immiscible with water.

Synthesis of New Tetraalkylated Ferrocenes. The synthesis of a larger, more lipophilic ferrocene is currently being pursued in the Strauss Labs. The compound DoDEC, which has tertiary alkyl groups consisting of 12 carbon atom chains, is larger than DEC and has been isolated as an isomerically pure solid, although in a very small yield of < 5%.[10] The resulting product has been prepared in the same manner as HEP and DEC, but is a mixture of mono-, di-, tri-, and tetraalkylated species, and thus requires a very difficult separation. The purified compound has been characterized by ^{1}H-NMR and mass spectroscopy. One reason for incomplete reaction mixture may be the purity of the starting 2-chloro-2-methylundecane alkylating agent. Further work needs to be done in order to isolate DoDEC as pure product in good yield.

The usefulness of DoDEC would be in studying the selectivity of the tetraalkylated ferrocenium extractants. As proposed in both Chapters 4 and 5, the size of HEP and DEC have been predicted to have reached a point of "thermodynamic diminishing returns" for selectivity. The study of the ion-exchange properties of physisorbed DoDEC materials could determine if this point of diminishing returns has in

fact been reached. Functionalization of this molecule with an 11-thiolundecanoyl group and subsequent electrochemical selectivity experiments could also be used to study this phenomenon. It should be noted that liquid-liquid ion-exchange experiments should not be used for this study since aggregation almost certainly will be a factor for this larger, more lipophilic cationic extractant.

Functionalization of Tetraalkylated Ferrocenes. The advantage of the functionalization reactions developed and discussed in Chapter 3 is the ease of further functionalization. Though the goals in this work were the functionalization of surfaces or materials, functional groups could also be introduced into the tetraalkylated ferrocenes that provide for anion recognition. Several recent reviews discuss a variety of functional groups that recognize various anions by either shape selectivity, hydrogen bonding, electrostatic interactions, or a combination of all of these.[9,11] Such functional groups typically consist of amines, amides, guanidines, esters, carboxylic acids or a combination of these, and have been shown to be useful for the detection of a variety of anions. Further functionalization of some of the compounds synthesized and discussed in Chapter 2 could be designed to include some of these functional groups. The resulting combination of recognition with the selectivity already demonstrated for the tetraalkylated ferrocenium cations may result in further advancement of the R^2ER process for both remediation and detection. Furthermore, such functionalities may enable the detection and extraction of anions in water, such as phosphonates, that have previously been unextractable using the current R^2ER extractants.

Electrochemical Sensors. As proposed in Chapter 4, tetraalkylated ferrocenes should make good electrochemical sensors due to the large potential shifts observed for the oxidation of these ferrocenes in the presence of various anions. An obvious area of research for this application would be the lowering of detection limits to useful levels for the detection of pollutant anions. These detection limits are typically in the micromolar to nanomolar range for most anionic pollutants. Since these potential shifts grow smaller

as the concentration of the analyte anion decreases, it will be necessary to develop ways to increase the magnitude of the potential shift at these lower anion concentrations.

One possible way to maintain a large potential shift at low anion concentrations may be through the use of microelectrodes or microelectrode arrays that have been functionalized with the tetraalkylated ferrocenes. Also the introduction of anion recognition functionalities, as discussed above, would help to maintain a large potential shift as the anion concentrations grow smaller. Various electrochemical techniques may also be incorporated. Though chronoamperometry was discussed in Chapter 4, more sensitive methods such as differential pulse voltammetry may be needed for detections at these lower concentrations. Thin films of tetraalkylated ferrocenes may also be applicable to voltammetric stripping systems. In such a system, the oxidized ferrocenium cations would be allowed to ion-exchange at an oxidizing potential and then subsequent reduction of the thin film would allow for quantification of the anion being detected.

One last improvement to the electrochemical sensor would be to demonstrate long-term use and durability. Though thiol monolayers on gold are fairly stable, over time a significant amount of desorption is observed, especially if oxidation potentials greater than 0.8 V vs. Ag/AgCl are used. For this reason, a more durable sensor material will eventually be necessary. One such material may be the functionalization of indium-tin oxide (ITO). This conducting material can be functionalized with siloxy moieties through the formation of a covalent Si–O–ITO bond. The siloxy functionality could be incorporated into the tetraalkylated ferrocenes. Alternatively, the ITO surface could first be modified with a siloxane containing a reactive group and surface functionalization could then be accomplished by reaction of an appropriately functionalized ferrocene with this surface confined group. Both methods have been previously demonstrated.[12,13] This covalent bond would be much more durable then the currently used chemisorbed thiols, provided the sensor material was not used in basic media.

References

1. Clark, J. F.; Clark, D. L.; Whitener, G. D.; Schroeder, N. C.; Strauss, S. H. *Environ. Sci. Technol.* **1996**, *30*, 3124.
2. Clapsaddle, B. J.; Clark, J. F.; Clark, D. L.; Gansle, K. M.; Gash, A. E.; Miller, S. M.; Anderson, O. P.; Hughes, R. P.; Strauss, S. H., 2002 *Synthesis and Characterization of Polyalkylated Ferrocenes and Ferrocenium Salts.*
3. Chambliss, C. K.; Odom, M. A.; Morales, C. M. L.; Martin, C. R.; Strauss, S. H. *Anal. Chem.* **1998**, *70*, 757.
4. Odom, M. A. Development of Strategies for the Detection, Extraction, and Recovery of Aqueous Anions Using Highly Selective Redox-Recyclable Materials. Ph.D. Dissertation, Colorado State University, Fort Collins, CO, 2001.
5. Strauss, S. H.; Odom, M. A.; Hebert, G. N.; Clapsaddle, B. J., 2001 *ATR-FTIR Detection and Quantification of Anionic Pollutants in Water.*
6. Moyer, B. A.; Bonnesen, P. V. In *Supramolecular Chemistry of Anions*; Bianchi, A., Bowman-James, K., Garcia-Espana, E., Eds.; VCH: New York, 1997.
7. Hebert, G. N.; Strauss, S. H. *unpublished results.*
8. Rowe, G. K.; Creager, S. E. *Langmuir* **1991**, *7*, 2307.
9. Beer, P. D.; Gale, P. A. *Angew. Chem. Int. Ed. Eng.* **2001**, *40*, 486.
10. Clapsaddle, B. J.; Strauss, S. H., Colorado State University, Fort Collins, CO. Unpublished results, 2001.
11. Beer, P. D.; Gale, P. A.; Chen, G. Z. *J. Chem. Soc., Dalton Trans.* **1999**, 1897.
12. Chen, K.; Herr, B. R.; Singewald, E. T.; Mirkin, C. A. *Langmuir* **1992**, *8*, 2585.
13. Herr, B. R.; Mirkin, C. A. *J. Am. Chem. Soc.* **1994**, *116*, 1157.

Appendix A.

Structures, tables, and experimental data for the X-ray crystallographic structural determination of 1,1',3,3'-tetrakis(2-methyl-2-hexyl)ferrocene (HEP), 1,1',3,3'-tetrakis(2-methyl-2-nonyl)ferrocene (DEC), and 1,1',3,3'-tetrakis(2-methyl-2-nonyl)ferrocenium nitrate ($DEC^{+}NO_3^{-}$).

Table A.1. Crystal data and structure refinement for HEP.

Identification code	HEP	
Empirical formula	C38 H66 Fe	
Formula weight	578.76	
Temperature	170(2) K	
Wavelength	0.71073 Å	
Crystal system	Orthorhombic	
Space group	Fdd2	
Unit cell dimensions	a = 18.833(12) Å	α= 90°.
	b = 43.00(2) Å	β= 90°.
	c = 8.849(5) Å	γ = 90°.
Volume	7166(7) $Å^3$	
Z	8	
Density (calculated)	1.073 Mg/m^3	
Absorption coefficient	0.443 mm^{-1}	
F(000)	2560	
Crystal size	0.07 x 0.20 x 0.40 mm^3	
Theta range for data collection	1.89 to 28.27°.	
Index ranges	-23<=h<=24, -57<=k<=44, -11<=l<=11	
Reflections collected	11530	
Independent reflections	4237 [R(int) = 0.1002]	
Completeness to theta = 28.27°	98.8 %	
Refinement method	Full-matrix least-squares on F^2	
Data / restraints / parameters	4237 / 1 / 178	
Goodness-of-fit on F^2	0.756	
Final R indices [I>2sigma(I)]	R1 = 0.0726, wR2 = 0.1602	
R indices (all data)	R1 = 0.1362, wR2 = 0.1952	
Absolute structure parameter	0.67(4) Racemic Twin	
Largest diff. peak and hole	0.628 and -0.375 $e.Å^{-3}$	

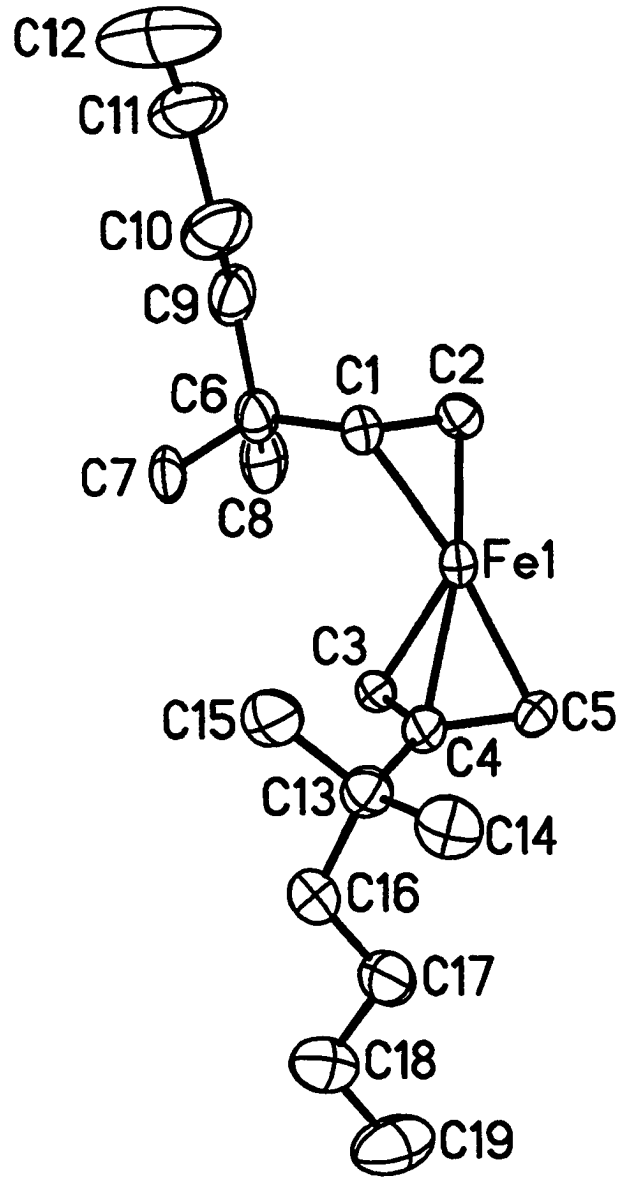

Figure A.1. Diagram showing the asymmetric unit of the HEP structure (50% probability ellipsoids). Hydrogen atoms have been omitted for clarity. HEP = 1,1',3,3'-tetrakis(2-methyl-2-hexyl)ferrocene.

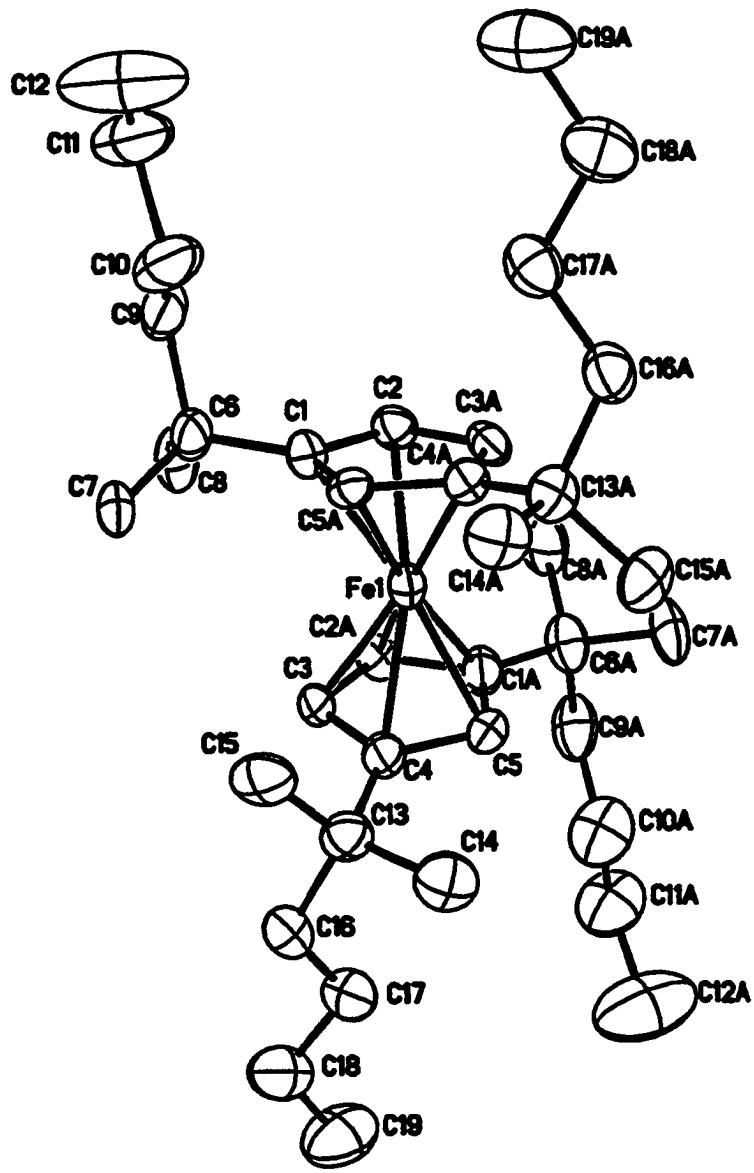

Figure A.2. Diagram showing the HEP structure (50% probability ellipsoids). Hydrogen atoms have been omitted for clarity. HEP = 1,1',3,3'-tetrakis(2-methyl-2-hexyl)ferrocene.

Table A.2. Atomic coordinates (x 10^4) and equivalent isotropic displacement parameters ($Å^2$x 10^3) for HEP. U(eq) is defined as one third of the trace of the orthogonalized U^{ij} tensor.

	x	y	z	U(eq)
Fe(1)	2500	2500	1443(1)	27(1)
C(1)	3257(3)	2189(1)	738(6)	35(1)
C(2)	2597(3)	2135(1)	23(7)	32(1)
C(3)	2920(3)	2933(1)	1109(6)	33(1)
C(4)	2599(3)	2929(1)	2570(7)	33(1)
C(5)	1872(2)	2852(1)	2317(6)	27(1)
C(6)	3968(3)	2231(1)	-57(6)	40(1)
C(7)	4504(3)	2395(1)	982(7)	49(2)
C(8)	3882(3)	2424(2)	-1502(7)	56(2)
C(9)	4244(3)	1908(1)	-525(8)	53(2)
C(10)	4393(4)	1686(2)	699(8)	66(2)
C(11)	4694(4)	1380(2)	121(10)	78(2)
C(12)	4911(6)	1161(2)	1278(12)	126(5)
C(13)	2950(3)	3037(1)	4031(6)	38(1)
C(14)	2439(3)	3009(2)	5356(6)	50(2)
C(15)	3619(3)	2847(1)	4396(6)	48(2)
C(16)	3189(3)	3378(1)	3797(7)	44(1)
C(17)	2624(3)	3615(1)	3371(8)	49(2)
C(18)	2947(4)	3932(1)	3022(8)	60(2)
C(19)	2396(4)	4176(2)	2707(10)	85(3)

Table A.3. Bond lengths [Å] and angles [°] for HEP.

Fe(1)-C(2)	2.019(6)	C(2)-Fe(1)-C(3)	125.7(2)
Fe(1)-C(2)#1	2.019(6)	C(2)#1-Fe(1)-C(3)	40.3(2)
Fe(1)-C(3)#1	2.044(5)	C(3)#1-Fe(1)-C(3)	163.4(3)
Fe(1)-C(3)	2.044(5)	C(2)-Fe(1)-C(1)#1	112.4(2)
Fe(1)-C(1)#1	2.052(5)	C(2)#1-Fe(1)-C(1)#1	40.6(2)
Fe(1)-C(1)	2.052(5)	C(3)#1-Fe(1)-C(1)#1	106.30(19)
Fe(1)-C(5)	2.070(5)	C(3)-Fe(1)-C(1)#1	68.4(2)
Fe(1)-C(5)#1	2.070(5)	C(2)-Fe(1)-C(1)	40.6(2)
Fe(1)-C(4)	2.105(6)	C(2)#1-Fe(1)-C(1)	112.4(2)
Fe(1)-C(4)#1	2.105(6)	C(3)#1-Fe(1)-C(1)	68.4(2)
C(1)-C(2)	1.414(7)	C(3)-Fe(1)-C(1)	106.30(19)
C(1)-C(5)#1	1.428(7)	C(1)#1-Fe(1)-C(1)	144.6(3)
C(1)-C(6)	1.522(7)	C(2)-Fe(1)-C(5)	148.48(19)
C(2)-C(3)#1	1.399(7)	C(2)#1-Fe(1)-C(5)	67.2(2)
C(3)-C(2)#1	1.399(7)	C(3)#1-Fe(1)-C(5)	119.9(2)
C(3)-C(4)	1.427(8)	C(3)-Fe(1)-C(5)	67.0(2)
C(4)-C(5)	1.426(7)	C(1)#1-Fe(1)-C(5)	40.55(19)
C(4)-C(13)	1.525(8)	C(1)-Fe(1)-C(5)	170.7(2)
C(5)-C(1)#1	1.428(7)	C(2)-Fe(1)-C(5)#1	67.2(2)
C(6)-C(8)	1.534(8)	C(2)#1-Fe(1)-C(5)#1	148.48(19)
C(6)-C(7)	1.537(7)	C(3)#1-Fe(1)-C(5)#1	67.0(2)
C(6)-C(9)	1.538(7)	C(3)-Fe(1)-C(5)#1	119.9(2)
C(9)-C(10)	1.472(9)	C(1)#1-Fe(1)-C(5)#1	170.7(2)
C(10)-C(11)	1.518(8)	C(1)-Fe(1)-C(5)#1	40.55(19)
C(11)-C(12)	1.451(12)	C(5)-Fe(1)-C(5)#1	136.1(3)
C(13)-C(14)	1.522(8)	C(2)-Fe(1)-C(4)	165.5(2)
C(13)-C(15)	1.536(7)	C(2)#1-Fe(1)-C(4)	67.7(2)
C(13)-C(16)	1.546(7)	C(3)#1-Fe(1)-C(4)	154.2(2)
C(16)-C(17)	1.523(8)	C(3)-Fe(1)-C(4)	40.2(2)
C(17)-C(18)	1.524(8)	C(1)#1-Fe(1)-C(4)	68.5(2)
C(18)-C(19)	1.503(9)	C(1)-Fe(1)-C(4)	130.82(19)
C(2)-Fe(1)-C(2)#1	103.1(3)	C(5)-Fe(1)-C(4)	39.94(18)
C(2)-Fe(1)-C(3)#1	40.3(2)	C(5)#1-Fe(1)-C(4)	114.4(2)
C(2)#1-Fe(1)-C(3)#1	125.7(2)	C(2)-Fe(1)-C(4)#1	67.7(2)

Table A.3. (continued)

C(2)#1-Fe(1)-C(4)#1	165.5(2)	C(3)-C(4)-Fe(1)	67.6(3)
C(3)#1-Fe(1)-C(4)#1	40.2(2)	C(13)-C(4)-Fe(1)	135.0(4)
C(3)-Fe(1)-C(4)#1	154.2(2)	C(4)-C(5)-C(1)#1	110.2(5)
C(1)#1-Fe(1)-C(4)#1	130.82(19)	C(4)-C(5)-Fe(1)	71.4(3)
C(1)-Fe(1)-C(4)#1	68.5(2)	C(1)#1-C(5)-Fe(1)	69.1(3)
C(5)-Fe(1)-C(4)#1	114.4(2)	C(1)-C(6)-C(8)	110.9(4)
C(5)#1-Fe(1)-C(4)#1	39.94(18)	C(1)-C(6)-C(7)	110.8(4)
C(4)-Fe(1)-C(4)#1	123.5(3)	C(8)-C(6)-C(7)	108.6(5)
C(2)-C(1)-C(5)#1	105.5(5)	C(1)-C(6)-C(9)	108.4(5)
C(2)-C(1)-C(6)	125.8(5)	C(8)-C(6)-C(9)	107.5(5)
C(5)#1-C(1)-C(6)	128.0(5)	C(7)-C(6)-C(9)	110.6(5)
C(2)-C(1)-Fe(1)	68.4(3)	C(10)-C(9)-C(6)	116.9(5)
C(5)#1-C(1)-Fe(1)	70.4(3)	C(9)-C(10)-C(11)	112.7(6)
C(6)-C(1)-Fe(1)	132.4(4)	C(12)-C(11)-C(10)	115.5(7)
C(3)#1-C(2)-C(1)	109.8(5)	C(14)-C(13)-C(4)	110.8(4)
C(3)#1-C(2)-Fe(1)	70.8(3)	C(14)-C(13)-C(15)	108.3(5)
C(1)-C(2)-Fe(1)	71.0(3)	C(4)-C(13)-C(15)	111.9(4)
C(2)#1-C(3)-C(4)	108.9(4)	C(14)-C(13)-C(16)	111.2(5)
C(2)#1-C(3)-Fe(1)	68.9(3)	C(4)-C(13)-C(16)	107.5(5)
C(4)-C(3)-Fe(1)	72.2(3)	C(15)-C(13)-C(16)	107.1(4)
C(5)-C(4)-C(3)	105.5(5)	C(17)-C(16)-C(13)	117.7(4)
C(5)-C(4)-C(13)	128.4(5)	C(16)-C(17)-C(18)	111.7(5)
C(3)-C(4)-C(13)	125.4(4)	C(19)-C(18)-C(17)	112.7(6)
C(5)-C(4)-Fe(1)	68.7(3)		

Symmetry transformations used to generate equivalent atoms: #1 -x+1/2,-y+1/2,z

Table A.4. Anisotropic displacement parameters ($Å^2 x\ 10^3$) for HEP. The anisotropic displacement factor exponent takes the form: $-2\pi^2[\ h^2\ a^{*2}U^{11} + ...\ + 2\ h\ k\ a^*\ b^*\ U^{12}]$

	U^{11}	U^{22}	U^{33}	U^{23}	U^{13}	U^{12}
Fe(1)	21(1)	33(1)	27(1)	0	0	-3(1)
C(1)	27(2)	36(3)	42(3)	-3(2)	-3(2)	-2(2)
C(2)	36(3)	33(3)	27(3)	-5(2)	1(2)	-4(2)
C(3)	27(2)	24(3)	48(4)	-1(2)	7(2)	-3(2)
C(4)	30(3)	30(3)	38(3)	1(2)	-1(2)	1(2)
C(5)	27(3)	28(3)	25(3)	5(2)	3(2)	5(2)
C(6)	31(3)	50(3)	38(3)	-12(3)	6(2)	-4(2)
C(7)	21(2)	57(4)	68(5)	-19(3)	7(2)	-8(2)
C(8)	40(3)	79(5)	49(4)	3(3)	13(3)	-11(3)
C(9)	33(3)	65(4)	60(4)	-20(3)	5(3)	2(3)
C(10)	69(5)	64(5)	66(5)	-24(4)	2(4)	20(3)
C(11)	90(5)	55(5)	88(6)	-22(4)	-8(5)	23(4)
C(12)	224(13)	64(6)	90(8)	-22(5)	-35(8)	47(7)
C(13)	39(3)	41(3)	33(3)	-7(2)	-3(3)	3(2)
C(14)	65(4)	55(4)	32(3)	-2(3)	-3(3)	-1(3)
C(15)	54(3)	51(4)	40(3)	-15(3)	-18(3)	6(3)
C(16)	41(3)	42(3)	51(4)	-5(3)	-2(3)	-5(2)
C(17)	51(4)	44(4)	51(4)	-7(3)	2(3)	-5(3)
C(18)	78(4)	49(4)	53(4)	-5(3)	7(3)	-3(3)
C(19)	114(7)	50(4)	90(6)	9(4)	28(5)	19(4)

Table A.5. Hydrogen coordinates (x 10^4) and isotropic displacement parameters ($Å^2$x 10^3) for HEP.

	x	y	z	U(eq)
H(2)	2514	2142	-1092	38
H(3)	3431	2979	896	39
H(5)	1509	2824	3130	32
H(7A)	4958	2417	454	73
H(7B)	4572	2271	1900	73
H(7C)	4322	2601	1255	73
H(8A)	3539	2323	-2174	84
H(8B)	4342	2441	-2015	84
H(8C)	3711	2633	-1239	84
H(9A)	3890	1813	-1211	63
H(9B)	4686	1938	-1112	63
H(10A)	3948	1643	1259	80
H(10B)	4735	1780	1413	80
H(11A)	4332	1279	-524	93
H(11B)	5110	1427	-525	93
H(12A)	5098	972	798	189
H(12B)	4501	1107	1907	189
H(12C)	5281	1255	1909	189
H(14A)	2674	3081	6281	75
H(14B)	2297	2791	5478	75
H(14C)	2018	3137	5164	75
H(15A)	3831	2924	5336	72
H(15B)	3962	2868	3569	72
H(15C)	3491	2627	4516	72
H(16A)	3418	3449	4743	53
H(16B)	3557	3380	2998	53
H(17A)	2282	3637	4215	58
H(17B)	2360	3540	2475	58
H(18A)	3241	3999	3891	72
H(18B)	3263	3913	2133	72
H(19A)	2631	4375	2486	127

Table A.5. (continued)

H(19B)	2089	4201	3594	127
H(19C)	2109	4113	1836	127

Table A.6. Crystal data and structure refinement for DEC.

Identification code	DEC	
Empirical formula	C50 H90 Fe	
Formula weight	747.07	
Temperature	170(2) K	
Wavelength	0.71073 Å	
Crystal system	Monoclinic	
Space group	C2/c	
Unit cell dimensions	a = 18.7606(8) Å	α= 90°.
	b = 8.7418(4) Å	β= 101.7360(10)°.
	c = 28.8086(12) Å	γ = 90°.
Volume	4625.9(3) $Å^3$	
Z	4	
Density (calculated)	1.073 Mg/m^3	
Absorption coefficient	0.356 mm^{-1}	
F(000)	1664	
Crystal size	0.09 x 0.30 x 0.40 mm^3	
Theta range for data collection	1.44 to 28.44°.	
Index ranges	-24<=h<=19, -11<=k<=11, -35<=l<=32	
Reflections collected	11942	
Independent reflections	5317 [R(int) = 0.0934]	
Absorption correction	SADABS	
Refinement method	Full-matrix least-squares on F^2	
Data / restraints / parameters	5316 / 0 / 231	
Goodness-of-fit on F^2	0.865	
Final R indices [I>2sigma(I)]	R1 = 0.0675, wR2 = 0.1385	
R indices (all data)	R1 = 0.1387, wR2 = 0.1622	
Largest diff. peak and hole	1.450 and -0.441 $e.Å^{-3}$	

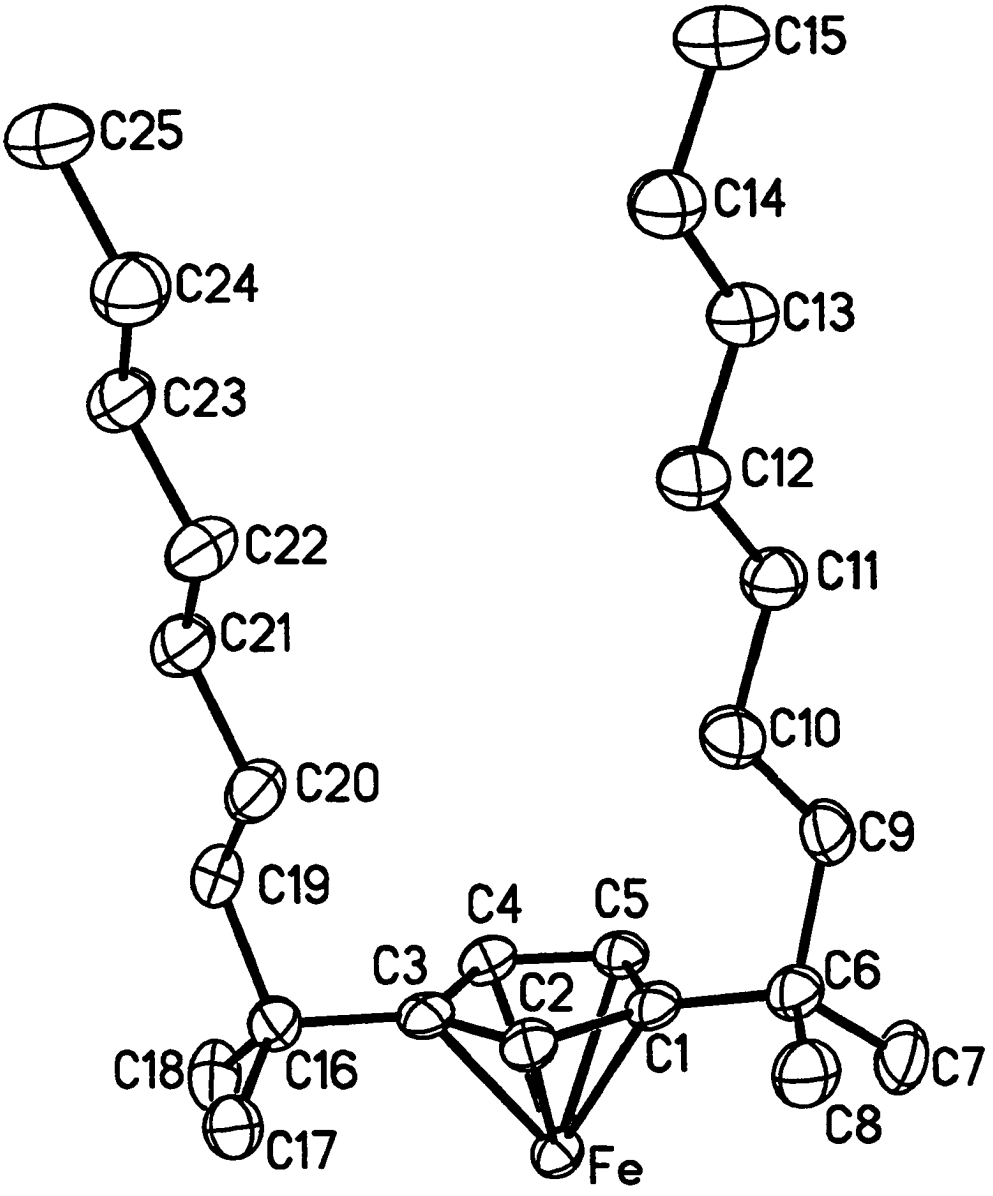

Figure A.3. Diagram showing the asymmetric unit of the DEC structure (50% probability ellipsoids). Hydrogen atoms have been omitted for clarity. DEC = 1,1',3,3'-tetrakis(2-methyl-2-nonyl)ferrocene.

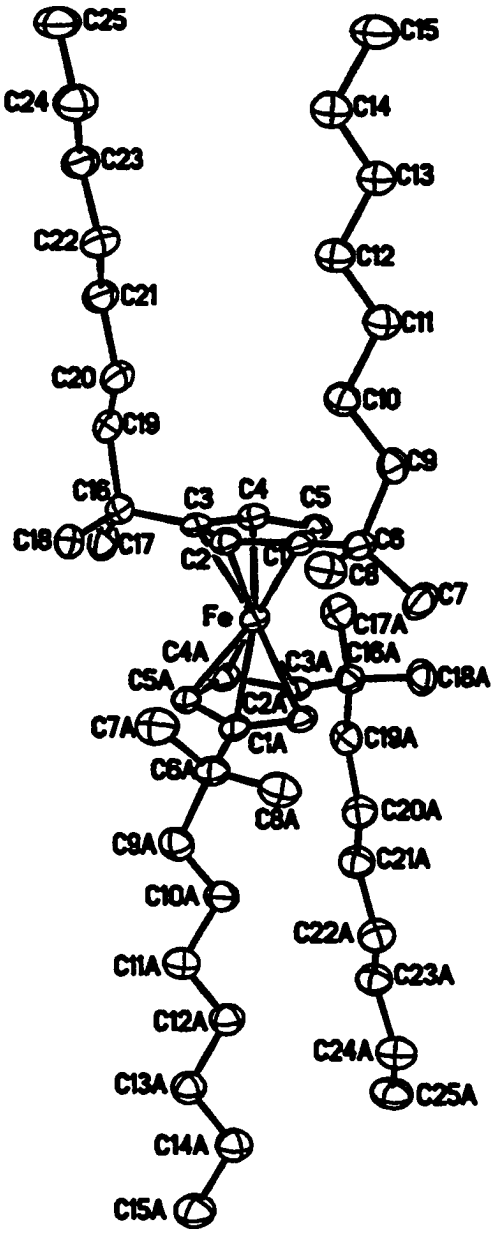

Figure A.4. Diagram showing the DEC structure (50% probability ellipsoids). Hydrogen atoms have been omitted for clarity. DEC = 1,1',3,3'-tetrakis(2-methyl-2-nonyl)ferrocene.

Table A.7. Atomic coordinates (x 10^4) and equivalent isotropic displacement parameters ($Å^2$x 10^3) for DEC. U(eq) is defined as one third of the trace of the orthogonalized U^{ij} tensor.

	x	y	z	U(eq)
Fe	5000	4666(1)	2500	26(1)
C(1)	4831(2)	5819(3)	1847(1)	27(1)
C(2)	4163(2)	5515(4)	1990(1)	27(1)
C(3)	4072(2)	3937(4)	2046(1)	28(1)
C(4)	4708(2)	3210(4)	1941(1)	29(1)
C(5)	5166(2)	4355(3)	1822(1)	28(1)
C(6)	5105(2)	7288(4)	1662(1)	31(1)
C(7)	5902(2)	7593(4)	1887(1)	46(1)
C(8)	4652(2)	8652(4)	1776(1)	41(1)
C(9)	5036(2)	7160(4)	1124(1)	34(1)
C(10)	4283(2)	6889(4)	824(1)	36(1)
C(11)	4277(2)	6770(4)	300(1)	37(1)
C(12)	3529(2)	6756(4)	-12(1)	39(1)
C(13)	3524(2)	6735(4)	-540(1)	38(1)
C(14)	2778(2)	6832(4)	-857(1)	43(1)
C(15)	2793(2)	6831(5)	-1380(1)	53(1)
C(16)	3415(2)	3073(4)	2140(1)	29(1)
C(17)	3636(2)	1726(4)	2477(1)	42(1)
C(18)	2929(2)	4140(4)	2362(1)	38(1)
C(19)	2982(2)	2414(4)	1673(1)	34(1)
C(20)	2654(2)	3516(4)	1282(1)	37(1)
C(21)	2219(2)	2693(4)	855(1)	40(1)
C(22)	1807(2)	3702(4)	470(1)	42(1)
C(23)	1365(2)	2819(4)	56(1)	41(1)
C(24)	917(2)	3793(4)	-329(1)	50(1)
C(25)	497(2)	2885(5)	-739(1)	57(1)

Table A.8. Bond lengths [Å] and angles [°] for DEC.

Fe-C(4)	2.037(3)	C(24)-C(25)	1.508(5)
Fe-C(4)#1	2.037(3)	C(4)-Fe-C(4)#1	102.7(2)
Fe-C(3)	2.054(3)	C(4)-Fe-C(3)	41.14(12)
Fe-C(3)#1	2.054(3)	C(4)#1-Fe-C(3)	111.46(13)
Fe-C(2)#1	2.058(3)	C(4)-Fe-C(3)#1	111.46(13)
Fe-C(2)	2.058(3)	C(4)#1-Fe-C(3)#1	41.14(12)
Fe-C(5)	2.059(3)	C(3)-Fe-C(3)#1	143.9(2)
Fe-C(5)#1	2.059(3)	C(4)-Fe-C(2)#1	146.35(12)
Fe-C(1)	2.100(3)	C(4)#1-Fe-C(2)#1	67.55(12)
Fe-C(1)#1	2.100(3)	C(3)-Fe-C(2)#1	172.24(12)
C(1)-C(2)	1.421(4)	C(3)#1-Fe-C(2)#1	39.90(12)
C(1)-C(5)	1.435(4)	C(4)-Fe-C(2)	67.55(12)
C(1)-C(6)	1.520(4)	C(4)#1-Fe-C(2)	146.34(12)
C(2)-C(3)	1.403(4)	C(3)-Fe-C(2)	39.90(12)
C(3)-C(4)	1.438(4)	C(3)#1-Fe-C(2)	172.24(12)
C(3)-C(16)	1.516(4)	C(2)#1-Fe-C(2)	137.7(2)
C(4)-C(5)	1.407(4)	C(4)-Fe-C(5)	40.17(12)
C(6)-C(7)	1.527(4)	C(4)#1-Fe-C(5)	126.81(13)
C(6)-C(9)	1.531(4)	C(3)-Fe-C(5)	68.13(12)
C(6)-C(8)	1.538(4)	C(3)#1-Fe-C(5)	106.89(12)
C(9)-C(10)	1.519(4)	C(2)#1-Fe-C(5)	118.94(12)
C(10)-C(11)	1.510(5)	C(2)-Fe-C(5)	67.13(12)
C(11)-C(12)	1.505(4)	C(4)-Fe-C(5)#1	126.80(13)
C(12)-C(13)	1.521(5)	C(4)#1-Fe-C(5)#1	40.17(12)
C(13)-C(14)	1.510(4)	C(3)-Fe-C(5)#1	106.89(12)
C(14)-C(15)	1.513(5)	C(3)#1-Fe-C(5)#1	68.14(12)
C(16)-C(17)	1.529(4)	C(2)#1-Fe-C(5)#1	67.13(12)
C(16)-C(18)	1.532(4)	C(2)-Fe-C(5)#1	118.94(12)
C(16)-C(19)	1.536(4)	C(5)-Fe-C(5)#1	164.8(2)
C(19)-C(20)	1.514(4)	C(4)-Fe-C(1)	67.99(12)
C(20)-C(21)	1.513(4)	C(4)#1-Fe-C(1)	167.05(12)
C(21)-C(22)	1.502(5)	C(3)-Fe-C(1)	67.98(12)
C(22)-C(23)	1.517(4)	C(3)#1-Fe-C(1)	132.28(12)
C(23)-C(24)	1.510(5)	C(2)#1-Fe-C(1)	114.84(12)

Table A.8. (continued)

C(2)-Fe-C(1)	39.97(11)	C(3)-C(4)-Fe	70.1(2)
C(5)-Fe-C(1)	40.36(11)	C(4)-C(5)-C(1)	109.0(3)
C(5)#1-Fe-C(1)	152.73(12)	C(4)-C(5)-Fe	69.1(2)
C(4)-Fe-C(1)#1	167.05(12)	C(1)-C(5)-Fe	71.4(2)
C(4)#1-Fe-C(1)#1	67.98(12)	C(1)-C(6)-C(7)	111.7(3)
C(3)-Fe-C(1)#1	132.28(12)	C(1)-C(6)-C(9)	109.2(3)
C(3)#1-Fe-C(1)#1	67.98(12)	C(7)-C(6)-C(9)	108.4(3)
C(2)#1-Fe-C(1)#1	39.97(11)	C(1)-C(6)-C(8)	109.7(3)
C(2)-Fe-C(1)#1	114.84(12)	C(7)-C(6)-C(8)	108.0(3)
C(5)-Fe-C(1)#1	152.73(13)	C(9)-C(6)-C(8)	109.6(3)
C(5)#1-Fe-C(1)#1	40.36(11)	C(10)-C(9)-C(6)	117.7(3)
C(1)-Fe-C(1)#1	122.6(2)	C(11)-C(10)-C(9)	113.4(3)
C(2)-C(1)-C(5)	105.7(3)	C(12)-C(11)-C(10)	114.4(3)
C(2)-C(1)-C(6)	129.9(3)	C(11)-C(12)-C(13)	114.4(3)
C(5)-C(1)-C(6)	123.5(3)	C(14)-C(13)-C(12)	114.8(3)
C(2)-C(1)-Fe	68.4(2)	C(13)-C(14)-C(15)	113.5(3)
C(5)-C(1)-Fe	68.3(2)	C(3)-C(16)-C(17)	111.8(3)
C(6)-C(1)-Fe	136.1(2)	C(3)-C(16)-C(18)	110.2(3)
C(3)-C(2)-C(1)	110.6(3)	C(17)-C(16)-C(18)	108.1(3)
C(3)-C(2)-Fe	69.9(2)	C(3)-C(16)-C(19)	109.6(3)
C(1)-C(2)-Fe	71.6(2)	C(17)-C(16)-C(19)	107.1(3)
C(2)-C(3)-C(4)	106.5(3)	C(18)-C(16)-C(19)	109.9(3)
C(2)-C(3)-C(16)	129.3(3)	C(20)-C(19)-C(16)	118.4(3)
C(4)-C(3)-C(16)	123.8(3)	C(21)-C(20)-C(19)	111.9(3)
C(2)-C(3)-Fe	70.2(2)	C(22)-C(21)-C(20)	115.7(3)
C(4)-C(3)-Fe	68.8(2)	C(21)-C(22)-C(23)	113.5(3)
C(16)-C(3)-Fe	131.0(2)	C(24)-C(23)-C(22)	115.1(3)
C(5)-C(4)-C(3)	108.2(3)	C(25)-C(24)-C(23)	113.8(3)
C(5)-C(4)-Fe	70.7(2)		

Symmetry transformations used to generate equivalent atoms: #1-x+1,y,-z+1/2

Table A.9. Anisotropic displacement parameters ($Å^2 x\ 10^3$) for DEC. The anisotropic displacement factor exponent takes the form: $-2\pi^2[\ h^2\ a^{*2}U^{11} + ... + 2\ h\ k\ a^*\ b^*\ U^{12}\ ]$

	U^{11}	U^{22}	U^{33}	U^{23}	U^{13}	U^{12}
Fe	24(1)	29(1)	23(1)	0	-1(1)	0
C(1)	22(2)	34(2)	21(2)	-3(2)	-4(1)	-1(1)
C(2)	23(2)	31(2)	22(2)	1(2)	-3(1)	2(1)
C(3)	24(2)	38(2)	17(2)	-1(2)	-4(1)	0(1)
C(4)	28(2)	29(2)	25(2)	-4(2)	-2(1)	2(1)
C(5)	25(2)	35(2)	21(2)	-2(2)	1(1)	2(1)
C(6)	31(2)	33(2)	26(2)	-1(2)	-1(1)	-3(1)
C(7)	39(2)	51(2)	43(2)	5(2)	-2(2)	-20(2)
C(8)	59(2)	27(2)	36(2)	2(2)	6(2)	-3(2)
C(9)	36(2)	31(2)	34(2)	6(2)	8(2)	-5(1)
C(10)	37(2)	41(2)	29(2)	5(2)	3(2)	0(2)
C(11)	43(2)	35(2)	31(2)	1(2)	3(2)	-1(2)
C(12)	41(2)	43(2)	31(2)	2(2)	2(2)	2(2)
C(13)	40(2)	40(2)	32(2)	-1(2)	3(2)	1(2)
C(14)	46(2)	46(2)	35(2)	1(2)	3(2)	1(2)
C(15)	56(3)	66(3)	32(3)	-3(2)	-3(2)	5(2)
C(16)	27(2)	31(2)	28(2)	0(2)	5(1)	-1(1)
C(17)	37(2)	41(2)	49(3)	5(2)	9(2)	-8(2)
C(18)	28(2)	50(2)	37(2)	-6(2)	9(2)	-3(2)
C(19)	31(2)	36(2)	37(2)	-3(2)	7(2)	-9(2)
C(20)	34(2)	37(2)	36(2)	-4(2)	1(2)	-6(2)
C(21)	40(2)	42(2)	35(2)	-1(2)	1(2)	-7(2)
C(22)	43(2)	41(2)	36(2)	-8(2)	-2(2)	-6(2)
C(23)	41(2)	43(2)	34(2)	-1(2)	-1(2)	-8(2)
C(24)	58(3)	48(2)	40(3)	4(2)	1(2)	-6(2)
C(25)	61(3)	71(3)	31(3)	1(2)	-6(2)	-7(2)

Table A.10. Hydrogen coordinates (x 10^4) and isotropic displacement parameters ($Å^2$x 10^3) for DEC.

	x	y	z	U(eq)
H(2A)	3810(2)	6316(4)	2048(1)	32
H(4A)	4803(2)	2084(4)	1946(1)	35
H(5A)	5649(2)	4177(3)	1734(1)	33
H(7A)	6060(2)	8545(4)	1759(1)	68
H(7B)	6203(2)	6744(4)	1814(1)	68
H(7C)	5956(2)	7686(4)	2231(1)	68
H(8A)	4831(2)	9596(4)	1655(1)	62
H(8B)	4697(2)	8731(4)	2120(1)	62
H(8C)	4140(2)	8498(4)	1625(1)	62
H(9A)	5230(2)	8114(4)	1012(1)	40
H(9B)	5355(2)	6313(4)	1063(1)	40
H(10A)	4082(2)	5932(4)	930(1)	43
H(10B)	3960(2)	7739(4)	876(1)	43
H(11A)	4553(2)	7644(4)	207(1)	44
H(11B)	4534(2)	5821(4)	243(1)	44
H(12A)	3261(2)	7673(4)	60(1)	47
H(12B)	3264(2)	5845(4)	67(1)	47
H(13A)	3820(2)	7604(4)	-615(1)	45
H(13B)	3762(2)	5781(4)	-616(1)	45
H(14A)	2536(2)	7780(4)	-781(1)	52
H(14B)	2482(2)	5954(4)	-788(1)	52
H(15A)	2294(2)	6896(5)	-1565(1)	80
H(15B)	3020(2)	5884(5)	-1460(1)	80
H(15C)	3074(2)	7711(5)	-1453(1)	80
H(17A)	3199(2)	1196(4)	2529(1)	64
H(17B)	3914(2)	2104(4)	2781(1)	64
H(17C)	3937(2)	1014(4)	2338(1)	64
H(18A)	2507(2)	3569(4)	2421(1)	57
H(18B)	2763(2)	4989(4)	2145(1)	57
H(18C)	3207(2)	4544(4)	2662(1)	57
H(19A)	3307(2)	1711(4)	1544(1)	41

Table A.10. (continued)

H(19B)	2581(2)	1788(4)	1749(1)	41
H(20A)	2334(2)	4246(4)	1404(1)	44
H(20B)	3049(2)	4108(4)	1184(1)	44
H(21A)	2556(2)	2044(4)	718(1)	48
H(21B)	1867(2)	2005(4)	964(1)	48
H(22A)	2157(2)	4368(4)	351(1)	50
H(22B)	1476(2)	4369(4)	606(1)	50
H(23A)	1701(2)	2185(4)	-86(1)	49
H(23B)	1033(2)	2117(4)	179(1)	49
H(24A)	571(2)	4410(4)	-190(1)	60
H(24B)	1246(2)	4511(4)	-449(1)	60
H(25A)	220(2)	3584(5)	-975(1)	85
H(25B)	161(2)	2189(5)	-625(1)	85
H(25C)	836(2)	2290(5)	-885(1)	85

Table A.11. Crystal data and structure refinement for $DEC^{+}NO_3^{-}$.

Identification code	$DEC^{+}NO_3^{-}$	
Empirical formula	C50 H90 Fe N O3	
Formula weight	809.08	
Temperature	177(2) K	
Wavelength	0.71073 Å	
Crystal system	Monoclinic	
Space group	P2/n	
Unit cell dimensions	a = 9.3903(15) Å	α= 90°.
	b = 8.6829(14) Å	β= 93.772(3)°.
	c = 29.713(5) Å	γ = 90°.
Volume	2417.4(7) $Å^3$	
Z	2	
Density (calculated)	1.112 Mg/m^3	
Absorption coefficient	0.351 mm^{-1}	
F(000)	894	
Crystal size	0.20 x 0.25 x 0.30 mm^3	
Theta range for data collection	3.09 to 23.30°.	
Index ranges	-10<=h<=10, -9<=k<=9, -33<=l<=32	
Reflections collected	14904	
Independent reflections	3481 [R(int) = 0.0688]	
Completeness to theta = 23.30°	99.6 %	
Absorption correction	None	
Refinement method	Full-matrix least-squares on F^2	
Data / restraints / parameters	3481 / 0 / 250	
Goodness-of-fit on F^2	1.084	
Final R indices [I>2sigma(I)]	R1 = 0.0580, wR2 = 0.1158	
R indices (all data)	R1 = 0.0817, wR2 = 0.1242	
Largest diff. peak and hole	0.701 and -0.540 $e.Å^{-3}$	

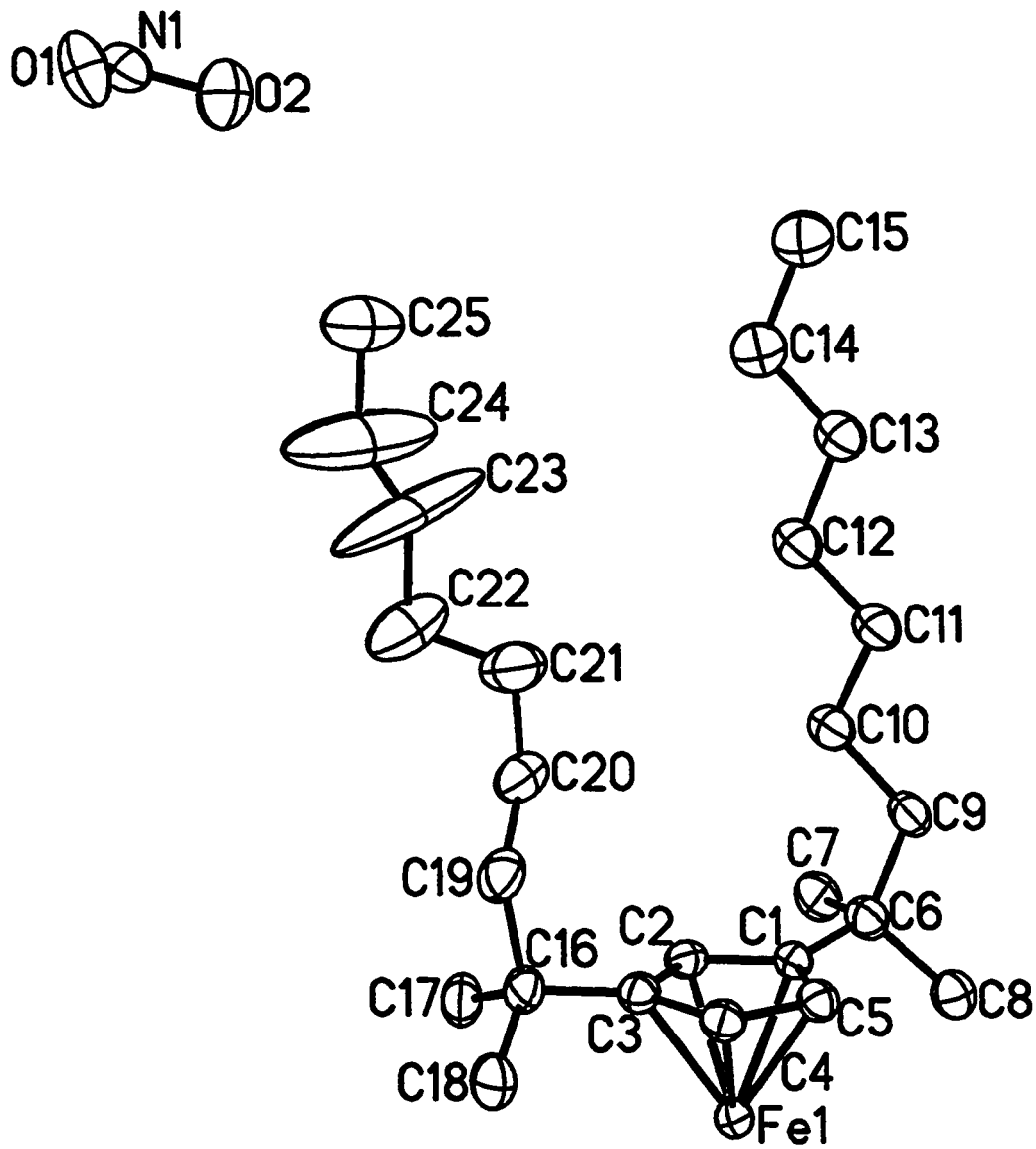

Figure A.5. Diagram showing the asymmetric unit of the $DEC^{+}NO_3^{-}$ structure (50% probability ellipsoids). Hydrogen atoms have been omitted for clarity. DEC = 1,1',3,3'-tetrakis(2-methyl-2-nonyl)ferrocene.

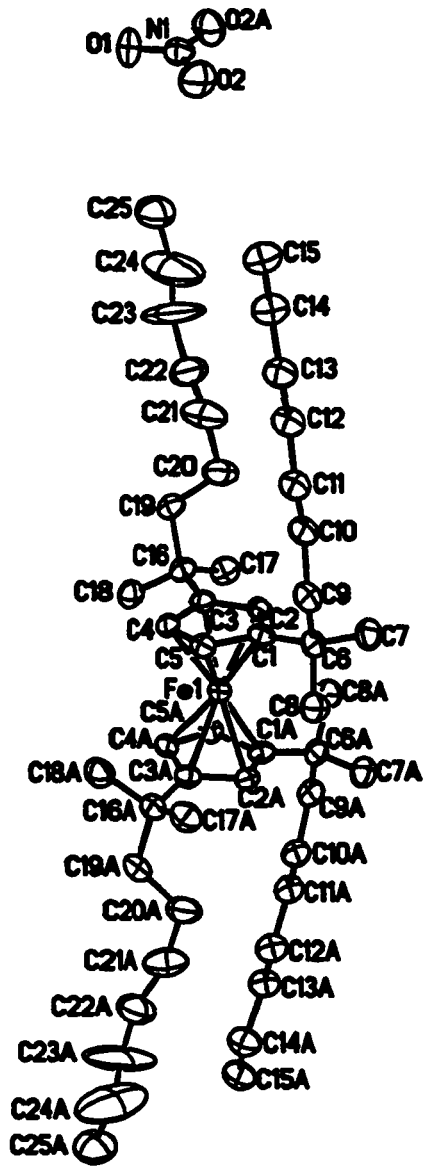

Figure A.6. Diagram showing the $DEC^{+}NO_3^{-}$ structure (50% probability ellipsoids). Hydrogen atoms have been omitted for clarity. DEC = 1,1',3,3'-tetrakis(2-methyl-2-nonyl)ferrocene.

Table A.12. Atomic coordinates (x 10^4) and equivalent isotropic displacement parameters ($Å^2$x 10^3) for $DEC^+NO_3^-$. U(eq) is defined as one third of the trace of the orthogonalized U^{ij} tensor.

	x	y	z	U(eq)
Fe(1)	2500	7633(1)	7500	26(1)
C(1)	1014(3)	8784(4)	7026(1)	28(1)
C(2)	2345(3)	8560(4)	6838(1)	27(1)
C(3)	2682(3)	6966(4)	6820(1)	28(1)
C(4)	1543(3)	6189(4)	7019(1)	30(1)
C(5)	528(3)	7285(4)	7146(1)	29(1)
C(6)	151(3)	10258(4)	7049(1)	33(1)
C(7)	1038(4)	11673(4)	6946(1)	41(1)
C(8)	-437(4)	10460(4)	7516(1)	43(1)
C(9)	-1129(3)	10104(4)	6695(1)	37(1)
C(10)	-757(4)	9838(4)	6208(1)	40(1)
C(11)	-2051(4)	9612(4)	5880(1)	40(1)
C(12)	-1667(4)	9280(5)	5405(1)	45(1)
C(13)	-2943(4)	9057(5)	5065(1)	44(1)
C(14)	-2543(4)	8643(5)	4594(1)	53(1)
C(15)	-3819(4)	8470(5)	4258(1)	58(1)
C(16)	3879(4)	6201(4)	6590(1)	33(1)
C(17)	5187(3)	7265(4)	6574(1)	41(1)
C(18)	4343(4)	4694(4)	6824(1)	42(1)
C(19)	3291(4)	5803(4)	6102(1)	42(1)
C(20)	2837(5)	7150(5)	5801(1)	58(1)
C(21)	2065(5)	6685(7)	5358(1)	75(2)
C(22)	2946(6)	6021(6)	5017(2)	79(2)
C(23)	2033(12)	5571(12)	4585(2)	218(6)
C(24)	2141(10)	5466(11)	4237(2)	196(5)
C(25)	1228(5)	4970(6)	3834(2)	81(2)
O(1)	2500	3663(4)	2500	50(1)
O(2)	1708(3)	5805(3)	2747(1)	66(1)
N(1)	2500	5103(6)	2500	41(1)

Table A.13. Bond lengths [Å] and angles [°] for $DEC^{+}NO_3^{-}$.

Fe(1)-C(4)	2.063(3)	C(24)-C(25)	1.492(7)
Fe(1)-C(4)#1	2.063(3)	O(1)-N(1)	1.250(5)
Fe(1)-C(5)	2.090(3)	O(2)-N(1)	1.238(3)
Fe(1)-C(5)#1	2.090(3)	N(1)-O(2)#2	1.238(3)
Fe(1)-C(3)	2.119(3)	C(4)-Fe(1)-C(4)#1	105.1(2)
Fe(1)-C(3)#1	2.119(3)	C(4)-Fe(1)-C(5)	39.85(12)
Fe(1)-C(2)	2.123(3)	C(4)#1-Fe(1)-C(5)	126.32(13)
Fe(1)-C(2)#1	2.123(3)	C(4)-Fe(1)-C(5)#1	126.32(13)
Fe(1)-C(1)#1	2.161(3)	C(4)#1-Fe(1)-C(5)#1	39.85(12)
Fe(1)-C(1)	2.161(3)	C(5)-Fe(1)-C(5)#1	163.41(18)
C(1)-C(2)	1.417(4)	C(4)-Fe(1)-C(3)	39.84(12)
C(1)-C(5)	1.431(4)	C(4)#1-Fe(1)-C(3)	115.85(13)
C(1)-C(6)	1.518(5)	C(5)-Fe(1)-C(3)	66.74(12)
C(2)-C(3)	1.421(5)	C(5)#1-Fe(1)-C(3)	108.43(12)
C(3)-C(4)	1.426(4)	C(4)-Fe(1)-C(3)#1	115.85(14)
C(3)-C(16)	1.508(4)	C(4)#1-Fe(1)-C(3)#1	39.84(12)
C(4)-C(5)	1.416(4)	C(5)-Fe(1)-C(3)#1	108.43(13)
C(6)-C(7)	1.526(5)	C(5)#1-Fe(1)-C(3)#1	66.74(12)
C(6)-C(8)	1.537(5)	C(3)-Fe(1)-C(3)#1	148.32(18)
C(6)-C(9)	1.550(5)	C(4)-Fe(1)-C(2)	65.65(13)
C(9)-C(10)	1.526(5)	C(4)#1-Fe(1)-C(2)	150.87(13)
C(10)-C(11)	1.520(5)	C(5)-Fe(1)-C(2)	65.38(12)
C(11)-C(12)	1.509(5)	C(5)#1-Fe(1)-C(2)	121.74(13)
C(12)-C(13)	1.527(5)	C(3)-Fe(1)-C(2)	39.15(12)
C(13)-C(14)	1.516(5)	C(3)#1-Fe(1)-C(2)	169.29(12)
C(14)-C(15)	1.517(5)	C(4)-Fe(1)-C(2)#1	150.87(13)
C(16)-C(18)	1.531(5)	C(4)#1-Fe(1)-C(2)#1	65.65(13)
C(16)-C(17)	1.540(5)	C(5)-Fe(1)-C(2)#1	121.74(12)
C(16)-C(19)	1.556(5)	C(5)#1-Fe(1)-C(2)#1	65.38(12)
C(19)-C(20)	1.516(5)	C(3)-Fe(1)-C(2)#1	169.29(13)
C(20)-C(21)	1.515(5)	C(3)#1-Fe(1)-C(2)#1	39.15(12)
C(21)-C(22)	1.468(6)	C(2)-Fe(1)-C(2)#1	135.42(18)
C(22)-C(23)	1.545(8)	C(4)-Fe(1)-C(1)#1	164.99(12)
C(23)-C(24)	1.050(8)	C(4)#1-Fe(1)-C(1)#1	66.20(13)

Table A.13. (continued)

C(5)-Fe(1)-C(1)#1	155.14(13)	C(3)-C(4)-Fe(1)	72.22(18)
C(5)#1-Fe(1)-C(1)#1	39.30(12)	C(4)-C(5)-C(1)	108.3(3)
C(3)-Fe(1)-C(1)#1	131.15(12)	C(4)-C(5)-Fe(1)	69.01(18)
C(3)#1-Fe(1)-C(1)#1	66.08(12)	C(1)-C(5)-Fe(1)	73.02(18)
C(2)-Fe(1)-C(1)#1	115.50(13)	C(1)-C(6)-C(7)	111.7(3)
C(2)#1-Fe(1)-C(1)#1	38.61(12)	C(1)-C(6)-C(8)	111.1(3)
C(4)-Fe(1)-C(1)	66.20(13)	C(7)-C(6)-C(8)	108.7(3)
C(4)#1-Fe(1)-C(1)	164.99(13)	C(1)-C(6)-C(9)	106.9(3)
C(5)-Fe(1)-C(1)	39.30(12)	C(7)-C(6)-C(9)	110.1(3)
C(5)#1-Fe(1)-C(1)	155.14(13)	C(8)-C(6)-C(9)	108.3(3)
C(3)-Fe(1)-C(1)	66.08(12)	C(10)-C(9)-C(6)	116.1(3)
C(3)#1-Fe(1)-C(1)	131.15(12)	C(11)-C(10)-C(9)	113.8(3)
C(2)-Fe(1)-C(1)	38.61(12)	C(12)-C(11)-C(10)	113.3(3)
C(2)#1-Fe(1)-C(1)	115.50(12)	C(11)-C(12)-C(13)	114.6(3)
C(1)#1-Fe(1)-C(1)	124.90(18)	C(14)-C(13)-C(12)	114.1(3)
C(2)-C(1)-C(5)	106.1(3)	C(15)-C(14)-C(13)	113.6(3)
C(2)-C(1)-C(6)	128.3(3)	C(3)-C(16)-C(18)	111.6(3)
C(5)-C(1)-C(6)	125.2(3)	C(3)-C(16)-C(17)	111.6(3)
C(2)-C(1)-Fe(1)	69.22(18)	C(18)-C(16)-C(17)	108.8(3)
C(5)-C(1)-Fe(1)	67.68(17)	C(3)-C(16)-C(19)	106.9(3)
C(6)-C(1)-Fe(1)	133.2(2)	C(18)-C(16)-C(19)	107.8(3)
C(1)-C(2)-C(3)	110.7(3)	C(17)-C(16)-C(19)	109.9(3)
C(1)-C(2)-Fe(1)	72.17(18)	C(20)-C(19)-C(16)	116.5(3)
C(3)-C(2)-Fe(1)	70.29(19)	C(21)-C(20)-C(19)	113.9(4)
C(2)-C(3)-C(4)	105.7(3)	C(22)-C(21)-C(20)	116.4(4)
C(2)-C(3)-C(16)	128.3(3)	C(21)-C(22)-C(23)	111.4(6)
C(4)-C(3)-C(16)	125.5(3)	C(24)-C(23)-C(22)	139.0(10)
C(2)-C(3)-Fe(1)	70.56(19)	C(23)-C(24)-C(25)	136.8(10)
C(4)-C(3)-Fe(1)	67.94(18)	O(2)#2-N(1)-O(2)	121.0(5)
C(16)-C(3)-Fe(1)	131.5(2)	O(2)#2-N(1)-O(1)	119.5(3)
C(5)-C(4)-C(3)	109.2(3)	O(2)-N(1)-O(1)	119.5(3)
C(5)-C(4)-Fe(1)	71.14(18)		

Symmetry transformations used to generate equivalent atoms: #1 -x+1/2,y,-z+3/2 #2 -x+1/2,y,-z+1/2

Table A.14. Anisotropic displacement parameters ($Å^2 x\ 10^3$) for $DEC^+NO_3^-$. The anisotropic displacement factor exponent takes the form: $-2\pi^2[\ h^2\ a^{*2}U^{11} + ... + 2\ h\ k\ a^*\ b^*\ U^{12}]$

	U^{11}	U^{22}	U^{33}	U^{23}	U^{13}	U^{12}
Fe(1)	24(1)	29(1)	26(1)	0	2(1)	0
C(1)	23(2)	36(2)	25(2)	3(2)	-1(2)	0(2)
C(2)	28(2)	30(2)	24(2)	4(2)	-1(2)	-5(2)
C(3)	28(2)	32(2)	25(2)	-1(2)	0(2)	-2(2)
C(4)	28(2)	35(2)	27(2)	-4(2)	-3(2)	-3(2)
C(5)	24(2)	35(2)	29(2)	1(2)	-2(1)	-5(2)
C(6)	30(2)	33(2)	35(2)	4(2)	0(2)	4(2)
C(7)	40(2)	34(2)	48(2)	2(2)	-2(2)	3(2)
C(8)	42(2)	45(2)	41(2)	-1(2)	3(2)	13(2)
C(9)	26(2)	42(2)	41(2)	7(2)	-2(2)	4(2)
C(10)	32(2)	48(2)	38(2)	6(2)	-3(2)	2(2)
C(11)	30(2)	49(2)	39(2)	4(2)	-3(2)	-2(2)
C(12)	34(2)	57(3)	43(2)	4(2)	-2(2)	-2(2)
C(13)	35(2)	55(3)	41(2)	2(2)	-2(2)	-3(2)
C(14)	50(3)	64(3)	45(2)	-5(2)	1(2)	1(2)
C(15)	61(3)	65(3)	47(3)	-9(2)	-3(2)	-3(2)
C(16)	34(2)	35(2)	31(2)	-5(2)	4(2)	2(2)
C(17)	32(2)	50(2)	42(2)	-6(2)	9(2)	2(2)
C(18)	41(2)	43(2)	42(2)	-5(2)	6(2)	9(2)
C(19)	45(2)	47(2)	34(2)	-10(2)	7(2)	0(2)
C(20)	69(3)	73(3)	33(2)	-2(2)	6(2)	14(2)
C(21)	65(3)	117(4)	40(3)	11(3)	-7(2)	-9(3)
C(22)	112(4)	84(4)	42(3)	-14(3)	12(3)	-36(3)
C(23)	356(14)	275(11)	23(3)	-30(5)	11(6)	-201(10)
C(24)	244(10)	262(11)	70(5)	46(6)	-75(6)	-169(9)
C(25)	86(4)	99(4)	55(3)	3(3)	-20(3)	-2(3)
O(1)	30(2)	35(2)	84(3)	0	9(2)	0
O(2)	64(2)	65(2)	69(2)	-11(2)	12(2)	20(2)
N(1)	30(3)	51(3)	69(2)	0	–4(2)	0

Table A.15. Hydrogen coordinates (x 10^4) and isotropic displacement parameters ($Å^2$x 10^3) for $DEC^+NO_3^-$.

	x	y	z	U(eq)
H(2A)	2960	9406	6730	33
H(4A)	1449	5047	7048	36
H(5A)	-392	7049	7283	35
H(7A)	1842	11762	7173	62
H(7B)	441	12597	6955	62
H(7C)	1401	11568	6646	62
H(8A)	358	10557	7744	64
H(8B)	-1018	9562	7584	64
H(8C)	-1028	11391	7516	64
H(9A)	-1733	9238	6785	44
H(9B)	-1709	11054	6704	44
H(10A)	-203	10731	6108	48
H(10B)	-138	8916	6198	48
H(11A)	-2628	8748	5987	48
H(11B)	-2647	10552	5879	48
H(12A)	-1072	8338	5408	54
H(12B)	-1080	10141	5301	54
H(13A)	-3558	8232	5176	52
H(13B)	-3510	10019	5049	52
H(14A)	-1907	9453	4486	64
H(14B)	-2002	7664	4608	64
H(15A)	-3488	8222	3960	87
H(15B)	-4358	9437	4240	87
H(15C)	-4435	7640	4355	87
H(17A)	5539	7529	6882	62
H(17B)	4913	8208	6409	62
H(17C)	5940	6735	6421	62
H(18A)	4732	4915	7131	62
H(18B)	5077	4195	6654	62
H(18C)	3518	4008	6835	62
H(19A)	4034	5218	5953	50

Table A.15. (continued)

H(19B)	2459	5111	6122	50
H(20A)	2206	7830	5966	70
H(20B)	3695	7753	5736	70
H(21A)	1319	5927	5423	90
H(21B)	1576	7606	5226	90
H(22A)	3444	5096	5143	95
H(22B)	3679	6778	4940	95
H(23A)	1667	4543	4664	261
H(23B)	1202	6268	4596	261
H(24A)	2997	4807	4223	235
H(24B)	2457	6508	4152	235
H(25A)	1831	4546	3607	122
H(25B)	696	5857	3707	122
H(25C)	555	4179	3922	122

Appendix B.

Final concentrations of $HClO_4$ used in electrochemical determinations of K_{eff}.

Table B.1. Volumes of 1 M $HClO_4$ added to 10 mL of 1 M H_2SO_4 electrolyte and resulting concentrations of $HClO_4$ used for electrochemical determination of K_{eff}.

vol. of 1 M $HClO_4$ added (mL)[a]	tot. vol. of electrolyte (mL)[b]	tot amt. of $HClO_4$ ($\times 10^5$ mol)	final [$HClO_4$] (mM)
0.0	10	0	0
0.05	10.05	5.0	0.50
0.05	10.10	10	9.9
0.15	10.25	25	24
0.25	10.50	50	48
0.25	10.75	75	70
0.40	11.15	115	103
2.00	13.15	315	240

a. The 1 M $HClO_4$ solution was prepared in 1 M H_2SO_4 in order to keep the concentration of H_2SO_4 in the electrolyte constant during $HClO_4$ addition. b. The initial volume of the 1 M H_2SO_4 electrolyte before addition of $HClO_4$ was 10 mL.

Appendix C.

Derivation of equation 4.2.

(Reproduced from Rowe, G. K.; Creager, S. E. *Langmuir* **1991**, *7*, 2307.)

Consider the electrochemical oxidation of ferrocene coupled with two independent ion-pairing reactions of ions X and Y with ferrocenium

$$Fc' \rightleftharpoons Fc'^{+} + e^{-} \qquad E^{o\prime}$$

$$Fc' + X^{-} \rightleftharpoons Fc'^{+}X^{-} \qquad K_X = \frac{\Gamma_{Fc'^{+}X^{-}}}{\Gamma_{Fc'^{+}} C_{X^{-}}}$$

$$Fc' + Y^{-} \rightleftharpoons Fc'^{+}Y^{-} \qquad K_Y = \frac{\Gamma_{Fc'^{+}Y^{-}}}{\Gamma_{Fc'^{+}} C_{Y^{-}}}$$

The total amount of oxidized ferrocene at any time is given by

$$(\Gamma_{Fc'^{+}})_{tot} = \Gamma_{Fc'^{+}} + \Gamma_{Fc'^{+}X^{-}} + \Gamma_{Fc'^{+}Y^{-}}$$

Combining this with the definitions of K_X and K_Y gives

$$(\Gamma_{Fc'^{+}})_{tot} = \Gamma_{Fc'^{+}}(1 + K_X C_X + K_Y C_Y)$$

The Nernst equation for the surface-confined ferrocene/ferrocenium redox reaction is

$$E_{pk} = E^{o\prime} - \frac{RT}{nF} \ln\left(\frac{\Gamma_{Fc'^{+}}}{\Gamma_{Fc'^{0}}}\right)$$

Substituting for $(\Gamma_{Fc'^{+}})$ gives, after rearrangement

$$E_{pk} = E^{o\prime} - \frac{RT}{nF} \ln\left(\frac{(\Gamma_{Fc'^{+}})_{tot}}{\Gamma_{Fc'^{0}}}\right) - \frac{RT}{nF} \ln(1 + K_X C_X + K_Y C_Y)$$

We can assume that ferrocene itself does not ion pair, e.g., that $(\Gamma_{Fc^{+0}})_{tot} = \Gamma_{Fc^{+0}}$. We then note that at E_{pk} (for a symmetric wave), $(\Gamma_{Fc^{+\cdot}})_{tot} = \Gamma_{Fc^{+0}}$. Then the second term on the right side of the equation above goes to zero, and

$$E_{pk} = E^{\circ\prime} - \frac{RT}{nF}\ln(1 + K_X C_X + K_Y C_Y) \tag{4.2}$$

Appendix D.

Complete Tables of Observed Distribution Ratios for the Liquid-Liquid Extraction of $ReO_4^-(aq)$ by $HEP^+NO_3^-$ and $DEC^+NO_3^-$ in Chlorobenzene

Table D.1. Observed distribution ratios for the extraction of ReO_4^- from 1 M $NaNO_3(aq)$ by chlorobenzene solutions of $HEP^+NO_3^-$.[a.]

[Extr.] M	$[ReO_4^-]$ M	$D(ReO_4^-)$ [b.]
0.00100	4.00×10^{-4}	2.4(1)[c.]
	3.50×10^{-4}	2.54(7)
	3.00×10^{-4}	2.7(1)
	2.50×10^{-4}	2.85(6)
	2.00×10^{-4}	3.0(1)
	1.50×10^{-4}	3.37(7)
0.0100	3.00×10^{-3}	24.4(4)
	2.50×10^{-3}	25.9(4)
	2.00×10^{-3}	27(1)
	1.50×10^{-3}	28(1)
	1.00×10^{-3}	29.0(5)
0.100	3.00×10^{-2}	200(6)
	2.50×10^{-2}	280(10)[c.]
	2.00×10^{-2}	299(3)
	1.50×10^{-2}	320(4)
	1.00×10^{-2}	383(1)[c.]

[a.] Extractions were done with equal volumes of the organic phase and the aqueous phase (see the Experimental Section in Chapter 5). [b.] Value reported is an average of three measurements. Numbers in parentheses represent one standard deviation. [c.] Average of only two measurements.

Table D.2. Observed distribution ratios for the extraction of ReO_4^- from 1 M $NaNO_3(aq)$ by chlorobenzene solutions of $DEC^+NO_3^-$.[a.]

[Extr.] M	$[ReO_4^-]$ M	$D(ReO_4^-)$ [b.]
0.00100	4.00×10^{-4}	2.10(7)
	3.50×10^{-4}	2.36(5)
	3.00×10^{-4}	2.42(6)
	2.50×10^{-4}	2.43(6)[c.]
	2.00×10^{-4}	2.47(9)
	1.50×10^{-4}	2.60(5)
0.0100	3.00×10^{-3}	21.4(7)
	2.50×10^{-3}	23.3(2)
	2.00×10^{-3}	23.5(8)
	1.50×10^{-3}	24(1)[c.]
	1.00×10^{-3}	25.3(1)
0.100	3.00×10^{-2}	260(10)
	2.50×10^{-2}	288(4)
	2.00×10^{-2}	296(7)
	1.50×10^{-2}	310(10)
	1.00×10^{-2}	318(6)

[a.] Extractions were done with equal volumes of the organic phase and the aqueous phase (see the Experimental Section in Chapter 5). [b.] Value reported is an average of three measurements. Numbers in parentheses represent one standard deviation. [c.] Average of only two measurements.